PLGA-DS REVERSES CHEMORESISTANCE IN MALIGNANT MESOTHELIOMA BY TARGETING HYPOXIA INDUCED CANCER STEM CELLS

Garima Tyagi
Student number: 1731271

A thesis submitted in fulfilment of the requirement of the University of Wolverhampton for the degree Master of Philosophy

Research Institute in Healthcare Science Faculty of Science and Engineering University of Wolverhampton

September 2020

Abstract

Background: Malignant Mesothelioma (MM) is a malignancy related to asbestos exposure which causes a wide variety of molecular aberrations. MM has a very dismal treatment outcome with an overall survival of fewer than 12 months, with less than five drugs available for its treatment. MM recurrence is unavoidable due to chemoresistance. Long-term inflammation triggered by asbestos activates a key transcription factor, nuclear factor-κB (NF-κB), which is further upregulated in cancer stem cells (CSCs) by hypoxia. Both hypoxia and NF-κB pathway plays a pivotal role in the maintenance of stemness in hypoxia-induced CSCs leading to upregulation of anti-apoptotic signalling, chemo-radiation resistance and metastasis. Therefore, the development of drugs targeting hypoxia-NF-κB-CSCs axis is of clinical significance for MM treatment. Our previous studies have shown that Disulfiram (DS), a clinically used anti-alcoholism drug, in combination with Copper (II) (Cu) has substantial toxicity in CSCs in a wide range of cancer types. The clinical application of DS in Cancer is limited by its very short half-life (< 2 minutes) in the bloodstream. MM is Cancer which mainly infiltrates local organs and tissues with rare distant metastasis. Considering this growing feature of MM, we developed a biodegradable and controlled released poly (lactic-co-glycolic acid) microparticle-encapsulate disulfiram (PLGA-DS) for local treatment of MM. This study aims to examine the anti-MM effect of PLGA-DS and elucidate its molecular mechanisms.

Methodologies: In order to determine drug sensitivity, stemness, apoptosis, invasiveness and NFκB status, the following methodologies were performed in this study: MTT cytotoxicity assay, flow cytometry, analysis of CSC markers, hypoxic cell

cultures, western blot, stable transfection of MM cell line with NFκB, CRISPR-Cas9 knock out of NF-kB-p65, CSC sphere reformation, invasion and migration assay.

Results and conclusions: Two MM cell lines were examined and cultured in a hypoxic environment. MM cell lines were highly resistant to Pemetrexed (PMT) and Cisplatin (CIS), the first-line chemotherapeutic agents for MM. Hypoxia cultured MM cells showed high NF-κB activity and CSC markers and manifested strong migration/invasion ability. The NF-κB-p65 over expressed transfected cell lines did not demonstrate CSC traits along with no increase in resistance to first line drugs. PLGA-DS/Cu completely abolished CSC population in a culture which is demonstrated by sphere reformation assays and flow cytometry analysis of CSC markers such as CD24, CD133 and ABCG2. PLGA-DS/Cu also inhibited the hypoxia-induced NF-kB expression and blocked the migration and invasion ability of MM cells. It showed substantial toxicity to MM cell lines and reversed hypoxia-induced chemoresistance. Also, PLGA-DS/Cu potentiated the cytotoxic effect of Cisplatin/Pemetrexed in vitro. Isobologram analysis indicates moderate synergistic effect between PLGA-DS and cisplatin and pemetrexed in MSTO 211 and JU77 cell lines, respectively. As an FDA approved a drug with all preclinical safety data available, further studies may quickly translate it into MM clinical treatment. This is very promising *in vitro* data and indicate that PLGA-DS could be a promising formulation for localised MM treatment.

Acknowledgements

I want to use this opportunity to appreciate the effort of the people who have assisted me in this research journey. Firstly, I am deeply grateful to my Principal Supervisor, Prof. Weiguang Wang, for his guidance, patience, advice and unending words of encouragement, especially on the days when I needed the most. I have been fortunate to have a supervisor who cared so much about the efforts and research interests of his students. His positive outlook inspired and gave me confidence. More than that, he helped me become a much better person inside and out.

My sincere gratitude goes to Dr Vinodh Kannappan for his excellent co-supervision, assistance and advice. More than a supervisor, he has been a great friend and well wisher. He polished my scientific skills and helped me become an independent researcher.

I am feeling short of words to thank Dr Mark Morris for his invaluable guidance and unconditional support. He helped me understand the complexity of topics by breaking things down to my level and then building up. This has helped me to understand diverse topics and mechanisms and to gain confidence in my abilities. He helped me develop professional and scientific communication skills. Thank you for believing in me.

Completing this work would have been all the more difficult were it not for the support and friendship provided by my colleagues Ogechi Nkeonye, Dr Satish Kumar Kurusamy, Karim Azhar, Gautham Rajendran, Amandeep Kaur, Adam Morgan, Maciej trybull and Manraj Bhela for contributions to this research and making lab a

fun place to work. I would also like to appreciate the academic and technical staff of the Research Institute in Healthcare Science (RIHS), Faculty of Science and Engineering, the University of Wolverhampton, for their assistance throughout my research.

I enjoyed my time here, and it was made fun with the company of my friends Amtul, Harry, Yvonne, Shivraj and Rose. Their constant love and support kept me motivated and focused. My deep gratitude goes to my friend Shelly, Deepika and Ruhi who put up with my odd hours and provided me with lifts and practical help. Thank you for having my back! My special thanks go to Sathish, Reshma, Karim and Ogechi, my basketball team and my friends back home Tarana, Dr Anshul, Preeti Rupinder, Pragati, Shweta and Varun.

I am very grateful to my parents and my brother and sister-in-law who supported me with all their might to pursue my dreams. The support extended by my parents and their positivity moved me leaps and bounds. I don't even have the words to thank my better half, Sourabh for his continued support, unconditional love and encouragement. I was amazed by his willingness to listen to countless discussions about science and my daily struggles. I am blessed to have such strong pillars of support in my life, thank you.

Table of contents

List of Tables

List of Figures

Abbreviations

ABC *ATP-binding cassette*

ABCG2 *ATP-binding cassette transporter G2*

ALDH *Aldehyde dehydrogenase*

APS *Ammonium persulphate*

ATP *Adenosine triphosphate*

AJCC *American Joint Committee on Cancer*

BAX *BCL2-associated X protein*

BAX *BCL2-associated X protein*

BAP1 *BRCA1-associated protein–1*

BCR *B cell receptor*

cDNA *Complementary DNA*

CIS *Cisplatin*

CI *Combination index*

CO_2 *Carbon dioxide*

COX-2 *cyclooxygenase-2*

CSC *Cancer stem cell*

CT *computed tomography*

Cu *Copper*

$CuCl_2$ *Copper chloride*

Cu-DDC *Bis (n, N-diethyldithiocarbamate)-copper (II)*

CuGlu *Copper gluconate*

CXR *Chest X-ray*

DALYs *Disability-adjusted life years*

DAPI *4',6-diamidino-2-phenylindole*

DDC *Diethyldithiocarbamate*

DHFR *dihydrofolate reductase*

DMEM *Dulbecco's modified Eagle's medium*

DMEM-F12 *Dulbecco's modified Eagle's medium/nutrient mixture F12*

DMSO *Dimethyl sulphoxide*

DNA *Deoxyribonucleic acid*

DS *Disulfiram*

DTT *DL-dithiothreitol*

ECL *Enhance chemiluminescence*

ECM *Extracellular matrix*

ED *Effective dose*

EGF *Epidermal growth factor*

EGFR *Epidermal growth factor receptor*

EMT *Epithelial-mesenchymal transition*

EPP *extrapleural pneumonectomy*

ESC *Embryonic stem cell*

FACS *Fluorescence-activated cell sorting*

FBS *Fetal bovine serum*

FDA *Food and Drug Administration*

FDG-PET *fluorodeoxyglucose positron emission tomography*

FITC *Fluorescein isothiocyanate*

FMISO [*F-18] fluoromisonidazole*

FPGS *folylpolyglutamate synthetase*

GAPDH *Glyceraldehyde 3-phoshate dehydrogenase*

HIF *Hypoxia inducible factor*

HIPEC *Hyperthermic intraoperative intraperitoneal chemotherapy*

HM *Human Mesothelial*

HMGB-1 *High Mobility Group Box -1*

HPP *Hypoxyprobe*

HPR *Horseradish Peroxidase*

HPRT1 *Hypoxanthine-guanine phosphoribosyl transferase Homologous recombination*

HRE *Hypoxia response element*

HSCs *Haematopoietic stem cells*

IASLC International Association for the Study of Lung Cancer

IC50 *Ideal Concentration at 50%*

IgG *Human immunoglobulin G*

IKBα *Inhibitor kappa B alpha*

Ikkβ *IKB kinase* β

IL *Interleukin*

i.v. *Intravenous injection*

Jab1 *Jun activating binding protein 1*

KRAS *Ras family of small GTPase*

LB medium *Luria Bertani medium*

LDH *lactate dehydrogenase*

MAPK *Mitogen-activated protein kinase*

MDR *Multiple drug resistance*

MET *Mesenchymal epithelial transition*

MEK *Member of MAPK family*

mM *Millie molar*

MMP *Matrix metalloproteinase*

MTT *3-(4, 5-Dimethylthiazol-2-yl)-2, 5-diphenyltetrazolium*

MRI *magnetic resonance imaging*

mRNA *Messenger RNA*

MRPs *multidrug-related proteins*

miRNA *microRNA*

NAC *N-acetyl-L-cysteine*

NADPH *Nicotinamide adenine dinucleotide phosphate*

NANOG *Homeobox protein NANOG*

NF-κB *Nuclear factor kappa B*

NLR *neutrophil to lymphocyte ratio*

nM *Nano molar*

O_2 *Oxygen*

OCT4 *Octamer-binding transcription factor 4*

PFS *progression-free survival*

PBS *Phosphate-buffered saline*

PCP *Planar cell polarity*

PCI *peritoneal carcinomatosis index*

PD-1 *Programmed-cell death protein-1*

PD-L1 *Programmed-cell death ligand-1*

P-gp *P-glycoprotein*

PLGA *Poly (lactic-co-glycolic acid)*

PVDF *Polyvinylidene difluoride*

P53 *Tumour suppressor gene*

Raf *Proto-oncogene serine/threonine-protein kinase*

RFC *Reduce folate carrier*

RECIST *Solid Tumors Response Evaluation Criteria*

RELA *REL-associated protein p65 involved in NF-κB*

RIPA *Radio-immunoprecipitation assay*

RNA *Ribonucleic acid*

ROS *Reactive oxygen species*

RPM *Rotation per minute*

RT-PCR *Reverse transcription polymerase chain reaction*

SCM *Stem cell medium*

SDS *Sodium dodecyl sulphate*

SDS-PAGE *Sodium dodecyl sulphate polyacrylamide gel electrophoresis*

S-Me-DDC *S-methyl-N, N-diethyldithiocarbamate*

SNAIL *Snail family transcriptional repressor 1*

SSC *Side scatter*

STAT1 *Signal Transducer and Activator Of Transcription 1*

SOX2 *SRY (sex determining region Y)-box 2*

TBS *Tris-buffered saline*

TBS-T *Tris-buffered saline- Tween*

TCR *T cell receptor*

TEMED *Tetramethylethylenediamine*

TF *Transcription factor*

TGF *Transforming growth factor*

TLR *toll-like receptor*

TNF *Tumour necrosis factor*

TNFR *(IL-1R), tumour necrosis factor receptor*

TNM *Tumour, node and metastasis*

TOP2A *Topoisomerase II*

TWIST *Twist-related protein 1*

TVT *tunica vaginalis testis*

TYMS *Thymidylate Synthase*

VATS video-assisted thoracoscopic surgery

VHL *Von Hippel-Lindau*

WHO *World Health Organization*

Wnt *Wingless gene*

ZEB *Zinc finger E-box-binding homeobox 1*

CHAPTER 1

Introduction

1.0 Introduction

1.1 Cancer

Cancer is not a single disease and caused by the uncontrolled growth of abnormal or mutated cells in the body. Cancer cells have the potential to grow and divide rapidly and undergo unchecked proliferation (B Kalyanaraman.,2017). It is major cause of worldwide death and in countries of all income levels (Torre et al.,2015). According to the WHO, Cancer imposes the largest worldwide burden, i.e. 244.6 million Disability-adjusted life years (DALYs), both in men (137.4 million DALYs) and in women (107.1 million DALYs).The cancer-related burden is slightly but non-significantly higher in men than in women (9.6% vs 8.6%; p = 0.219).

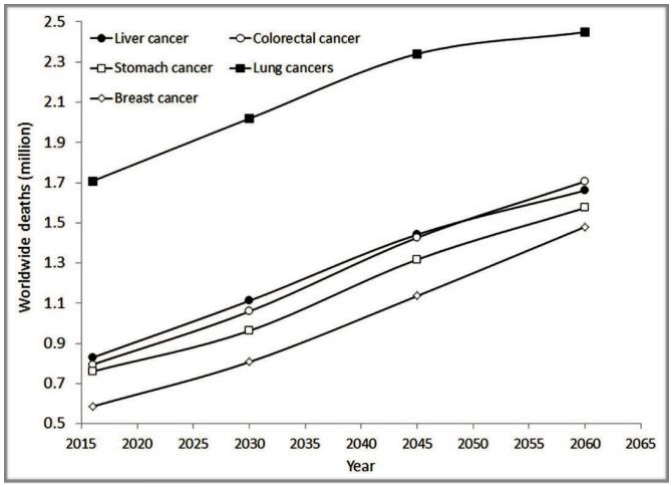

Figure 1: Showing the estimated epidemiological trend of the five leading causes of cancer death from the years 2016 to 2060 (Mattiuzzi and Lippi.,2019).

As per last WHO update, corresponding to the year 2016 states that cancer is the second leading cause of death, accounting for 8.97 million deaths worldwide.

Especially, the rank of cancer was among the leading reasons for mortality which differs in the different WHO regions. It remains first in the Western Pacific and America Regions, second in South-East Asia, Eastern Mediterranean Regions and European, but only fourth in the African Region (Mattiuzzi and Lippi.,2019)

2.0 Mesothelioma

Mesothelioma is characterised as an insidious neoplasm because of its long latency period, for about 40 years (Frank et al.,2012). Malignant Mesotheliomas (MM) are rare and aggressive tumors. It arises from the mesothelium of pleura and peritoneum and the rare sites are pericardium and tunica vagnilis testis. More than 80% of mesotheliomas localises in the pleura (Tischoff et al.,2017). Previous exposure to asbestos is the leading risk factor for MM. Clinical signs are late and unspecific (Delourme et al.,2018). The precise prevalence of the disease is not known, but MM expects to represent 1% of all the known cancers (Alastair J Moore et al., 2008).

2.1 Epidemology

Europe (Belgium, Malta, The Netherlands) and Oceania (New Zealand and Australia) have reported the highest MM incidence. Fifty-five countries have banned asbestos. However, only 16% of the inhabitants contribute to the world population. The second group includes a significant part of Europe and the USA. The incidence rates of MM are misleading as inside a single country; the incidence of the disease shows substantial variations depending on the areas (Bianchi et al.,2014).

The incidence and mortality rates of global mesothelioma are uncertain because there is no data available from developed countries which continue to use large quantities of asbestos. The accuracy of diagnosis for MM has improved due to novel molecular and immunohistochemical markers. However, still, 14 per cent (high-resource countries) to 50 per cent (developing countries) of diagnoses are incorrect, leading to insufficient diagnosis (Carbone et al., 2019).

Men get affected even more often than women. The mean patient age is > 60 years. The most significant risk factor is asbestos exposure, which persists in 54–90% of all affected patients (Tischoff and Apple.,2017). In environmentally exposed subjects, the male to female ratio reports about 1.2: 1.4 (Marinaccio et al.,2018). In 9 countries (United Kingdom, Sweden, France, Germany, Netherlands, Canada, United States, Australia, and New Zealand), MM mortality has decreased dramatically among males. It was significantly rising in 5 countries (Poland, Spain, China-Hong Kong, Japan, and the Republic of Korea) over the last ten years.

Among females and in the last ten years MM mortality has declined significantly in only one country (Italy); while in 3 countries (Poland, Argentina, and the Republic of Korea), it has increased substantially. In the remaining countries, APC (Annual Percentage Change) was stable. The burden and patterns of mesothelioma mortality are globally variable. Furthermore, MM is still a significant cause of mortality despite the ban on asbestos in many countries (Rahman. ,2018).

2.2 Etiology

Exposure to airborne asbestos fires is mainly associated with the development of MM

(Porpodis et al., 2013). Asbestos belongs to silicate family minerals which are further divided into two major groups: The serpentine form and the amphibole form. Asbestos is known to cause various diseases like laryngeal cancer, plaques/fibrosis and majorly Mesothelioma (Michele et al.,2012). Most pleural mesotheliomas are due to asbestos (70% to 90%) in men in Europe and North America. However, this proportion is lesser for peritoneal mesothelioma. In North America, asbestos exposure is lesser in women at any location, but in Europe, the ratio is higher and differs significantly by locale. Other types of mineral fibers (erionite, fluoro-edenite, and possibly balangeroite) can induce MM at specific geographic locations. For other malignancies, therapeutic radiation is a well-established cause of mesothelioma. Chronic pleural inflammation can cause MM, but there is insufficient data. A small number of mesotheliomas (probably 1%) is caused by germline mutations/deletions of BRCA1-associated protein–1 (BAP1). All of these alternative etiologies account for a small proportion of tumours, and most mesotheliomas are not caused by asbestos exposure (Attanoos et al.,2017).

2.3 Types and features

2.3.1 Anatomic classification

Mesothelioma arises from mesothelial surfaces and can be classified by location and pathology. According to the site, mesothelioma occurs majorly in pleura (65%-70%), peritoneum (30%), tunica vaginalis testis, and pericardium (1%-2%) (Ahmed et al.,2013).

1. Pleural Malignant Mesothelioma: It is the most common and accounts for the predominant subtype-80% of all cases. Pleural mesothelioma has an unusually dismal prognosis; its 5-year survival rate is only 10%, making it the most fatal among rare cancers (Tolani et al.,2018).

2. Peritoneal Malignant Mesothelioma -Peritoneal Malignant Mesothelioma is a rare tumour, less common than its pleural equivalent. It emerges from the peritoneum overlying mesothelial cells, it occurs preferentially in males with an average age ranging from 47 to 60.5 years, clinical symptoms are not specific, and the imagery remains little or non-contributive (Mery et al.,2014).
3. Primary cardiac and pericardial tumours - These are rare entities with an autopsy frequency of 0.001-0.03%. Cardiac and pericardial metastases are much more common than primary tumours. Pericardial malignant mesotheliomas account for up to 50% of primary pericardial tumours (Barroso et al.,2017).

4. Mesothelioma of the tunica vaginalis - It arises from the serosal membranes of the tunica vaginalis testis (TVT) (Butnor et al.,2019). It represents 0.3 to 0.5% of all malignant mesotheliomas. Asbestos exposure is frequently accompanied by sickness. It is often mistakenly diagnosed during surgery for other causes, due to its low occurrence and non-specific clinical presentation, and the prognosis is typically low (Trenti et al.,2019).

2.3.2 Pathological classification

According to pathology, malignant mesothelioma is divided into four histologic types:

1. Epithelioid: Composes roughly 60% of cases. Tumours of this kind have higher chances of survival since they are easier to be identified and removable with surgery. They are characterised by square-shaped cells with a visible nucleus and is the most common (50-70%) and tend to have a much more favourable prognosis (Boneli et al.,2017).
2. Fibrous sarcomatoid: Roughly 25% of cases are more aggressive than epithelial, and patients often do not respond to the treatment. 10-20% with elongated and spindle-shaped cells is the most aggressive one (Boneli et al.,2017).

3. Biphasic/mixed: They are most challenging to cure and thus with abysmal prognosis. It also contributes roughly to 15% of the total occurrence and consist of both epithelial and sarcomatoid cell types. It is a mixture of epithelial cells and sarcomatoid cells (20–35%) (Boneli et al.,2017).
4. Other (rare) histologies include desmoplastic, lymphohistiocytosis, deciduous, anaplastic, multicystic, and well-differentiated papillary mesothelioma (Terence et al.,2009). Papillary type is the most common which coexist with other patterns and mostly tubular design (Shavekke et al.,2017).

2.3.3 Modified pathological classification

Recently, a revised classification was also suggested (Blyth et al.,2018). The authors suggest that epithelioid and sarcomatoid classifications to be retained, but biphasic tumours were split into biphasic-E and biphasic-S. 68% of tumours are histologically classified as epithelioid; further molecularly classified as biphasic-E. Moreover, it had a significantly worse prognosis than other molecular subtypes.

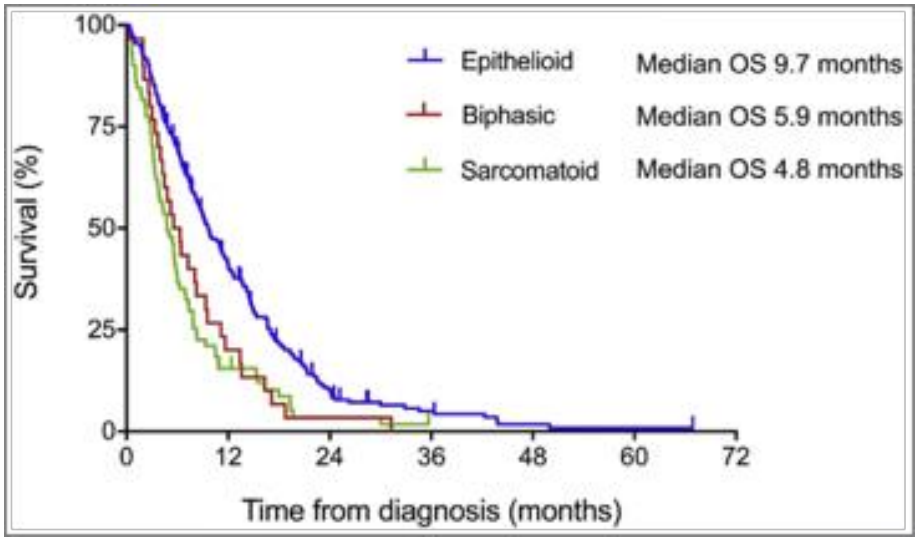

Figure 2: Showing the median survival of mesothelioma patients depending upon the cell type (Blyth et al.,2018).

2.4 Prognosis

MM has reduced life expectancy, with median survival varying between 8 and 14 months. For mesothelioma patients, the prognostic markers were categorised into the following four basic categories: clinical and patient-reported prognostic markers, predictive blood or serum markers, prognostic imaging markers, and molecular prognostic markers. Inflammatory markers like WBC, neutrophil to lymphocyte ratio (NLR) and C-reactive protein in various MM, prognosis studies have also found to be significantly elevated (Zandwijk et al.,2013). Multiple organisations have analysed quite a large number of MM patients who enrolled in the treatment trials and identified the following poor prognostic factors: WBC count - 8.3 × 109/L or higher, older age, i.e. more than 75, Male, chest pain, Non-epithelioid histology, Platelets greater than 400,000 μL, poor performance status, LDH greater than 500 IU/L (Alastair J Moore et al., 2008). Decreased levels of haemoglobin, thrombocytosis, and elevated serum

lactate dehydrogenase (LDH) also contributed to the poor prognosis (Zandwijk et al.,2013). Epithelioid is the most common amongst the subtypes and is associated with the best prognosis. The worst prognosis is of sarcomatoid variants consisting of spindle morphology (Frank et al., 2012).

2.5 Symptoms

MM was discovered incidentally during laparoscopy for other indications. Usually, MM is diagnosed between 40 and 65 years of age and can show ambiguous, non-specific symptoms which may be quite variable depending on the degree and distribution of the disease in the peritoneum. Plaques are very common with mesothelioma patients. Patients most often complain of increased abdominal distension and abdominal pain (Enomoto et al., 2019. Typical patients with malignant pleural mesothelioma may have an unproductive cough, chest wall pain, dyspnea, pleural effusions mainly on the right side (60 per cent of cases)). The common symptoms are shortness of breath and pain (90%), while others include fatigue (36%), worry (29%), cough (22%), sweating (22%), and constipation (22%) (Porpodis et al.,2013).

2.6 Staging of MM

The staging method for TNM ((T) tumours, (N) nodes, and (M) metastases is primarily focused on surgical and pathological variables and cross-sectional imaging. Due to the impracticality of measuring tumours with irregular and highly variable morphology,

unlike TNM staging of most solid tumours, MM classification does not require consideration of tumour size. The lung cancer diagram, which suggests that tumours invade pulmonary lymphatics, follows the N classification of MM. M classification of MM is binary. M1 indicates documented blood-borne metastasis. Distant metastases to the brain, bone, kidney and adrenal glands have reported. Still, they are rarely diagnosed, likely due to the comparatively rapid and fatal progression of local T4 disease involving vital intrathoracic organs (Richard et al.,2017). Tertemiz et al. found extrapleural dissemination in 87.7% of cases during postmortem studies. Tumour dissemination in extrathoracic sites seen in the liver (31.9%), spleen (10.8%), thyroid (6.9%), and the brain (3.0%) (Tertemiz et al.,2014)

The precision and reproducibility of TNM staging for MM are impeded by the absence of a quantitative measure, representing the size of the tumour, the number and complexity of criteria for T classification, and the growing inclination to use lung-sparing surgical procedures that leave many unassessed margins and lymph nodes. These facts led the International Association for the Study of Lung Cancer (IASLC) staging committee to suggest the concept of a "best" stage (bTNM) incorporating available staging data from multiple (clinical, surgical, pathological) evaluations to minimise missing data and increase the efficacy of TNM by using chest computed tomography (CT), magnetic resonance imaging (MRI) and fluorodeoxyglucose positron emission tomography (FDG - PET), clinical staging of MM usually requires radiographic evaluation of TNM classification criteria. Some groups used staging to monitor metastatic diseases which would avoid surgical resection and could be missed by imaging.

Pathological staging classifies cases from surgical resection based on gross and microscopic analyses of pathological specimens (Richard et al.,2017). Review of the database of MM by the IASLC indicated that therapeutic (cTNM) staging minimally stratified survival and was inconsistent with pathological (pTNM) staging. Alternative staging models based on quantitative parameters explored, to improve the prognostic classification of MM. The rarity of this disorder, the difficulty of its diagnosis and the general ineffectiveness of available treatment have impeded attempts to improve MM staging (Gill et al.,2018). RECIST (Solid Tumors Response Evaluation Criteria) is the most used MM measurement system. It is based on the unidimensional measurements of tumour thickness perpendicular to the chest wall or mediastinum. Tumour stage remains the most important prognostic factor in many malignancies, and it is often used to stratify patients in clinical trials. Since not every patient had both therapeutic and pathological stages, data was put together to obtain the best TNM.

Beyond TNM, histology remains the most significant prognostic determinant (Bonomi et al., 2017). The peritoneal carcinomatosis index (PCI) is the most frequently used and accepted classification to measure the peritoneal disease burden. The eighth edition of the Staging Manual of the American Joint Committee on Cancer (AJCC) has a staging system for pleural mesothelioma. Still, it has no staging system for Malignant Peritoneal Mesothelioma (MPM). A new TNM staging method, proposed by Yan and colleagues, addresses this issue. T was allocated under this method based on the magnitude of the disease burden quantified by intraoperative PCI and classified into four subgroups: T1 (PCI 1–10), T2 (PCI 11–20), T3 (PCI 21–30), and T4 (PCI 31–39). Node status (N) allocated for histopathology of surgical specimens based on the presence (N1) or absence (N0) of positive lymph nodes. Any extra-abdominal metastasis discovered on pre-operative imaging was assigned M1. Stage I disease

included T1N0M0, stage II included T2- 3N0M0, and stage III included T4N0M0 and N1 or M1 disease. Using this staging system, 5-year survival for stage I, II, and III was 87%, 53%, and 29%, respectively (Enomoto et al.,2019). Efforts are underway to further refine criteria and to validate 3-dimensional quantitative estimates of tumour size to potentially augment T classification in future editions of the staging system (Richard et al.,2017).

2.7 Pathogenesis

Asbestos has demonstrated to induce the production of reactive oxygen and nitrogen species from mesothelial cells and macrophages. These species are potent mutagens which can react with DNA, resulting in a plethora of damage (Quinna et al.,2015). The underlying pathogenesis of the disease is that the inhaled asbestos fibres enter the visceral pleura and the pleural space and then to the parietal pleura through the alveoli or retrograde through the lymphatic vessels (Roe and Stella.,2015). Molecular changes are also involved in the development of MM and accumulate over many decades, eventually resulting in malignant transformation of the mesothelial cell. The typical molecular landscape of MM consists of multiple chromosomal losses leading to loss or inactivation of several tumour suppressor genes. Mainly, chromosomes 3p, 9p and 22q, harbouring tumour suppressor genes, are critically involved in the pathogenesis of MM, leading to loss of p16INK4A-p14ARF (CDKN2A) located at 9p21, neurofibromatosis type 2 (NF2) at 22q12 and BRCA1-associated protein 1 (BAP-1) at 3p21.31-p21.2 (Hjerpe, Own and Dobra.,2020). Several MM consists of very complex karyotypes along with extensive aneuploidy and the rearrangement of many chromosomes. The single most common karyotypic change found is the loss of one

copy of chromosome 22. Moreover, dysregulation in signal transduction pathways, related to cell survival and proliferation, has also been demonstrated (Boneli et al.,2017). The fibres themselves can also cause aberrant separation of chromosomes during mitosis and direct activation of tyrosine kinase receptors, in the absence of driver mutations (Abbott et al.,2020).

2.8 Diagnosis

As the clinical presentations and imaging are complex and non-specific, diagnosis of MM is difficult. Chest X-ray (CXR) typically starts with imaging and then goes on to computed tomography (CT). A novel approach may help differentiate malignant from benign lesions, such as quantitative textural and form analysis. Ultrasound is especially important to analyse pleural effusion. Thoracoscopy is used in the diagnostic phase as a standard procedure that allows good visualisation of the endothoracic anatomy with the direct evaluation of the locoregional tumour extension and to practice, where necessary, effective chemical pleurodesis (Abbott et al.,2020). It is a reliable diagnostic tool since it can give additional tissue confirmation. Computed tomography (CT) may show pleural-based nodularity. PET (Positron emission tomography) is very beneficial as mesothelioma has hypermetabolic characteristics. Thus, this technique cannot only be used for staging, but post-treatment follows up as well (Frank et al., 2012). The ultra-structural features of MM can be revealed by using electron microscopy. As thin and tall microvilli on the surface of the cell, whose length exceeds the width by a margin of 15:1 (Murinello et al.,2010).

2.9 Biomarkers

Currently, there is no routine test used for testing prognostic or predictive biomarkers for MM. Emerging data suggest that the histologic type of mesothelioma show different associations with different predictive biomarkers (Brcic and Kern.,2020). Over the years, numerous candidate biomarkers have proposed the significance of screening, early diagnostic and prognostic markers. A combination of two positive (mesothelial) and two negatives (cancer-related) markers are considered the gold standard for immunohistochemical diagnosis of epithelioid and biphasic MM, while the rare sarcomatoid type has no specific markers. Among biomarkers in body fluids such as a serum, plasma, and pleural effusion (PE), soluble mesothelin-related peptide (SMRP), also known as mesothelin, is the best characterised and well known displaying high specificity for MM, but low sensitivity. Therefore, levels of SMRP in the body fluids cannot be considered as the sole modality of a diagnostic marker. Osteopontin has been reported as a promising biomarker to discriminate early-stage MM patients among an asbestos-exposed population, but its usefulness in screening is compromised by the low specificity (Lacerenza et al.,2020).

Claudin-4 now viewed by many expert mesothelioma pathologists, and supported by the literature, as a superior marker of epithelial differentiation. While historically described mesothelial markers remain in use, more recently, HEG1 (heart development protein with EGF-like domains), is described as a sensitive and specific marker of mesothelial differentiation with an excellent discriminatory expression between mesothelial and epithelial proliferation (Schulte and Husain.,2020). MM stains were positive for cytokeratin 5/6 (CK 5/6), calretinin, vimentin, epithelial membrane antigen, Wilms tumour 1 (WT-1) (Enomoto et al.,2019). Until today the

only tumour biomarker to receive the approval of US Food and Drug Administration for clinical use is mesothelin. It has a very confined expression on non-cancerous healthy tissue; thus, it is a desirable therapeutic target for mesothelin-positive tumours. In a few situations, mesothelin can be shed from the surface of the cells by the action of tumour necrosis factor-a-converting enzyme and identified in the blood (Creaney et al.,2017). The low sensitivity of SMRPs for early MM limits its value; therefore, additional biomarkers are required (Santarelli et al.,2015).

3.0 Treatment

Unfortunately, few treatment options exist for MM (Abbott et al.,2020). Current treatments for MM are limited to surgery, radiation, and chemotherapy (Tolani et al.,2018).

3.1 Surgery

In terms of pleurectomy, surgical therapy is only for patients who can handle surgical risks and have a low tumour stage (Abbott et al.,2020). Various surgical procedures are surgical pleurodesis by video-assisted thoracoscopic surgery (VATS), debulking surgery and extrapleural pneumonectomy (EPP) (Alastair J Moore et al., 2008). Several non-randomised series reported long-term survivors following extra-pleural pneumonectomy (EPP), which involves removal of the diseased pleura in addition to the lung, pericardium and hemidiaphragm, usually as part of a multi-modality regime including neoadjuvant chemotherapy and adjuvant Hemi-thoracic radiotherapy (Blyth et al.,2018). In MM surgery, microscopic radical (R0) resection is not possible because

of the anatomy, and the target of MM surgery is full macroscopic resection (R1). Surgery alone is not effective, it is generally undertaken with chemotherapy and/or radiation therapy and reserved for a subset of patients with early tumour, epithelioid histology and good results (Cantini et al., 2020)

3.2 Radiotherapy

Radiation therapy (RT) may have a role in MM, as it can be used in combination with chemotherapy and can provide local tumour control if the patient has a good performance status (Abbott et al. ,2020). Intensity-modulated radiotherapy (IMRT) allows effective moulding of large RT doses, even to the complex morphology of the pleura. However, some of the apparent radio-resistance associated with MM may reflect intrinsic radio-resistant tumour biology and development of effective radiosensitisers which may be necessary for maximum effect. Combinations of RT with relevant agents, e.g. DNA-damage repair inhibitors and/or immunotherapies may deliver new treatment options (Blyth et al.,2018). Intensity-modulated radiotherapy (IMRT) is a sophisticated modality using small radiation beams at different angles in a 3-D conformal pattern, which allows more intense radiation at the target with high precision (Frank et al., 2012). However, the toxicity may be important and, thus, RT unless it helps to alleviate symptoms such as chest pain or bronchial/oesophagal obstruction, it alone has no benefit (Abbott et al. ,2020).

3.3 Chemotherapy

The combination of Cisplatin and Pemetrexed is floowed as a standard first line

therapy for MM. In 2003, a phase III randomised trial compared Cisplatin alone versus Cisplatin plus Pemetrexed in untreated malignant pleural mesothelioma with the combination, and the response rate was 41.3% compared to 16.7% for Cisplatin alone, Median time to progression was 5.7 vs 3.9 months. Median overall survival was 12.1 vs 9.3 months, both in favour of the combination arm. Therefore, it has also become a standard recommendation in the adjuvant combined modality approach to resectable disease (Frank et al., 2012). The National Comprehensive Cancer Network's recommendations for 2018 identify that the first-line systemic therapy for MM is Pemetrexed combined with Cisplatin and probably Bevacizumab (Abbott et al. ,2020).

3.3.1 Cisplatin

Cisplatin is a small and surprisingly simple molecule made up of one atom of Platinum bound to two amides and two chlorides; it is a potent drug considering its size. Cisplatin undergoes a mechanism known as aquation, under conditions of low chloride concentration, as found in the cytosol, in which water molecules substitute one or two chlorides. By the process of aquation, Cisplatin becomes highly reactive and binds readily within the cell to a variety of biomolecules. Cisplatin covalently binds in its reactive form to the DNA bases, forming adducts of DNA. In a coordinated effort by the cells to remove the lesions, these DNA adducts block transcription and DNA synthesis, which in turn activates a complex intracellular signal transduction cascade. The cell cycle is arrested, providing adequate time for DNA repair mechanisms to remove the lesions. In cases of impaired repair or excessive damage, the cells undergo apoptosis (Rocha et al.,2018).

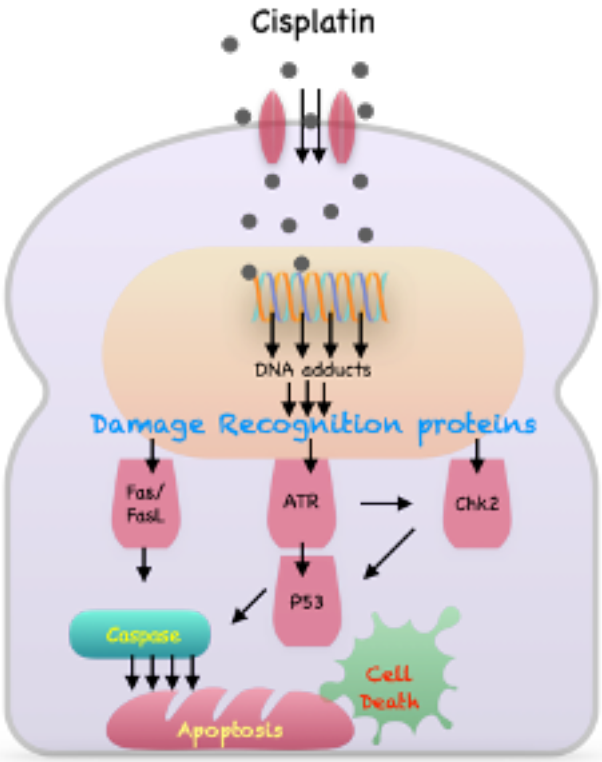

Figure 1.3: Mechanism of Cisplatin action for mesothelioma treatment.

Platinum responsiveness is high primarily, but many cancer patients will ultimately relapse with the Cisplatin-resistant disease. The major mechanisms leading to Cisplatin resistance inside the tumour cell is decreased drug import, increased drug export, increased drug inactivation by detoxification enzymes, increased DNA damage repair, and inactivated cell death signalling. Hence, drug resistance has been observed in many patients who relapsed from interactions between a cell, and its environmental components which promote these internal mechanisms and subsequent Cisplatin resistance (Chen and Chang.,2019). To overcome resistance, Cisplatin is commonly used in combination with some other drugs in treating various cancers, including mesothelioma (Dasari et al.,2014).

3.3.2 Pemetrexed

Pemetrexed belongs to the class of antifolic agents, but it is distinguished from the other antifolates for its novel structure, possessing a unique 6-5 fused pyrrolo-[2,3-d] pyrimidine nucleus instead of the classical 6-6 core structure (pteridine or quinazoline) (Facchetti et al.,2017).

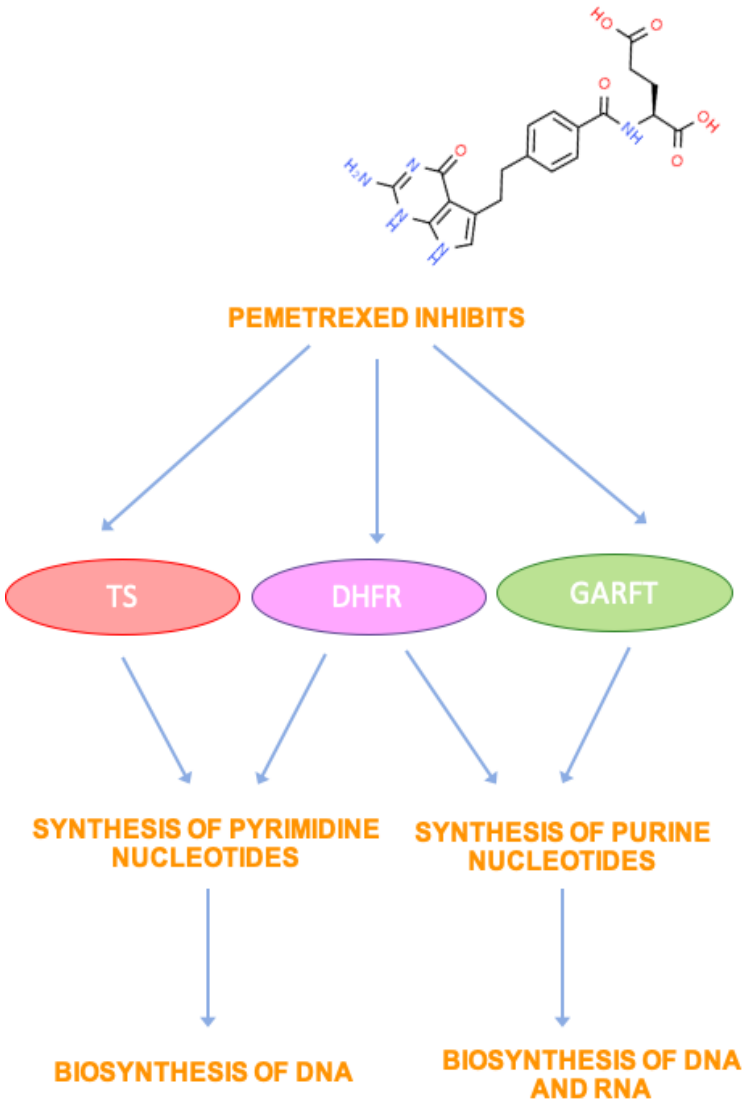

Figure 1.4: Mechanism of Pemetrexed action for mesothelioma treatment.

Pemetrexed is an antagonist against folates. Because folate donate one-carbon units to the biosynthesis of purines, thymidine, and hence DNA, the interruption of folate metabolism by Pemetrexed contributes to ineffective DNA synthesis and failure of growth in tumour cells (Liang et al.,2019).

Pemetrexed is rapidly converted to polyglutamate forms once the folylpolyglutamate enzyme synthetase enters the cell. The types of polyglutamate are stored in cells and are also more powerful Inhibitors of TS and GARFT. The process of polyglutamation is concentration and time-dependent process, which occurs in tumour and lesser in normal cells. Polyglutamated metabolites have prolonged drug action in malignant cells due to increased intracellular half-life., Therefore, Pemetrexed prevents the formation of DNA and RNA by inhibiting the formation of precursor purine and pyrimidine nucleotides, required for the growth and survival of both normal cells and cancer cells.

The primary adverse effect of Pemetrexed is the dose-limiting toxicity of the drug and is associated with elevated pretreatment levels of plasma homocysteine which predicts severe myelosuppression (Xin et al.,2014). In first-line therapy, Pemetrexed is always administered in combination with other more emetogenic agents, such as Cisplatin; therefore, adequate antiemetic prophylaxis is necessary.

3.3.3 Resistance of MM to Cisplatin and Pemetrexed

A widely held misconception contends that all elderly patients, because of the toxicity of some chemotherapeutic agents, even with good performance status (performance status [PS] 0–1), are unable to tolerate aggressive chemotherapy (Xin et al.,2014).

However, the effect of this therapy is reversible; preclinical testing showed that exogenous hypoxanthine and thymidine were necessary to prevent growth inhibition by Pemetrexed (Curtin and Hughes 2001). In Pemetrexed-resistant cells, TYMS (Thymidylate Synthase) overexpression is one of the major factors leading to resistance and the regulation of DHFR (dihydrofolate reductase), RFC (Reduce folate carrier) and FPGS (folylpolyglutamate synthetase) expression is associated with acquired resistance to pemetrexed (Obata et al.,2013).

Although Cisplatin is the most frequently used chemotherapeutic agent used, in association with Pemetrexed, usually the results are disappointing. Since the score of residual peritoneal seeding after cytoreductive peritonectomy is the principal prognostic indicator; selected patients can support it. Hyperthermic intraoperative intraperitoneal chemotherapy (HIPEC), followed by early postoperative intraperitoneal chemotherapy, is a good strategy for a much longer survival (Murinello et al.,2010). Therefore, despite the improvement shown with the combination of Cisplatin and Pemetrexed, nearly two-thirds of patients still fail to show a response to this regimen (Frank et al., 2012).

MM treatment is not guided by histological or molecular features of the tumour. It mainly depends on the clinical stage and patient characteristics. Moreover, there are no other approved regimens for relapsed or refractory MM as Platinum-based chemotherapies and have also failed to show improvements in survival benefits and (Porpodis et al., 2013). There is no alternative when MM patients fail this treatment option as the combination confers a median progression-free survival (PFS) of 5.7 months (Porpodis et al., 2013). Moreover, an overall Response rate of combination

chemotherapy is approximately 40%; almost half of all patients are primary resistant and develop resistance ultimately (Kim et al.,2018).

4.0 Chemoresistance

MM is incurable and chemoresistant cancer (Riedel et al.,2017). There is no standard chemotherapy for refractory or relapsing MM (Staumont et al.,2020). The standard of care in the first-line treatment is a combination of Platinum-based chemotherapy with antifolate Pemetrexed. Interestingly, Raz and collaborators showed that severe hypoxia-induced a complete antifolate resistance and caused simultaneous suppression of crucial genes in folate homoeostasis. Lactate production due to hypoxia also contributes to extracellular acidosis, thus supporting tumour invasiveness and exerting immunosuppressive effects (Petri et al.,2020). The genetic and molecular profiling of MM led to the discovery of pathways involved in the development and invasion of MM. Analyses of alterations in signalling pathway activities have identified consistent upregulation of the PI3K/AKT/mTOR pathway (Li et al.,2018). ROS are usually increased in MM cells due to oncogene activation and involved in the initiation and progression of MM. Overproduction of reactive oxygen and ROS, aberrant inflammatory cytokine and chemokine expression, increased cyclooxygenase-2 (COX-2), and nuclear factor kappa B (NF-kB) expression are just some of the molecular factors that contribute to inflammation-induced carcinogenesis (Benedetti et al.,2015).

One of the multidrug resistance mechanisms (MDRs) is the overexpression of ATP-binding cassette (ABC) transporters. Such as P-glycoprotein (Pgp) and multidrug-

related proteins (MRPs), which extrude anti-cancer drugs, leading to a reduction in the accumulation of intracellular chemotherapy and its cytotoxic effects (Mungo et al.,2018). Cancer Stem Cells (CSCs) represent a small subpopulation of tumour bulk and are mainly responsible for tumour mass renewal, recurrence and chemoresistance. MM CSCs were first identified from commercial cell lines as a side population, ranging from 0.05 to 1.32% cells, positive for CD133, CD9, CD24, CD26, CD44, octamer-binding transcription factor 4 (Oct4), Nanog, sex-determining region Y-box 2 (SOX2), ATP-binding cassette transporter G2 (ABCG2), aldehyde dehydrogenase (ALDH). A shared feature of CSCs is their resistance to Cisplatin and Pemetrexed (Milosevic et al.,2020). The utmost barrier for efficient drug delivery in solid tumours is the morphologically and functionally abnormal tumour vasculature characterised by chaotic angiogenesis and highly permeable blood vessels that lead to elevated tumour interstitial fluid pressure. High interstitial fluid pressure is believed to delay convection and, for this reason, to cause unfavourable drug transport conditions within tumours. The latter is is believed to be responsible for the inadequate response of tumours to chemotherapy and their recurrence (Riedel et al.,2017).

4.1 Hypoxia

The rapid proliferation of tumours makes them too large than their surrounding vasculature, resulting in a drop of normal oxygen levels of 2 –9% to hypoxic levels of less than 2% (Jing et al.,2019) Oxygen can diffuse only 100-180Am from a capillary to the cells before completely metabolising (Powis et al.,2018). Regions with fewer oxygen levels are termed as hypoxic regions. Hypoxia plays a crucial role during embryonic development in determining cell fate (Saxena and Jolly.,2019). Oxygen

tension in tumours varies from 0.02 to 8%. Oxygen levels at about 3% induce EMT, while severe oxygen depletion (< 0.02%) inhibits DNA synthesis (Najafi et al.,2019).

Normal cells cannot withstand prolonged hypoxia and undergo either apoptosis or necrosis depending on nutrient availability along with oxygen deprivation (Saxena and Jolly.,2020). Hypoxic cells become resistance to programmed cells death, convert to glycolytic metabolism and migrate to lesser hypoxic areas of the body. They relate to pro-angiogenic factors like VEGF (vascular endothelial growth factor) stimulating new blood vessel from existing vasculature leading to increased tumour oxygenation and, ultimately, tumour growth. For this reason, hypoxic tumours are the most pro-angiogenic and aggressive tumour (Kim et al.,2020). Tumours are composed of regions with oxygenated cells which are situated near to the blood vessels. They become highly hypoxic with increased distance from a functional blood supply (Tameemi et al.,2019). Regions with extreme hypoxia are regarded as niches, where poorly differentiated and more aggressive cell types called cancer stem cells (CSCs) aggregated. CSC enrichment in these hypoxic regions finally causes tumour relapse at local or distant sites (Najafi et al., 2019).

Hypoxia also generates intertumoral oxygen gradients, contributing to the plasticity and heterogeneity of tumours. Hypoxia-induced by the acidic TME leads to MDR by various mechanisms. It includes a decreased concentration of the drug caused by "ion trapping," reduced apoptotic potential, genetic alterations (such as p53 mutations), and elevated activity of a multidrug transporter p-glycoprotein (P-gp) (Jing et al.,2018).

Mesotheliomas are particularly hypoxic solid tumour masses as evidenced by binding of pimonidazole as exogenous hypoxia markers and elevated levels of HIF-1α as endogenous hypoxia marker. Imaging evidence from [F-18] fluoromisonidazole

(FMISO) PET-CT scanning confirms hypoxia being integral to mesotheliomas (Nabavi et al.,2016).

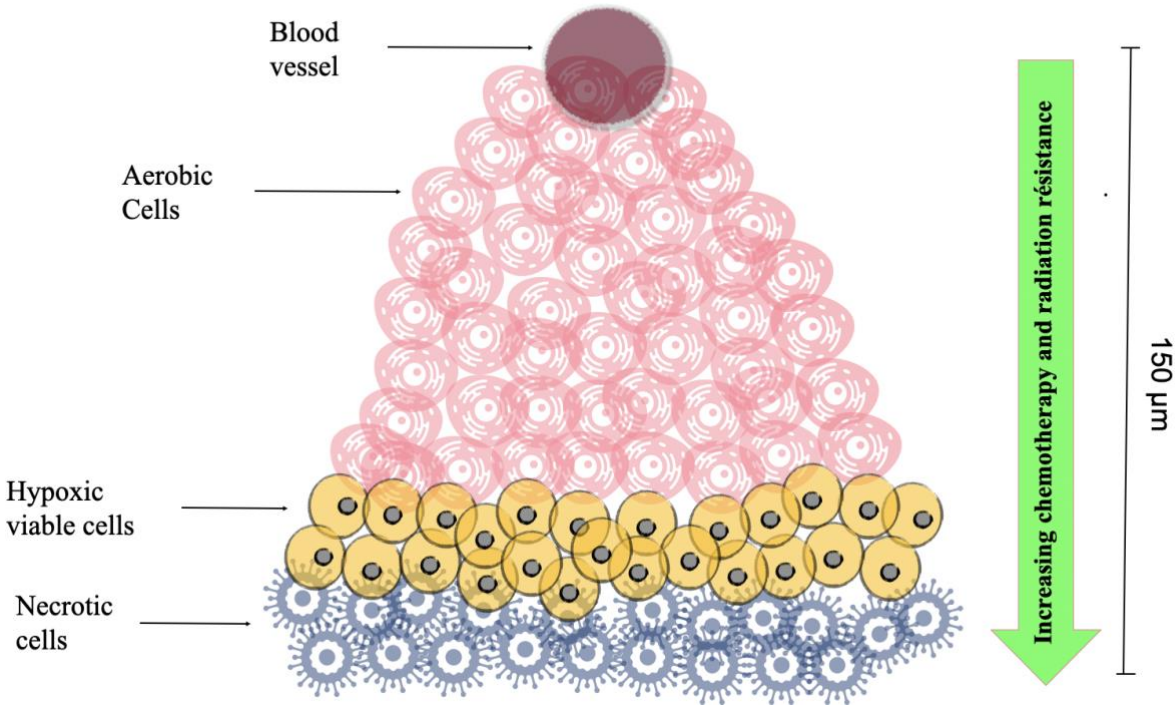

Figure 1.5: Hypoxic regions of solid tumors

Mechanistically, hypoxia shows to influence invasive and migratory behaviour of cancer cells via EMT (Epithelial to Mesenchymal Transition), a trans-differentiation of cells to acquire plastic and mobile abilities. This process alters its gene expression prior to migration. EMT is physiologically involved during embryogenesis and tissue regeneration, as well as in carcinogenesis in many forms of solid tumours and

haematological malignancies. Hypoxia-induced EMT is characterised by a decrease in epithelial-associated gene expressions, such as E-cad, β-catenin and an increase in mesenchymal-like gene expressions, such as N-cad and vimentin. The TGF-β is the master regulator and promotes EMT. EMT is also increased by hypoxia inhibiting the expression of E-cad and increasing the expression of downstream transcription factors like Smads, Snail, Slug, and Twist. Interestingly, radio and chemoresistance have also shown to be associated with EMT phenotype; expression of Snail and Slug antagonises p53-mediated apoptosis and promotes resistance to radiation and chemotherapeutic agents such as Paclitaxel and Cisplatin in ovarian cancer cells (Barbara Muz et al.,2015).

Hypoxia induces several complex intracellular signalling pathways such as the major hypoxia-inducible factor (HIF) pathway. Other hypoxia-associated pathways include PI3K/AKT/mTOR, MAPK is also known as ERK pathways, and the NFκB. These pathways include cell proliferation, survival, apoptosis, metabolism, migration, and inflammation. PI3K / AKT / mTOR, MAPK, and NF-kB signalling pathways are also activated in a hypoxia-independent manner, which could eventually contribute to the activation of HIF (Barbara Muz et al.,2015). Hypoxia-inducible factors (HIFs) are mediators of hypoxia and responsible for monitoring cellular responses to oxygen levels (Najafi et al.,2019). They play a central role in cellular mechanisms triggered in response to hypoxia (Jing et al.,2019). HIF-1α and HIF-2α support formation of blood vessels, prevent cellular differentiation, regulate apoptosis and activate DNA repairing enzymes, all of which are related to therapy resistance (Najafi et al.,2019). HIF-1α is stabilised only during the acute phase, while HIF-2α is high and stable under the chronic hypoxia (Chen et al. 2018). Despite being highly homologous, HIF-1α and HIF-2α take diverse roles in chemoresistance; this is possibly due to the diversity of

oxygen demand for activation of HIF-1α and HIF-2α, different regulation over their activation and their diverse functioning on a target gene (Najafi et al.,2019).

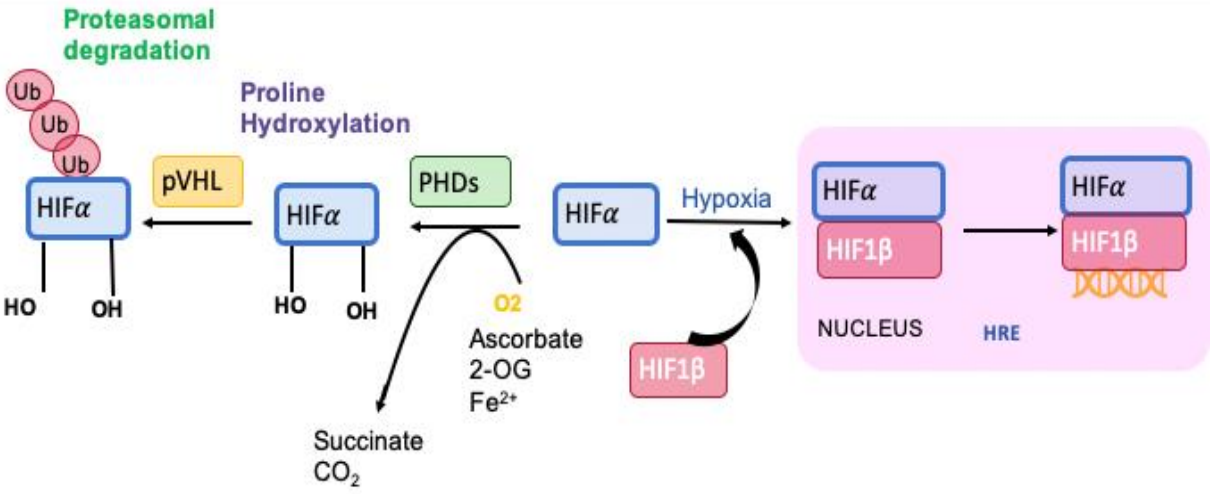

Figure 1.6: Hypoxic HIFa Stabilization and Transactivation

Under non-hypoxic conditions, HIF1-a subunits (HIF-1a or HIF-2a) undergo O2-dependent hydroxylation (-OH) catalysed by prolyl-4-hydroxylases (PHDs) that utilise 2-OG, ascorbate, and Fe2+ as co-substrates. This post-translational modification allows binding of HIF1-a to the von Hippel–Lindau (pVHL) tumour suppressor, resulting in HIF1-a ubiquitination and proteasomal degradation. Hypoxia results in inhibition of PHD activity leading to stabilisation of HIF1-a, dimerisation with HIF1-b, nuclear translocation, and transactivation of target genes by consensus hypoxia-responsive elements (HREs) (Abbreviations: 2-OG, 2-oxoglutarate; Ub, ubiquitination). In well-oxygenated cells (>5% O2), HIFa undergoes enzymatic hydroxylation at proline residues by prolyl-4-hydroxylases (PHDs) which utilise O2 as substrate and 2-oxoglutarate, Fe2+, and ascorbate as co-substrates. O2-dependent hydroxylation allows recognition of HIF1-a by the von Hippel–Lindau (pVHL) tumour suppressor, recruiting E3-ubiquitin ligases which target HIF-1a for proteasomal degradation. Hypoxia inhibited HIF-1a hydroxylation (<1% O2), resulting in HIF-1a stabilisation, dimerisation with HIF-1b, and binding to cis-acting hypoxia-responsive elements (HREs) bearing the DNA consensus sequence 50-[A/G] CGTG-30, thereby inducing target gene transcription (Schito and Rey.,2018).

HIF-1α induced genes are primarily involved in anaerobic glycolysis, angiogenesis, and apoptosis. On the other hand, HIF-2α regulates genes that promote invasion and

stemness (Saxena and Jolly.,2020). In a hypoxic environment, activated HIF-1α increases the activity of Snail and Twist, two transcription factors that reduce E-cadherin expression and promote EMT (Jing et al.,2019). Several studies demonstrated that HIF-1α and HIF-2α have a complementary action in angiogenesis: HIF-1α drives vessel growth whilst HIF-2α enhances vessel maturation (Tirpe et al.,2019). Tumour cells display an increase in glucose consumption, and for this, they make an essential metabolic switch to glycolysis; hence, the pyruvate is converted into lactate. This switch to glycolysis in tumour cells is present even in aerobic conditions and is called the Warburg effect. (Tirpe et al.,2019). This phenomenon is clinically assessed in mesotheliomas through PET/CT imaging with 2-[19F]-fluoro-2-deoxy-D-glucose (F-FDG) tracers. HIF-1a activation increases glucose transport (via GLUT-1) as well as glutamine and L-type amino acid transport (via LAT1) in pleural mesotheliomas (Nabavi et al.,2016).

Hypoxic cells within the tumour mass are distant from blood vessels, resistant to most anti-cancer drugs, and present a significant obstacle to the delivery of targeted therapies. Targeting hypoxia is a potential therapy to eradicate the progression of various cancers and enable long-term survival for patients.

4.2 Cancer stem cells

CSCs are a minor subpopulation of cancer cells located within the tumour and is another cellular source of chemoresistance. These cells have similar characteristics to non-transformed stem cells, such as the ability of self-renewal and expression of embryonic factors Oct4, Sox2 and Nanog. They can differentiate into committed tumour cells. Due to their inherent quiescent state, CSCs can evade the actions of drugs

which target rapidly proliferating cells and can limit drug toxicity due to increased expression of aldehyde dehydrogenase (ALDH), drug efflux pumps, and pro-survival proteins. Ultimately, these characteristics allow CSCs to re-populate the tumour, resulting in tumour relapse and chemoresistance (Chiodi and Mondello.,2020).

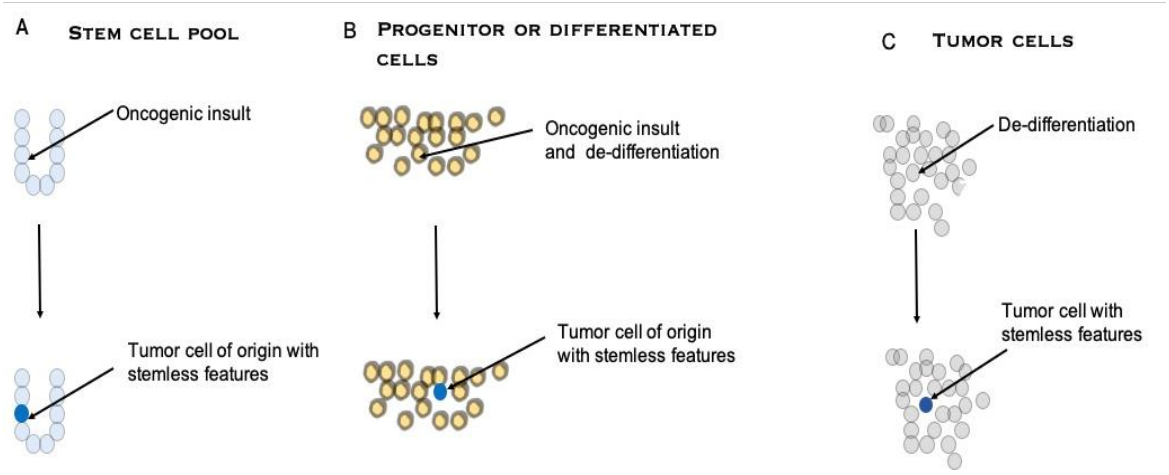

Figure 1.7: Schematic representation of CSC genesis

(A) Oncogenic insults can hit stem cells, leading to transformed stem cells, or
(B) progenitor/differentiated cells, which then acquire stemness features through de-differentiation;
(C) CSCs can be generated by de-differentiation of bulk tumour cells.

CSCs are in specific niches and determined by tumour microenvironment (TME) peculiarities that empower them to be phenotypically better adapted and more susceptible to retrieve fitness. Moreover, these niches are thought to help protect CSCs from the immune system, resist conventional treatments by reducing their proliferation state and/or evading apoptosis, and facilitate their metastatic potential (Linden and Corbet.,2019). The main factor that phenotypically differentiates CSCs from embryonic or adult stem cells is their unregulated, and primarily symmetric, cell division. It has been observed that cancer stemness is exceptionally heterogeneous.

Different pathways may be indicated to varying times in different tumour types, resulting in distinct stemness characteristics. Activation of stemness pathways was identified in cells expressing distinct CSC markers (Lathia, Liu and Matei.,2020).

As there is no clear CSC marker, one major challenge with regard to CSC is their accurate detection. However, there is some cell surface marker that seems robust enough to use them as indicators for CSC. Two of these biomarkers are CD44 and CD133. Naturally, there are more surface molecules, and usually, combinations of these markers are used to identify and isolate CSCs depending on the type of tumour that is investigated. It is important to emphasise that CSC differ between tumour entities, both phenotypically and functionally, results from one type of cancer should not translate to other types (Arnold et al.,2020).

CSCs that can form spheres maintain their stem cell properties for many passages, whereas most differentiated cells die from anoikis. The high expression of telomerase in CSCs has also helped to preserve their ability to self-renew, thus enabling cells to proliferate indefinitely and promoting CSC EMT thus retaining their stem properties (Liu et al.,2020). HIFs are related to MDR, such as ABCG2, and influence drug efficacy. VEGF is also induced by hypoxia, leading to chemo/radiotherapy resistance (Sun et al.,2019).

In tumours, hypoxia leads to a low ROS level that in turn can be protective for CSCs and lead to therapy failure. HIF's influence pathways that contribute to the quiescence of CSCs, such as cell cycle control via cyclin-dependent kinase, metabolic control via pyruvate dependent kinase, anti-apoptosis via BCL-XL, and self-renewal via OCT- 4 (Sun et al.,2019). Traditionally, CSCs prefer hypoxic conditions and the CSC niche described as hypoxic and acidic. CSCs can create spheroids in blood circulation. The

ability to form spheroids is considered a unique feature of CSC's. The study concluded that CSCs containing spheroids in the blood of cancer patients might generate a "micro-niche" that supports CSC-survival and adaptation in the bloodstream. Furthermore, CSCs up-regulate reactive oxygen species (ROS) scavengers and increase DNA-repair capabilities protecting them from the oxidative stress encountered in the blood circulation. CSCs become resistant to nutritive stress encountered in the blood circulation by increasing their capacity to produce ATP by oxidative mitochondrial metabolism. MET returns CSCs to a highly proliferative but less migratory phenotype, enabling the development of macrometastasis like the primary tumour (Steinbichler et al.,2020).

CSCs are considered to have innately higher radio-resistance, invasive capacity and metastatic capacity than their differentiated cancer cell counterparts. Complex cellular and molecular mechanisms like stemness maintenance, reactive oxygen species (ROS) production epithelial-mesenchymal transition (EMT), are indulging in the process of CSC initiation and facilitation of cancer recurrence and metastasis after treatment (Liu et al.,2020). There is new evidence emerging which indicate that some of these anti-cancerous drugs not only fail to remove CSCs but selectively enrich CSCs possibly by inducing de-differentiation or trans-differentiation (Ahmed et al.,2016).

CSCs can switch between quiescent and proliferative state. Quiescence has found to be associated with the capacity of CSCs to survive anti-cancer treatments and escape from the immune system (Chiodi and Mondello.,2020). By becoming quiescent, CSCs up-regulate enzymes (such as ALDH), and multidrug resistance pumps to increase chemotherapy elimination from the cell and the upregulation of anti-apoptotic

proteins. Given their link with tumour initiation and drug resistance, they have pushed to the forefront of cancer therapy (Cole et al.,2020).

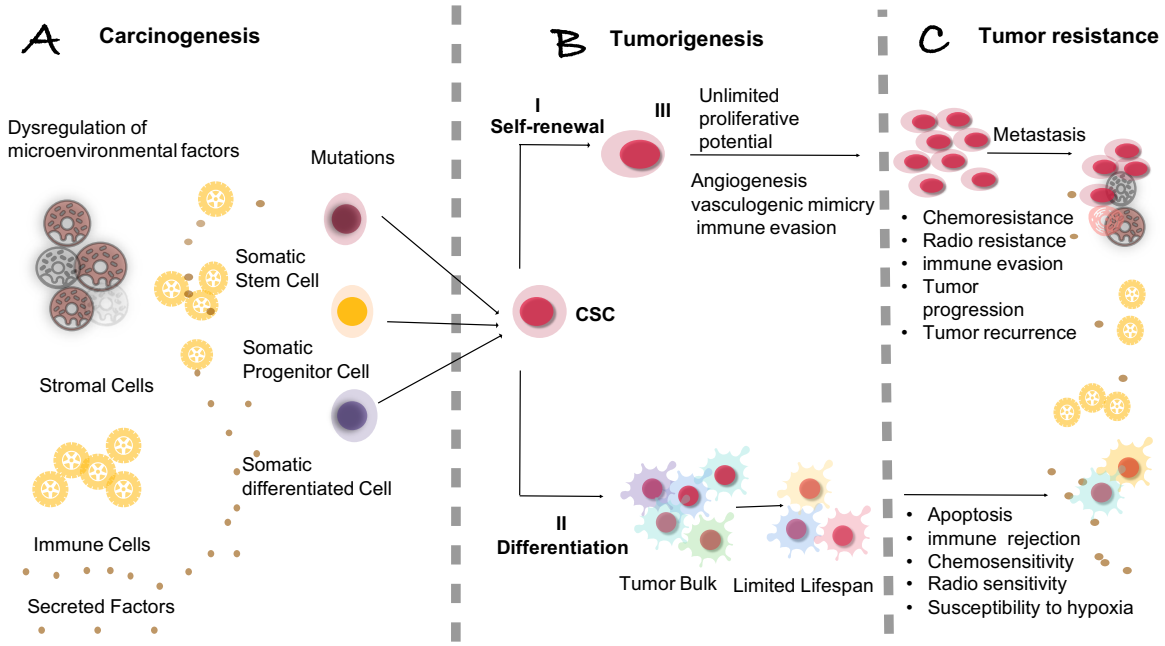

Figure 8: CSCs, carcinogenesis, tumorigenesis, and tumour resistance.

(A)Tumours can arise from somatic cells through genetic mutations of cancer-critical genes. Also, dysregulation of microenvironmental factors can contribute to the carcinogenic process. (B) Such events might primarily affect long-lived somatic stem cells, which can illustrate the cancer cell of origin, (i) their ability for long-term self-renewal, (ii) their capacity to differentiate into tumour bulk populations devoid of CSC characteristics, and (iii) their limitless potential for proliferation and tumorigenic growth. Further, CSCs in certain malignancies possess the capacity to drive tumour angiogenic responses and/or to retain in vasculogenic mimicry, potential means of promoting tumour growth. Also, immunoevasive features of CSC increase tumorigenesis and leads to tumour progression. (C) CSCs show high resistance to chemotherapeutic drugs and ionising radiation.

Resistance to chemotherapy occurs by conversion of aldehydes into weak carboxylic acids, and thereby reducing the chance of deposition for the toxic aldehydes within

CSCs. This conversion is mediated by the activity of ALDHs in CSCs. High ALDH activity is a unique feature for CSCs that distinguish them from normal stem cells. Among 19 members of ALDHs, ALDH1 considered as a CSC biomarker primarily linked to stemness and chemotherapy resistance (Najafi et al.,2019).

CSC plasticity is the main predicament in cancer targeted therapies. CSCs can sequentially transit between stem (an EMT phenotype) and non-stem (a mesenchymal-epithelial transition [MET] phenotype), and between quiescence (drug resistance) and proliferation (drug-sensitive) states. It is for the promotion of a heterogeneous population of cells within a tumour, making it hard to combat by conventional chemotherapies (Najafi et al.,2019).

There is growing evidence that CSC is also inherently resistant to radiation, by initiating DNA repair, re-distributing the cells in the cell cycle, raising activation of the DNA damage checkpoint, and re-populating and reoxygenating areas of hypoxia in the tumour (Das et al.,2020. Since they are the "seeds" of cancer, the way CSCs respond to treatment is crucial to the prognosis of tumours (Liu et al. ,2020). More attention should be focused on targeting stem cells by the use of the analogy of beehive, and the most efficient manner to destroy beehive is to target the queen bee. Likewise, the most effective way to remove a tumour would be to target the cancer stem cell, which is the queen bee.

4.3 NF-KB

The nuclear factor-κB (NF-κB) pathway plays a vital role in regulating immune and inflammatory responses. NF-kB pathway is also involved in cellular survival, proliferation, and differentiation. The process of tumour development and progression

produces cytokines, growth, angiogenic factors and proteases to activate NF-κB signalling. Inflammation has been recognised as a hallmark of cancer. However, in human cancers, direct or altered molecular mutations in NF-kB have rarely been identified. Based on recent research, NF-κB regulates several genes implicated in cell survival, proliferation, metastasis, and tumorigenesis of cancer. NF-κB activation is also directly or indirectly linked to the expression of key angiogenesis factors and adhesion molecules, such as growth-regulated oncogene and IL-8, vascular endothelial growth factor (VEGF). The NF-κB pathway has an essential connection in regulating inflammation, self-renewal, or maintenance and metastasis of CSCs (Yang et al.,2019).

The half-life of NF-kB is less than 30min, and maintenance of its activity requires ongoing protein synthesis and continuous stimuli. Thus, the high NF-kB activity in drug-resistant cells is a constitutive and intrinsic feature of the resistant cell lines (Lin et al.,2010). High NF-kB activity has been observed in drug-resistant cancer cell lines. Ectopic overexpression of NF-kB blocks apoptosis (Wang et al., 2003, 2004; Guo et al., 2010; Yip et al., 2011).

In MM different fiber types are found in various areas of the lung, where they can interrupt the phagocytosis of the mesothelial cells, which causes cytotoxicity, damaging DNA through oxidative stress and hence leads to an inflammatory response. The deposition of asbestos fibres causes the release of pro-inflammatory molecules such as HMGB-1 (High Mobility Group Box -1) and TNF-a, contributing to the carcinogenesis of asbestos (Quinna et al.,2015). HMGB-1 is the master switch that starts the inflammatory process. HMGB-1 release causes macrophage accumulation and the secretion of TNF-alpha, which in turn activates NF-kB. Activation of the NF-

kB pathway can stimulate proliferation and reduce the effectiveness of chemotherapy and ionising radiation (Bianchi et al.,2007). Thus, it leads to the survival of HM (Human Mesothelial) cells that have accumulated genetic damage because of asbestos exposure (Michele et al. .2012). HMGB1 acts as a 'master switch' which initiates and maintains the chronic inflammation and drives mesothelioma formation. Overall HMGB1 plays a crucial role in MM onset, and progression relative to the following mechanisms: (i) asbestos-induced effector as its secretion by mesothelial or immune cells is highly responsive to asbestos fibre stimulation (ii) inflammatory and epithelial-to-mesenchymal transition mediator (Abbott et al.,2020).

The in vitro studies of MM cells exposed to asbestos had cytotoxic effects. Still, these effects were negated by TNF-α, which acts by the activation of (NF-κB) translocation and activation pathway. Nuclear factor-κB increases cell survival by inducing cellular proliferation and inhibition of apoptosis. It results in favour of tumorigenesis. This study provided a mechanistic rationale to the observation by Liu et al. (1998) that asbestos did not show any pathogenesis in transgenic mice which do not express TNF-alpha receptor. On the one hand, TNF-alpha protects HM cells from asbestos-induced cell death, and on the other hand, it promotes the growth of HM that have accumulated DNA damage following asbestos exposure (Michele et al.,2012).

NF-κB consists of five different proteins (p65, RelB, c-Rel, NF-κB1, and NF-κB2). The primary physiological function of NF-κB is the p50-p65 dimer. The primary mode of NF-κB regulation takes place at the level of subcellular localisation (Yang et al.,2019). To release the NF-κB complex, signalling pathways are activated by pro-inflammatory cytokine receptors, such as IL-1 receptor (IL-1R), tumour necrosis factor receptor (TNFR) and toll-like receptor (TLR) family members(TLR3, TLR4,

TLR7); antigen receptors, such as B cell receptor (BCR) and T cell receptor (TCR); and, growth factors, like (EGFR) Epidermal growth factor receptor, family members. All these receptors can initiate the IkB kinase (IKK) complex (IKKα, IKKβ and IKKγ) NF-kB essential modulator (NEMO), which further phosphorylates and facilitates the ubiquitination of IkB and its subsequent degradation by the 26s proteasome. The dimers p65/p50, and c-Rel/p50 is then translocated into the nucleus and activate target gene expression.

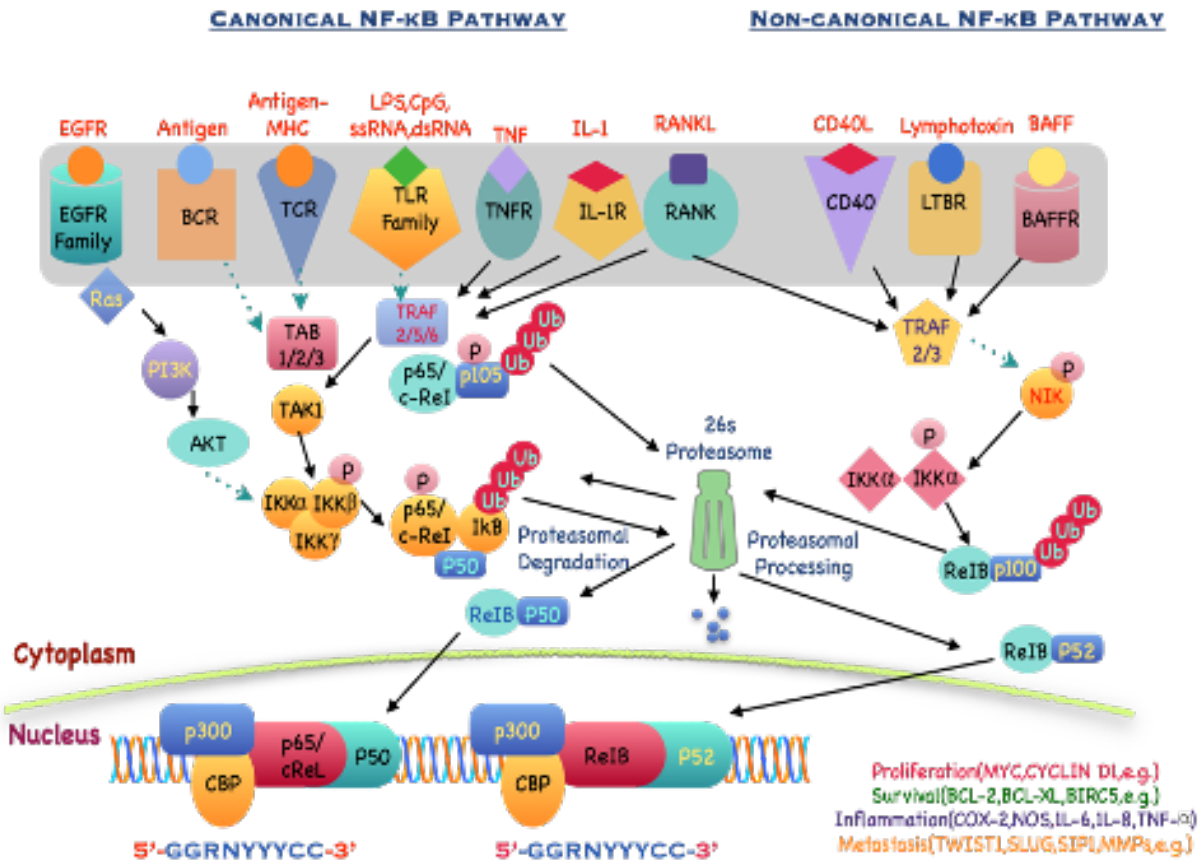

Figure 1.9: Schematic overview of canonical and non-canonical NF-κB

In the non-canonical pathway, there is no IκB, but the RelB/p100 complex is inactive in the cytoplasm. Signaling from the cluster of differentiation 40 ligands (CD40L), lymphotoxin β receptor (LTβR), and (BAFFR) B cell-activating factor receptor leads to NF-κB-inducing kinase (NIK) activation, phosphorylating the homodimer IKKα/IKKα, which further transfers the phosphate group to the C-terminal residues of p100 to be ubiquitinated and proteasomal processed into p52. It finally leads to the nuclear translocation of RelB/p52 and the induction of target gene expression (Pires et L.,2018).

The NF-κB complex attached to sequence-specific target DNA, known as κB sites in the nucleus, (5′-GGGRNYYYCC-3′, where R: purine, and N: any nucleotide and Y: pyrimidine), further which exist in promoters of the target genes, gather with the basal transcriptional machinery, and associate with other transcription factors, including AP-1 (c-Jun/c-Fos complex) and chromatin remodelling proteins, such as CREB-binding protein (CBP) and p300. Also, NF-κB can be influenced by other transcription factors that can associate physically, changing its ability to bind to the DNA and genes that will be activated. This diversity of players who can control and activate NF-kB nuclear translocation will be responsible for the different and often competing functions of NF-kB as both a pro- and an anti-inflammatory mediator (Pires et L.,2018).

NF-κB is a crucial mediator of inflammation (acute and chronic) in tumours linking inflammation with stemness. NF-κB activates hypoxia-related stemness signalling and is associated with both early (through induction of EMT) and late stage of tumorigenesis. NF-κB reverts ROS-induced apoptotic cell death in CSCs (Najafi et al.,2019). Among the broad range of NF-κB target genes and associated pathways,

epithelial-to-mesenchymal transition (EMT) is one of the most well-known ones in regulating CSC-functionality. Here, NF-κB regulates transcription of SNAIL, Slug, ZEB1, ZEB2, and Twist, which repress the epithelial phenotype and are directly associated with cancer invasiveness and aggressiveness as well as poor patient survival.

NF-κB also regulates expression of Matrix metalloprotease MMP-2 and MMP-9, as well as vimentin. Particularly Vimentin-positive CSCs seem to represent the end-stage progression of EMT, concomitant with a completely dedifferentiated state, which is highly proliferative and invasive. In line with these observations, EMT shows to generate cells with properties of stem cells from human mammary epithelial cells. Stem-like cells have shown increased expression of stem cell markers, sphere formation ability, and more efficient capability for tumour formation (Kaltschmidt et al.,2019).

4.3.1 Hypoxia - CSC- NF-kB

Hypoxia functions to increase CSC number and helps maintaining their stem-like state allowing the subsequent growth and metastasis and hence considered as a critical physiological component of CSC niche (Yadav and Desai.,2019). Hypoxia-induced HIF overexpression and NF-kB pathway activation is responsible for chemoresistance and also determines the factors responsible for maintaining the stemness in CSCs (Conley et al., 2012). Increasing evidence suggests intracellular signalling pathways mediated by NF-κB to be of particular importance for CSC characteristics and functionality (Kaltschmidt et al.,2019). Studies have also demonstrated that CSCs drive cancer cell proliferation, aggressiveness, and recurrence through the activation

of specific signalling pathways, such as the Notch, Hedgehog, Wingless (WNT) and NF-kB circuits (Castagnoli et al.,2020). NF-κB activates hypoxia-related stemness signalling and is associated with both early (through induction of EMT) and late stage of tumorigenesis (Najafi et al.,2019). Together with the ability to neutralise ROS more efficiently, CSCs are, more resistant to radiation treatment. NF-kB is essential for CSCs to withstand stress exerted by ROS (Schulz et al.,2019). NF-κB also reverts ROS-induced apoptotic cell death in CSCs (Najafi et al.,2019).

HIFs also regulates the stemness of CSCs. Previous studies have shown that HIF-1 alpha and HIF-2 alpha need to be activated by CSCs to maintain their self-sustainability under hypoxic conditions and achieve pluripotency by up-regulation of Sox2 and Oct4 genes. HIF-1α manages the proliferation and fate of CSCs in medulloblastoma and glioblastoma multiforme and activates the NF-κB pathway to nurture CSC survival and tumorigenesis. HIF-2α retains the survival and phenotype of CSCs (Yang et al.,2019). In tumours, hypoxia leads to a low ROS level that in turn, can be protective for CSCs and lead to therapy failure (Sun et al.,2019). HIF-1α maintains the CSC niche and directly modulate the CSC population. It also protects CSCs from DNA damage and enhances stemness by slowing down cell cycle progression by acting as an antagonist to c-Myc activation (Yadav and Desai.,2019).

5.0 Drug Repurposing and Disulfiram

5.1 Drug repurposing

Drug repurposing, repositioning, re-profiling, or re-directing defines the process of identifying a novel application of already approved drugs. Drug repurposing can

surpass several challenges associated with de-novo drug discovery. The traditional drug discovery involves a cost of ~2.5 billion US dollars, which represents a loss of about 85 % as compared to drug repositioning which costs ~ 300 million US dollars (Kaushik et al.,2020). Moreover, searching for specific molecules for a novel drug target may be perceived as unrealistically slow, especially during emerging disease outbreaks (Dinic et al.,2020). Drug repurposing is dependent on two major approaches: 1) Activity-based reporting, where drugs are assessed in cancer models in vitro and in vivo 2) In silico drug repurposing, where the drug interactions and their molecular targets are modelled in silicon by the use of bioinformatics tools and public databases. By the usage of these approaches, several drugs showed potent anti-cancerous effects and successfully repurposed to target specific pathways (Boyer et al.,2018). Strategising drug repurposing involves three significant steps before taking the drug across the development pipeline: recognition of the right drug, i.e. hypothesis generation; systematic evaluation of the drug effect in clinical models; and estimation of usefulness in phase II clinical trials—these steps are accomplished by various computational and experimental approaches (Kirtonia et al.,2020). For example, in tumours such as breast cancer, genomics-based tools have been used to identify Food and Drug Administration (FDA)-approved drugs and repurpose them to treat patients through targeting CSCs within the tumour. Also, data-driven computational methods were utilised in glioblastoma multiforme (GBM) to identify compounds and drugs that repositioned to inhibit GBM CSCs (Bahamad et al.,2020).

Drug repositioning arises from the exploitation of the promiscuity of small molecule drugs, i.e., the ability to disturb two or more independent proteins causing undesired side effects. The growing appreciation of network pharmacology as the next drug discovery paradigm encourages scientists to understand better and make use of such

polypharmacological effects of promiscuous compounds (Chaudhari et al., 2017). Polypharmacological effects offer significant advantages for finding novel therapeutics, particularly for the treatment of complex and multifactorial diseases such as cancer (Dinic et al.,2020). Repurposing can be on-target, i.e. validation of already identified drug target for its potential anti-cancer activity or off-target effects that identifies novel molecular targets for already FDA approved drugs. Several clinical and non-clinical studies have revealed that among 200 off target drugs, 50 % of drugs have efficacy against Cancer (Kaushik et al.,2020).

Moreover, once the cancer target has been identified and validated for a repositioned drug, and pharmacokinetic data from the literature, indicate that the in vitro antitumor activity of the candidate drug is pharmacologically achievable, proceeding to clinical trials can be faster as there is knowledge on safety and toxicity, including rare adverse events. Also, there is an extensive clinical experience derived from its original indication. Most importantly, repurposing candidates usually are of low cost, particularly those who are generic and have multiple manufacturers. Finally, drug candidates have widespread availability if they are included in the WHO Essentials Medicine list (Gonzalez-Fierro et al.,2019).

The majority of the biochemical and clinical proprieties such as bioavailability and safety profiles, proven formulation and manufacturing routes, and reasonably characterised pharmacology, are known for most approved molecules which favour the inclusion of these repositioned drugs in clinical phases more rapidly and at a lower cost than novel therapeutic agents. For rare diseases such as MM that are understudied at the preclinical and clinical levels, the development of new compounds is problematic. It needs worldwide collaboration from numerous clinical trial centres to

achieve a successful outcome from innovative drugs. Drug repositioning may be an attractive strategy for diseases such as MM, by offering a reduced timeframe from preclinical research to the bedside. Furthermore, with the expected increase in the incidence of MM in developing countries, drug repositioning could provide solutions for patients living in these countries. Repositioning may apply to a wide variety of drugs and perform in a variety of ways. Recent research used the DRUGSURV database to target individual genes/proteins that identified as important for mesothelioma based on computational modelling of TP53 and stratified patient data (Guazzeli et al.,2020).

5.2 Disulfiram

Disulfiram is the oxidised form of two diethyldithiocarbamate molecules, linked together by a central disulphide bond. It has a molecular weight of 296.4 Da and consists of sulfhydryl group, thiuram structure and the ethyl groups. (Papaioannou et al., 2014). The earliest clinical evidence that showed DS has anti-cancer activity traced back to the 1970s. It reported that DS could induce apoptosis, reduce angiogenesis, and show metal ion-dependent antineoplastic activity. These findings attracted significant interest (McMahon Chen, and Li.,2020). DS is an established FDA-approved agent to treat alcoholism dependent on its activity to inhibit acetaldehyde dehydrogenase (ALDH) for decades (Ren et al.,2020). In vivo, DS is rapidly metabolised to diethyldithiocarbamate (DDTC), which further gets converted to S-methyl-N, N-diethyldithiocarbamate (DETC) and S-methyl-N, N-diethyldithiocarbamate (Me-DDTC). Subsequent P450-catalyzed oxidation of DETC and Me-DDTC produces DETC-sulfoxide (DETC-SO) and S-methyl-N, N-

diethyldithiocarbamate-sulfoxide (Me-DTC-SO) and sulfone (Me-DTC-SO2), metabolites that are most likely involved directly in ALDH inhibition. Importantly, when a chemical P450 inhibitor blocks downstream steps of DS metabolism, liver ALDH remains uninhibited, thus unambiguously proving that metabolites of DS are genuine inhibitors of ALDH in vivo. Even though this knowledge is published and accepted in some research fields, most cancer-focused studies regard DS as a direct ALDH inhibitor (Skrott et al.,2019).

DS is widely researched due to its relatively good safety profile and reasonable financial cost (Li et al., 2015). In the conclusion of high-throughput cell-based drug screening, Disulfiram is found to be an anti-cancer drug as it shows reducing tumour growth (Turanli et al., 2018). Prolonged treatment with this drug has negligible side effects and thus considered safe by the FDA (Rae et al., 2013). Disulfiram is postulated to form carbamate complex with Cupric ions, resulting in the inhibition of proteasome activity, activation of apoptosis leading to cell death (Georgewill et al.,2014).

DS is a member of the dithiocarbamate family comprising a broad class of molecules possessing an R1R2NC(S)SR3 functional group, which gives them the ability to complex metals and react with sulfhydryl groups (Li et al., 2015). It can respond with redox-sensitive sulfhydryl groups (thiols) and bind Copper (Cu), an essential cofactor for key cellular enzymes (e.g. cytochrome c oxidase and superoxide dismutase 1 (SOD1)) involved in oxidative stress response. Notably, DS is a redox modulator whose induction of ROS is enhanced by the addition of Cu, and it has reported to inhibit the activity of NF-kB (Allensworth et al., 2015).

The anti-cancerous activity of Disulfiram is dependent on Copper (Cu). DS quickly gets reduced to diethyldithiocarbamate (DDC), a potent chelator of Copper (II). The

biological activity of Disulfiram is dependent on binding divalent cations and thus disrupting processes dependent on these metals, particularly Copper and Zinc. Disulfiram treatment removes essential Copper and Zinc ions from the enzymes which regulate the extracellular matrix degradation and metabolism of oxygen, leading to cancer suppression, cancer invasion and angiogenesis in vitro and in vivo. Current literature of DS focuses on its capacity to bind copper ions by metal-binding regions in its structure (Wiggins et al., 2015).

Suggested mechanisms for DS toxicity include inhibition of proteasome activity, G2/M cell cycle arrest, induction of apoptosis, inhibition of Nrf2 expression, inhibition of TGF-beta induced EMT transitions, and inhibition of the p97-NPL4 pathway (Hubert et al.,2020). Moreover, DS shows high toxicity to CSCs in a copper (Cu)-dependent manner (Li et al., 2015). Also, DS as cancer therapeutic is well tolerated, with few toxicities at blood levels of 1.3 μM. Clinical trials in cancer patients suggest that dosing up to 500 mg is possible and well-tolerated in combination with chemotherapy (Hubert et al.,2020).

5.2.1 Disulfiram toxicity is copper dependent

Cellular Copper in excess causes cytotoxicity and damages different types of biomolecules by mediating generation of highly reactive hydroxyl radicals. There is growing evidence that Copper plays a vital role in inflammation and the growth of tumours (Li et al., 2015). Copper plays an essential role in inflammation and the growth of tumours. Copper can stimulate the proliferation and migration of endothelial cells at high concentrations (Li et al., 2017). Copper has a long history for treating

cancer, but intracellular transport is still a significant hurdle for its clinical efficacy (Li et al., 2015).

Since Copper is required for DS cytotoxicity and DS acts as a copper ionophore, the intracellular deposition of Copper can be cytotoxic through the generation of oxidative stress, resulting from Fenton reactions or enzymatic inhibition due to copper binding to peptide bonds. Further, Copper complexes tend to intercalate between the base pairs of DNAs due to their planar conformation (Tesson et al., 2017).

As Copper is a bivalent metal ion chelator, DS forms a complex with Cu (DS/Cu) which is more readily taken up by cells. Also, DS and its metabolite diethyldithiocarbamate (DDC) inhibit superoxide dismutase (SOD) by Cu chelation. By shifting the thiol redox balance, both DS and DDC may also induce oxidative stress. Cellular thiol pools have proven to be important in regulating redox status of the cells, resulting in a sizeable antioxidant pool which consists of free thiols, thiols bound to proteins and thiols bound to disulfide bonds (Wu et al., 2018).

This Cu (DDC)2 complex is believed to play a significant role in DSF-based cancer therapy. A stated above the anti-cancer efficacy of DS is copper ion dependent. Since many cancers have higher levels of Copper ions than normal tissues, it is hypothesised that DS could form relatively higher levels of Cu (DDC)2 in cancer and selectively kill cancer cells (McMahon, Chen, and Li.,2020). Cu-DDC is damaging to lung cancer cells by targeting CSC-like cells. It was observed that along with the thiol groups, thiuram structure is also essential for the anti-cancer activity of DS and DDC (Butcher et al., 2018). Studies indicated that Cu (DDC)2 killed cancer cells through the induction of paraptosis. Paraptosis is a non-apoptotic cell death that does not need the activation of caspases. Therefore, it is a promising approach to kill resistant cancer

cells with defective apoptotic pathways. Besides, DS or DS/Cu could effectively overcome drug resistance caused by multiple other mechanisms, including cancer stem cells (CSCs) and over-expression of drug-resistant transporters (McMahon Chen and Li.,2020). DDC-Cu is more cytotoxic than Ds/Cu as the IC50 for Ds/Cu is 449 nM, and IC50 for DDC-Cu shown to be 238.7 nM, $p < 0.01$). It indicates that the final product of DS/Cu might play an essential role in DS/Cu induced cell death (Tawari et al., 2015).

Cells treated with Cu (DDC)2 showed similar phenotypic characteristics as those treated with proteasome inhibitors, including the accumulation of poly-ubiquitinated proteins in the cytoplasm. Because of these observations, early studies believed that DS was a proteasome inhibitor. Recent studies revealed that Cu (DDC)2 did not directly inhibit proteasome but instead targeted the p97-NPL4-UFDI pathway. The binding of Cu (DDC)2 to the zinc (II) binding thiolate site present in NPL4 proteins resulted in the aggregation of NPL4. The aggregation of NPL4 caused the deactivation of P97 segregase, which caused the accumulation of misfolded proteins in the endoplasmic reticulum (ER) and eventually cell death (McMahon Chen, and Li.,2020).

Cu (II) interacts directly with various molecules and promotes their oxidation in redox reaction leading to the formation of Cu (I). This Cu (I) further reacts with molecular oxygen and generates superoxide anion O2, which disputes to O2 and H2O2, producing hydroxyl radicals and other reactive oxygen species (ROS). ROS causes oxidative damage to DNA and is accountable for clastogenic property of Copper, resulting in cell death. Although the half-life of ROS is merely 10−9 s (HO•) to 1 ms (H2O2) But when equal molar of Disulfiram and Copper is mixed, the reaction is

triggered immediately and completed in 150 minutes. The study suggests that the cytotoxicity from Ds/Cu is due to the following actions: (1) Disulfiram and Copper reaction-generated ROS (2) toxic effect of DDC-Cu. The chelation of DS with Cu is indispensable for both two actions. (Tawari et al., 2015).

The observation by Rae et al., 2013, have suggested that apart from the presence of Copper, the concentration of Copper relative to Disulfiram is also a significant determinant of the cytotoxicity of Disulfiram. The equimolar level of Copper and DS resulted in a maximum clonogenic kill. Presence of surplus DS resulted in the competition amongst DS/Cu and free DS complexes for cellular uptake or intracellular binding. This competition explains the increased survival, observed after increasing the concentration of Copper beyond DS (Rae et al., 2013).

Recently, DTC copper complex CuET was detected by Skrott et al. in DS treated cell cultures. It is a complex that spontaneously develops in vivo and cell cultures and is present in tumour counterparts at higher concentrations than the corresponding natural liver and brain tissues of CuET is enhanced in humans undergoing DS treatment for alcoholism. They showed that Copper anion supplementation allowed its development, exerting a further deteriorating effect on cancer cells, precisely at the stage when DS is introduced.

The copper transporter, Ctr1 regulate the transport of Cu into cells. To maintain redox homoeostasis, intracellular Cu levels are strictly controlled. As a strong bivalent metal ion chelator, DS and its derivative, N, N-diethyldithiocarbamate (deDTC), can form a complex [Cu(deDTC)2] with Copper. This DS/Cu complex can transport Cu into cancer cells in a Ctr1 independent manner, thus overcoming the transporter-controlled regulation of intracellular Cu homoeostasis (Liu et al., 2012).

Disulfiram and Copper also target cells by simultaneous modulation of ROS and NF-KB (Peng Liu et al.,2014). Moreover, it has been found that the induction of apoptosis mediates the anti-cancer effect of DS/Cu. It also is seen that DS/Cu induces autophagy, which impedes DS/Cu-induced apoptosis. Cancer cells contain a high level of Cu in vivo. However, it is reported that Cultured cancer cells possess low to trace levels of Cu (Wu et al., 2018). Addition of Cu to DS was needed for CSC targeting and induction of cancer cell apoptosis in vitro. However, exogenous Cu may not be required for DS to work in vivo. Therefore, elevated Cu serves as a specific cancer target for Cu-chelating agents, such as DS (Cong et al., 2017). In comparison with Cu, the DS/Cu complex is a more potent ROS inducer. Reactive oxygen species even have a crucial role in signalling transduction in cancer cells. Considering the higher ROS load in cancer cells, it has been proposed that further ROS exposure induced by ROS-generating agents will exhaust their cellular antioxidant capacity and selectively lead cancer cells into apoptosis (Liu et al., 2012).

5.2.2 Mechanism of action of Disulfiram by Targeting NF-KB pathway

An essential mechanism of DS-induced cell death involves proteasome inhibition. Proteasome activity was elevated in cancer cells. DS inhibits proteasome activity and induces selective apoptosis in the cancer cells and spare normal healthy cells. The copper-binding ability of DS can also be responsible for this action as the formation of Copper complexes tend to be accountable for pro-apoptotic proteasome inhibition (Rae et al., 2013). Proteasome inhibition in cancer cells leads to accumulation of pro-apoptotic target proteins and induction of cell death (Owunari et al.,2014). NF-kB is a protein complex found in most animal cells. Activated NF-kB can induce a large

number of anti- apoptosis-related genes, thereby inducing drug resistance and rendering cells insensitive to chemotherapeutic drugs. Thus, NF-kB is considered one of the major drug resistance-related anti-apoptotic factors. Notably, DS/Cu combined with chemical drugs, can not only inhibit NF-kB activity but also enhance the cytotoxicity of an anti-cancer drug (Li et al.,2020).

Chemotherapeutic agents and radiation activate NF-κB, and both constitutive and therapy-induced NF-κB activation is generally anti-apoptotic. Blocking NF-κB has been tested and found to sensitise cancer cells to radiotherapy and a variety of chemotherapeutics in numerous tumour cell types. As discussed above, the induction of anti-apoptotic factors is one of the primary mechanisms involving NF-κB in cancer cell resistance to therapy (Lin et al.,2010). Dithiocarbamates are widely used as inhibitors of canonical NF-kB pathway both in vitro and in vivo despite their lack of specificity. Since the beginning of this research in the early 1990s, it has suggested that dithiocarbamates can block the release and degradation of IkB. A popular explanation that persists is that the dithiocarbamate effect NF-kB pathway through oxidative stress attenuation. The canonical NF-kB pathway is (in a cell-free system) blocked by dithiocarbamates via E3 ubiquitin ligase inhibition, and this ligase depends on CSN5 (COP9 signalosome subunit 5) also known as Jab1 (Jun activating binding protein 1). CSN5 and the key proteasome subunit Poh1/Rpn11 both have the JAMM domain, the active site sensitive to both metals and ligands (1,10-phenanthroline). Taking all these into consideration, dithiocarbamates would seem to be primarily proteasome inhibitors, and their ability to inhibit NF-kB inhibition is secondary (cvek et al.,2008).

DS regulates NF-kB and mitogen-activated protein kinase (MAPK) signalling pathways, leading to the death of various types of the cancer cell. Activation of NF-kB signalling associated with the epithelial-mesenchymal transformation (EMT) and tumorigenesis. Ying et al. confirmed that DS could potently inhibit osteoclast differentiation by attenuating NF-kB activity in vitro. Chiba et al. found that 90 % of cells showed an increase in phosphorylated p38 level when tumour-initiating hepatocellular carcinoma (HCC) treated with DS. It indicates that p38 MAPK activated in HCC cells, and DS inhibits tumour-initiating HCC cells in a p38-dependent manner. Therefore, DS could exert antitumor effects in part by downregulating the NF-kB and MAPK signalling pathways (Li et al.,2020).

Zeng et al. found that both the Wnt and NF-kB pathways, which are involved in cancer cell proliferation, apoptosis, and progression, were inhibited by Disulfiram (Zhang et al.,2020). Further, DS generates oxidative stress through the inhibition of NF-κB activation and inhibition of superoxide dismutase (SOD) and because of its induction of an increased ratio of oxidised glutathione to its reduced form (Tesson et al., 2017). DS/Cu inhibits both NF-kB and TGF-b signalling, including the nuclear translocation of NF-kB subunits and the expression of Smad4, leading to down-regulation of Snail and Slug, which contributed to phenotype epithelial-mesenchymal transition (EMT). In the field of metastasis, studies showed that DS inhibits invasion of both tumour cells and endothelial cells at non-toxic concentrations by inhibiting MMP-2 and MMP-9 activity (Li et al., 2017).

5.2.3 PLGA - Disulfiram

In many other clinical studies, DS was used in combination with Copper which can

Increase the intratumor Copper concentrations and generate higher levels of Cu (DDC)2 to kill cancer cells more effectively. In most of these clinical trials, the oral administration of DS yields low concentrations of Cu (DDC)2 in tumour regions because DS has low bioavailability and it is rapidly metabolised and degraded in the body (McMahon Chen, and Li.,2020).

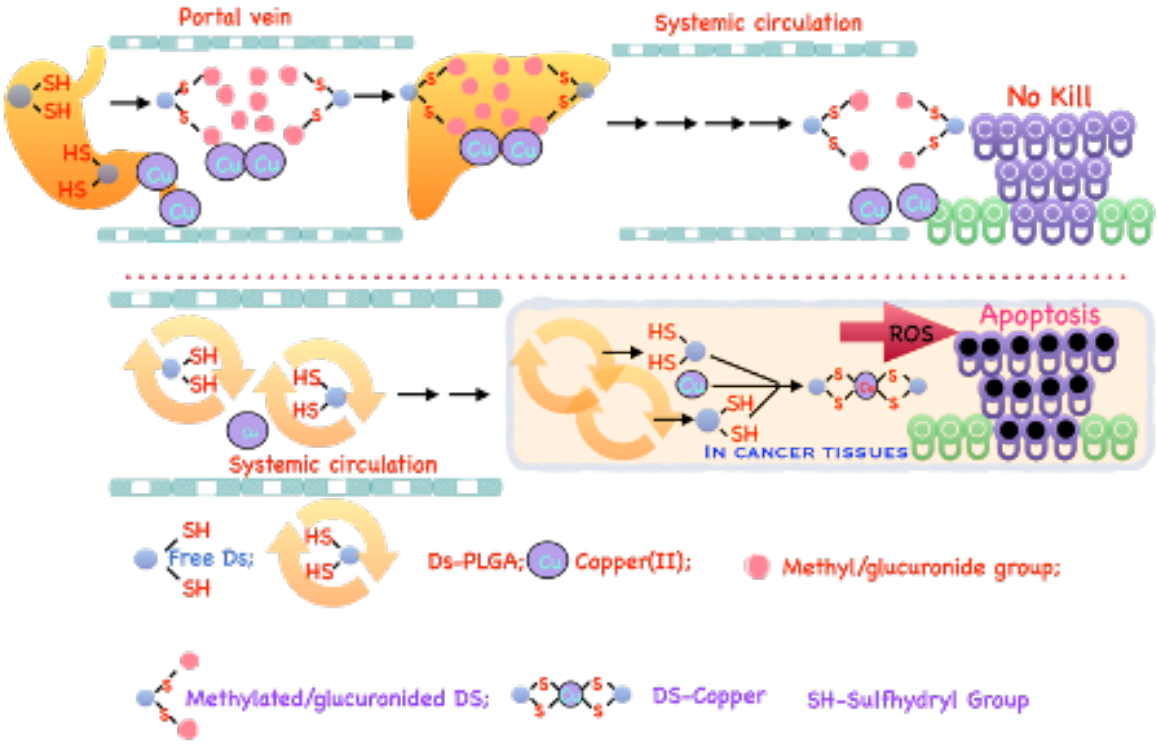

Figure 1.10. Comparison between the action of free Disulfiram and PLGA - coated Disulfiram on tumor cells

The underlying reason is that DS is instantly reduced to DDC in the bloodstream *in vivo*, which is also very unstable and promptly gets converted into the irreversible downstream metabolites, e.g., DDC-glucuronide, methylated DDC and other degraded

products. Thus, the functional group, i.e. sulfhydryl group of DDC is destroyed, making DDC lose its chelating ability (Tawari et al., 2015). The half-life of DS pH 7.4 is 1-1.5 minutes. It may introduce the discrepancy between the anti-cancer activities in vitro, in vivo and the clinic (Wang et al.,2017).

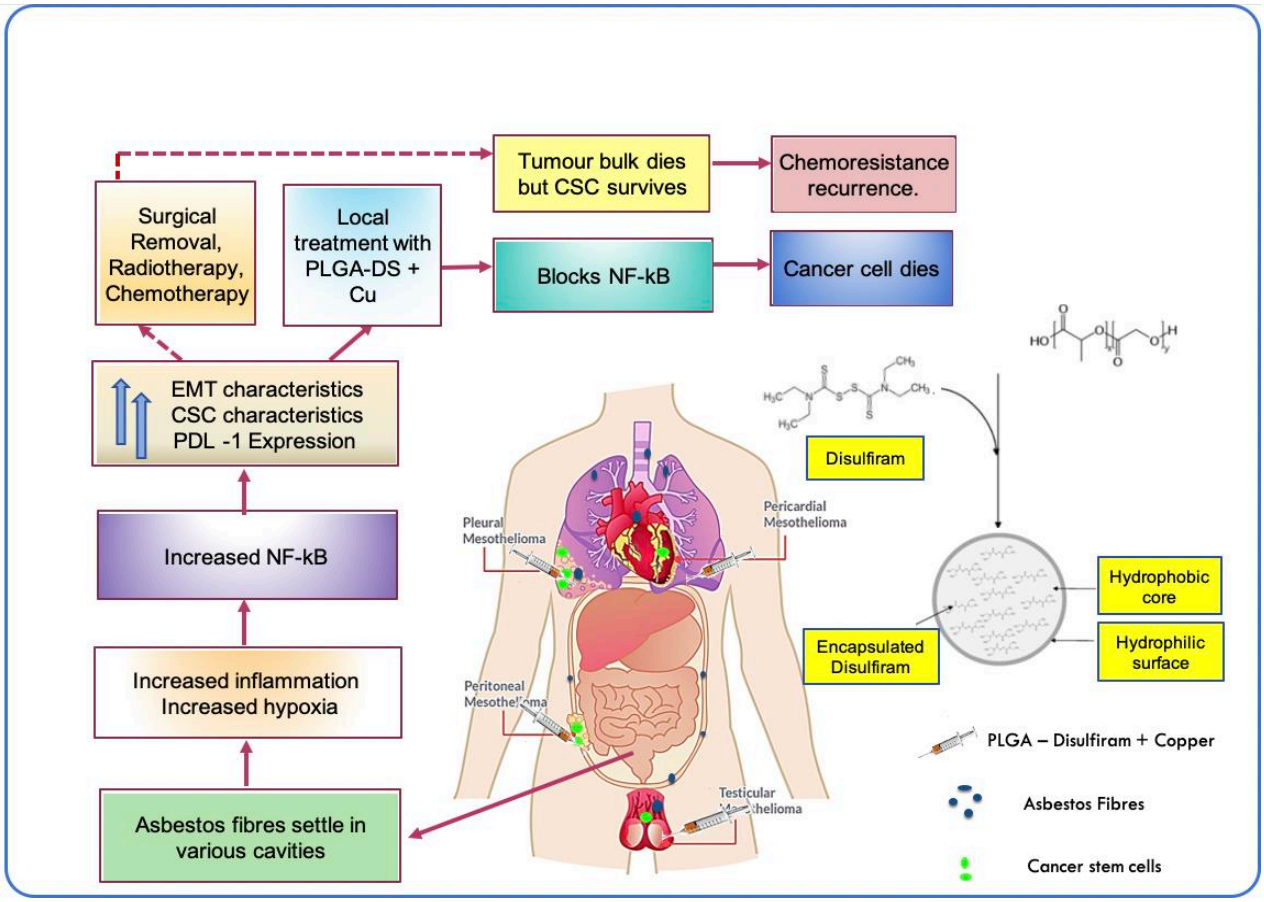

Figure 1.11 Proposed model for treating Mesothelioma by PLGA-coated Disulfiram + Copper by local injection.

Therefore, advanced delivery systems are much needed for DS-based cancer therapy. Delivery systems should have the promise to enhance intratumor drug delivery,

improve anti-cancer potency and reduce toxicity. Nanomedicine can protect and deliver drugs in the bloodstream. Porous microparticles based on polymers are useful for the pulmonary administration due to its unique properties such as low density, adaptive aerodynamic diameter, and favourable lung deposition. PLGA, which is a biodegradable polymer, has been widely used as constructing porous-microparticle to deliver many types of drugs to lungs, such as proteins and plasmid DNA. (Wang et al.,2017).

Thus, in vivo anti-cancer efficacy of DS can be improved by liposomal encapsulation (half-life~25 min). Therefore, our group prepared porous PLGA microparticle, through the emulsion solvent evaporation method, where ammonium carbonate was used as a porogen. PLGA encapsulation has improved DS half-life. In serum, from less than 2 minutes to 7 hours. DS-PLGA, in conjunction with Copper, was significantly inhibited by cancer stem cells population in the liver. Therefore, nanomedicine may be a novel strategy for protection of the sulfhydryl group in DS and translation of DS into cancer treatment (Wang et al.,2017).

Since mesothelioma is known to metastasize rarely, we propose a local treatment by injecting PLGA-Disulfiram and Copper to the affected sites. The anti-cancerous properties of PLGA Microparticles were evaluated on mesothelioma cell lines MSTO and JU77.

Aims: I aim to determine the effect of microparticles encapsulated Disulfiram on malignant mesothelioma cells. The success of my project will lead to future animal study and potentially clinical trials.

Objectives : My study intends to elucidate the following phenomena.

1. Hypoxia induces chemoresistance and invasiveness in MM cell lines

2. Hypoxia induces cancer stem cell and invasiveness-related markers in malignant Mesothelioma cell lines

3. PLGA-DS and Copper targeted MM CSCs, reversed chemoresistance and blocked MM cell invasiveness in vitro

4. The status of NF-kB activity on drug sensitivity and invasiveness in MM cell lines.

CHAPTER 2

Materials and Methods

2.1 Materials

2.1.1. Mesothelioma cell lines

The MM cell lines MSTO-211H and JU77 were very kindly provided by Professor Peter Sziosarek from the Queen Mary University of London.

2.1.2. Reagents, Enzymes and Kits

- copper chloride (CuCl2), poly-2-hydroxyethyl methacrylate (Poly-HEMA), insulin, D-Glucose, human EGF, heparin, LB Broth, sodium chloride, trizma base, hydrogen peroxide, methanol, 100% ethanol, 99.9% dimethyl sulfoxide (DMSO), tween 20, tetramethyl ethylenediamine (TEMED), DL-dithiothreitol solution (DTT), fixative, developer, crystal violet solution, propidium iodide (powder), agarose, tris HCl, SDS, Triton X-100, sodium deoxycholate, NaCl, 5% glycerol (Sigma, Dorset, UK)

- Dulbecco's Modified Eagle's Medium (DMEM), Dulbecco's Modified Eagle's Medium/nutrient mixture F12 (DMEM-F12), L-Glutamine, Penicillin-Streptomycin, Amphotericin B Mix (Lonza, Basel, Switzerland)

- RPMI-1640, Trypsin-EDTA (10x), Sterile phosphate buffer saline (PBS) - Biowhittaker®, USA

- Fetal Bovine Serum (FBS) - Hyclone®, USA

- B-27 Supplement, DNase/RNase free water (Gibco, Thermo fisher scientific Inc, UK)

- 99.9% Dimethyl sulfoxide (DMSO), N, N,N′,N′-Tetramethyl ethylenediamine - Sigma®, UK
- 99.7% Dimethyl sulfoxide (DMSO)- Fisher bioreagents, UK
- RL buffer, wash solution A – Norgen Biotek Corporation, Canada
- Vector shield (Vector Laboratories Inc, Burlingame, CA)
- Reverse Transcription kit (Applied Biosystems, CA, USA)
- Total RNA purification kit (Norgen Biotek Corp, Ontario, Canada)
- Hypoxyprobe Kit (Hypoxyprobe, Massachusetts, USA)
- ActinRed^{TM}, Lipofectamine^{TM} 2000 Reagent, S.O.C. Medium, DH5 competent *E. coli* bacterial cells (Invitrogen, Thermo fisher scientific Inc, UK)
- Image-it Fix-Perm kit (Molecular probes by life technologies, Massachusetts, USA)
- QuantiPro™ BCA Assay Kit (BIO-RAD, Hertfordshire, UK)
- EZ-ECL chemiluminescence detection kit for horse radish peroxidases solution A and B - (Thermo Fisher Scientific Inc., UK)
- AccuGel 19:1 40%(w/v) 19:1 Acrylamide: Bis-Acrylamide Solution, 4X ProtoGel Resolving Buffer (1.5M Tris-HCl, 0.4% SDS, pH 8.8), ProtoGel Stacking Buffer (0.5 Tris-HCl, 0.4% SDS, pH 6.8), Pre-stained Blue Protein Ladder (Gene Flow, Lichfield, UK)
- Matrigel (BD biosciences).

- Crystal violet solution, Contains 2.3% certified crystal violet, 0.1% ammonium oxalate and 20% ethyl alcohol, (Sigma – Aldrich)

- PLGA-DS stock solution (1mM) was prepared in H2O.

2.1.3 Antibodies

Table 2.1. Primary monoclonal antibodies used for Western blot analysis

Antibody	Reference No.	Company	Dilution in buffer
NF-kB p 65	Ab 16502	Abcam	1:1000
IKB alpha	Ab32518	Abcam	1:1000
Beta Actin	A2228	Sigma	1:5000
Tubulin	T5168	Sigma	1:5000
Vinculin	V9131	Sigma	1:5000
HIF -2 Alpha	Ab199	Abcam	1:1000

Conjugated secondary antibodies used for Western blot analysis:

ECL^{TM} Anti-Rabbit IgG Horseradish Peroxidase (HPR) linked whole antibody (from donkey), ECL^{TM} Anti-Mouse IgG HPR linked whole antibody (from sheep) (GE Healthcare, Life Sciences, Buckinghamshire, UK)

Fluorescently labelled antibodies used for flow cytometry:

FITC Mouse Anti-Human CD44, APC Mouse Anti-Human CD338 (BD Biosciences, New Jersey, USA) CD133/2 VioBrightTM FITC human (Macs Miltenyi Biotec, Surrey, UK)

2.1.4. Buffers

Phosphate Buffered Saline (PBS)

Prepared by dissolving 5 abets of PBS in 1 litre of deionised water.

Freezing Buffer

Prepared by adding 10% DMSO in FBS. Used to suspend cell lines for storage in liquid nitrogen.

Flow Buffer

Used for staining cells with antibody for flow cytometric analysis. Prepared by adding 4% FBS in PBS.

RIPA buffer

RIPA is used for whole protein extraction. Stock buffer was prepared from the following reagents detailed in **Table 2.2** to make a volume of 100 mL and pH 7.4. RIPA buffer protease and phosphatase inhibitors were added to an aliquot of 5 ml.

Chemicals	Concentration	W/100 ml
Tris Hcl	25 mM	395 mg
SDS	0.1%	0.1 g
Triton X-100	1%	1 ml
Sodium deoxycholate	0.5%	0.5 g
NaCl	0.15 M	0.88 g
EDTA	1 mM	37.2 mg
Sodium orthovanaldate	1 mM	18.4 mg
Leupetin	1µm (1-10 µm/ml)	1 mg
Aprotinin	1µm (1-10 µm/ml)	1 mg
PMSF	1µm	17.4 mg

Sorensen's glycine buffer

Prepared by dissolving 3.75 g glycine and 2.92 g NaCl in deionised water. NaOH (5 M) was used to adjust the pH to 10.5.

10× Tris-buffered saline (10×TBS)

Prepared by dissolving 12.11 g tris base and 81.8 g NaCl per 1 litre of deionised water. HCl (1 M) was used to adjust the pH to 7.4

1×Tris-buffered saline-Tween-20 (TBS-T)

Prepared by mixing 100 mL 10×TBS with 900 mL of deionised water and 500 µL of Tween-20. Used for washing membrane in Western blot technique.

Running Buffer

Used for gel electrophoresis in Western blot analysis. Prepared by mixing 100 mL of 10x stock (tris/glycine/SDS), with 900 mL of deionised water.

Transfer buffer

Prepared by mixing 200 mL methanol, with 100 mL of 10x stock (tris/glycine) and 700 mL of deionised water. Used in western blot analysis for blotting proteins onto a nitrocellulose membrane.

Blocking buffer

Prepared by dissolving 5 g of milk powder in 100 mL of TBS-T. 5% (w/v) milk in TBS-T was used to prevent non-specific binding on the nitrocellulose membrane in western blot analysis.

2.1.5. Equipment Consumables

	Primer (Thermofisher)	TaqMan Gene Expression Assays ID Assay Cat no (4331182)
1	P65	Hs01042014_m1
2	HIF1a	Hs00936371_m1
3	HIF2a	Hs01026149_m1
4	SOX2	Hs01053049_s1
5	NANOG	Hs02387400_g1
6	OCT4	Hs00999632_g1
7	MMP2	Hs01548727_m1
8	MMP7	Hs01042796_m1
9	MMP9	Hs00957562_m1
10	SNAIL 1	Hs00195591_m1
11	SNAIL 2	Hs00161904_m1
12	TWIST	Hs01675818_s1
13	ZEB 1	Hs00232783_m1
14	HPRT1	hs99999909_m1
16	E-CAD	Hs01023895_m1
17	VIM	Hs00958111_m1
18	N-CAD	Hs00983056_m1

- Microamp Optical 96-well Plate (Applied Biosystems, CA, USA)
- Sterile pipette ZAP filter tips (Alpha laboratories, Eastleigh, UK)
- Fixative procedure tray (Cell Path PLC, Newton, UK)
- Blotting papers, Amersham Hybond P 0.45 polyvinylidine difluoride (PVDF) (GE Healthcare Life Sciences, Buckinghamshire, UK)
- 0.5, 1.5 mL Eppendorf tube, 10, 25 mL serological pipette, 10, 20 50 and 100 mL tubes, 6-well, 12-well, 24-well, 96-well flat bottom tissue culture plates, T25, T75, T175 tissue culture flask, with vented caps, vacuum filter, cell scrapper (Sarstedt Ltd., Leicester, UK)
- Cryogenic vials, Black 96-well Immuno plate, EZ single Cyto funnel with white filter cards (Thermo Scientific, Massachusetts, USA)

- Polysine^{TM} (VWR International, Pennsylvania)

Scientific instruments

- Quant Studio 6 Flex (Applied Biosystems, CA, USA)
- TE70 ECL Semi-Dry Transfer Unit, Hyper cassette (Amersham, Biosciences)
- BD Accuri C6 Flow Cytometer (BD, New Jersey, USA)
- Mini protein electrophoresis chamber kit, tank with lid, gel plate gaskets, 1.5mm glass plate and 1.5mm 10 well combs, gel cutter, buffer dam, power pack (BIO- RAD, Hertfordshire, UK)
- BioMAT2 Class 2 microbiological safety cabinet (Contained Air Solutions, Manchester, UK)
- PIPETBOY (Integra, Hudson, USA)
- Evos FL Cell Imaging System (Invitrogen, California, USA)
- Multifuge 3 S-R (Heraeus, Hanau, Germany)
- Spectrafuge mini centrifuge, Micropipette for volumes: 0.1-2 µL, 0.5-10 µL, 2- 20 µL, 10-100 µL, 20-20 µL, 100-1000 µL (Labnet, New Jersey, USA)
- MP220 pH meter (Mettler Toledo, Ohio, USA)
- Eclipse TS1000 (4×, 10×, 20× lenses) (Nikon, Amsterdam)
- CO_2 Incubators, O_2/CO_2 Incubators (Panasonic, Leicestershire, UK)
- Refrigerated centrifuge sigma 6-16KS (Sigma, Dorset, UK)
- Block heater, see-saw rocker, heat-stir UC152 (Stuart, Staffordshire, UK)

- Multichannel pipette, Transfer pipette S-8

- Multidrop 384, Multiskan Ascent, Fluoroskan Ascent FL, Nanodrop 2000, Shandon Cytospin 4 (Thermo Scientific, Massachusetts, USA)

- Ultrasonic Cleaner (VWR, Pennsylvania, USA)

Cell culture inserts, transparent PET membrane 24 well 8.0µM Pore size, (Falcon).

2.2 Methods

2.2.1 Cell Culture of adherent cells

Cell lines: Two mesothelioma cell lines (MSTO-211H and JU77) were used in this study.

2.2.1.1 Media:

Serum containing medium (SCM)

RPMI media was used which consists of Fetal bovine serum 1% (v/v) L - Glutamine 1% (v/v) and antibiotics i.e. penicillin and streptomycin 1% (v/v)

Serum free medium (SFM)

It consists of L - Glutamine 1% (v/v) and antibiotics (penicillin and streptomycin) 1% (v/v).

Trypsin

Working stock i.e. 10x is prepared from 1x stock solution by diluting with sterile PBS.

Freezing medium (To store cells at -180 °C in liquid nitrogen)

The Medium was prepared by adding 10% DMSO to 90% fetal calf serum.

2.2.2 Recovering cells from liquid Nitrogen

The labelled cell lines were collected from liquid Nitrogen, quickly defrosted at 37 °C and transferred to T-75 vented flask containing 19 ml of RPMI (serum-containing medium). The cells were incubated overnight at room temperature, i.e. 37°C. It was followed by changing media the next day to ensure that the trace amounts of DMSO was removed and no unattached or dead cells remained.

2.2.3 Trypsinization of healthy adherent cells

The cells were observed for ~90% confluency under the microscope, which should also relate to the colour change of media; the cells were then ready for Subculturing. The consumed media was aspirated, followed by washing with 5 mL sterile PBS. It was further followed by addition of 2 mL trypsin from working stock, and the cells were incubated at 37 °C for approximately 10 minutes. The flask was lightly tapped from the sides to detach the cells gently. After ten minutes, it was checked for complete detachment of the cells under the microscope. The trypsin was then neutralised with 2 mL serum-containing medium. The mixture should be mixed well in the flask to break any clumps left after trypsinisation. It was then transferred to the tube and centrifuged at 1200 r.p.m for 10 minutes; the pellet was collected and again suspended into fresh medium for subculturing.

2.2.4 Maintenance of the cell lines

The number of cells in the flask determines the number of days it should be a subcultured. The cells were checked for a change in the colour of media and confluency accordingly. When the cells were ~90% confluent, they are ready for subculture. The cells are again trypsinised, collected as pellet, counted, and added accordingly to the flask.

2.2.5 Storage of cell lines in liquid nitrogen

The fully confluent flask was trypsinised, and cells centrifuged at 1200 r.p.m for 5

minutes. The used media was aspirated. The cells were then counted using cell counter, and $1x10^6$ cells were collected and released in 1 mL freezing medium. It was then aliquoted to carefully labelled cryovial mentioning details of the cell lines, date, passage number (if patient-derived). The cryovial is then wrapped in a thick layer of tissue paper and stored at -80 °C. It was followed by transfer of these vials to liquid nitrogen tank (-160 °C) to maintain long term viability of the cells. The location of the vials was updated in the liquid nitrogen logbook.

2 .2.6 Sphere Reformation

Poly-HEMA coating for sphere cell culture

- JU77 and MSTO-211H cell lines were stimulated to form spheres by using nutrient-rich media DMEM F12 supplemented with growth factors by using coated flask and plates with low adherence. These plates were prepared by using Poly-HEMA (poly-2-hydroxyethyl methacrylate) 10mg/mL mixed with 95% ethanol. The solution was sterilised using the filter and stored at 4°C. The following volumes used for coating the flasks/plates:

- 2 ml for T 25
- 0.4 ml/well for six wells

The coated flasks kept in the incubator at 50- 60 °C to form a coating of dried polyhema on the bottom of the flask. Before using, the flasks were washed twice thoroughly with 2ml PBS for T-25 and 500 ul for six-well plates.

Growing sphere cells

MSTO-211H and JU77 cell lines were trypsinised from T-75 cultured flask, and cells were counted using a cell counter. For sphere cells culture, 0.5x106 cells were grown in selective stem cell media with all the growth factors. The cells were grown in ploy-HEMA coated flasks and incubated for seven days at 37 °C and the consumed media was changed carefully on Day-5 with fresh media. After incubation, the cells were observed under the microscope for the formation of sphere cells.

Dosing the sphere cells

The cultured cells were collected and centrifuged at 600 r.p.m for 5 minutes. The liquid was aspirated, and the pellet was mixed with 7 mL of stem cell media. 1 mL of media containing cells was distributed equally in 6 test tubes labelled for different treatments, i.e. Negative, Pemetrexed, Cisplatin, Copper, Disulfiram, Disulfiram + copper. The drug concentrations are as follows (according to the IC-50 values of cell lines): MSTO-211H and JU77:

- PMT - 1 µM
- CIS - 10 µM
- PLGA-DS - 1 µM
- Cu - 10 µM
- PLGA- Ds/Cu - 1 µM/10 µM

The labelled test tubes were then topped up with 3 mL SCM containing the above concentration of drugs making the volume to be 4 mL in all the six test tubes and

mixed well. 4 mL solution from the above mixture containing cells + drug was transferred to already prepared six-well plate coated with Poly-HEMA and washed twice with 2 mL PBS. The plate was incubated for 48 hours.

Regrowing sphere cells

Six test tubes were labelled carefully for different drugs (mentioned above). Individually collected content from each well (incubated for 48 hours) was transferred to each test tube. The test tubes were centrifuged at 600 r.p.m for 5 minutes, aspirated and 4 mL PBS was added to the pellet and centrifuged again at 600 r.p.m for 5 minutes. PBS was aspirated, and 200 µL of trypsin was added and mixed well until no spheres were visible. It was followed by a short incubation of 5 minutes and repeated twice making the volume of trypsin to 400 µL. The volume was made up to 1 mL by adding 600 µL of serum-containing media. 5 mL of stem cell media was added further, and the volume was made up to 6 mL. Cells were counted for each test tube using the cell counter. Fifty thousand cells from each tube were collected and added to 2 mL to stem cell media. Poly-HEMA coated Six well plates were prepared by washing with 2 mL PBS. Stem cell media + cells were added to each labelled well with different drugs concentrations and placed in the incubator for seven days to identify the ability of spheres to regrow. The cells were observed under the microscope. Each well was then counted separately for the presence of sphere cells. Images were taken at 4x magnification.

Statistical Tests

Graph pad prism analysis tool was used to perform all statistical data analysis. The

cut-off chosen for statistical significance between samples was p=0.05. Values less than 0.05 indicate that the difference between the samples is statistically significant. P-value<0.001 denotes that the difference between the samples is extremely significant, and p≥0.05 defines that the difference between the two samples is not statistically significant. The statistical "student t-test" was used for means to determine the statistical significance between MM cell lines that tested under the same conditions for two samples. The statistical test "One-Way Annova" used to determine the statistical significance of the same MM cell line that tested under the varying condition and more than two samples.

2.2.7. Stable Transfection

Gene of interest	Vector	Target sequence
NF-kB (knockout)	NF-kB-p65sgRNA CRISPR/Cas9 All in one Lentivector set (Human)	T1 57 GCTCAATGATCTCCACATAG T2 98 GCTTCCGCTACAAGTGCGAG T3 266 AGCTTGTAGGAAAGGACTGC S GCACTCACATCGCTACATCA

Table 2.4: showing gene of interest, lentiviral vector, and target sequences

2.2.7.1 NF-kB knock out - All-in-One lentivector sets of sgRNA CRISPR/Cas9 for NF-KB (Rel A) purchased from Abm (BC, Canada). Each lentiviral set consists of multi-guide sgRNA that target the same gene but will introduce three fragment deletion in the DNA of the target gene.

Preparation of LB plates

LB (Luria -Bertani) agar medium (Sigma, UK) prepared by adding, 50 g of LB broth powder to 2 L of deionised water, 6 gm of agar medium was mixed in one of the aliquots and autoclaved. To select successfully transformed bacteria 100 μg/mL ampicillin (for antibiotic selection) added to the broth-agar autoclaved medium. Each 10 cm2 petri dish prepared with 15 mL of medium containing ampicillin and allowed to set at room temperature and stored at 4°C.

Transformation

The JM109 *E. coli* strain (Promega USA) chosen as competent bacterial cells for transformation. They were stored as aliquots of 50 mL at -80°C. One aliquot of JM109 was thawed on ice, 20 ng of each plasmid (T1, T2, T3) DNA was added to the 50 μL of competent cells and incubated on ice for 20 minutes. To enhance the uptake of DNA by bacterial cells, the tube containing JM109 and DNA were exposed to heat shock for one and a half minute at 42°C water bath. The samples were quickly placed on ice for 2 minutes. Subsequently, 950 μl of LB broth without containing ampicillin was added to the mixture and incubated at 37°C for 1 hour on a shaker. After incubation 150 mL of each target was spread on the agar plate containing antibiotic ampicillin with the help of an L-rod and incubated overnight at 37°C to allow the formation of bacterial colonies which were not resistant to ampicillin. A single colony was picked per target and added to 20 ml of the sterile tube containing 3 mL of LB broth containing ampicillin to a final concentration of 100 mg/mL and incubated overnight in a shaker at 240 r.p.m, 37°C. The next day solution on each tube was divided into two 1 mL and 2 mL aliquots for mini-prep and maxi prep respectively.

Plasmid preparation

Miniprep

The QIAGEN Kit, UK (QIAprep Spin Miniprep) was used for preparing high copy plasmid. The tubes with 1 ml of the transformed plasmid were centrifuged at 8000 r.p.m. for 3 minutes at room temperature. The pellet was collected and suspended into 250 mL of buffer P1 (composition: 50 mM Tris-Cl, pH 8.0; 10mM EDTA; 100 mg/mL RNase A). The mixture was transferred to a microcentrifuge tube, and 250 µL of buffer P2 was added (composition: 200 mM NaOH, 1% SDS (w/v) for cell lysis. The sample was mixed gently by inverting the tubes until the solution became clear. It was followed by adding chilled buffer P3 (composition: 3.0 M potassium acetate pH 5.5) and mixed well to neutralise cell lysis. The solution incubated on ice for 20 minutes. The mixture was centrifuged for 30 minutes at 13,000 r.p.m and 4°C. The supernatant was collected into a QIAprep and centrifuged again for 1 minute at 20,000 g, 4 °C. The flow-through was discarded. The QIAprep column was washed with buffer PB and centrifuged for one minute. The flow-through was discarded. The column was then washed a second time with 750 µL of buffer PE, centrifuged for 1 minute and flow-through was discarded. Additionally, centrifugation was repeated for 1 minute to remove any residual wash buffer. The column was transferred in a microcentrifuge tube, and 50 µL of buffer EB (pH-8.5) then added to the middle of the column and incubated for 1 minute at room temperature. The eluted DNA was quantified using nanodrop and stored at -20°C.

Maxiprep

1.5 mL of previously transformed plasmid was added into a 500 mL of a sterile glass bottle containing 9 mL of LB broth with ampicillin (100 µg/mL). The mixture was placed in a shaker at 37°C for 6 hours. After incubation, the mixture was transferred in a 500 mL sterile maxi prep bottle and centrifuged for 4,500 r.p.m. for 15 minutes. The supernatant was discarded, and the pellet resuspended and carefully combined into a 10 mL P1 buffer. The solution transferred into 50 mL maxi-prep flasks, 10 mL of Buffer P2 was added to the mixture for cell lysis, mixed well by inverting and incubated for 5 minutes at room temperature. The solution was incubated on ice for 20 minutes. It was followed by centrifugation at 9,600 r.p.m for 30 minutes. Meanwhile, 10 mL buffer QBT was used to equilibrate maxi-prep columns. After centrifugation, the supernatant was collected and transferred in a maxi prep column and allowed to flow by gravity. 30 ml of buffer QC used to wash the QIAGEN columns. 15 mL of buffer QF was added to elute the DNA, and a 50 uL was placed under the column for collection. 10.5 mL of isopropanol (room temperature) was added to the collected elute and immediately mixed and centrifuged for 1-hour min at 9,600 r.p.m, 4°C. Isopropanol aid in DNA precipitation. The supernatant was removed, and the pellet was washed with 1.5 mL of 70% ethanol (room temperature) and centrifuged for 10 min at 13,000 r.p.m, 4°C. The supernatant was decanted, and tubes were centrifuged again to remove the residual ethanol and pellet was left to air dry. DNA was dissolved in the TE buffer to measure the concentration of DNA by using nanodrop spectrophotometer. The three targets, i.e. T1, T2 and T3, were aliquoted to a concentration of 3 µg/µL and stored at -20°C for future use.

Each target (T1, T2, T3) was diluted to a final concentration of 3 µg/µL of plasmid DNA, and 10 µL was added in a 1.5 mL tube. For stable transfection (knock out) Mesothelioma cell line (MSTO-211H) were seeded at a density of 0.4x106 and cultured in 6 well plates, in serum-containing media and incubated for 24 hours at 37°C, 5% CO_2. To determine the efficiency of transfection, scrambled (empty vector), and Negative (no plasmid) was used as controls. To perform transfection 250 µL of OPTIMEM was mixed with 10µL of lipofectamine 2000 in tube A. In tube B 250 µL of OPTIMEM was mixed with 3µg/µL of plasmid DNA (the plasmids containing the above sequences were mixed in equal proportions) In tube C 3 µg/µL of an empty plasmid (scrambled) was mixed with 250 µL of OPTIMEM and 10µL of lipofectamine 2000. The tubes were incubated for 5 minutes at room temperature. After incubation, tube A and B were mixed and incubated for 20 minutes.

The mixture was then transferred to well labelled six-well plates containing MSTO-211H culture and incubated for 24 hours at 37°C and 5% CO2. The following day cell culture was trypsinised with 500 µL of trypsin and neutralised with 1.5 mL of serum containing media. Each transfection was then subcultured to well labelled petri dishes containing 15mL fresh RPMI media with 150 ng/mL puromycin as selecting agent. The cells were incubated at 37 °C and allowed to grow for a few days, according to preliminary screening. They were checked routinely, and media was changed approximately after every two days. The plates were observed for the presence of colonies. The Negative containing no resistance to puromycin died, and the successfully transfected cells formed colonies. The individual colonies were picked

by trypsinising and transferred to T-25 flask contains fresh RPMI with 150 ng/mL puromycin. The cells were then collected and screened by western blot for the expression of NF-kB on the protein level followed by screening by qRT-PCR on RNA level. For about, 40 colonies were picked and screened for no expression of NF-kB in the clones through western blot and RT-PCR. Amongst which only two clones for the best expression and one for scrambled was chosen for further experiments.

2.2.7.2 NF-kB ectopic expression

For stable transfection (overexpression) Mesothelioma cell line (MSTO-211H) were seeded at a density of $0.4x10^6$ and cultured in 6 well plates, in serum-containing media and incubated for 24 hours at 37°C, 5% CO_2. To determine the efficiency of transfection, mock (empty vector), and Negative (no plasmid) were used as controls. To perform transfection 250 µL of OPTIMEM was mixed with 10µL of lipofectamine 2000 in tube A. In tube B 250 µL of OPTIMEM was mixed with 3µg/µL of plasmid DNA. In tube C 3 µg/µL of the empty plasmid (mock) was mixed with 250 µL of OPTIMEM and 10µL of lipofectamine 2000. The tubes were incubated for 5 minutes at room temperature. After incubation tube, A and B were mixed and incubated for 20 minutes.

The mixture was then transferred to well labelled six-well plates containing MSTO-211H culture and incubated for 24 hours at 37°C and 5% CO2. The following day cell culture was trypsinised with 500 µL of trypsin and neutralised with 1.5 mL of serum containing media. Each transfection was subcultured to well labelled Petri dishes containing 15mL fresh RPMI media with 50 mg/mL hygromycin was the selecting agent. The cells incubated at 37°C and allowed to grow for a few days, according to

preliminary screening. The cells were checked routinely, and media was changed approximately every two days. The plates observed for the presence of colonies. The Negative containing no resistance to hygromycin died, and the successfully transfected cells formed colonies. The individual colonies were picked by trypsinising and transferred to T-25 flask contains fresh RPMI with 50 mg/mL hygromycin. The cells were then collected and screened by western blot for the expression of NF-kB on the protein level followed by screening by qRT-PCR on RNA level. For about, 40 colonies were picked and screened for ectopic expression of NF-kB in the clones through western blot and RT-PCR. Amongst which only two clones for the best expression and one mock were chosen for further experiments

2.2.8. SDS - PAGE / Western Bolt

Pellet Collection

Cells were collected and centrifuged at 1200 r.p.m for 5 minutes. The collected pellet was washed with 1mL PBS and centrifuged. The washed pellet was transferred to Eppendorf (1.5 mL) and centrifuged with 1 mL PBS. PBS was removed, and the pellet was stored at -80 °C.

Protein extraction

For cell lysis 100-200 µL of RIPA buffer (with protease and phosphates inhibitors see Table 2.2 for its preparation) was added according to the pellet size and mixed every well. The samples were sonicated for 1 minute and centrifuged for 20 min (4°C) at 14000 r.p.m. The supernatant was collected and stored at -20°.

Protein concentration

The protein concentration was estimated with BCA assay, by comparing the values to a protein standard calibration curve, which is prepared by plotting absorbance versus protein concentration graph by using a serially diluted BSA in RIPA buffer. The protein sample was thawed and placed on ice. 2.5 µL of each protein sample aliquoted in duplicate in 96 well plates. Followed by the addition of reagent (A+S) which was prepared by mixing A:S = 20:1 µL (prepared according to the number of samples). 25 µL of A+S solution aliquoted in the well-containing protein followed by addition of 200 µL of reagent B. The mixture was incubated for 10 minutes at room temperature. The protein concentration was determined by using a multi-scan. BSA protein determination assay was followed which was prepared by serially diluting the 3.0mg/mL BSA solution in RIPA buffer to the following concentrations: 3.0mg/mL, 1.5 mg/mL, 1.0 mg/mL, 0.75 mg/mL, 0.50 mg/mL, 0.25 mg/mL and 0 mg/mL (30µL RIPA buffer). The absorbance was read at 650 nm, and protein concentration of the samples was calculated from plotting the absorbance versus protein concentration of the BSA. The protein estimates were used to equalise protein concentrations across the samples ranging between 30-150 µg/lane.

Preparing samples for loading

The samples were calculated using Excel software. A mixture of protein about 50-100 µg, 1 µL of 0.5 M DTT, deionised water and 4x loading dye was prepared to the specified final volume (maximum loading volume 40 µL) and vortexed for 1 min. The labelled vials containing loading mixture was kept on heat block for 10 min at 96°C. The vials were removed after 10 minutes and vortexed for a few seconds.

Preparation of separating gel

Before the preparation of gel mixture, 1.5 mm spacer plates were used and placed together and secured with clamps. The separating gel was prepared, as described in Table 2.3. TEMED was added in the end whilst preparing the mixture. The mixture was mixed thoroughly, and 7.5 mL added to the gel plates. After the addition of gel, approximately 200 µL of isopropanol was added to cover the top of separating gel solution to remove any bubbles. The gel was left undisturbed for 20 minutes. The isopropanol was removed once the gel was set. The solidified gel was washed thrice with distilled water.

Reagents:

10% Ammonium persulphate: It was prepared by dissolving 0.1 g APS in 1 mL of distilled water.

Table 2.5: Components of separating gel with corresponding volumes.

SEPERATING GEL	10% GEL	6% GEL
40% 19:1 acrylamide: bis (mL)	4.4 mL	4.4 mL
Resolving Buffer (mL)	5.5 mL	5.5 mL
H2O (mL)	5 mL	6.6 mL
TEMED (µL)	15 µL	15 µL
10% (w/v) APS (µL)	125 µL	120 µL

Preparation of stacking gel: The stacking gel was prepared, as shown in Table 2.4. The stacking gel mixture was added on top of the separating gel, and 1.5 mm comb was placed immediately but carefully to avoid the formation of bubbles. This comb helps in forming the required wells for protein loading. The combs were removed after solidification of the gel.

Table 2.6: Preparation of stacking Gel SDS - PAGE electrophoresis

REAGENTS	VOLUME
30% 19:1 acrylamide: bis	1.2 mL
Stacking Buffer (mL)	4.2 mL
H2O (mL)	6.6mL
TEMED (µL)	20 µL
10% (w/v) APS (µL)	250 µL

Previously prepared SDS-PAGE gels were assembled into the electrophoresis tank, by using the cassette adapter and placed in the tank containing in 1x running buffer. Comb was removed, and the wells were cleaned with a syringe to remove any trapped gel inside the wells. The prepared protein samples were loaded into the wells, and 5µL of protein marker was added in one of the wells to monitor protein size. The gel was then run at 200 V, 300 mA for 1 hour. The current was maintained to allow protein separation by molecular weight.

Membrane Blotting

3MM blotting paper was cut into 9 x 10 cm size. PVDF cut into 8 x 4.5 cm size and was soaked in transfer buffer for a while, and PVDF was dipped in methanol (to activate it for protein binding) for 5 minutes and then soaked in transfer buffer before being transferred. Four Blotting papers were dipped in transfer buffer and kept on top of each other on the semi-dry transfer unit. PVDF membrane was placed carefully on top of blotting papers. SDS gel was carefully removed from the casket and placed on top of the PVDF membrane and again covered by four blotting papers from the top. The sandwich was flooded with transfer buffer, and the lid was closed. The SDS-PAGE was run for 1 hour 30 minutes at 20V and 200 mA.

Blocking the PVDF membrane

After botting was completed, the membrane was placed in a tray and submerged in blocking buffer. Blocking buffer was prepared by using 5% of fat-free milk in 1xTBS-T solution. It was added to the freshly transferred protein-membrane for 1 hour and was used to prevent unspecific binding of antibodies.

Staining by primary antibody

PVDF membrane was incubated for 1 hour by using a primary antibody (Concentrations according to table 1.3) prepared in blocking buffer. The membrane was placed in a clean plastic bag and sealed around the corner using heat. The primary antibody was poured into the bag carefully without bubbles, sealed and was left overnight at 4°Con a shaker. The membrane was removed the next day and washed thrice with TBST for 10 minutes. It was then placed in 10 mL secondary antibody, prepared in blocking buffer (dilution from Table 1.3) and incubated for 2 hours at

room temperature. The PVDF membrane was then washed thrice with TBS -T (1x) for 10 minutes and prepared for signal detection.

Table: 2.7: Antibodies and their working dilutions with corresponding volume in µl.

ANTIBODY	DILUTION
p65	1:1000
HIF2α	1:500
VINCULIN	1:8000
TUBULIN	1:8000
VIMENTIN	1:2000
SECONDARY ANTI MOUSE	1:5000
SECONDARY ANTI RABBIT	1:5000

Protein Detection

The ECL detection kit was used to detect the chemiluminescence signal. The washed membrane was placed in a hyper cassette layered with cling film. EZ-ECL solution was prepared by mixing solution A with solution B in 1:1 ratio and added to PVDF membrane for 4 minutes. The ECL solution was removed by tilting the cassette and draining off the solution without touching the membrane. For the extra sensitive proteins, the luminescence was detected using x-ray films in a completely dark room. The membrane was covered with cling film, and the x-ray was kept on the top. The lid of the cassette was closed, and it was left undisturbed in a completely dark room for 15 minutes. The film was developed by immersing in the developer solution briefly

rinsed with water, followed by brief exposure to the fixative solution. The bands were observed as dark spots due to chemiluminescent light affecting x-rays. The intensity of bands is directly proportional to the protein content, therefore darker the band more the protein and vice versa. The membrane was washed for 1 hour in TBS-T to remove any previously bound antibodies. The protein loading efficiency was determined by using b acting as a loading control. The membrane stained with b-actin primary antibody (1:5000) was prepared in blocking buffer. It was washed twice for 15 minutes and was followed by HPR conjugated secondary antibody (1:8000) in blocking buffer. The protein bands detected should be equivalent to all the samples. It further determines the accuracy of the technique throughout the western blot analysis.

2.2.9. Quantification of RNA gene expression (qRT-PCR)

RNA isolation

Mesothelioma cells (0.25 x 10^6) were cultured in T-25 flask and placed in a hypoxic chamber for five days without changing media. Normoxic samples were collected by culturing 1x10^6 cells in overnight Normoxia. Media was aspirated, and cells were washed with 2 mL PBS. PBS was aspirated, and 300 µL of RL buffer was added and incubated for 2 minutes. The lysate was collected and placed in -80 °C if not processed further. RNA purification was performed by using total RNA purification kit (Norgen Biotek). To process the sample further, the solution was added to the genomic DNA column, and a collection tube was placed at the bottom of the column. It was then centrifuged at 10,000 r.p.m at room temperature for 1 minute. The column was disposed, and 200 µL of 100% ethanol was added to 300 µL of flow-through and

vortexed. This 500 µL of the solution was transferred to RNA purification tube with collection tube placed at the bottom and centrifuged at 10,000 r.p.m for 1 minute. The flow-through was discarded. 400 µL of wash solution A was added to the column and centrifuged for 1 minute at 10,000 r.p.m. The procedure was repeated three times. The column was carefully removed to prevent any ethanol binding to the column. The collection tube was discarded, and the column was placed into a fresh elution tube. 50 µL of elution solution A was added to the column and left for 1 minute. The samples were centrifuged at 2000 r.p.m at room temperature for 2 minutes, followed by centrifugation at 10,000 rpm, room temperature for 1 minute. The final solution collected in the elution tube is the required the RNA sample.

RNA Quantification

RNA concentration and quality of each sample were measured using a Nanodrop 2000 spectrophotometer (Thermo Scientific, UK). The ratio of absorbance at 260nm and 280nm was used to assess the purity of RNA in the sample. To blank the machine, 1.5 µL of the RNA samples were added and measured in ng/µL.

Complementary DNA (cDNA) synthesis

500 ng of the RNA required for RT (Reverse Transcriptase Chain Reaction), and therefore the obtained samples were diluted to 500 ng in 10µL using nuclease-free water (Invitrogen, UK). This 10µL of total RNA (50 ng/µL) mixed with 10µL of a 2x Reverse Transcription mixture containing 2x Transcription buffer, 8mM dNTP mix, 2x random primers (as shown in table 2.6). This 2x RT master mix was used for reverse transcription, in thermocycler using the following conditions: 25°C for 10 minutes, at 37°C for 120 minutes, 85°C for 5 minutes. The cDNA samples obtained

was placed on ice for immediate use or stored at -20ºC for long term storage. The cDNA product (20µL) was assumed to have 500 ng of DNA concentration and was diluted with 80 µL of DNase/Rnase free water (1:5 dilution) to make a final concentration of 5 ng/µL, cDNA stored at -80°C.

Table 2.8: Reagents required for preparing RT master mix with volume (µL)

RT COMPONENT	VOLUME *(µL) x 1Reaction*
10 x RT Buffer	2
10 x RT Random Primers	2
DNase/Rnase free Water	4.2
25 x dNTP mix	0.8
Reverse Transcriptase Enzyme	1
Total	10.0

Quantitative real-time PCR (qRT-PCR)

The quantification of gene-specific mRNA expression was determined by qRT-PCR using TaqMan Gene Expression Assays (Thermo Scientific, UK) with FAM reporter. The master mix was prepared for a calculated number of reactions required, as detailed in Table 2.7. The master mix was prepared for each specific TaqMan primer used, once these mixed 5.5 µL of the master mix added to one well of Microamp® fast optical 96-well reaction plates (Applied Biosystems, UK) followed by 4.5 µL of the required cDNA.

A negative control sample that contained 5.6 µL of nuclease-free water instead of cDNA solution was included in the assay to verify the fidelity of the PCR amplification—after setting up the reaction, the plates were sealed with an optically clear seal, gently tapped to remove any air bubbles and centrifuged at 200 r.p.m. for 1 minute. The reaction plate was placed on a Real-Time PCR System (Applied Biosystems, UK). PCR cycling conditions consisted of an initial enzyme activation step at 95ºC for 10 minutes, following denaturation at 95ºC for 15 seconds and annealing and extension at 60ºC for 1 minute for 40 cycles. Data was exported to GraphPad Prism for statistical analysis. The expression of the *GAPDH* gene was determined and used for internal control and normalisation.

Table 2.9: Showing the components for master mix for (qRT-PCR) and their corresponding volumes.

COMPONENT	VOLUME
2x TaqMan Universal Master Mix II	5 µL
20x TaqMan Assay Primers	0.5 µL
DNase/RNase free water	4.5 µL
Total	10 µL

2.2.10. Detection of Cancer stem cell markers using Flow Cytometry

Mesothelioma cells were collected and aliquoted at a density of 100,000 cells/well. They were plated in a six-well plate and incubated in the hypoxic chamber for four

days. On third-day cell samples at a density of 250,000/well were plated in Normoxia and incubated overnight. The samples were trypsined by adding 500 µL of trypsin and neutralised with 1.5 mL of media. The solution was centrifuged at 1200 r.p.m for 5 minutes. The pellet was washed with 2 ml flow buffer (4% FBS in PBS stored at 4°C) by centrifuging at 1200 rpm for 5 minutes. The cells were counted, and 200,000 cells suspended in each tube. The tube containing cells were washed with 2 mL of flow buffer at 2000 r.p.m for 5 minutes.

Detection of CD133 positive population – The CD-133-FITC reagent was diluted (2.5 µL stain/100 µL of flow buffer). The cell pellet was resuspended in 100 µL of diluted CD133-FITC and incubated for 1 hour at 4°C. Followed by incubation, the cells were rinsed with flow buffer and centrifuged at 2000 r.p.m for 5 minutes. The medium was aspirated, and the pellet was resuspended in 200µl of flow buffer. The samples were analysed with FL-1 green filter to detect CD133 positive population.

Detection of ABCG2 positive population – ABCG2 is also known as CD338w. The 338w -APC reagent diluted (2.5 µL stain/100 µL of flow buffer). The cells were resuspended in 100 µL of diluted CD338w and incubated for 30minutes at 4°C. Followed by incubation, the cells were rinsed with flow buffer and centrifuged at 2000 r.p.m for 5 minutes. The medium was aspirated, and the pellet was resuspended in 200µl of flow buffer. The samples were analysed with FL-3 red filter to detect positive ABCG2 population by using BD flow cytometer.

Detection of CD 24 positive population – The CD 24-FITC reagent was diluted (2.5 µL stain/100 µL of flow buffer). The cell pellet was resuspended in 100 µL of diluted CD24 and incubated for 30 minutes at 4°C. Followed by incubation, the cells were rinsed with flow buffer and centrifuged at 2000 r.p.m. for 5 minutes. The medium was aspirated, and the pellet was resuspended in 200µl of flow buffer. The samples were analysed with the FL-1 filter to detect positive CD24 population by using BD flow cytometer.

.

2.2.10.1 Measurement of hypoxia in cell culture

The hypoxic status of the cell was examined by immunohistochemistry and flow cytometry. The attached cells (10,000/dish) in hypoxia were cultured for four days using a HypoxyprobeTM-1 Plus Kit (HPP). On the fourth day, the consumed medium was replaced with HPP containing medium at a concentration of 100 µM. The cells were incubated overnight. Cells for Normoxia (50,000 cells/well) were plated on the third day, and HPP probe (100 µM) was added on the fourth day for overnight. The hypoxic and normoxic culture were processed together on day five. The media was removed, and cells were washed with PBS. The Image-it Fix-Perm kit was used to fix the cells and prepare a slide for staining purposes. Fixative (which contained 4% formaldehyde) was added to the cells and incubated for 15 minutes.

The cells were washed three times for five minutes each and kept on see-saw rocker at room temperature. Permeabilisation solution (containing 0.5% Triton X-100 in DPBS) was then added to the cells and left for 15 minutes. The slide was then washed three times for 5 minutes each with 500 µL of washing buffer. The cells were treated with 200 µL of blocking buffer (containing 3% BSA in DPBS) for 60 minutes.

Blocking buffer was discarded, and the cells were stained with the fluorescently labelled primary antibody to bind to the HPP. FITC anti-HPP was conjugated monoclonal antibody prepared in blocking buffer in the ratio 1:1000 dilution. It was incubated in the dark at room temperature for 1 hour. The cells were then washed with wash buffer thrice for 5 minutes. Two drops of beta actin- PI antibody was added in 1 mL blocking buffer to stain the cytoskeleton. After half an hour, the solution was discarded, and a solution of vector shield containing DAPI was added directly to the cells, and well covered by 12 mm coverslip. The dishes were covered with aluminium foil to prevent the loss of fluorescence. The cells were then analysed using the Evos microscope for high magnification images.

HPP staining was also detected by using flow cytometric analysis. Mesothelioma cells (100,000 cells/well) were plated in a six-well plate and incubated in the hypoxic chamber for four days. On the third day, 250,000 cells /well were incubated in normoxic conditions overnight. On the fourth day, HPP (1:1000) was added to the respected wells (1µL/mL) in normal and hypoxia samples for 2 hours. The samples were trypsinised by adding 500 µL of trypsin, rinsed with PBS, collected and centrifuged at 1200 r.p.m for 5 minutes. The pellet was washed with 2 mL PBS and centrifuged twice at 1200 rpm for 5 minutes. The final pellet was resuspended in 200 µL of sterile PBS and fixed adding 2 mL of ice-cold 70% ethanol (stored at - 80 °C) drop by drop whilst mixing, followed by incubation for 10 minutes. This ice-cold ethanol was slowly added to the test tubes whilst placing them on the vortex, and cells were left untouched for 10 minutes. The cells were rinsed with PBS and centrifuged, at 1200 r.p.m for 5 minutes, the ethanol was aspirated, and cells were washed with 9 mL PBS. The PBS was removed, and the fixed cells stained with 200 µL of HPP-FITC conjugated antibody was prepared in blocking buffer (1:1000) and stored in the

dark for 2 hours at 4°C. The cells were washed with 2mL of PBS and centrifuged at 1200 r.p.m for 5 min. The pellet was mixed in 200 µL of PBS, and cells were analysed using FACS. The positive hypoxic population was detected by FL-1 green filter using BD flow cytometer.

2.2.11. Migration Assay

MSTO-211H and JU77 cell lines (0.25 x 10^6) were cultured in hypoxia for four days. For normoxic culture, 1x10^6 cells were on the third day for 24 hours. The normoxic and hypoxic cells were trypsinised together on the fourth day, and a pellet was obtained. The cells were trypsinised, and the pellet was collected again. It was resuspended in fresh medium, and cells were counted. Ten thousand cells for MSTO-211H and 50,000 for JU77 were taken per sample and transferred to 2 ml PBS. The solution was centrifuged at 1200 r.p.m for 5 minutes. The pellet was resuspended in 50 µL serum-free media and mixed very well, and it was then topped up with 1950 µL serum-free media and mixed well.

Boyden chambers were placed in 24 well plates. 200 µL of SFM containing cells were transferred to the chamber. 700 µL of serum-containing media was transferred to the well in which Boyden chamber was placed, to immerse the chamber in serum-containing media from the bottom. The hypoxic cells were treated with 25 nM of PLGA - DS, which was added in 700 µL of the serum-containing medium. So, one cell line had four samples per condition, i.e. Normoxia, hypoxia and Treated. The plates were incubated overnight. Following day media was removed from the chambers, and the chamber containing cells were transferred to another 24 well plates containing 700 µL of crystal violet/well. Crystal violet was prepared in the ratio of 1:3

with PBS. The chamber was left untouched for 20 minutes and then washed twice with water and left to dry. The dried chambers were placed back in the fresh 24 well plates and observed under the microscope. The cells were counted for different conditions and were analysed using INNOVA graph pad.

2.2.12 Invasion Assay

MSTO-211H and JU77 cell lines (0.25 x 10^6) were cultured in hypoxia for four days. For normoxic culture, 1x10^6 cells were cultured on the third day for 24 hours. The normoxic and hypoxic cells were trypsinised together on the fourth day, and the pellet was obtained. It was resuspended in fresh medium, and cells were counted. 10,000 cells for MSTO -211H and 50,000 for JU77 were taken per sample and transferred to 2 ml PBS. The solution was centrifuged at 1200 r.p.m for 5 minutes. The pellet was resuspended in 50 µL serum-free media and mixed very well, and it was then topped up with 1.95 µL serum-free media and mixed well. Unlike migration, Boyden chamber was coated with matrigel for invasion. The gel aliquot for coating was prepared using stock (200ul) gel dilution of 1:15 with serum-free media. It was mixed well using cold tips, and 200 µL of the mixture was aliquoted in the Boyden chambers and incubated overnight.

The coated Boyden chambers were placed in 24 well plates. 200 µL of SFM and cells were transferred to the chamber. 700 µL of serum-containing media was transferred to the well in which Boyden chamber placed, to immerse the chamber in serum-containing media from the bottom. The hypoxic cells treated with 25 nM of PLGA-DS, which was added in 700 µL of the serum-containing medium. So, one cell line had four samples per condition, i.e. Normoxia, hypoxia and Treated. The plates were

incubated overnight. Following day media was removed from the chambers, and the chamber containing cells were transferred to another 24 well plates containing 700 µL of crystal violet/well. Crystal violet was prepared in the ratio of 1:3 with PBS. The chamber was left untouched for 20 minutes. They were then washed twice with water and left to dry. The dried chambers were placed back in the fresh 24 well plates and observed under the microscope. The cells were counted for different conditions and analysed using INNOVA graph pad.

2.2.13. Cytotoxicity Assay

Stock MTT solution

500 ml of MTT working reagent (5mg/ml MTT solution) prepared by adding 2.5 gm of 3-(4,5- Dimethylthiazol-2-yl)-2,5-diphenyltetrazolium bromide in 500 mL of sterile PBS solution. The mixture is sparingly soluble in water. Therefore, magnetic stirrer was used to dissolve it further. Since MTT is sensitive to light, the bottle was carefully covered with the foil and left overnight to dissolve completely. The following day, the MTT solution was filtered with the sterile vacuum flask, the opaque mixture is collected in the sterile bottle, wrapped with foil, and stored at 4°C.

MTT Assay

MTT assay is a renowned method to check the effect of drugs on cell viability. Cells were counted and seeded equally into 96 well flat-bottomed microtiter plates overnight at 37 °C—the outermost wells were filled with sterile water to maintain humidity. The following day, cells were checked for proper seeding number in each well. The cells were exposed to various concentrations of anticancer drugs, i.e. PMTXD,

CISPLATIN, PLGA-DS/Cu. It was prepared by a two-fold serial dilution using RPMI culture medium, i.e. 10μM, 5μM, 2.5 μM, 0.625 μM, 0.3125 μM. One side of the column was used as a negative control in which one column contained medium without cells, the second column contained medium, and cells (i.e. the far left) and the other side of the column (i.e. the far right) was used as a carrier control PLGA microparticles. The media used for seeding the cells for 24 hours was aspirated and replaced by 200 μL of a fresh drug-containing medium of different concentrations. The plates were incubated at 37°C for 72 hours. The experiment was done in triplets for each drug concentration with the same cell line, after 72 hrs. The cells were dosed with 25 μl of MTT reagent, and the plates are wrapped with foil paper and incubated for 3h at 37°C. The solution was removed and was followed by addition of 80 μl of 99.9% DMSO and 20 μl of Sorensen's buffer (to maintain a pH at 10.5) by 96 well multi-drop, in each well. The OD values were further calculated by using multi-well plate reader spectrophotometer at a wavelength of 540 nm. The viability percentage (%) calculated after treatment to determine the IC - 50 values of each drug. The mean and standard deviation was calculated, followed by Isolobologram.

MTT Assay for hypoxic cells

MTT assay for hypoxic cells involves culturing of the cells in the hypoxic conditions (oxygen level 1% as compared to Normoxia, i.e. oxygen level 21%) for 96 hours. The cells were trypsinised, seeded for the required density and incubated again for 48 hr. in the hypoxic condition. The cells were then treated with the desired concentration of drug/combination of drugs and incubated for 72 hrs. in hypoxia. It was then subjected to MTT assay followed by the calculations of viabilities and Isobologram as in Normoxia.

Isobologram analysis

Isobologram was used to measure the synergistic effect of two first-line anticancer drugs used for combinational chemotherapy for treating malignant mesothelioma. MTT assay investigated if PLGA-DS/Cu significantly enhanced the cytotoxicity of anticancer drugs, i.e. PMTXD and Cisplatin. The experiment was done in three dilutions respectively, e.g. dilution1 of PMTXD alone, dilution 2 PLGA-DS/Cu alone, dilution 3 PMTXD in combination with PLGA-DS + Cu. The same was done for Cisplatin. After incubating these drugs for 72 hours, cell cytotoxicity was calculated by MTT assay as mentioned above.

The synergy between two drugs was calculated using combination Index (CI). The CI index provided a quantitative measure and calculated using software Calcusyn^{TM}. The data for individual drugs and in combination, was processed in constant and non-constant ratios. Calcusyn^{TM} gives a detailed report of drug interaction which includes CI value at effective dose x (EDx), i.e. ED50, ED75 and ED90. A CI value <1 show synergy.

CHAPTER 3

Hypoxia induces chemoresistance and invasiveness in MM cell lines

3.1 Introduction

Mesothelioma is a highly chemoresistant neoplasm; only 40% of patients respond to standard chemotherapy causing median survival to be only 12 months (Hudson et al.,2014). Regardless of severe drug toxicities, chemotherapy for MM patients remains primary treatment choice, which can increase the median survival from 9 to 12 months in progressed stage for MM patients who cannot undergo surgery (Rossini et al., 2018). The root cause for this chemoresistance is cancer stem cells (CSCs) which are found to resist conventional chemotherapies and cause a relapse. Emerging studies suggest that these CSCs reside in a hypoxic/necrotic tumorous CSC niche (Triscott, Rose Pambid and Dunn, 2015). It has been shown that hypoxia plays a major role in the maintenance of the stemness in CSCs (Peng Liu et al.,2014).

Recent research has further shown that MM also contains hypoxic regions, which explains the link between tumour hypoxia and low therapeutic efficacy. However, the underlying mechanism of hypoxia in MM remains mostly unknown. The present study showed that hypoxia promotes aggressive phenotypes in MM cells. By inhibiting apoptosis and inducing drug resistance, hypoxia enhances *in vitro* clonogenicity, migration, invasion in MM cells (Kim at al.,2018). Mechanistically, hypoxia was shown to impact invasive and migratory behaviour of cancer cells via EMT, a process which alters their gene expression prior to migration (Barbara Muz et al.,2015).HIF's can induce epithelial plasticity and migratory phenotype by direct or indirect regulation of transcription factors related to EMT such as Snail, Slug and Zeb. Invasion of the surrounding extracellular matrix (ECM) can also be enhanced by HIF signaling by upregulation of enzymes such as MMPs to support the initial stages of metastasis by remodeling the ECM. Hypoxia is a critical microenvironmental factor

that contributes to metastatic tumour progression at the primary and distant tissue sites. HIF signaling can also be activated within tumour stromal cells through a variety of mechanisms, including hypoxia and secreted factors produced by tumour cells (Rankin et al.,2017). Hypoxic regions are found to be associated with increased genetic instability during malignant growth and more aggressive phenotype, which correlates with tumour metastasis risk (Challapalli et al.,2017).

Research studies has shown that EMT not only assist cells with migratory and invasive properties but also with stem cell properties. Moreover, EMT promotes the generation of stem-like cells from differentiated neoplastic cells (Han.,2015). Various molecular mechanisms and signaling network suggests the aggressive biological behaviors of MM cells is also dependent on EMT. Therefore, exploiting tumour hypoxia may be an alternative therapeutic strategy to reduce the aggressive behaviour of MM cells (Kim at al.,2018). Hypoxia causes slow-proliferation in stem-cell-like cells, reduce senescence, creates dysfunctional blood vessels, and promotes metastasis, which altogether results in causing resistance to various therapies (Barbara Muz et al., 2015).

Hypoxia plays a significant role in causing resistance to cancer treatments, such as reduced drug penetration, intrinsic chemoresistance and resistance to ionising radiation. Further, by supporting highly tumorigenic stem cell microenvironment, hypoxia, and HIF 1a cause treatment resistance. It is achieved by inducing cell cycle arrest (quiescence) and making drugs that target cycling cells ineffective. During adverse conditions such as prolonged or severe hypoxia, many cells undergo programmed cell death. But, some of the cancer cells get adjusted to the environmental stress and survive by avoiding necrosis, inhibition of apoptosis, and decreasing

senescence of cells, mediated by HIF alpha, resulting in an aggressive phenotype and resistance to treatment (Challapalli et al.,2017).

Hypoxia leads to the failure of chemotherapy in most solid tumours. Hypoxia in tumours can reduce the production of reactive oxygen species (ROS) in tumour cells and limit the efficacy of cytotoxic chemotherapeutic drugs through intracellular reactive oxygen species. Hypoxia can also downregulate the DNA repair pathways while upregulating resistance-related genes, thus reducing the sensitivity to p53-mediated apoptosis, thereby decreasing cell proliferation. Considerable evidence indicates that elevating oxygen levels in hypoxic tumours can overcome hypoxic-related chemoresistance (Chen et al.,2020).

We hypothesise that hypoxia is responsible for cancer stem cell characteristics and maintenance of cancer cell stemness. This study replicates the *in vivo* tumour microenvironment in 2D cultures subjected to hypoxic condition (1%). It determines the role of hypoxia to induce cancer stem-like cells in the fully differentiated cancer cell. By using this model, the study also intends to understand the resistance development to first-line drugs in MM. This study further aims to determine that the migration and invasiveness in MM is caused by cancer stems like cells when subjected to hypoxic conditions.

3.2 Material and Methods

This section describes the methods used within this specific study and any observed changes as compared to the general detailed methods explained in chapter 2.

3.2.1. Culture methods

In this study, two MM cell lines, MSTO-211H and JU77 were established as mono-layered cultures and maintained following standard subculture methods. Additionally, attached mono-layered cell line cultures were incubated under hypoxia. Cell lines cultured using RPMI were seeded at a density of ~5×10^4 cells/mL and incubated using tissue culture incubators maintained at 37°C, 5% CO2, 1% O2, for four days. The culture conditions were initially maintained for three days and later standardised for four days as the markers well expressed on day four.

3.2.2 Measurement of the hypoxic cell population

The Hypoxyprobe^{TM-1} Plus Kit was used to identify and quantify the hypoxic cell population in MM MSTO-211H and JU77 cell lines hypoxic cultures as compared to normoxic cultures, respectively. The two methods used for determination were immunocytochemistry and flow cytometry analysis as detailed in chapter 2.2.10

3.2.3 MTT cytotoxicity assay

The MM MSTO-211H and JU77 normoxic and hypoxic cultures were subjected to MTT cytotoxicity assay, as mentioned in 2.2.13 The first-line drugs for treating MM and highest concentrations used in this study are as follows: PMT (1μM) and CIS (10μM). The cell cultures were serially diluted with anti-MM first-line drugs for 72 hours in their respective cell culture incubators. After the treatment, cells were subjected to MTT reagent, and the percentage cell viability was determined.

3.2.4 Invasion Assay

The MM MSTO-211H and JU77 normoxic and hypoxic cell cultures were subjected to invasion assay as detailed in chapter 2.2.12 The normoxic and hypoxic MSTO-211H, and JU77 cell lines were seeded in Boyden chamber with nutrient-deprived RPMI medium whereas the chamber was surrounded by nutrient-rich RPMI medium. Matrigel was used to coat the bottom of the chamber, which acts as collagenase *in-vitro* to study the effect of invasion in MM cell lines. After that, the plate was incubated in the respective normoxic and hypoxic conditions for 24 hours at 37°C. The culture conditions were initially maintained for 12 hours and later standardised to 24 hours. The cells were fixed and stained with crystal violet after incubation; the number of the stained cell was counted manually. The comparison of the number of invaded cells in normoxic conditions, as compared to hypoxic conditions was made by using statistical analysis.

3.2.5 Migration Assay

The MM MSTO-211H and JU77 normoxic and hypoxic cell cultures were subjected to migration assay as detailed in chapter 2.2.11. The normoxic and hypoxic MSTO-211H and JU77 cell lines were seeded in Boyden chambers in nutrient-deprived RPMI medium whereas the chamber surrounded by nutrient-rich RPMI medium. The plates were then incubated in respective normoxic and hypoxic conditions for 24 hours. The culture conditions were initially maintained for 12 hours and standardised to 24 hours. The cells were fixed and stained with crystal violet after incubation, the number of cells was counted manually, and comparison was made between migration in normoxia as compared to hypoxia.

3.3 Results

3.3.1 Determination of the hypoxic status in hypoxia-cultured MM cell lines

The hypoxic status of normoxia and hypoxia cultures were determined using hypoxyprobe kit. Figure 3.1 (A) represents the positive hypoxic cell population as there is a visual increase of green fluorescence. Additionally, these findings were quantified by using flow cytometer analysis, which further confirms the result by showing a statistically significant increase in the hypoxic population for cells incubated under normoxia and hypoxia.

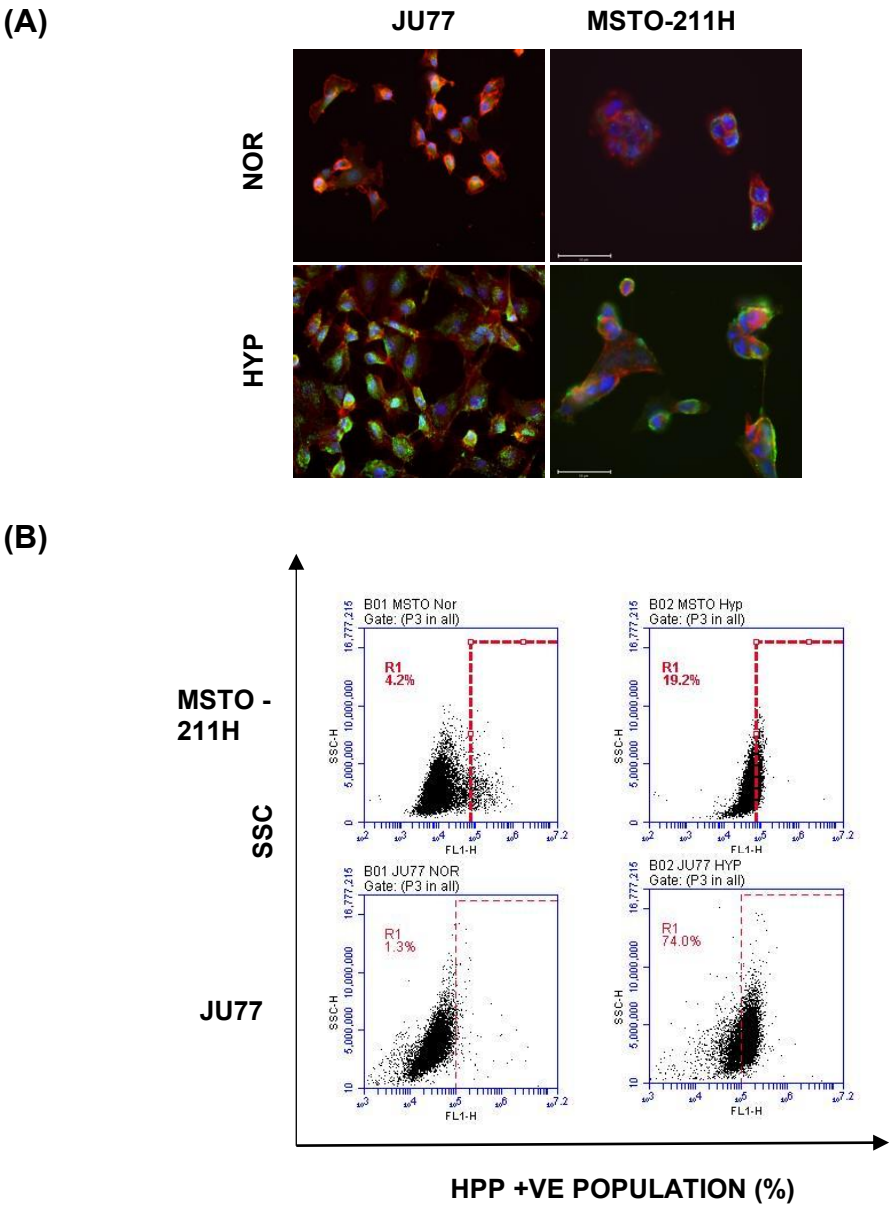

(C)

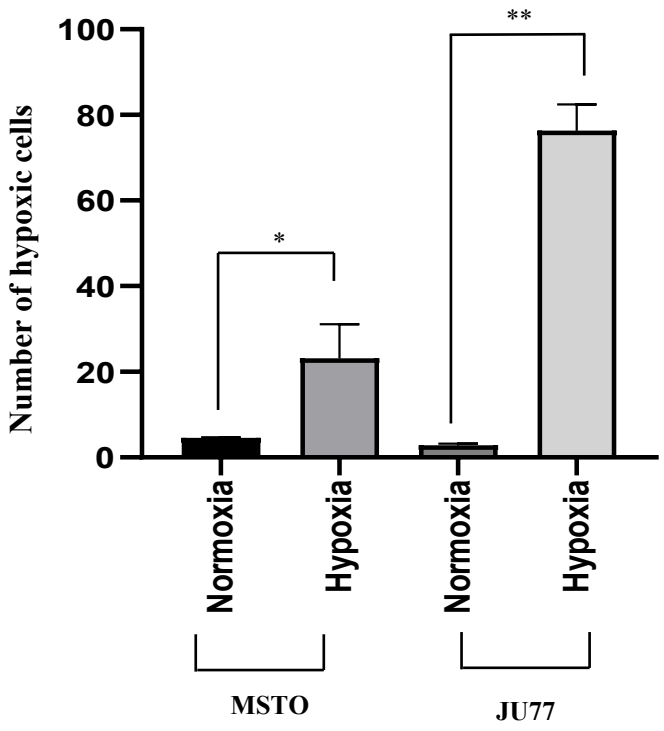

Figure 3.1 Hypoxic cell population in hypoxia cultured MM cells.

*Immunocytochemistry staining of MM cells subjected to normoxic and hypoxic conditions respectively, by using Hypoxyprobe TM-1 kit. (A) In Situ Detection of hypoxic cells in MM cells stained by green-FITC HPP and PI (red) counterstained nucleus (40x magnification) (B) Flow cytometric analysis used to measure the proportion of the hypoxic population in MM hypoxic cultures. (C) The bar chart displays the percentage of hypoxic cells detected in the cell population. n=6, *p<0.05, **p<0.01.*

3.3.2. Hypoxia-cultured MM cell lines are resistant to anticancer drugs

Studies have demonstrated that hypoxia induces resistance to fully differentiated neoplastic cells and induces resistance to anti-MM drugs *in vitro.* The cell lines were tested for cell viability after exposure to the first line anti-MM drugs, i.e. PMT and CIS, for 72 hours in normoxia and hypoxia respectively. MTT assay was used to

determine the cytotoxicity and cell viability after treatment. Figure 3.2 demonstrated cell viability curves. It depicts that the percentage of cell viability decreases with the increase in anti-MM drug concentration. To compare the effect of hypoxia on chemoresistance, IC-50 values, shown in Table 3.2, were calculated. The anti-MM drug was able to eradicate cells grown in normoxic condition, and their IC-50 values calculated accurately. Nevertheless, the cells subjected to hypoxia developed resistance to these first-line drugs and did not reach IC-50 values as shown by the plateau on the cell viability curves.

(A)

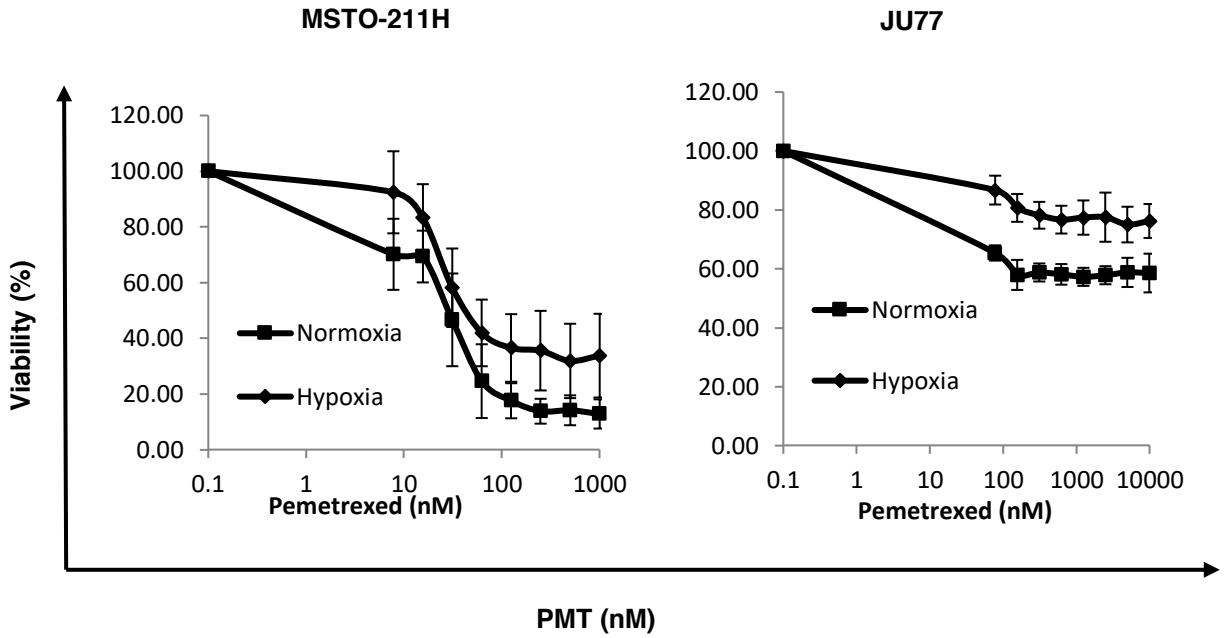

(B)

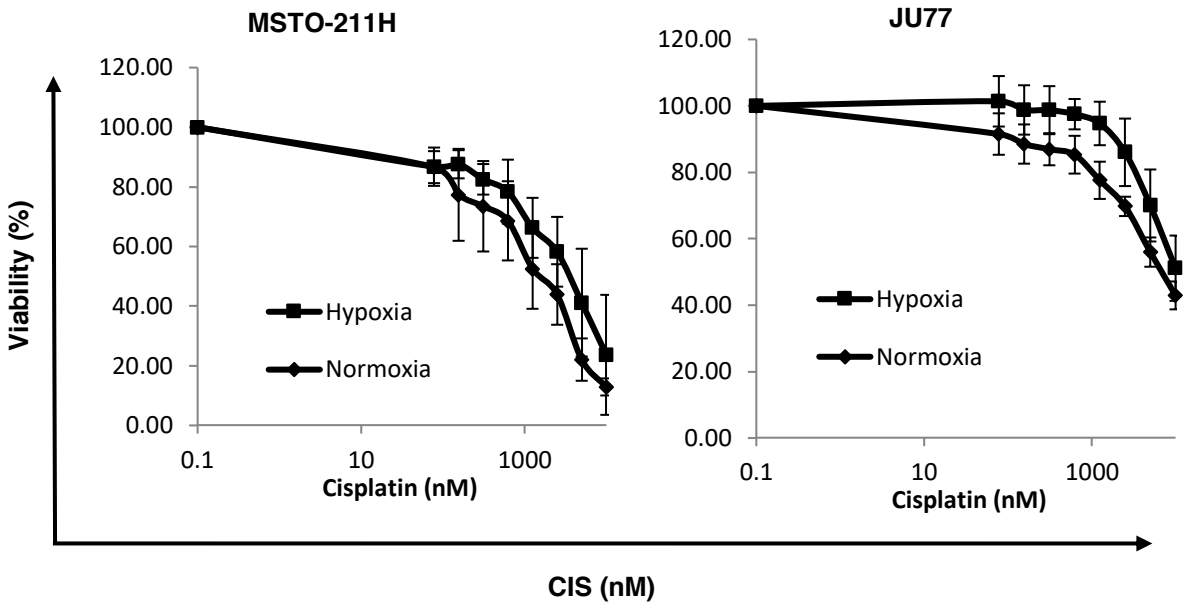

Figure 3.2 MM hypoxic cultures are resistant to first line anticancer drugs.

The cell viability curve shows the effect of first-line anti-MM drugs on normoxic and hypoxic cultures of MSTO-211H and JU77 cell lines. The cells were treated with (A) PMT (B) CIS for 72 hours and then subjected to MTT assay.

Table 3.1: IC-50 values for MSTO-211H and JU77 cell lines under normoxia and hypoxia after 72 hours of treatment with anticancer drugs (where nM = Nano Molar., ± = Mean + Standard deviation)

	Pemetrexed IC50 (nM)		**Cisplatin IC50 (nM)**	
	Normoxia	***Hypoxia***	***Normoxia***	***Hypoxia***
MSTO	*31.78 ± (8.81)*	*52.77 ± (21.14)*	*1532.48 ± (858.01)*	*4385.49± (3650.86)*
JU77	*>10000*	*>10000*	*7078.15± (1460.25)*	*11802.42± (5839.23)*

3.3.3 Hypoxic cells have higher migratory potential.

The migration potential of hypoxic cells was determined using a migration assay. Figure 3.4 shows the increased number of cells in the hypoxic cultures as compared to normoxia. The hypoxic cells were more aggressive and metastasised as a nutrition-rich medium drove them outside the Boyden chamber. The migrated cells were then fixed and counted by staining with crystal violet; the number of cells was manually counted and standardised using the normoxic conditions.

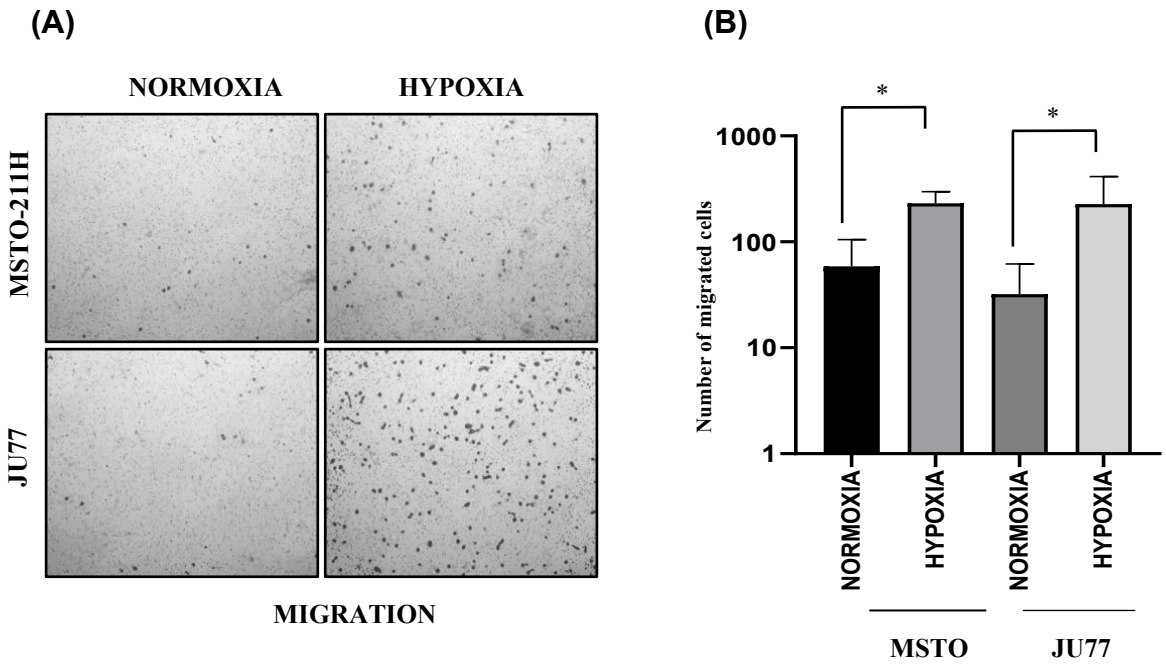

Figure 3.3 MM hypoxic cells have more migration potential *in vitro.*

The potential of MM cells was detected using migration assay with Boyden inserts ***(A)*** *Microscopic pictures of the migrated MM cells (40x magnification).* ***(B)*** *The bar chart is representing the mean number of migrated MM cells in hypoxia as compared to normoxia. n=12, *p<0.05*

3.3.4 Hypoxic cells are more invasive

The invasive properties of hypoxic cells were determined using invasion assay. Figure 3.3 shows the increased number of cells in the hypoxic cultures as compared to normoxia. In order to migrate hypoxic cancerous cells, need to invade by degrading extracellular matrix, which is presented by Matrigel coating *in vitro*. The invaded cells were then fixed and counted by staining with crystal violet; the number of cells was manually counted and standardised using the normoxic conditions.

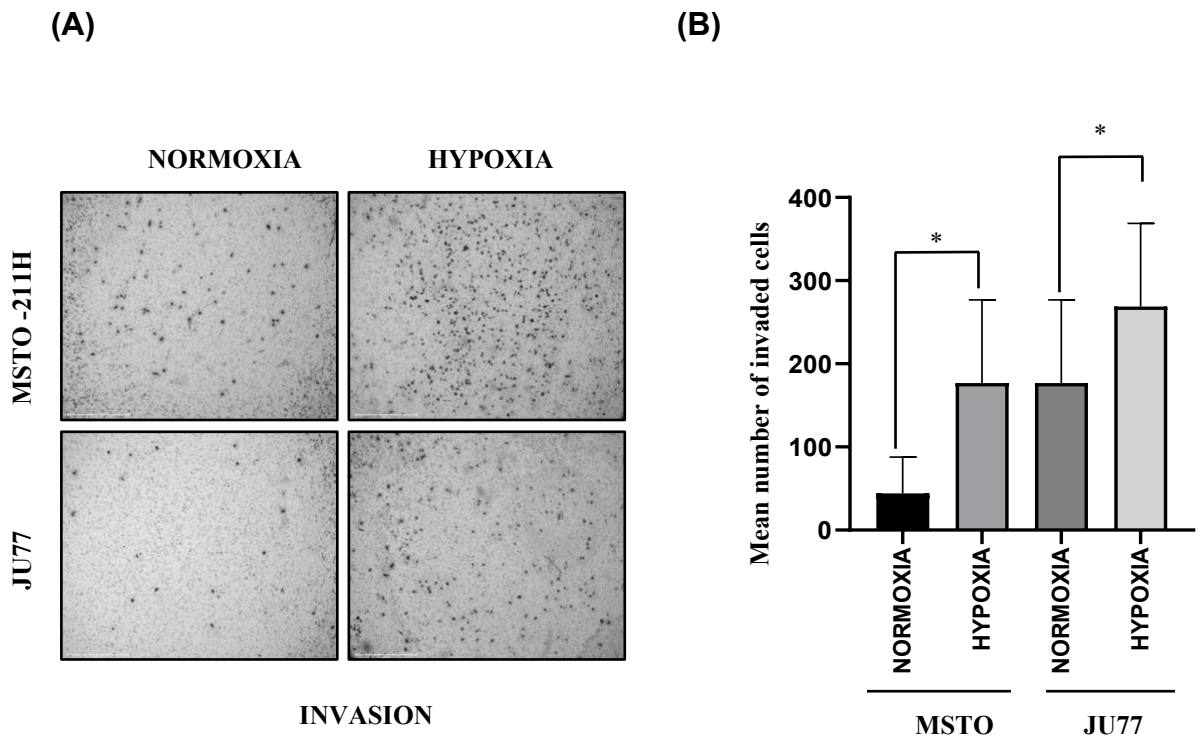

Figure 3.4 MM hypoxic cells shows increased migration.

*The potential of MM cells was detected using Matrigel invasion assay with Boyden inserts **(A)** Microscopic pictures of the invaded MM cells (40x magnification). **(B)** The bar chart is representing the mean number of invaded MM cells in hypoxia as compared to normoxia. n=12, *p<0.05*

3.4 Discussion

This study investigated the use of hypoxic cultures to mimic the hypoxic environment of tumour *in vivo* and to examine the chemoresistant potential of MM. It encouraged the study to investigate further if MM cells when subjected to the hypoxic environment can induce resistance and related properties in the fully differentiated neoplastic cells. The findings in this study indicate that cells in hypoxic conditions are more resistant and aggressive as compared to the cells in normoxic conditions. It also gives rise to speculation for the presence of cancer stem-like cells as the findings suggest that after initial treatment with first line drugs, the cancer cells subjected to hypoxia were still resistant. It further confirms the possibility of specialised residual cells, which can be CSCs leading to relapse of MM. This study also mimics the *in vivo* state in MM patients, who experience either resistance or relapse, as the first-line drugs are not capable to selectively target cancer stems like cells.

Hypoxia has implicated in resistance to multiple therapeutic modalities. As well as driving tumour progression through increased migration and dissemination, reduced apoptosis, and enhanced angiogenesis, hypoxia also links to treatment resistance through multiple mechanisms. The downstream processes driven by hypoxia can generate resistance to therapy, including EMT, aerobic glycolysis and autophagy (Redfern et al.,2019). Research also suggest that several hypoxia-inducible genes have the capacity to play an important role in promoting the breast to bone metastasis (Gikes.,2016). Hypoxia generates intra tumoural oxygen gradients, contributing to the plasticity and heterogeneity of tumours and promoting a more aggressive and metastatic phenotype (Jing et al.,2019). Although both acute and chronic hypoxia correlates with poor patient outcome and an aggressive tumour phenotype (Williams et al., 2001; Vaupel and Harrison, 2004). Acute hypoxia is found to be associated with

more aggressive tumour phenotype through the induction of spontaneous metastasis (Barbara Muz et al.,2015)

Hypoxia is a very dynamic and heterogenous feature and observed in many solid tumours. These hypoxic cells and hypoxia responsive mechanisms make these tumours resistant to both chemotherapy and radiotherapy leading to tumour progression (Zonneveld et al.,2019). Hypoxia induces activity and expression of MMP-2 and MMP-9 via HIF-1-dependent process, and increased levels of MMP-2 in breast cancer biopsies were associated with poor prognosis (Gikes.,2016). HIF-1α protects the tumour microvasculature from radiation-induced endothelial apoptosis during radiotherapy by inducing vascular endothelial growth factor (VEGF) and other pro-angiogenic factors and aid in the survival of tumour cell by increasing the antioxidant capacity of tumours to counteract radiation-induced oxidative stress. The irradiation further induces changes in the tumour microenvironment such as vascular, stromal, and immunological changes which may promote radioresistance and tumour recurrence. These effects eventually lead to the resistance of tumour cells to chemotherapy and radiation (Challapalli et al.,2017). The expression level of HIF-1α in oesophageal squamous cell carcinoma (ESCC) under hypoxic condition increased significantly, which boosted migration and invasion ability of ESCC (Jing et al.,2017). A meta-analysis of hypoxia-modifying modalities indicated that lowering tumour hypoxia increases treatment response and patient survival. To contribute to tumour regrowth after treatment or metastasis development, hypoxic cells must reoxygenate at some time (Zonneveld et al.,2019) A HIF-1α transcription factor is a central player in the hypoxic adaption of tumour cells, therapeutic resistance (Kim and Lee.,2017). HIFs coordinately regulate numerous signalling pathways in hypoxic cancer cells, which mediate invasive and metastatic phenotypes, including: (i) EMT pathway (ii)

basement membrane disruption and ECM remodelling, leading to intravasation; (iii) inhibition of anoikis (iv) extravasation (v) establishment of premetastatic niches (vi) transition from mesenchymal to epithelial phenotype for clonal expansion (Schito and Gregg.,2016). Therefore, hypoxia can induce many pathways and EMT is of utmost importance. The effect of this pathway on MM will be discussed in the next chapter. The findings in this chapter showed a remarkable effect of hypoxic condition on the cancer cell to become resistant to anticancer drugs. Many MM cancer patients experience relapse due to the development of chemoresistance, and this *in vitro* study indicated that conventional anti - MM drugs cannot eliminate highly resistant hypoxic MM cells.

CHAPTER 4

Hypoxia induces cancer stem cell and invasiveness related markers in malignant mesothelioma cell lines

4.1 Introduction

As discussed in the previous chapter hypoxia is a significant factor responsible for causing chemoresistance in MM cell lines. The underlying reason speculated to be is specialised cells that are resistant to all the therapies and termed as stem-like cells or cancer stem cells (CSCs). It is based on the findings that a small proportion (1%) of cancer cells possess typical stem cell markers, for example, CD133, Nanog, Oct4, Sox2 and ALDH and is shown to be responsible for tumour initiation (Clevers, 2011). Hypoxia in the stem cell and tumour microenvironment also promote CD133 expression via hypoxia-inducible factor-1α (HIF-1α) upregulation (Glumac and LeBeau.,2018). As a standard marker of CSCs, ALDH also possesses the responsibility to catalyse the oxidation of aldehyde, subsequently contributing to cellular homeostasis, which is identified to be related to the function as stem cells, such as self-renewal capability and stress-resistant properties (Xia et al.,2018).

The stemness status of CSCs is extremely microenvironment dependent as recent studies have indicated that hypoxia and some hypoxia-regulated transcription factors are the contributing factors for the stemness of CSCs (Conley et al., 2012). Hypoxia may be a major component of the CSCs niche, providing the CSCs with the maintenance of an undifferentiated state. The standard niche of hematopoietic stem cells (HSC) is hypoxic compared to other tissues, and normal HSCs represent a hypoxic population. Both normal bone marrow stem cells and normal brain stem cells are reported to reside in a hypoxic environment. Furthermore, human embryonic stem cells and adipocyte precursor cells differentiate unless cultured under hypoxic conditions (1–5% O_2) (Marie-Egyptienne et al.,2012).

HIFs target CSC-associated genes and mediate transcriptional responses to hypoxia during normal embryonic development, tumour growth, and stem cell differentiation (Yeo et al.,2017) Morel et al. showed that cancer cells possessing both stemness and tumorigenic characteristics of CSCs could be derived by EMT induction (Yeo et al.,2017). Moreover, CSCs has been shown to arise in part by EMT, and that hypoxia induced EMT lead the way to an increase in CSCs during tumour progression, which subsequently enhances invasion and metastasis (Yeo et al.,2017).

EMT is involved in cancer progression and metastasis, and HIF-1α has been identified as a regulator of EMT in human cancers. EMT can be adjusted by HIF, which regulates the expression and functional activity of principal transcription factors, including Twist, Snail, Slug, and ZEB1. Amongst which ZEB1 drives the induction of EMT with activation of stem cell traits, immune evasion and epigenetic reprogramming (Zhang et al.,2019). The promoter region of twist holds an HRE, which can be bound by HIF. Hypoxic microenvironment induces EMT master regulators that encourage EMT changes, such as E-cadherin attenuation by Snail up-regulation, and besides matrix metalloproteinase (MMP) production through activation of Slug (Yeo et al.,2017). Research has also suggested that hypoxia and HIF-1α upregulate the expression levels and activities of MMP-2 and MMP-9. Collagen is vital for cell migration during the invasion. When tumour size increases, collagen fibers straighten and align, which facilitates cancer cell invasion (Gao et al.,2016).

In addition to EMT, cancer stemness plays a role in metastasis and treatment resistance, which are associated with poor prognosis (Yeo et al.,2017). Hypoxia is also a significant factor for the development of tumour cell resistance to therapy, which is in part due to the generation of cancer stem cells (CSCs) (Terry et al.,2018). Hypoxia

is not only a significant feature of the tumour microenvironment but is also a potential contributor to the multidrug resistance (MDR) and enhanced tumorigenicity of CSCs (Ibrahim et al.,2018). Both EMT and stemness are linked with resistance to chemotherapy in tumours. ABC transporter genes included in chemoresistance can be upregulated by EMT-inducing transcription factors, such as Twist, Snail, and Slug, by their ability to induce EMT. The EMT process plays a role in generating the stem cell phenotype, and expression of CD44 or CD133 stemness genes confers chemoresistance (Yeo et al.,2017).

Among ABC transporters that are well known to cause MDR, ABCG2 is particularly interesting for its potential role in protecting cancer stem cells (Jian and Zhang et al.,2012). Many genes implicated in various processes are critical for cancer progression (such as angiogenesis, epigenetic changes, erythropoiesis, pH regulation, glycolysis, metastatic spread and undifferentiated phenotype) are affected by these transcription factors. Therefore, hypoxia, by modifying critical molecular pathways, allows the survival and proliferation of tumour cells under harsh conditions creating hypoxia tolerance. The highly dynamic hypoxic gradients in tumours provoke the manifestation of diverse mechanisms which can promote stemness, metastasis and treatment resistance (Marie-Egyptienne et al.,2012).

CSCs may indicate the microenvironment-dependent heterogeneity and EMT within tumour tissues. Although the role of CSCs in tumorigenesis is still debatable, the cancer cells expressing stem cell markers are widely accepted as highly resistant to radio and chemotherapy and are the sources of cancer recurrence. Also, the cells with CSC markers are resistant to all dissimilar anticancer drugs. Remarkable expression of the embryonic stem cell-associated genes Sox2, Oct4, and Nanog haven been

detected in the resistant cell line (Conley et al., 2012). CSCs possess the critical survival mechanisms and properties crucial for the maintenance and propagation of the tumour (Marwa M.,2018). Although CSCs are very small in number, they are believed to possess pluripotent and self-renewal capacity, which generates a heterogeneous cell population of the originating tumour, seeding at distant sites and driving the formation of macro metastasis (Han.,2015). We hypothesised that the hypoxic microenvironment/stress of the tumour is responsible for maintaining stemness in CSCs. This study aims to replicate the hypoxic tumour environment *in vitro* and elucidate the causal relationship between hypoxia and CSCs and EMT status in MM cell lines.

4.2 Materials and Methods

This section describes methods used for this and specifies any observed changes concerning the general detailed methods explained in chapter 2.

4.2.1. Culture Methods

In this study, two MM cell lines, MSTO-211H and JU77 were established as mono-layered cultures and maintained following standard subculture methods. Additionally, attached mono-layered cell line cultures incubated under hypoxia. Cell lines cultured using RPMI were seeded at a density of ~5×10^4 cells/mL and incubated using tissue culture incubators maintained at 37ºC, 5% CO2, 1% O_2, for four days.

4.2.2. Detection of CSC markers

The expression of CSC markers, i.e. CD 133, ABCG2, ALDH and CD 24 was measured by Flow cytometry technique in MM MSTO-211H and JU77 cell lines. A comparison made between hypoxic and normoxic cultures, respectively. The detailed methods are detailed in chapters 2.2.10 respectively.

4.2.3. Detection of ESC markers

Quantitative RT-PCR method used to determine the mRNA expression of SOX2, OCT4 and NANOG in MM MSTO-211H and JU77 cell lines and a comparison was made to the normoxic and hypoxic cell cultures, respectively. The RT-PCR procedure followed as detailed in chapter 2.2.9 respectively.

4.2.4. Detection of EMT and invasiveness related markers

Quantitative RT-PCR method used to determine the mRNA expression of EMT markers, i.e. Snail, Zeb, Slug, Twist, E-Cadherin, N-cadherin, Vimentin and invasiveness markers MMP-2, MMP-7, MMP-9 in MM MSTO-211H and JU77 cell lines and a comparison was made to the normoxic and hypoxic cell cultures, respectively. The RT-PCR procedure followed as detailed in chapter 2.2.9, respectively.

4.3 Results

4.3.1. Hypoxia-cultured MM cells express CSC markers

MM cells exposed to hypoxic conditions developed stress-induced alterations such as expression of CSC characteristics. MM cell lines MSTO-211H and JU77 were incubated at 37℃, 5% CO2, and <1% O2 for four days respectively to study the effect of hypoxia on CSC markers. Flow cytometry analysis of hypoxic MM cells, is shown in figure 4.1, compares the expression level of ABCG2, CD 24 and CD 133. Both the cell lines MSTO-211H and JU77 show a statistically significant increase in the cells incubated under hypoxia as compared to normoxia.

(A)

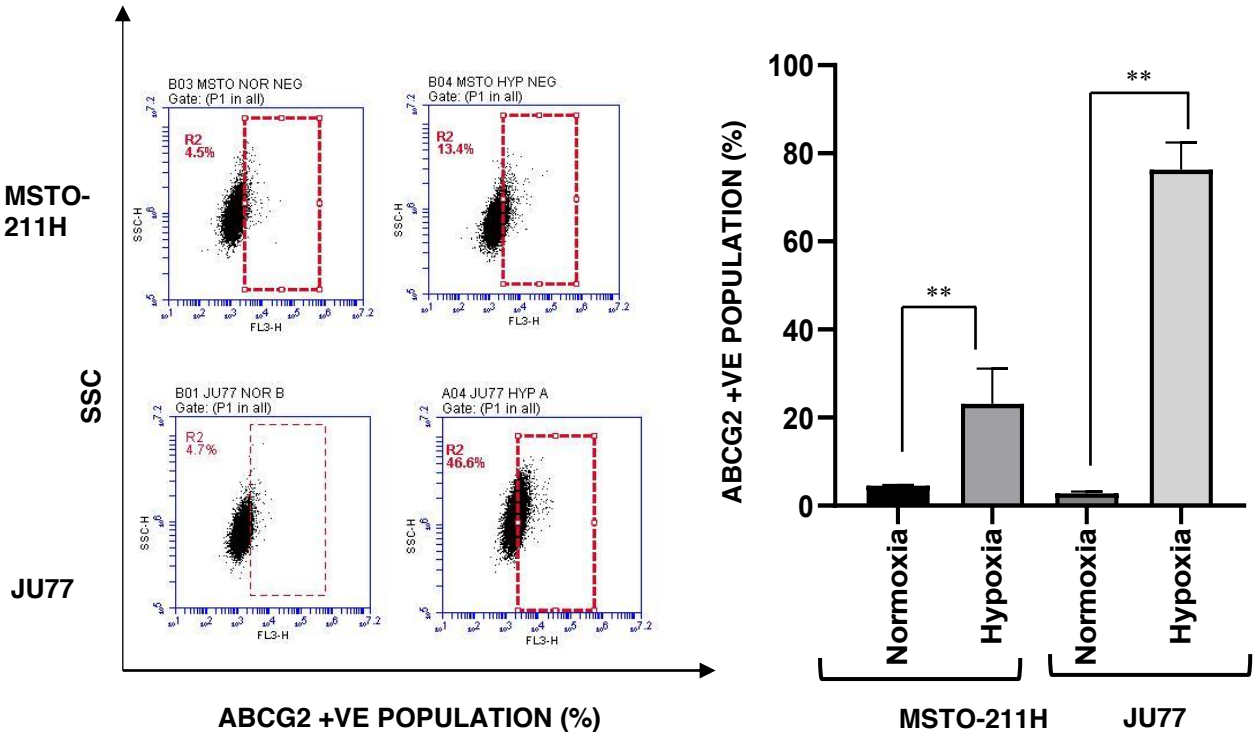

(B)

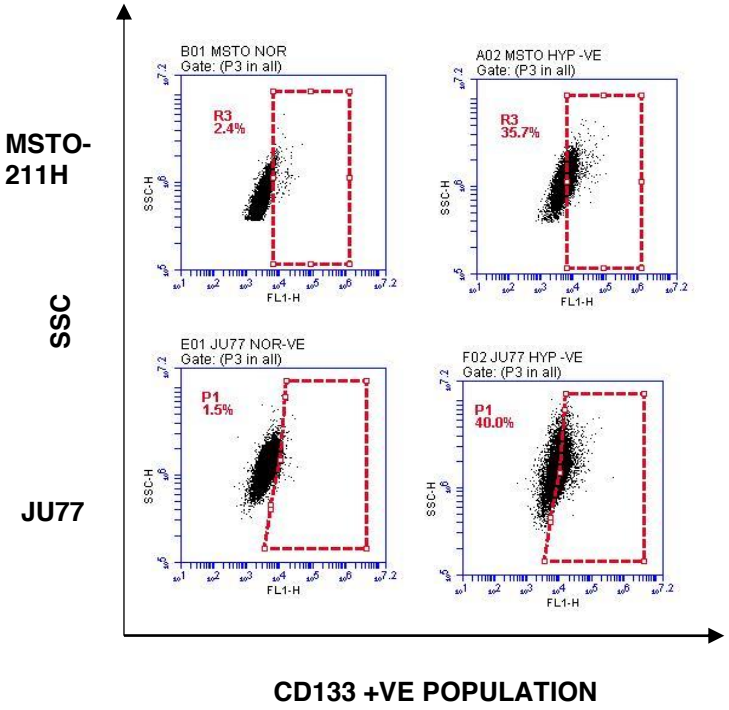
MSTO-211H
JU77
SSC
B01 MSTO NOR
Gate: (P3 in all)
R3
2.4%
A02 MSTO HYP -VE
Gate: (P3 in all)
R3
35.7%
E01 JU77 NOR-VE
Gate: (P3 in all)
P1
1.5%
F02 JU77 HYP -VE
Gate: (P3 in all)
P1
40.0%
SSC-H
FL1-H
CD133 +VE POPULATION

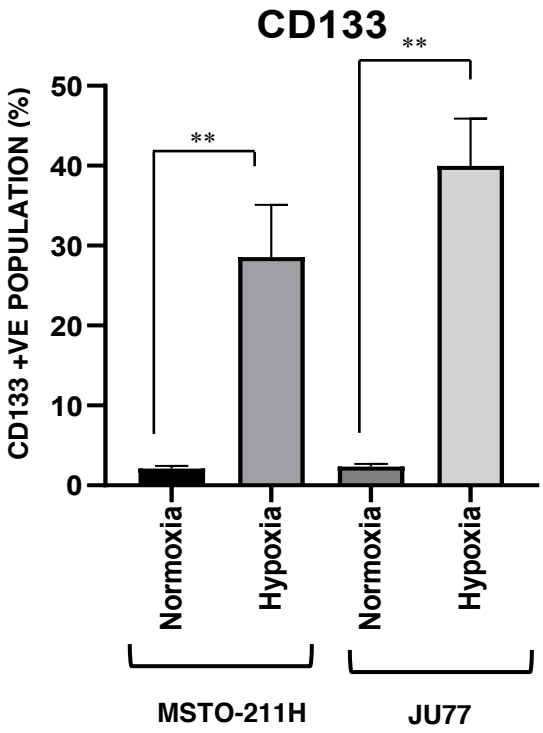
CD133
CD133 +VE POPULATION (%)
50
40
30
20
10
0
**
**
Normoxia
Hypoxia
Normoxia
Hypoxia
MSTO-211H
JU77

(c)

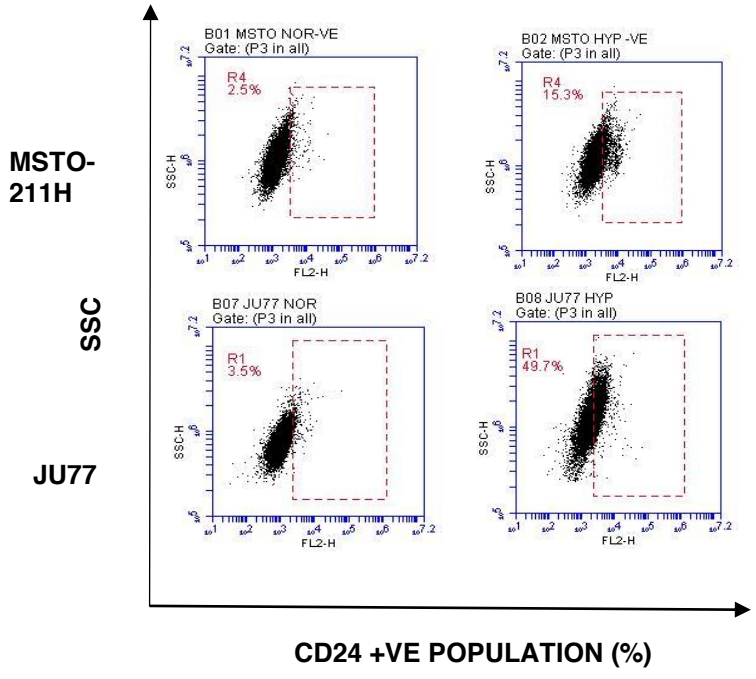
MSTO-211H
JU77
SSC
B01 MSTO NOR-VE
Gate: (P3 in all)
R4
2.5%
B02 MSTO HYP -VE
Gate: (P3 in all)
R4
15.3%
B07 JU77 NOR
Gate: (P3 in all)
R1
3.5%
B08 JU77 HYP
Gate: (P3 in all)
R1
49.7%
SSC-H
FL2-H
CD24 +VE POPULATION (%)

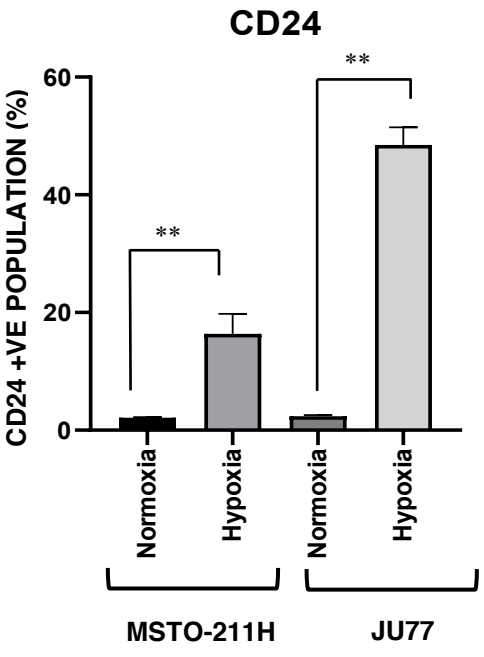
CD24
CD24 +VE POPULATION (%)
60
40
20
0
**
**
Normoxia
Hypoxia
Normoxia
Hypoxia
MSTO-211H
JU77

Figure 4.1 MM cells in hypoxic microenvironment demonstrate increased CSC characteristics.

*The expression level of CSC markers was analysed by using flow cytometry in MSTO-211H and JU77 cell lines. (A) ABCG2 using APC conjugated anti-ABCG2 (B) CD 133 using FITC conjugated anti-CD133 (C) CD 24 using PE-conjugated anti-CD24. n=6, **p<0.01.*

4.3.2 Hypoxia-cultured MM cells show increased ESC expression.

MM cells exposed to hypoxia developed cancer stem cell characteristics which were further confirmed by expression of ESC markers such as SOX-2, Nanog and OCT 4. MM cell lines MSTO-211H and JU77 incubated at 37℃, 5% CO2, and <1% O2 for four days respectively to study the effect of hypoxia on CSC markers. The qRT-PCR analysis technique was used to compare the relative mRNA expression level of SOX2, Nanog and OCT4 of hypoxic and normoxic cultures shown in figure 4.2. Both the cell lines MSTO-211H and JU77 shows a statistically significant increase in the expression level of Nanog, whereas SOX-2 showed an insignificant increase in the expression level in both MSTO-211H and JU77 cell line when MM cells were compared between normoxic and hypoxic conditions respectively.

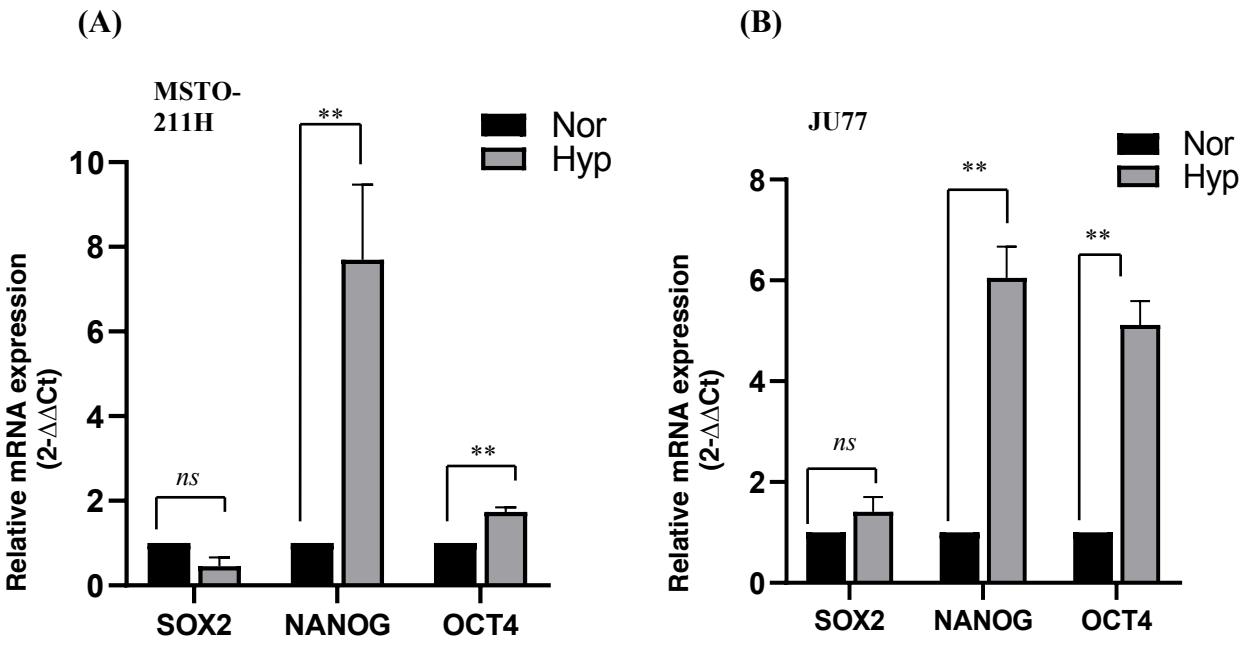

Figure 4.2 MM hypoxic cultures demonstrates increased of Nanog but decrease in SOX-2 expression.

*The relative mRNA expression of ESC markers SOX2, OCT4, NANOG was analysed in (A) MSTO-211H (B) JU77 cell lines, using RT-PCR 2-ΔΔCt method. n=4, **p<0.01, ns denotes no- significance (p ≥ 0.05)*

4.3.3 Hypoxia-cultured MM cells show increased expression of EMT markers

The increased expression level of Epithelial to Mesenchymal transition (EMT) and related markers such as Snail, Slug, Twist, Zeb, E-cadherin, N-Cadherin and Vimentin were compared between MM cells in the hypoxic and normoxic microenvironment. MM cell lines MSTO-211H and JU77 cell lines were incubated at 37℃, 5% CO2, and <1% O2 for four days respectively in hypoxic conditions. The qRT-PCR analysis

technique used to compare the relative mRNA expression level of EMT related markers in figure 4.3. Both the cell lines MSTO-211H and JU77 shows statistically increased expression level of Snail 1, Twist 1, Zeb,1 N-cadherin and Vimentin in hypoxia. MSTO-211H cell lines showed a non-significant increase in Snail 2, and there was no expression of for E-cadherin. Whereas JU77 cell line showed a decreased expression level of E-Cadherin when the two cell lines were compared to normoxic and hypoxic conditions, respectively.

(A)

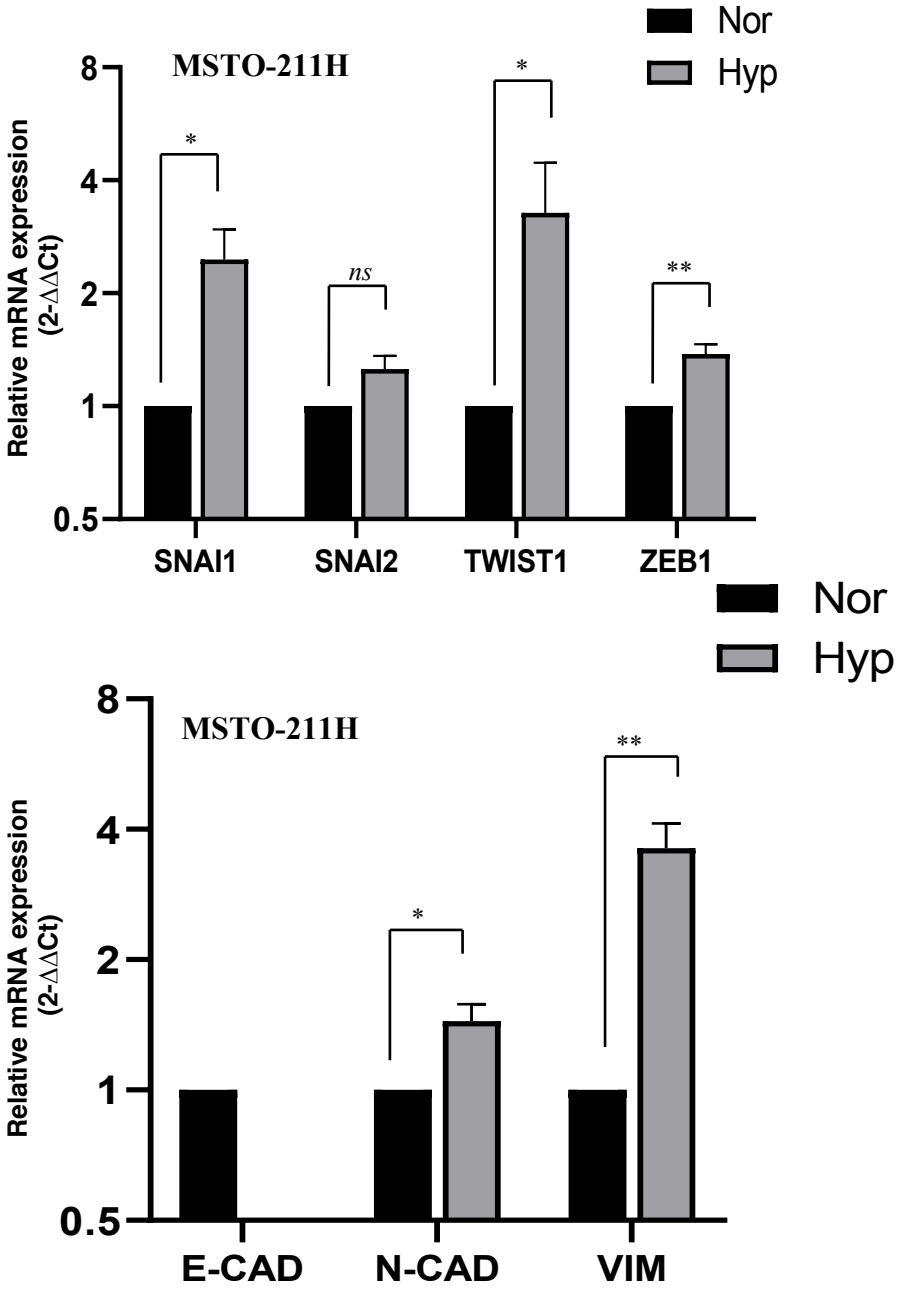

(B)

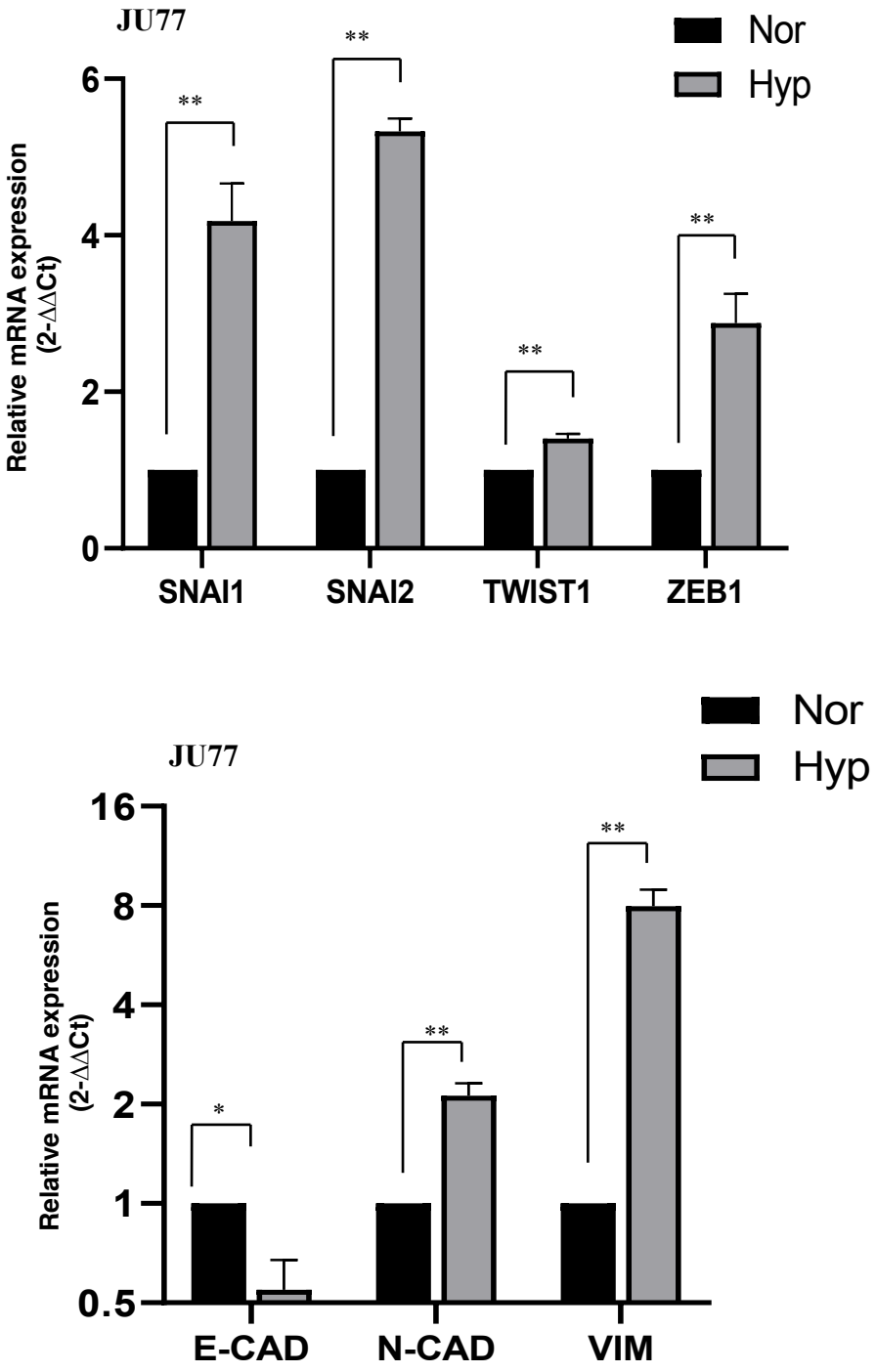

Figure 4.3. MM hypoxic cultures demonstrates increased expression of EMT markers but decrease in the expression of E - Cadherin.

*The relative mRNA expression of invasion related markers, i.e. Snail 1. Snail 2, Twist, Zeb 1, E cad, N cad and Vimentin, were analysed in (A) MSTO -211H (B) JU77 cell lines, using RT- PCR 2-ΔΔCt method. n=4, **p<0.01, *p<0.05, ns denotes no - significance (p ≥ 0.05).*

4.3.4 Hypoxia-cultured MM cells show increased expression of invasiveness related genes

The expression level of invasiveness related markers such as MMP-2, MMP-7 and MMP-9 was compared between MM cells in hypoxic and normoxic microenvironment. MM cell lines MSTO-211H and JU77 were incubated at 37℃, 5% CO_2, and <1% O_2 for four days respectively in hypoxic conditions. qRT-PCR analysis technique was used to compare the relative mRNA expression level of invasion related markers in figure 4.3. Both the cell lines MSTO-211H and JU77 shows statistically significant increase in the expression level of MMP2, and MMP-9, whereas MSTO-211H showed non-significant increase in MMP-7, in hypoxia as compare to normoxia respectively.

(A)

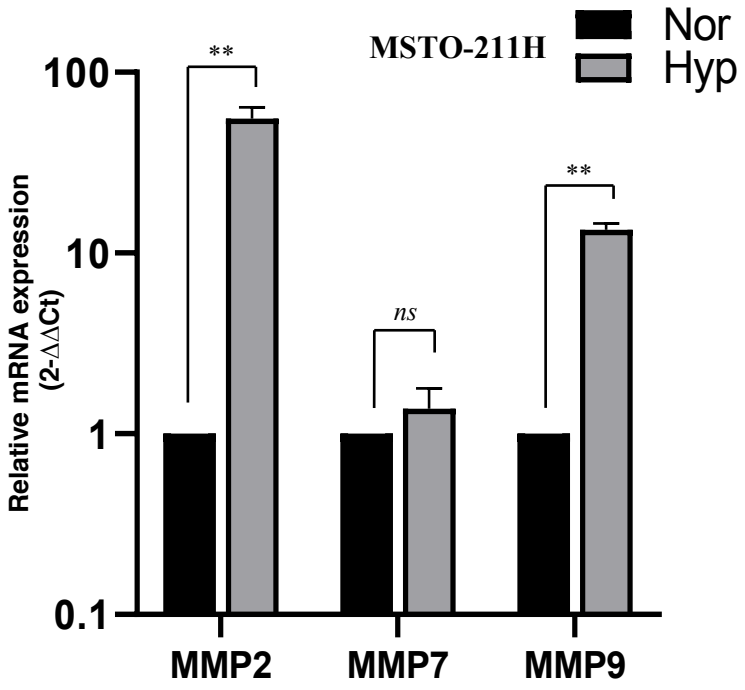

(B)

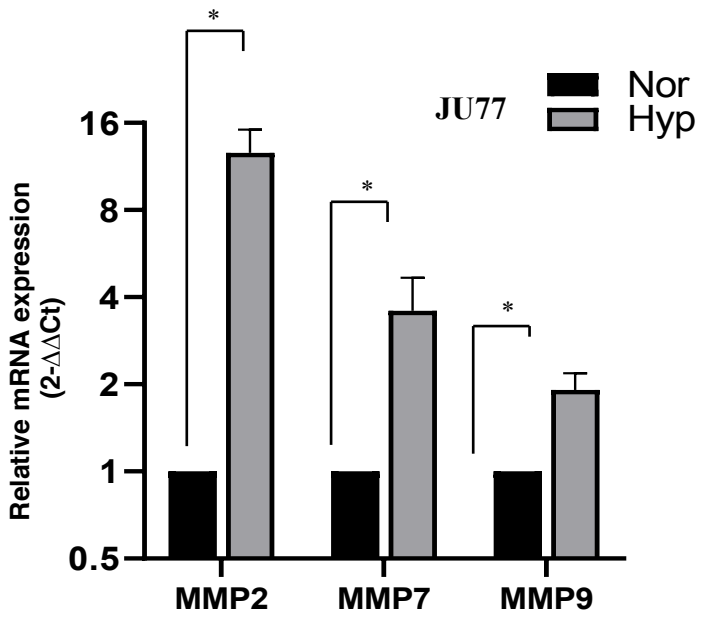

Figure 4.4. MM hypoxic cultures demonstrates increased expression of invasiveness related markers.

The relative mRNA expression of invasion related markers i.e. MMP-2, MMP-7 and MMP-9 were analyzed using RT- PCR $2^{-\Delta\Delta Ct}$ *method. n=4, **p<0.01, *p<0.05, ns denotes no - significance (p ≥ 0.05).*

4.4. Discussion

This study demonstrated the effects of hypoxia on the expression level of CSC and EMT pathway-related markers in MM. The experimental conditions mimicked tumour microenvironment in acute and hypoxic conditions. The results confirm that hypoxia induces significant changes on the molecular level and increases the expression of CSC, ESC and EMT related markers. CSCs are capable of uncontrolled self-renewal and metastasis, chemoresistance and tumour recurrence (Marwa M.,2018) Hepatocellular Carcinoma (HCC) has shown that hypoxia induce EMT transition, a typical character of CSCs involving in metastasis (Wang et al., 2017)

Tumours are "abnormal organs" encouraged by a CSC, enriched with the capacity to self-renew and with multipotent differentiation capacity to yield a heterogeneous cell progeny (Montreo et al.,2018). In this study, we showed the increased expression of CD133, ABCG2 and CD 24 in hypoxic conditions as these markers have shown a prominent role in maintaining stemness in CSCs. The expression of CD133 on the cell surface is known to be a specific marker for CSCs in several malignancies (Barzegar et al.,2019). Studies have also shown that CD24 expression induces increased cell proliferation, migration, and invasion, leading to rapid tumour spread, properties fostered by the EMT program and stemness capabilities (Montreo et al.,2018).

Among ABC transporters that are well known to cause multidrug resistance (Mo and Zhang.,2012). High expression levels of ABC transporters and aldehyde dehydrogenase (ALDH) may also cooperate in the development of drug resistance in CSCs (Wang et al., 2018). Drug resistance is associated with expression of various pluripotency markers, including NANOG, OCT4, and SOX2, since these genes further lead to a decrease in differentiation status (Weina and Utikal.,2014) Poorly

differentiated tumours shows preferential overexpression of genes usually enriched in embryonic stem cells, such as downstream targets of Nanog, Oct4 and Sox2 (Ben-Porath et al., 2008). Oct4 is most crucial transcription factor since it can reprogram adult stem cells to induced pluripotent cells (iPS) cells as an individual factor. Aberrant expression of Oct4, Nanog, and Sox2, is associated with abnormal tissue growth or tumorigenesis (Kumar et al.,2012) Sox2 is also linked to stemness through modulation of Oct4 levels in CSCs (Sun et al.,2019). This might also explain the decreased level of SOX 2 and insignificant increase of Oct 4 in MSTO-211H cell lines. Nanog regulates several aspects of cancer development such as tumour cell proliferation, self-renewal, motility, epithelial-mesenchymal transition, immune evasion, and drug-resistance, which are all defined features for cancer stem cells (Wang et al.,2013). EMT transcription factors and regulators transform the cancer cells from epithelial-cell like to mesenchymal-cell like by suppressing epithelial markers and upregulating mesenchymal markers. It leads to cancer metastasis, drug resistance and features of cancer stem cells.

Furthermore, the cancer cells undergoing EMT show increased resistance to apoptosis and chemotherapeutic drugs and traits expressed by stem cells (Shih and Yang.,2011). EMT initiated by overexpression of specific proteins, e.g. Snail, Slug, twist, and ZEB (1and 2) in cells which have been observed in progression from in situ to invasive forms (Grzegrzolka et al.,2015). EMT can also be defined by events such as the formation of specific epithelial cells, degradation of the basement membrane, disruption of epithelial tissue constitution, and development of a novel mesenchymal form (Koujan et al.,2015). The hallmark of EMT in cancer is the downregulation of E-cadherin, which is thought to be a repressor of invasion and metastasis. Several transcription factors are implicated within the transcriptional repression of E-cadherin,

including zinc finger proteins, Snail, Slug, Zeb1, and Zeb2 (Shih and Yang.,2011) In breast cancer cells, many studies have demonstrated that hypoxia leads to an increased expression of two transcriptional repressors of E-cadherin, SNAIL1 and SLUG, by the modulation of NOTCH1 signaling pathway (Gikes.,2016)

Fusion oncogenes generated as a result of chromosomal abnormalities associated with mesenchymal tumours block differentiation and have the ability to activate target genes such as Slug (also known as Snail-2, which promotes survival and migration of the defective target cells into different environments (Mancera et al.,2005). Slug enhances chemoresistance of several types of cancer, including malignant mesothelioma (Shih and Yang.,2011). The expression of Slug is linked to cancer stem cell formation, cell cycle regulation and apoptosis as well as invasion and metastasis (Wu et al.,2012) TWIST is also a predominant regulator of EMT, involved in the promotion of cellular differentiation, motility, and proliferation, and is associated with cancer stem cell phenotype (Grzegrzolka et al.,2015). HIF-1α has also shown direct binding to TWIST by HRE in the TWIST proximal promoter in hypopharyngeal and breast cancer cell lines (Tam et al.,2020) Snail, another gene studied in this study is a zinc-finger transcription factor, triggers EMT providing epithelial cells with migratory and invasive properties by both embryonic development and tumour progression (Vega et al.,2004) Snail mediates an increase in expression of mesenchymal markers such as vimentin, and matrix metalloproteinases (MMPs) (Smith and Mrah.,2012). Snail and ZEB also suppress other epithelial markers and activate mesenchymal genes (Cho et al.,2019).

Zeb-1 acts as an oncogene in metastatic and invasive lung cancer cells, in which ZEB1-induced EMT enhanced the loss of epithelial cell adhesion and polarity, induces

drives growth and cytoskeleton remodelling, migration, metastasis, and invasion (Zhang and Han.,2019). Vimentin's overexpression in cancer correlates well with increased tumour growth, invasion, and poor prognosis (Satelli and Li,2011) N-cadherin, as a marker of ongoing EMT, is not expressed in normal epithelial cells. However, its expression has demonstrated in several forms of carcinomas. Aberrant N-cadherin expression is related to various processes in tumour metastasis, such as angiogenesis, heterotypic adhesion, and invasion (Zhan-qi et al.,2019).

MMP's are capable of cleaving type IV basement membrane collagen (MMP-2 and -9) and add value for drug development (Brehmer et al.,2003). MMP-7 can deteriorate laminin, type IV collagen, and entactin, which are the main element of the basement membrane, and activate other important MMPs (MMP-1, MMP-2, and MMP-9)(Bavi et al.,2011) MMP-2 and MMP-9 are related to tumour invasion and metastasis and involved in tissue remodelling by ECM as well as basement membrane degradation and induction of angiogenesis. Thus, MMP-9, together with MMP-2, activate transforming growth factor β (TGF-β) signalling to promote the invasion of the tumour, angiogenesis, and metastasis (Gialeli et al.,2011). Although MMP-2 is mainly responsible for the regulation of inflammatory response, MMP-7 takes part in the degradation of the peritumoral stroma whereas MMP-9 may have an impact on the formation of the new blood vessels (Pryczynicz et al.,2016) Hypoxia induces activity and expression of MMP-2 and MMP-9 via HIF-1-dependent process, and increased levels of MMP-2 in breast cancer biopsies were associated with poor prognosis (Gikes.,2016).

Hypoxia is a major factor responsible for chemoresistance. This study confirms the elevated expression of CSC markers, metastasis and invasion related markers in

correlation with hypoxia. Studies have demonstrated the role of CSCs in the growth of tumours and inducing resistance to chemotherapeutic drugs and radiation therapy. Hence, the detection and targeting of CSCs could be examined as a therapeutic strategy in the future (Barzegar et al.,2019). It is highly convincing that tumour recurrence can be prevented if CSCs are specifically targeted. Development of drugs to target and eliminate CSCs represents a major challenge since they are resistant to all modes of conventional therapies (Jagupilli and Elkord.,2012)

This study demonstrated that hypoxia-induced CSC, ESC and EMT characteristics in MM cell lines. These characteristics are responsible for causing chemoresistance in MM. The next chapter will demonstrate the effect of Pemetrexed, Cisplatin, PLGA-DS and their combination on the above-studied markers.

CHAPTER 5

PLGA-DS and copper targeted MM CSCs, reversed chemoresistance and blocked MM cell invasiveness *in vitro*

5.1 Introduction

MM treatment is not guided by histological or molecular features of the tumour. It mainly depends on the clinical stage and patient characteristics. Moreover, there are no other approved regimens for relapsed or refractory MM, as platinum-based chemotherapies have also failed to show improvements in survival benefits. There is no alternative when MM patients fail this treatment option as the combination confers a median progression-free survival (PFS) of 5.7 months (Porpodis et al., 2013). Moreover, the overall response rate of combination chemotherapy is approximately 40%; almost half of all the patients are primary resistant, and all develop resistance ultimately (Kim et al.,2018). As discussed earlier, CSCs may reflect the microenvironment-dependent heterogeneity and epithelial-mesenchymal transition within tumour tissues. Although the role of CSCs in tumorigenesis is still debatable. But it is widely accepted that the cancer cells expressing stem cell markers are highly resistant to radio and chemotherapy and are the sources of cancer recurrence. Also, the cells with CSC markers are immune to all different anticancer drugs (Conley et al., 2012). Chapter 3 and 4 demonstrated that hypoxic stress stimulated the expression of CSC traits and significantly induced chemoresistance.

Given the high costs and time duration for producing new medicines, the repurposing of already existing drugs to combat both rare and common disease is an attractive approach (Pushpakom et al., 2019). The anticancer activity of DS was reported as early as 40 years ago, since then DS is widely considered as a strong candidate for repurposing due to its relatively good safety profile and reasonable financial cost (Li et al., 2015). DS repurposing is considered as an anticancer medication to decrease

tumour development as a consequence of high-throughput cell-based drug screening (Turanli et al., 2018). Despite its diverse range of pharmacologic activities, prolonged treatment with DS has negligible, reversible, adverse effects and is considered a safe drug (Rae et al., 2013). But the major drawback of DS is that it instantly reduces to DDC in the bloodstream *in vivo*, which is also very unstable and promptly converted into the irreversible downstream metabolites. Till date, various studies have successfully entrapped DS by different formulations in vitro and *in vivo* to achieve high antitumour efficacy. However, these systems could not trap DS with high drug load and also, they were not apt for the treatment of lung cancers, due to their low delivery ability to lungs in oral or intravenous administration (Wang et al., 2017). Our previous publication demonstrates that the new formulation significantly improves the half-life of DS. Our group developed a PLGA encapsulated DS. The PLGA-DS plus Copper showed very promising anticancer efficacy in liver cancer mouse model (Wang et al., 2017). These encouraging results prompted me to examine the cytotoxic effect of PLGA-DS and Copper (Cu) in MM cell lines.

The research aims to establish the cytotoxicity of PLGA-DS on MM cell lines in conjunction with Cu. We previously identified that hypoxic stress promotes CSC characteristics and chemoresistance in MM. This study will examine the ability of PLGA-DS/Cu to inhibit CSC traits leading to reversed chemoresistance. It will also confirm if PLGA-DS/Cu can synergistically enhance the cytotoxicity of conventional anti-MM drugs. To direct our in vivo MM analysis and potentially transform PLGA-DS into MM patient care, this research aims to provide preliminary in vitro cytotoxicity results.

5.2 Materials and Methods

In this analysis, the following section explains the primary methods used and defines any methodological improvements in comparison to the broadly comprehensive methods described in Chapter 2.

5.2.1 Detection of CSC markers

Flow cytometric analysis was used to measure the presence of CSC markers such as CD24, CD133 and ABCG2 after treatment with PLGA-DS (500 nM) in combination with CuCl2 (10 μM) for 24 hours in MM MSTO-211H and JU77 cell lines hypoxic cultures, respectively. A comparison was made between hypoxic and normoxic cultures, respectively. The detailed methods of staining and detection are detailed in chapters 2.2.10.

5.2.2. Sphere reformation assay

The MM MSTO-211H and JU77 spheroid cultures we subjected to sphere reformation assay as detailed in chapter 2.2.6. The specific drugs and doses used in this study are as follows: Cu (10 μM), CIS (10μM) PMT (1μM), PLGA-DS (1μM), and PLGA-DS in combination with CuCl2 (PLGA-DS/Cu). The spheroid cultures were treated for 48 hrs. at 37°C, 5% CO_2. After treatment, the samples were seeded at a low cell density in drug-free medium and incubated for seven days. The total numbers of spheres formed were manually counted, and images were taken at 4× magnification.

5.2.3 Migration Assay

The MM MSTO-211H and JU77 hypoxic cell cultures were subjected to migration assay as detailed in chapter 2.2.11. The hypoxic MSTO-211H and JU77 cell lines were seeded in Boyden chamber with nutrient-deprived RPMI medium whereas the chamber has surrounded by nutrient-rich RPMI medium containing PLGA-DS/Cu (25nM/10 μM). The plate was then incubated in hypoxia for 24 hours at 37 ºC. After incubation, the cells were fixed and stained with crystal violet; the number of stained cells were counted manually. The comparison of the number of migrated cells in hypoxia was compared to normoxia and hypoxia PLGA-DS/Cu, followed by statistical analysis.

5.2.4 Invasion Assay

The MM MSTO-211H and JU77 hypoxic cell cultures were subjected to invasion assay as detailed in chapter 2.2.12. The hypoxic MSTO-211H and JU77 cell lines were seeded in Boyden chamber with nutrient-deprived RPMI medium, whereas the chamber was surrounded by nutrient-rich RPMI medium containing PLGA-DS/Cu (25nM/10μM). To study the effect of MMP's on basement membrane degradation, in MM cell lines, the bottom of the chamber was coated with matrigel, which acts as collagenase/ECM *in vitro*. The plate was then incubated in hypoxia for 24 hours at 37 ºC. After incubation, the cells were fixed and stained with crystal violet; the number of stained cells were counted manually. The comparison of the number of invaded cells in hypoxia, normoxia and hypoxia PLGA-DS/Cu was compared, followed by statistical analysis.

5.2.5. Detection of ESC markers

Quantitative RT-PCR method was used to determine the mRNA expression of SOX2, OCT4 and NANOG in PLGA-DS/Cu treated MM MSTO-211H and JU77 cell lines. The hypoxic MM cells were treated with PLGA-DS/Cu (500nM/10μM) for 24 hrs and a comparison made to the hypoxic and PLGA-DS/Cu treated cell cultures, respectively. The RT-PCR procedure was followed as detailed in chapter 2.2.9. respectively.

5.2.6 Detection of EMT and invasiveness related markers

Quantitative RT-PCR method was used to determine the mRNA expression of EMT markers, i.e. Snail, Zeb, Slug, Twist, E-Cadherin, N-cadherin, Vimentin and invasiveness markers MMP-2, MMP-7, MMP-9 in MM MSTO-211H and JU77 cell lines. The hypoxic MM cells were treated with PLGA-DS/Cu (500nM/10μM) for 24 hrs. And comparison was made to the hypoxic and PLGA-DS/Cu treated cell cultures, respectively. The qRT-PCR procedure was followed as detailed in chapter 2.2.9. respectively.

5.2.7 MTT cytotoxicity assay

The MM MSTO-211H and JU77 normoxic and hypoxic cultures were subjected to MTT cytotoxicity assay as detailed in section 2.2.13. The first-line drugs for treating MM and highest doses used in this study are as follows: PMT (1μM), CIS (10μM), PLGA-DS (1μM) and (PLGA-DS/Cu) (1μM/10 μM)) as a combination. The cell cultures were incubated with serially diluted anti-MM drugs for 72 hours and placed

in their respective cell culture incubators. After the treatment, cells were treated with MTT reagent, and percentage cell viability was calculated.

5.2.8. Isobologram analysis

To measure the synergistic effect of the first line anti-MM drugs in combination with PLGA-DS/Cu, isobologram analysis was used. Hypoxic-cultured cell lines were seeded as described for the MTT cytotoxicity assay. Three serial drug dilutions were performed for each experiment as follows; anti-MM drug alone, PLGA-DS/Cu alone and anti-MM drug in combination with PLGA-DS/Cu. For analytical purposes this study required drugs to be added in a ratio of 1:1 or 1:10; the specific drugs and highest doses used were as follows: PMT (1μM), CIS (10μM), PLGA-DS (1μM) with copper supplementation at a consistent concentration of 10 μM. Cells were incubated in a drug-containing medium for 72 hours. After incubation, measurement of cell cytotoxicity was determined as above for the MTT assay, and the results were used to determine combination index (CI) using Calcusyn^{TM} software as detailed in chapter 2.2.13

5.3 Results

5.3.1. PLGA-DS/Cu inhibits CSC markers in hypoxic culture.

The expression of CSC markers was induced by MM hypoxic cultures and were subjected to PLGA-DS in combination with copper. The flow cytometric analysis determined the expression levels of CSC markers, i.e. CD133, ABCG2 and CD24, as shown in Figure 5.1. MSTO-211H and JU77 hypoxic cultures showed a significant reduction in the expression of positive CSC population after treating with (500 nM) in combination with $CuCl_2$ (10 μM). The results indicate that the treatment with PLGA-DS/Cu inhibits hypoxia-induced CSC traits. The cytotoxicity of PLGA-DS/Cu on normoxia and hypoxic MM cells were determined using MTT assay. The IC 50 table 5.1 shows cytotoxic response of normoxia and hypoxia-cultured MM cell lines to PLGA-DS/Cu treatment. Additionally, MTT assay determined that a very low concentration of PLGA-DS/Cu in combination with copper is required to show its cytotoxic effect on MM hypoxic cultures.

(A)

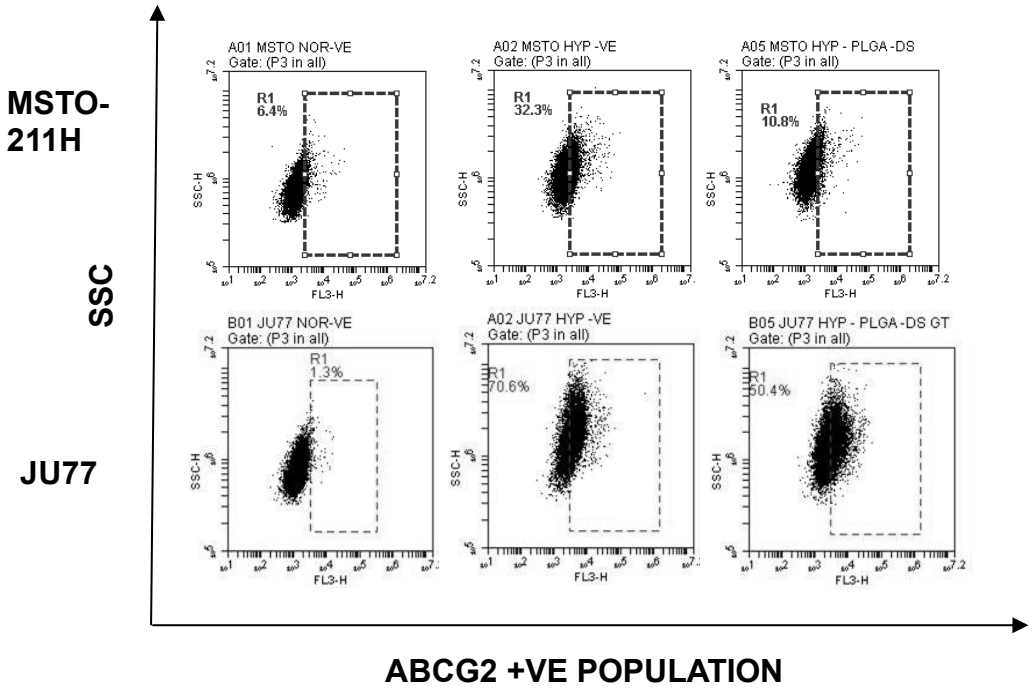
MSTO-211H
JU77
SSC
A01 MSTO NOR-VE
Gate: (P3 in all)
R1
6.4%
A02 MSTO HYP -VE
Gate: (P3 in all)
R1
32.3%
A05 MSTO HYP - PLGA -DS
Gate: (P3 in all)
R1
10.8%
B01 JU77 NOR-VE
Gate: (P3 in all)
R1
1.3%
A02 JU77 HYP -VE
Gate: (P3 in all)
R1
70.6%
B05 JU77 HYP - PLGA -DS GT
Gate: (P3 in all)
R1
50.4%
SSC-H
FL3-H
ABCG2 +VE POPULATION

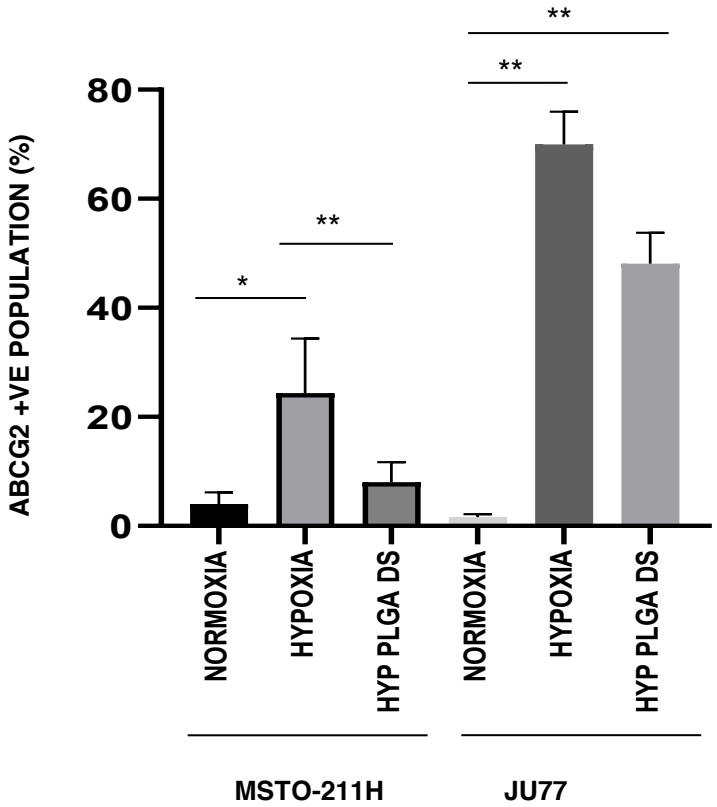
ABCG2 +VE POPULATION (%)
80
60
40
20
0
*
**
**
**
NORMOXIA
HYPOXIA
HYP PLGA DS
NORMOXIA
HYPOXIA
HYP PLGA DS
MSTO-211H
JU77

(B)

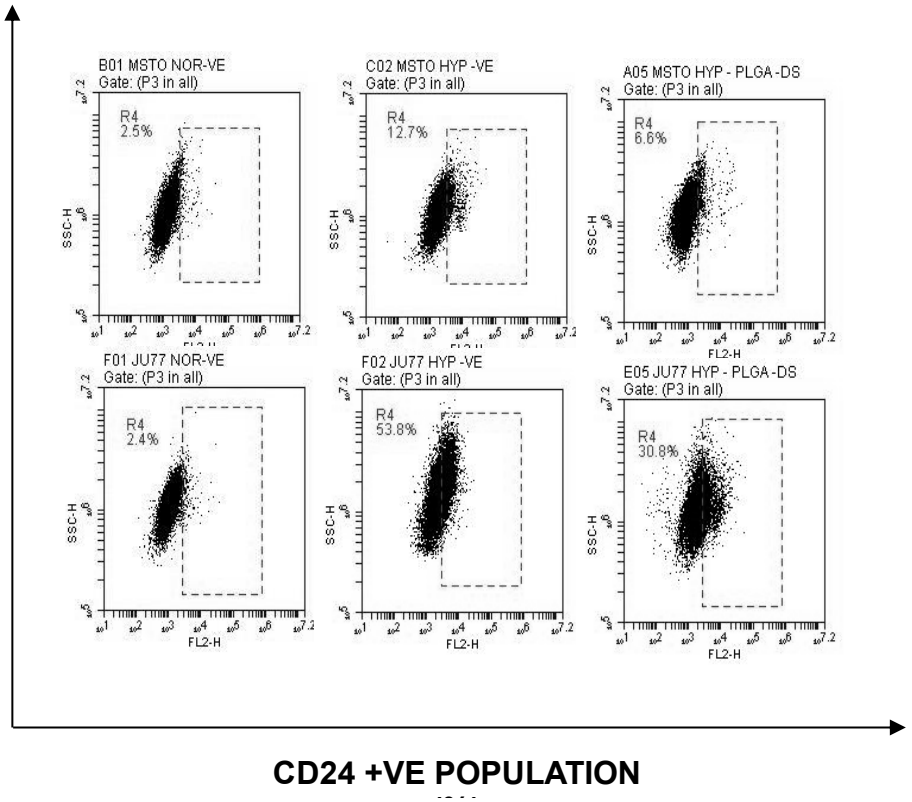
MSTO-211H
JU77
SSC
B01 MSTO NOR-VE
Gate: (P3 in all)
R4
2.5%
C02 MSTO HYP -VE
Gate: (P3 in all)
R4
12.7%
A05 MSTO HYP - PLGA -DS
Gate: (P3 in all)
R4
6.6%
F01 JU77 NOR-VE
Gate: (P3 in all)
R4
2.4%
F02 JU77 HYP -VE
Gate: (P3 in all)
R4
53.8%
E05 JU77 HYP - PLGA -DS
Gate: (P3 in all)
R4
30.8%
SSC-H
FL2-H
CD24 +VE POPULATION

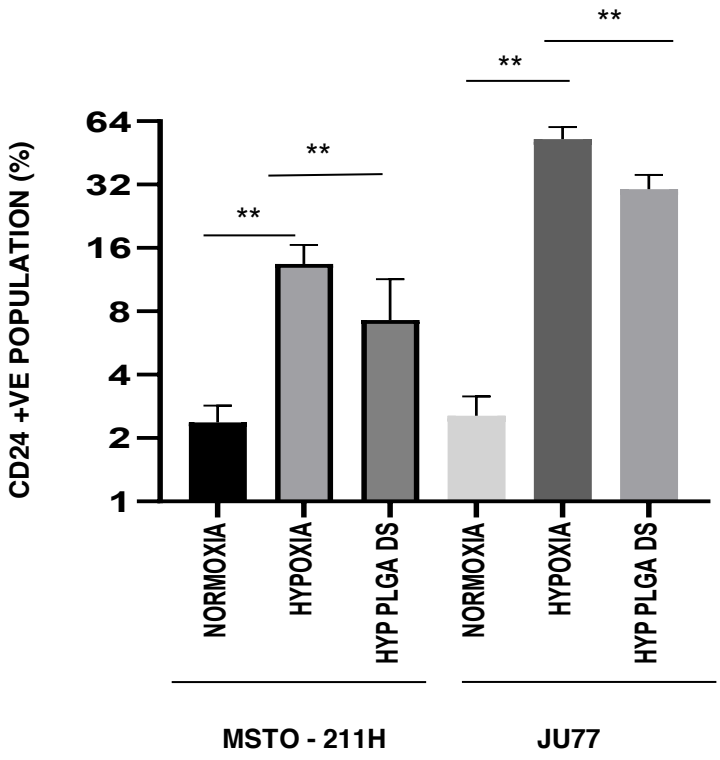
CD24 +VE POPULATION (%)
64
32
16
8
4
2
1
**
**
**
**
NORMOXIA
HYPOXIA
HYP PLGA DS
NORMOXIA
HYPOXIA
HYP PLGA DS
MSTO - 211H
JU77

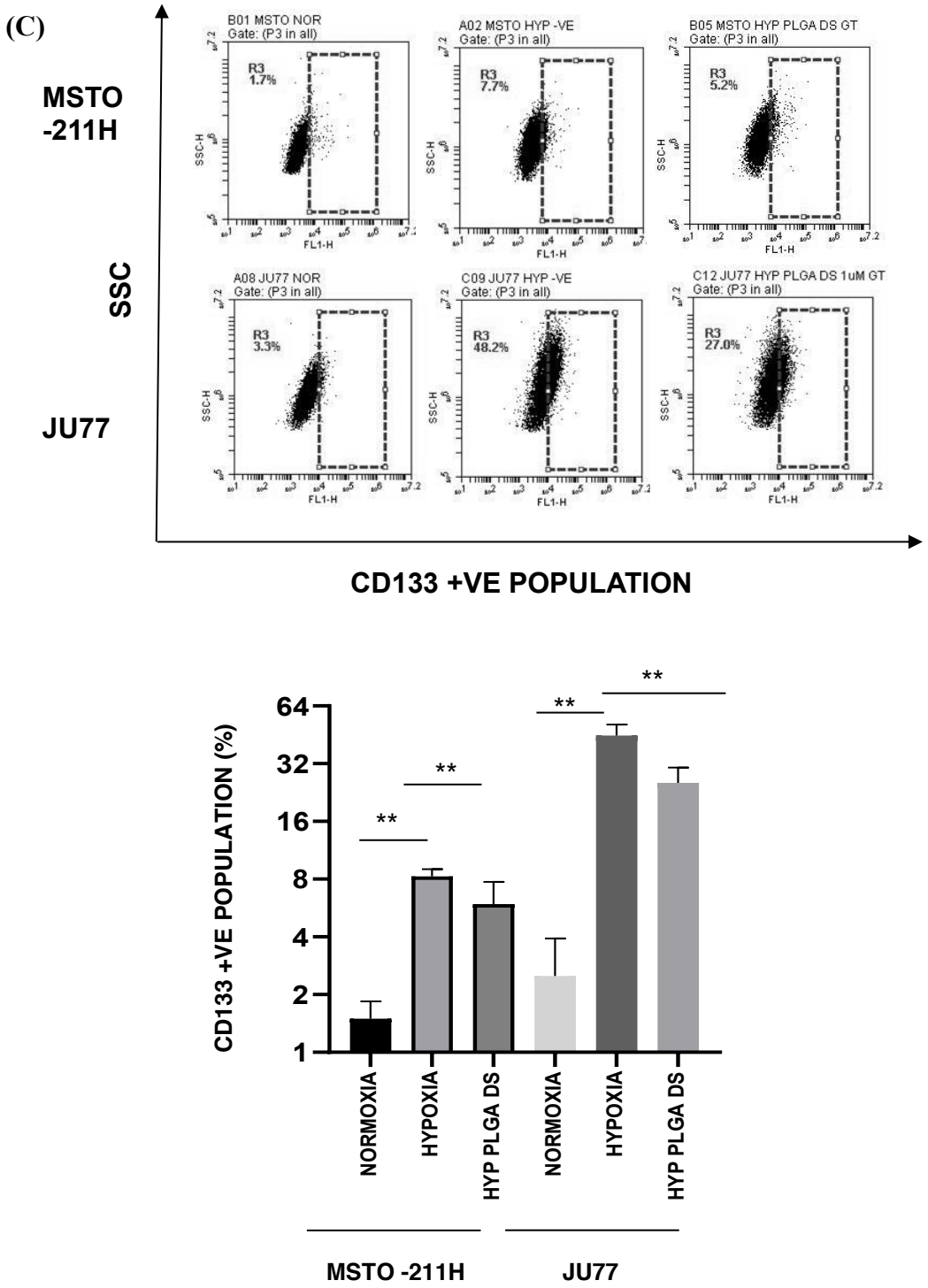

Figure 5.1. PLGA-DS/Cu inhibits MM CSC characteristics in hypoxic cultures.

The above results indicate the effect of PLGA-DS with CuCl2 on CSC markers i.e., ABCG2, CD133 and CD24. Results showed that CSC characteristics were increased in MSTO-211H and JU77 cell lines and statistically reduced in both MSTO-211H and JU77 cell lines after treatment with PLGA-DS 500nM and CuCl2 10 µM. PLGA DS in the figure represents PLGA-DS/Cu. *n=3, ns denotes no- significance ($p \geq 0.05$), *$p<0.05$ **$p<0.01$*

Table 5.1. IC50 values for MSTO 211H and JU77 cell lines under normoxia and hypoxia after 72 hours of treatment with PLGA-DS/Cu.

	MSTO 211H		JU77	
	Normoxia	**Hypoxia**	**Normoxia**	**Hypoxia**
PLGA-DS/Cu (nM)	*308.67 ± 114.99*	*299.78 ± 98.47*	*694.79 ± 122.61*	*559.20 ± 148.89*

5.3.2 PLGA-DS/Cu inhibits sphere reformation

MSTO-211H and JU77 spheroid cultures also showed sensitivity to PLGA-DS/Cu as compared to other first line drugs available for MM treatment. Additionally, PLGA-DS/Cu treatment eradicated the sphere reforming ability of MM cells. Figure 5.3 shows that the sphere reformation ability was not affected when the cells were treated with PLGA-DS (1 μM) or $CuCl_2$ (10 μM) alone and with anti-MM drugs. Whereas, the sphere-reformation was completely inhibited after treatment with PLGA-DS + Cu. The bar chart depicts that the number of spheres after the treatment. The result shows that the spheres treated with PLGA-DS/Cu lost the ability of sphere reformation. The results from this experiment indicate that PLGA-DS/Cu actively targets the CSC population and inhibits sphere reformation in MM.

(A)

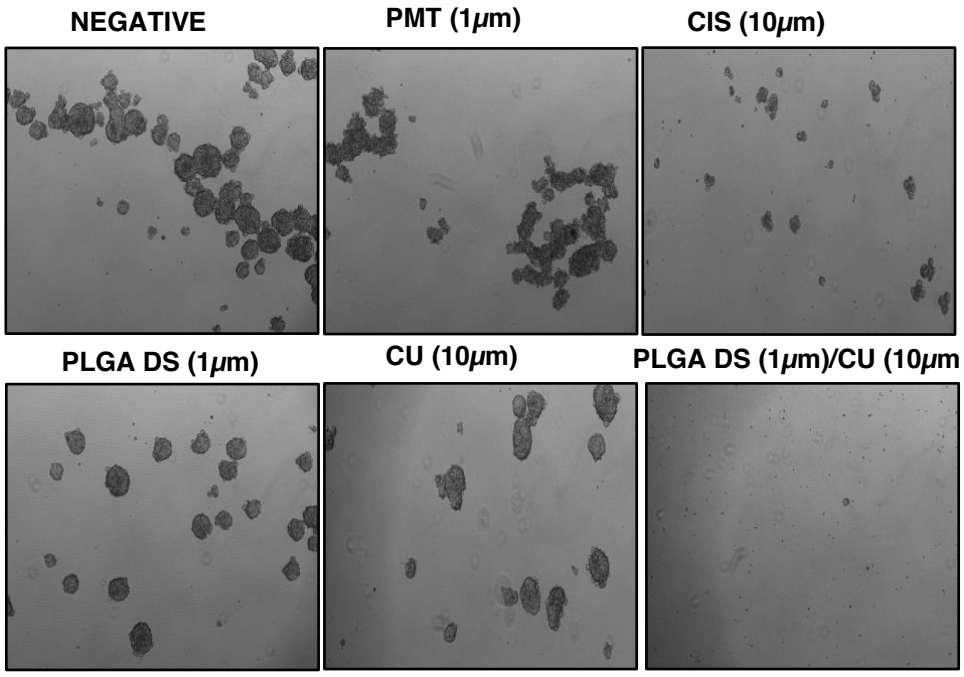
NEGATIVE
PMT (1μm)
CIS (10μm)
PLGA DS (1μm)
CU (10μm)
PLGA DS (1μm)/CU (10μm

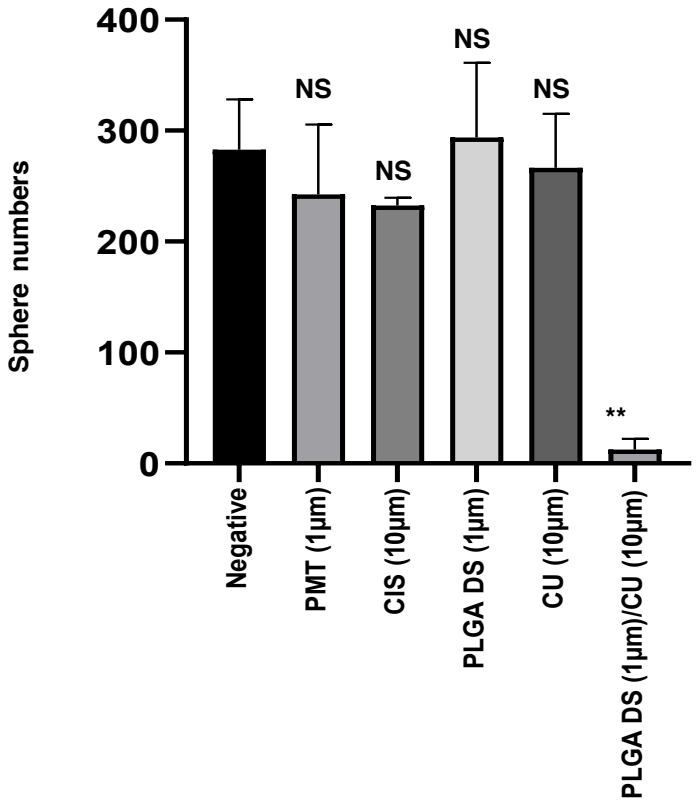
Sphere numbers
400
300
200
100
0
NS
NS
NS
NS
**
Negative
PMT (1μm)
CIS (10μm)
PLGA DS (1μm)
CU (10μm)
PLGA DS (1μm)/CU (10μm)

(B)

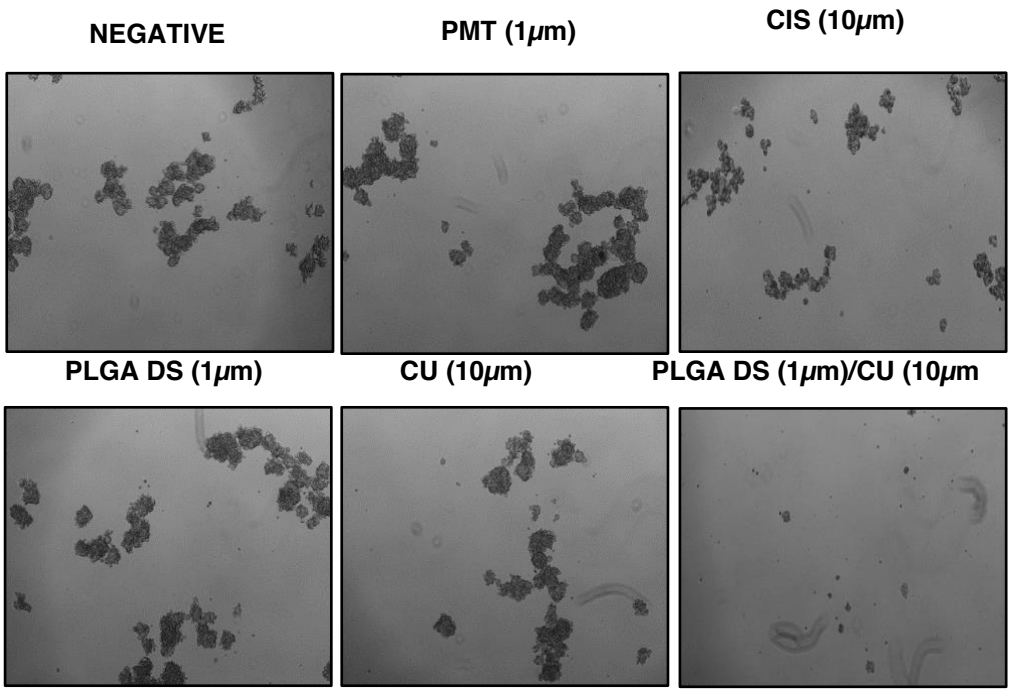

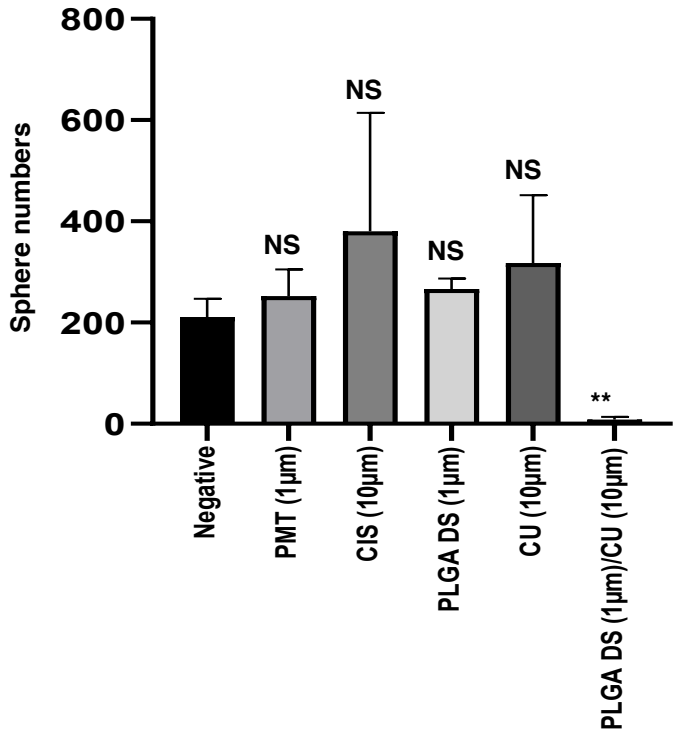

Figure 5.2. PLGA-DS/Cu inhibits sphere reformation in MM cell line.

The Normoxia and hypoxia cultures of MSTO-211H and JU77 cell lines were treated with PMT (1μM), Cisplatin (10 μM), CuCl2 (10 μM), PLGA-DS (1μM) and PLGA-

*DS in combination with CuCl2 for 48 hours. After treatment, MM cells were reseeded at a low density and maintained in respective conditions for sphere formation. (A) Images of sphere reformed for MSTO-211H cell lines with bar chart (B). Images of sphere reformed for JU77 cell line with bar chart. n=3, ns denotes no- significance (p ≥ 0.05), **p<0.01*

5.3.3 PLGA-DS/Cu inhibits migration in hypoxic culture.

Results from chapter 3 showed that hypoxia increases the migration potential of MM cells. To demonstrate that PLGA-DS/Cu inhibit migration in MM cell lines, Boyden chamber assay was performed. The cells were subjected to hypoxic conditions at 37℃, 5% CO2, and <1% O2. Hypoxia negative/untreated culture were used as a control, and hypoxic cells were treated with an extremely low dose of PLGA-DS/Cu, i.e. 25 nM in combination with 10µM of copper. Figure 5.4 (A) shows representative microscopic images of the cells stained with crystal violet, showing migration under hypoxia (negative) and hypoxia (treated) conditions. The results demonstrated that the migration potential of hypoxic cells was remarkably reduced after treatment with PLGA-DS/Cu at a very low dosage of 25 nM, as compared to untreated (hypoxic) cells in MSTO-211H and JU77 cell lines respectively. The number of cells that migrated through 8 µm pore size in the PET membrane was counted. The bar chart in Figure 5.4 (B) represents the mean number of migrated cells under each condition. The number of migrated cells was reduced after the treatment of PLGA-DS/Cu under hypoxic conditions. This number varies between each cell line and further depends on the migration potential of cells.

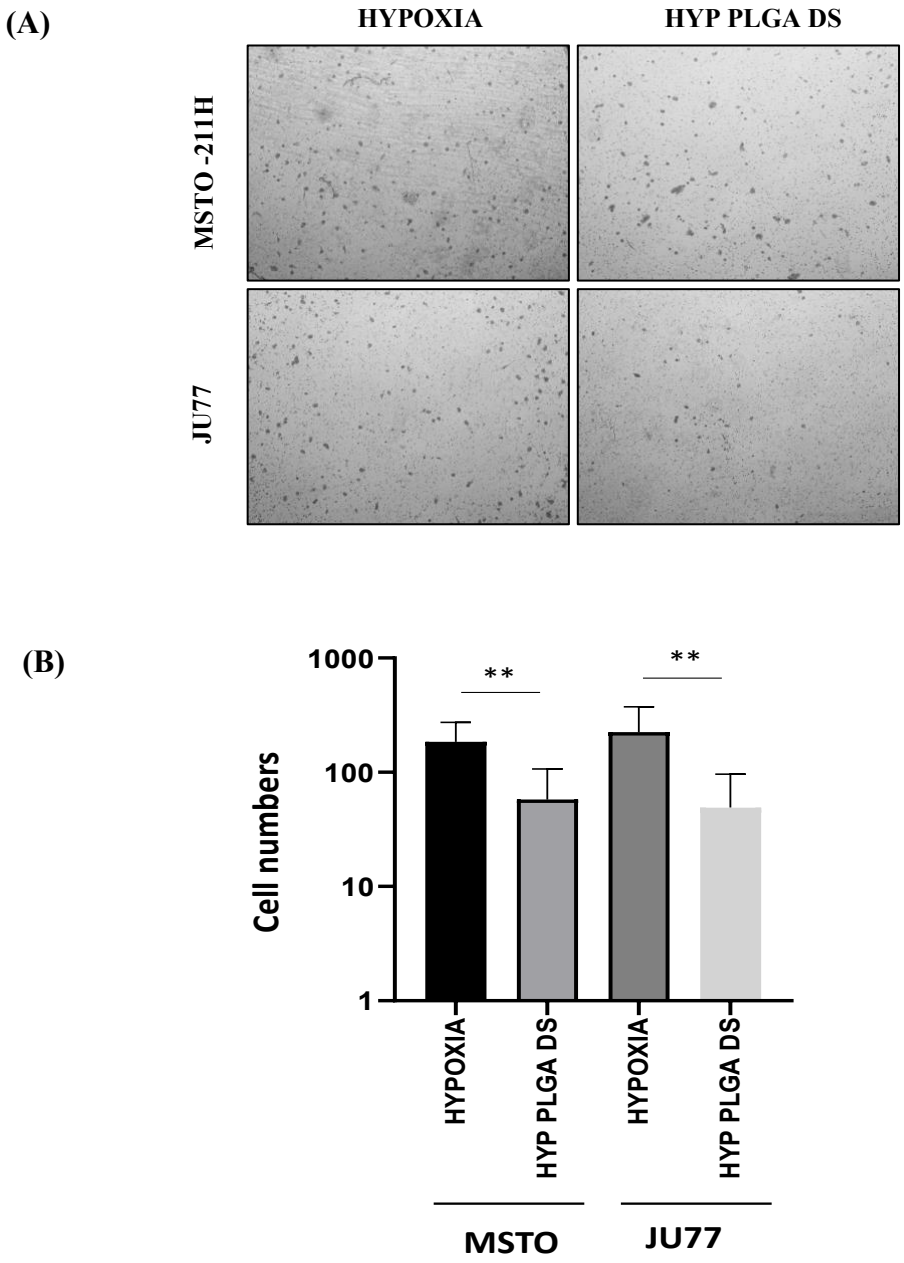

Fig 5.3. PLGA-DS/Cu inhibits migration potential of MM hypoxic culture in vitro

The potential of MM hypoxic cells was reduced after the treatment with a very low dose of PLGA-DS/Cu, i.e. 25 nM in combination with 10 µM of copper. ***(A)*** *Microscopic pictures of the reduced migrated MM cells (40x magnification).* ***(B)*** *The bar chart is representing the mean number of migrated MM cells in hypoxia as compared to normoxia. PLGA DS in the figure represents PLGA-DS/Cu. n=12, ($p \geq 0.05$), **$p<0.01$*

5.3.4 PLGA-DS/Cu inhibits invasion in hypoxic culture.

Results from chapter 3 showed that hypoxia increases the invasion potential of MM cells. To demonstrate that PLGA-DS/Cu inhibits invasion in MM cell lines, Boyden chamber assay performed. The cells subjected to hypoxic conditions at 37℃, 5% CO2, and <1% O2. Hypoxia negative/untreated cells were used as a control, and hypoxic cells were also treated with a very low dose of PLGA-DS/Cu, i.e. 25 nM in combination with 10µM of copper. Figure 5.5 (A) shows representative microscopic images of the cells stained with crystal violet, showing invasion under hypoxia (negative) and hypoxia (treated) conditions. The results demonstrated that invasion potential of hypoxic cells was remarkably reduced after treatment with PLGA-DS/Cu at a very low concentration, as compared to untreated (hypoxic) cells in MSTO-211H and JU77 cell lines respectively. The number of cells that invaded through the coated gel matrix chamber were counted. The bar chart in Figure 5.5 (B) represents the mean number of invaded cells under each condition. The number of invaded cells reduced after the treatment of PLGA-DS/Cu under hypoxic conditions. Interestingly, this number varies between each cell line and further depends on the invasion potential of cells.

(A)

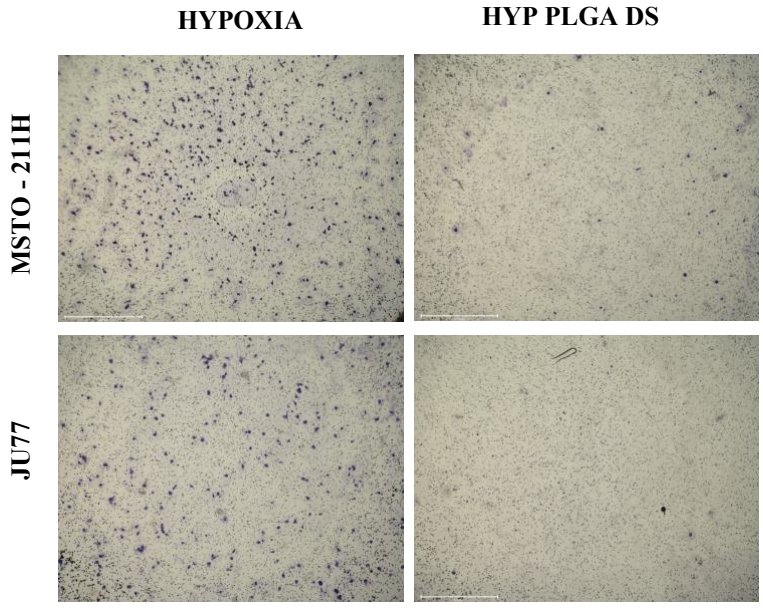

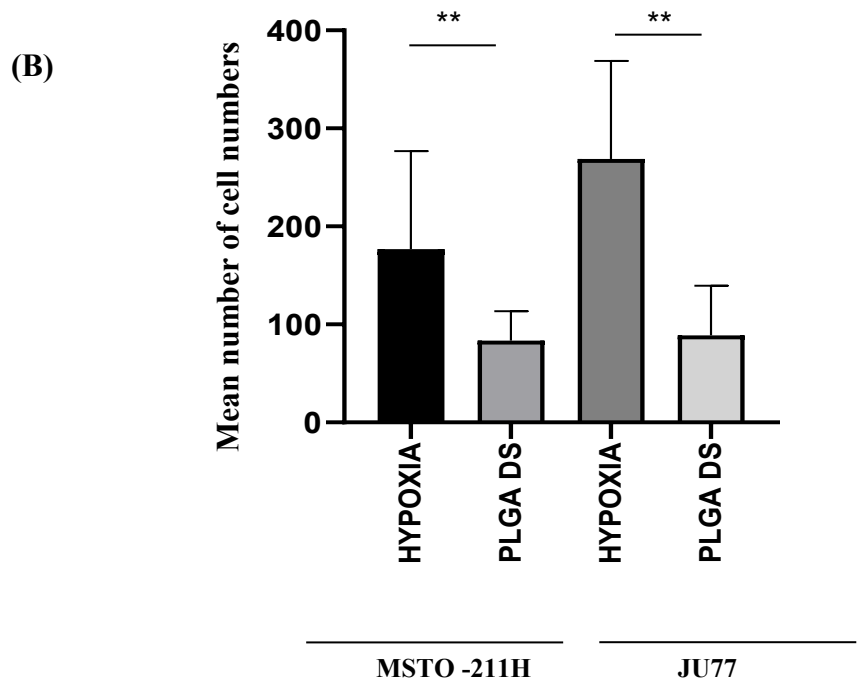

Figure 5.4. PLGA-DS inhibits invasion potential of MM hypoxic culture in vitro.

The potential of MM hypoxic cells was reduced after treatment with a very low dose of PLGA-DS/Cu, i.e., 25 nM in combination with 10µM of copper. ***(A)*** *Microscopic pictures of the reduced invaded MM cells (40x magnification).* ***(B)*** *The bar chart is representing the mean number of invaded MM cells in hypoxia as compared to normoxia. PLGA DS in the figure represents PLGA-DS/Cu.*

5.3.5 Hypoxia induced ESC traits are inhibited by PLGA-DS/Cu

Results from chapter 4 demonstrated that MM cells exposed to hypoxia develop cancer stem cell characteristics which was further confirmed by expression of ESC markers such as SOX-2, Nanog and OCT 4. MM cell lines MSTO-211H and JU77 were incubated at 37℃, 5% CO2, and <1% O2 for five days respectively to study the effect of hypoxia on CSC markers and normoxia was used as a control. The other set-in hypoxic condition was treated with 500 nM of PLGA-DS/Cu for five days. The

consumed media was changed with fresh medium after every three days. The qRT-PCR analysis technique was used to compare the relative mRNA expression level of SOX2, Nanog and OCT4 of hypoxic negative and hypoxic treated cultures shown in figure 5.5. JU77 showed a statistically significant decrease in the expression level of Nanog, SOX 2 and OCT 4. MSTO-211H showed a non-significant increase in SOX2 and OCT4 after treatment and a significant increase in Nanog when MM cells were treated with 500 nM of PLGA-DS/Cu in combination with copper

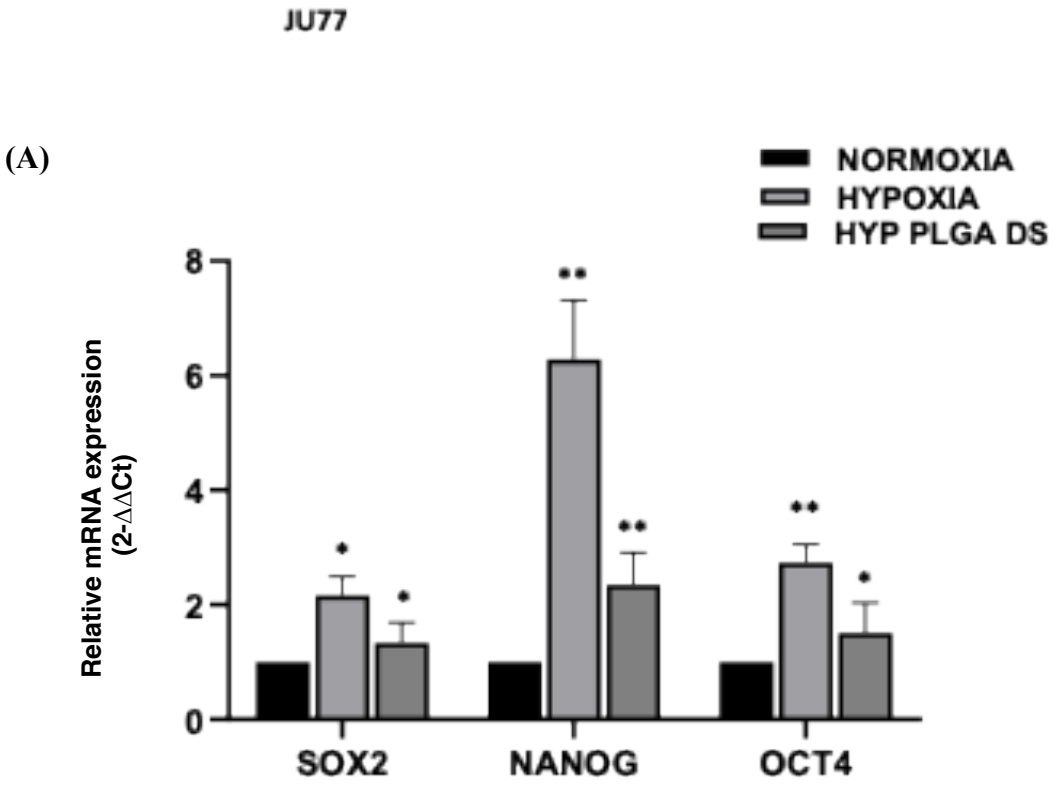

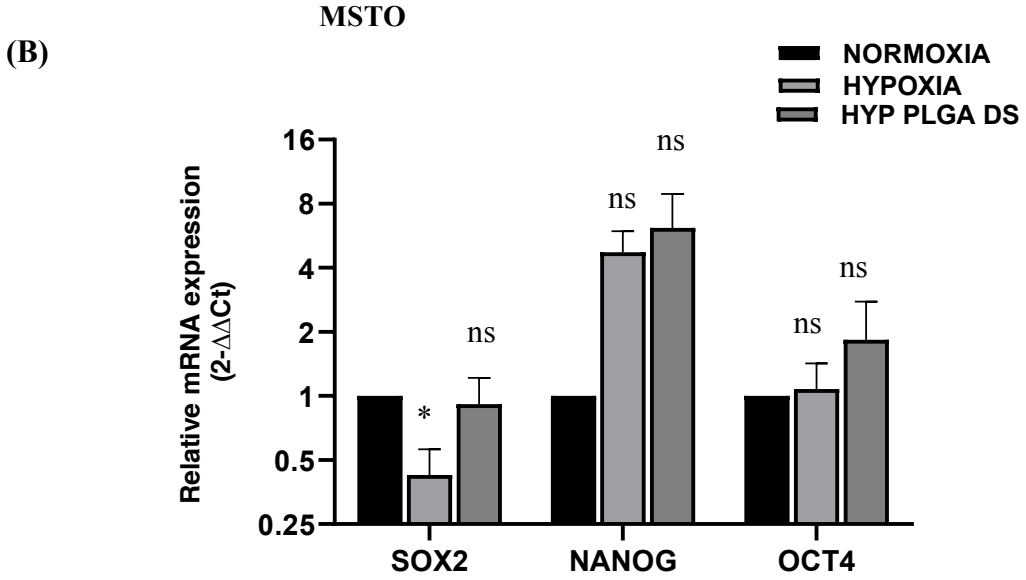

Figure 5.5. PLGA-DS/Cu inhibits hypoxia induced ESC characteristics in MM cell lines.

*The relative mRNA expression of ESC markers SOX2, OCT4, NANOG was analysed using RT-PCR 2-ΔΔCt method in (A) MSTO -211H (B) JU77 cell lines respectively. Results showed that ESC characteristics were increased in MSTO 211H cell lines and reduced in JU77 cell lines after treatment with PLGA-DS 500nM and CuCl2 10 μM. n=3, ns denotes no- significance (p ≥ 0.05), *p<0.05 **p<0.01*

5.3.6. PLGA-DS/Cu inhibits EMT related markers in hypoxic culture.

Results from chapter 4 demonstrated that MM cells exposed to hypoxia showed increased expression level of EMT related markers such as Snail, Slug, Twist, Zeb, E-cadherin, N-Cadherin and Vimentin. MM cell lines MSTO-211H and JU77 were incubated at 37℃, 5% CO_2, and <1% O_2 for five days respectively and normoxia was used as a control. The other set was treated with 500 nM of PLGA-DS/Cu for five

days. The consumed media was changed with fresh medium every three days. The qRT-PCR analysis technique was used to compare the relative mRNA expression level of EMT related markers for hypoxic negative and hypoxic treated cultures shown in figure 5.6. The expression level of Snail 1 and ZEB 1 was statistically increased in both MSTO-211H and JU77 cell lines. Whereas E-cadherin was increased only in JU77 and no expression of E cadherin was found in MSTO-211H. Both the cell lines MSTO-211H and JU77 showed a statistically significant decrease in the expression level of Snail 2, Twist, and Vimentin when MM cells were treated with 500 nM of PLGA-DS/Cu.

(A)

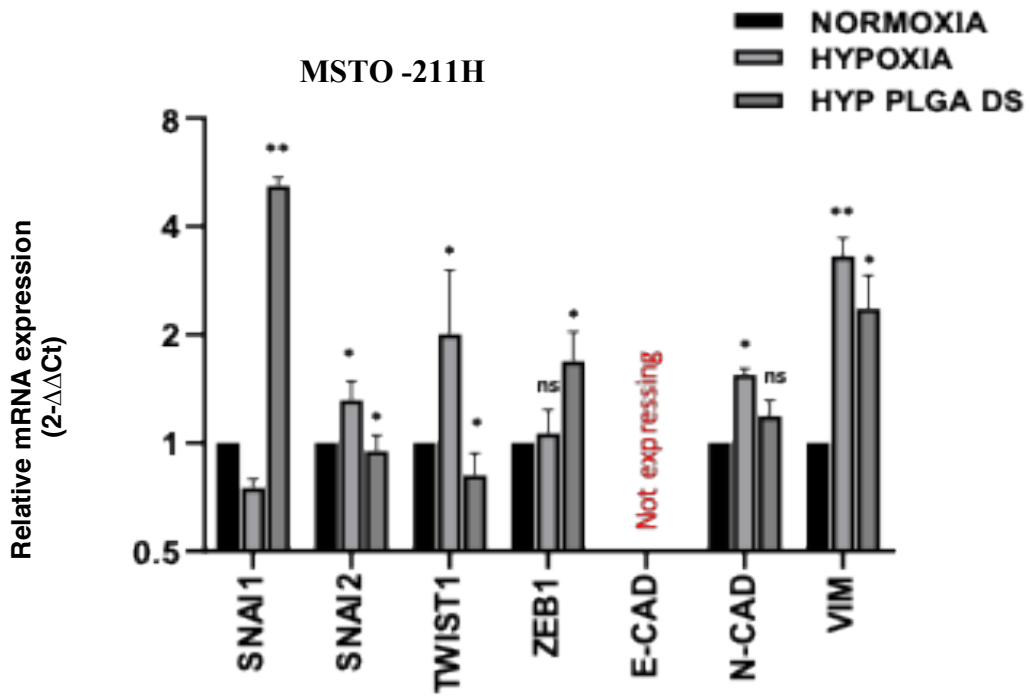

(B)

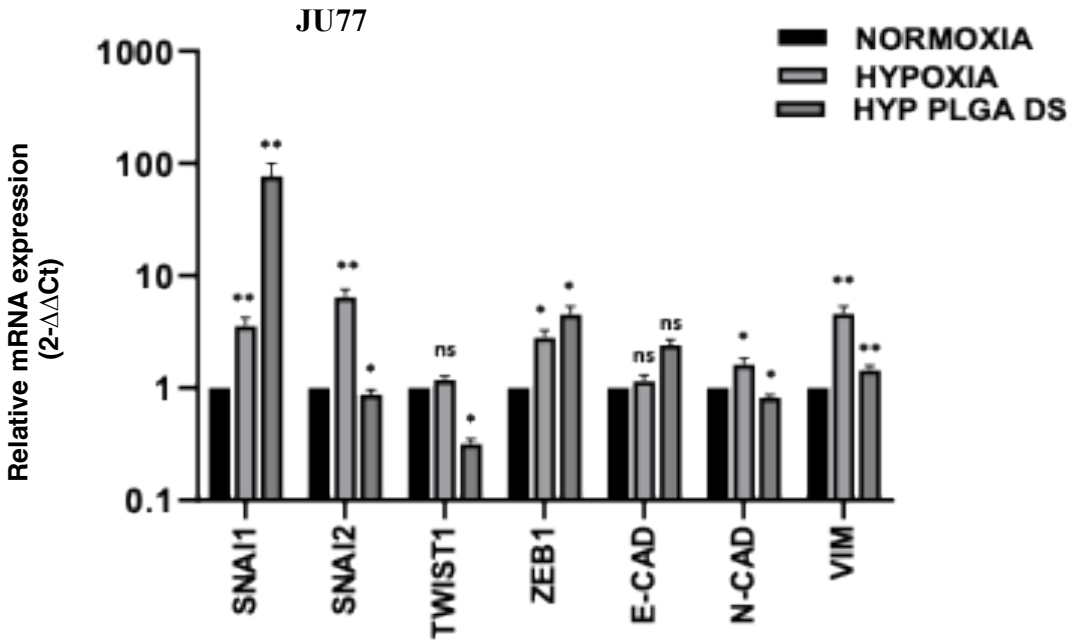

Figure 5.6. PLGA-DS/Cu inhibits hypoxia induced EMT characteristics in MM cell lines.

*The relative mRNA expression of EMT markers Snail, Slug, Twist 1, ZEB-1, E-Cadherin, N-Cadherin and Vimentin was analysed using qRT-PCR 2-ΔΔCt method in (A) MSTO -211H (B) JU77 cell lines respectively. Results indicated that the expression level of Snail 1 and ZEB 1 were statistically increased in both MSTO-211H and JU77 cell lines. Whereas E -cadherin was increased in only in JU77 and there was no expression of E cadherin in MSTO 211H cell line. Both the cell lines MSTO-211H and JU77 showed a statistically significant decrease in the expression level of Snail 2, Twist and Vimentin when MM cells were treated with 500 nM of PLGA-DS/Cu. n=3, ns denotes no- significance ($p \geq 0.05$), *$p<0.05$ **$p<0.01$*

5.3.7 PLGA-DS/Cu inhibits invasiveness related markers in hypoxic culture.

Results from chapter 4 demonstrated that MM cells exposed to hypoxia showed increased expression level of invasiveness related markers such as MMP-2, MMP-7 and MMP-9 in MM cell lines. MSTO - 211H and JU77 cell lines were incubated at 37℃, 5% CO2, and <1% O2 for five days respectively and normoxia was used as control. The other set was treated with 500 nM of PLGA-DS/Cu for five days. The consumed media was changed with fresh medium every three days. The qRT-PCR analysis technique was used to compare the relative mRNA expression level of invasiveness related markers for hypoxic negative and hypoxic treated cultures shown in figure 5.7. Both the cell lines MSTO -211H and JU77 showed statistically non-significant decrease in the expression level of MMP-7 and MMP-9 and a significant decrease in the level of MMP 2 when MM cells were treated with 500 nM of PLGA-DS/Cu in combination with copper.

(A)

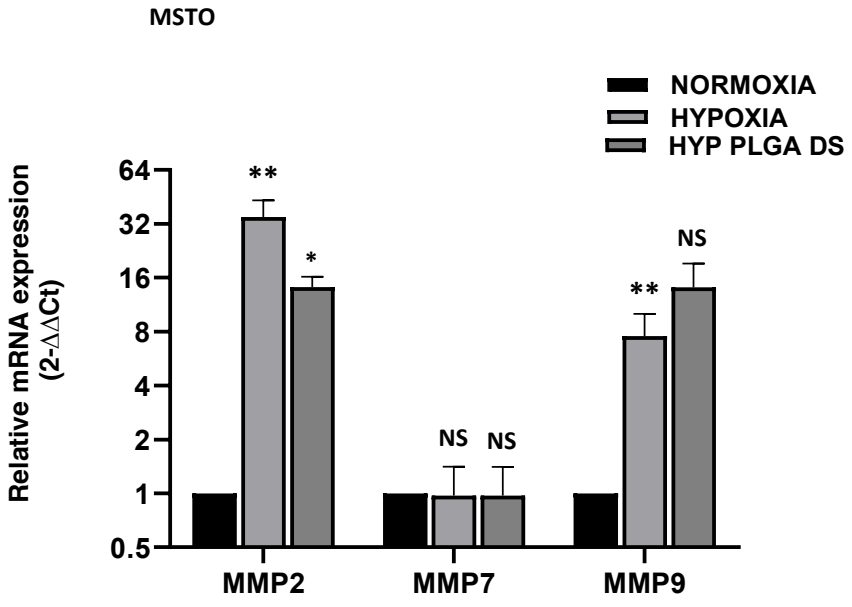

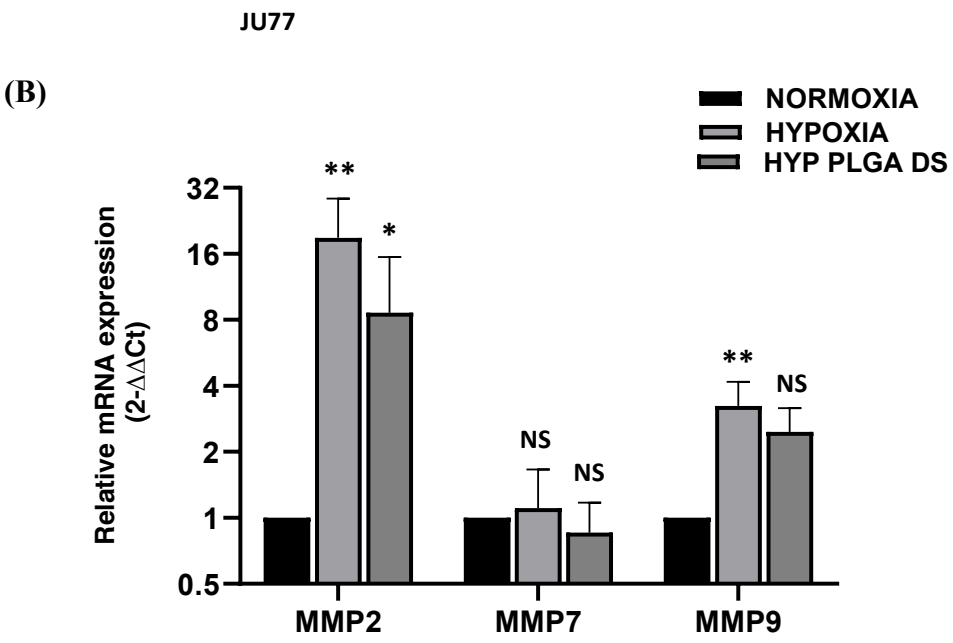

Figure 5.7. PLGA-DS/Cu inhibits hypoxia induced invasive characteristics in MM cell lines.

*The relative mRNA expression of invasiveness related markers MMP-2, MMP-9 and MMP-7 were analysed using RT-PCR 2-ΔΔCt method in (A) MSTO -211H (B) JU77 cell lines respectively. Results showed that both the cell lines MSTO-211H and JU77 showed statistically no-significant decrease in the expression level of MMP-7 and MMP-9 and a significant decrease in the level of MMP 2, when MM were cells treated with 500 nM of PLGA-DS/Cu in combination with copper. ns denotes no- significance ($p \geq 0.05$), *$p<0.05$ **$p<0.01$*

5.3.8. PLGA-DS/Cu enhances the cytotoxicity of the anti-MM drugs in MM cell lines

MM cell lines have demonstrated earlier that they are more sensitive to PLGA-DS in combination with copper as compared to conventional anti-MM drugs. The combinational treatment of PLGA-DS/Cu with anti-MM drugs enhances the

cytotoxicity of conventional drugs *in vitro*. The cell viability curves represent the anti-MM drugs in combination with PLGA-DS/Cu in Figure 5.8 These curves depicts the effect of various anti-MM drugs alone and in combination with PLGA-DS/Cu on MSTO-211H and JU77 cell lines. Treating MM cells alone with conventional drugs shows drug-resistance as depicted in chapter 3. However, when these drugs were combined with PLGA-DS/Cu, a significant decrease in the number of MM cells at a very low dosage was observed. These results indicate that PLGA-DS/Cu, when combined with anti-MM drugs, improves the cytotoxicity by reducing the required dose for killing the cells. To determine the synergy of the drug combinations, Calcusyn™ software used, and the Combination Index (CI) value calculated. A CI value of less than one is considered synergistic. Table 5.2 shows the calculated IC50 and CI values of anti-MM drugs in combination with PLGA-DS/Cu. The IC50 values show the dose required to kill 50% of the cell population. Table 5.3 shows the CI values were calculated using the Effective Dose (ED) at three points of the curve, ED50, ED75 and ED90.

(A)

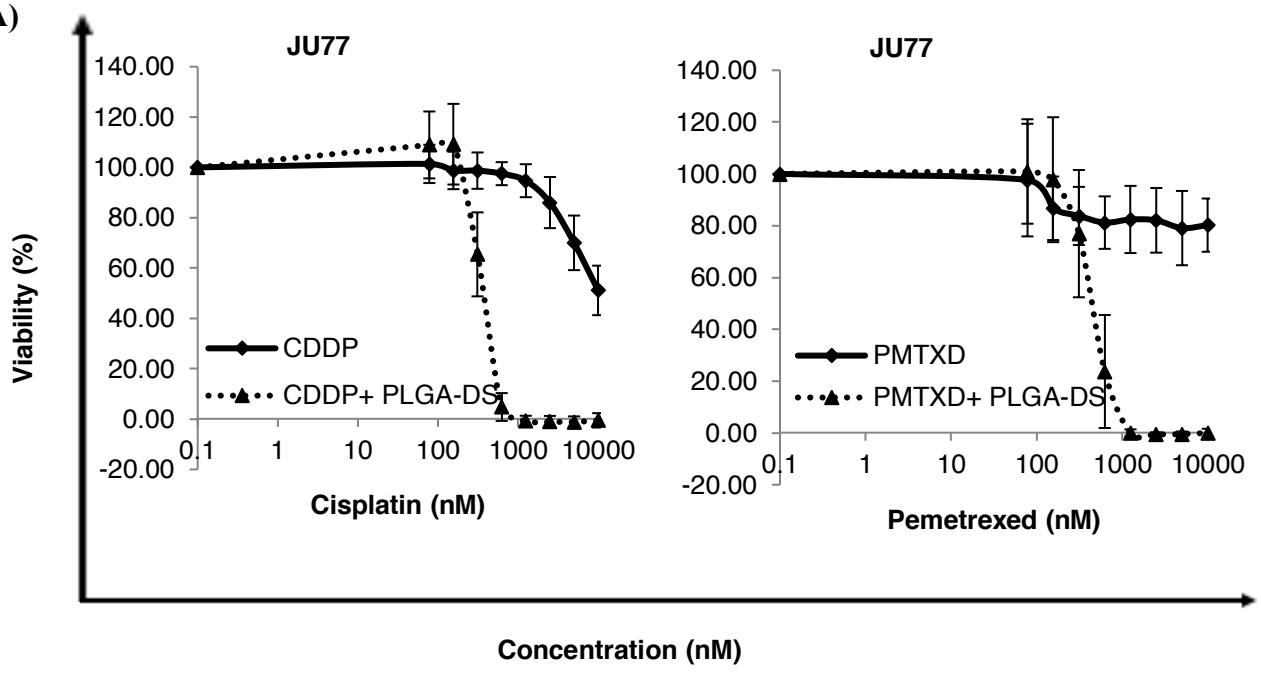

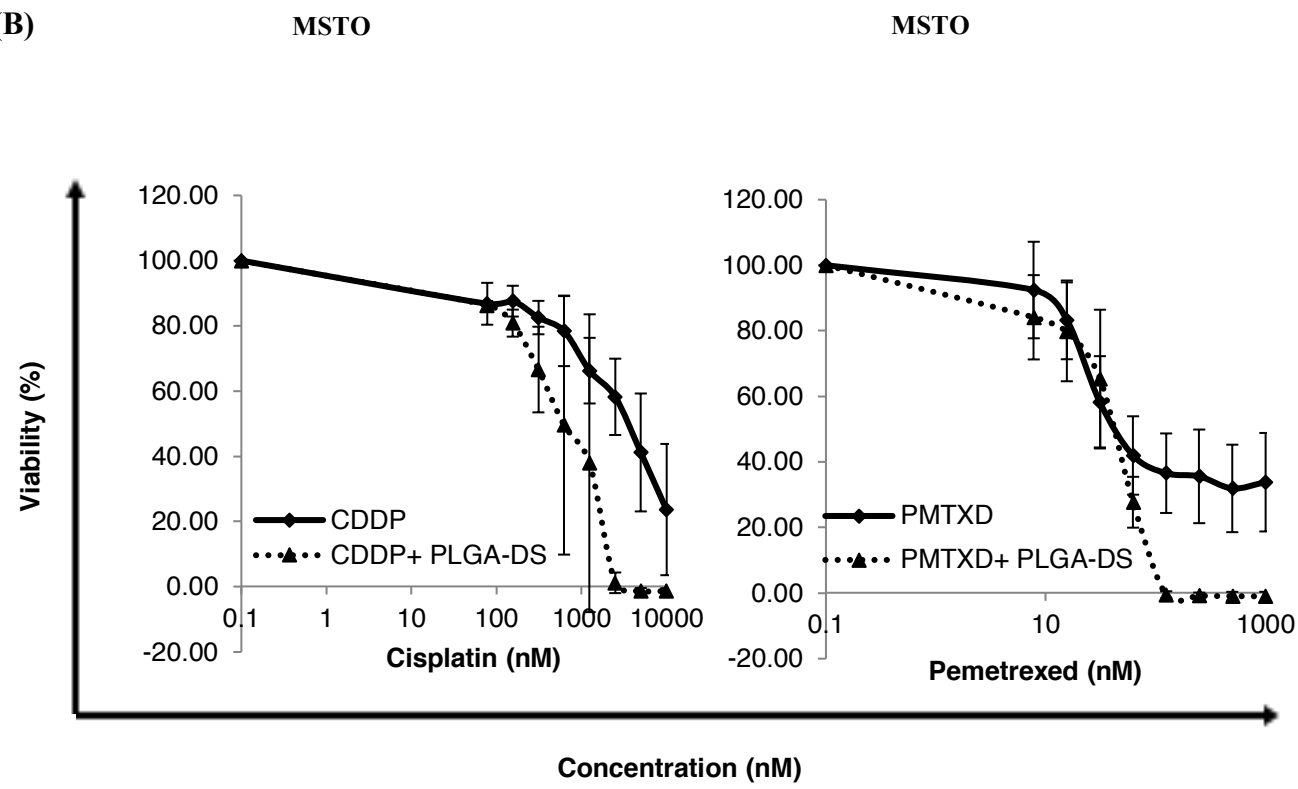

Figure 5.8. PLGA-DS/Cu enhances the anticancer activity of conventional anti-MM drugs.

The cell viability curves show the synergistic effect of PLGA-DS/Cu on the cytotoxicity of anticancer drugs on hypoxic cultured MM cell lines (A) JU77and (B) MSTO -211H. The cells were incubated with PLGA-DS and supplemented with $CuCl_2$(10 μM) in combination with anticancer drugs: PMT (1μm) and CISPLATIN (10 μM) for 72 hours and subjected to MTT assay.

Table 5.2. IC 50 values of anti-MM drugs after 72 hours of treatment on MSTO-211H and JU77 MM hypoxic cultures.

	MSTO-211H hypoxia	JU77 hypoxia
Cisplatin (nM)	*4385.49± 3650.86*	*11802.42 ± 5839.23*
Cisplatin + PLGA - DS (nM)	*822.99± 486.30*	*356.2 ± 43.4*
Pemetrexed (nM)	*52.77 ± 21.14*	*<10,000*
Pemetrexed + PLGA-DS (nM)	*43.13± 17.26*	*472.20 ± 130.9*

Table 5.3. Isobologram analysis of anti-MM drugs in combination with PLGA DS/Cu after 72 hours on MSTO 211H and JU77 hypoxic cultures: Combination Index (CI) values.

Drug in combination with PLGA-DS/Cu (nM)	MSTO 211H Hypoxia			JU77 hypoxia		
	CI values			*CI values*		
	ED50	ED75	ED90	ED50	ED75	ED90
Cisplatin (nM)	1.08	0.96	0.90	1.14	1.08	1.03
Pemetrexed (nM)	1.43	1.21	1.09	0.84	0.89	0.94

Discussion

The prognosis of MM is poor due to late diagnosis, rapid progression, high invasiveness and the lack of effective treatment (Zhang et al.,2015). A front-line regime for this disease is the combination of Pemetrexed and Cisplatin, resulting in a response rate of 41% and a median survival of 12.1 months. Despite continuous efforts to implement new therapeutic modalities, none of these, have prolonged patient survival primarily due to chemoresistance. It is hypothesised that tumour relapse may be associated with the drug resistance caused by CSC. Hence, the identification and complete elimination of CSC looks promising for treating MM (Dericks et al.,2017) Although there is an improved understanding of the biology of MM, response to targeted therapies is hampered by intra-tumour heterogeneity, and it is still unclear whether most of the mutations constitute clonal or sub-clonal driver events (Cantini et al.,2020)

It has been shown that combination chemotherapy is superior to monotherapy, with higher response rates to Platinum-based regimens. But several complications have been associated with the treatment strategies and can result in significant morbidity (Murphy and Gill.,2017) There is no single drug or combination therapy that can be considered as the standard treatment for MM. A variety of single-agent and combination regimens have been tried in clinical trials with response rates of between 0% and 45% (Moore, Parker and Wiggins., 2008)

The findings from chapter four showed a strong detection of hypoxia-induced CSC traits which induces resistance to anti-MM drugs in hypoxic cultures. Hence, indicating that conventional anti-MM drugs do not selectively target the CSC population. This study demonstrates the significant anti-CSC activity of PLGA-DS in

combination with Cu in MM cell lines, which suggests that conventional drug combinations with PLGA-DS/Cu may provide better outcomes for patients. This anticancer property of Disulfiram and copper has been shown in lung cancer, prostate cancer, leukaemia, breast cancer and cervical adenocarcinoma and depends on copper (Cu), as Cu plays an important role in the redox reactions and triggers generation of reactive oxygen species (ROS) which induces apoptosis in human cells (Boyd et al.,2014)

In this study, PLGA-DS/Cu treatment inhibits the expression of CSC markers CD133, CD 24 and ABCG2 in MSTO-211H and JU77 hypoxic cultures. Current studies have established ALDH and CD44 as putative CSC markers that exhibit elevated chemoresisitive properties in solid cancers, making them potential indicators of drug tolerance in MM (Dericks et al., 2017). High ALDH activity has been shown to maintain a drug-resistant phenotype in cancer cells (Triscott, Rose Pambid and Dunn, 2015). ALDH inhibition with DS, by modulation of reactive oxygen species, could overcome this drug-resistant phenotype and delay disease recurrences (Rezk et al., 2015) Wang et al demonstrated that hypoxia increased CSC population in Hepatocellular carcinoma (HCC) cell lines, and DS-PLGA/Cu significantly inhibited the ALDH and CD133 positive CSC population in both hypoxic and spheroid HCC cultures. DS-PLGA/Cu also showed very strong anti-metastatic effect on HCC in vitro and in vivo (Wang et al.,2017)

This study also demonstrates that after treatment with PLGA-DS/Cu, the detection of specific CSC markers was significantly reduced in MM hypoxic cultures. Despite the current evidence linking CSC markers such as ALDH and CD44 to drug resistance in solid tumours, the variability in the different studies still warrants further investigation

to delineate the present roles of these potential CSC markers (Dericks et al.,2017). DS has been reported to downregulate tumour growth through the inhibition of proteasome activity, induction of apoptosis, blockage of drug resistance, inhibition of invasion and angiogenesis and suppression of stem cell-like properties. Moreover, DS shows high toxicity to cancer cells in a Copper (Cu)-dependent manner and inhibits cancer stem cells (Li et al., 2015). It has shown that the DS-Cu complex is highly cytotoxic to the cancer cells but not the normal cells (Yang et al., 2017).

The intact sulfhydryl group is essential for the anticancer function of DS. The degradation of DS in the bloodstream destroys the sulfhydryl group making DS lose its cancer-targeting ability. The degradation of DS in the serum kinetically results from a covalent interaction of this drug with the free sulfhydryl of serum albumin. The half-life of DS pH 7.4 is 1-1.5 minutes. It may introduce the discrepancy between the anticancer activities *in vitro* and *in vivo* and in the clinic. Nanomedicine can protect and deliver drugs in the bloodstream. The *in vivo* anticancer efficacy of DS can be improved by liposomal encapsulation (half-life~25 min). Therefore, our group has successfully extended the half-life of DS to ~7 h by encapsulation of DS into PLGA (Zhipeng Wang et al.,2017)

DS-loaded PEGylated liposomes have relatively smaller sizes, and significantly lower polydispersity index (PI) than those of conventional liposomes (Najlah et al.,2019) The cytotoxicity of Lipo-DS/Cu is ROS dependent. ROS induces apoptosis by damaging DNA, RNA and protein. Cancer cells possess and also tolerate significantly higher levels of ROS due to the balance of anti-apoptotic mechanisms, e.g. NFκB (Peng Liu et al.,2014). Copper plays a key role in redox reactions which induces ROS to trigger apoptosis. DS can chelate Cu (II) to form a DS/Cu complex that enhances

Cu transport to cancer cells and is a much better inducer of ROS than Cu alone. Drug-induced ROS accumulation is usually counterbalanced due to the activation of NF-kB, an anti-apoptotic factor inhibiting ROS and ROS-induced cytotoxicity. However, DS is also capable of inhibiting the activity of NF-kB. Furthermore, it has been demonstrated that DS can potentiate the cytotoxic effect of other anticancer drugs and ionising radiation. These characteristics and its low toxicity make DS an attractive candidate for treating orphan diseases like MM (Zembko et al.,2014)

This study confirms that the cytotoxic activity of PLGA coated Disulfiram is dependent on copper supplementation. The results have clearly shown that CSC traits have inhibited by PLGA-DS/Cu in MM cell lines. CSCs can form spheres, which retain their stem cell properties for several passages, while most differentiated cells die from anoikis (Liu et al.,2020). PLGA-DS/Cu blocked the sphere reformation ability of CSCs after treatment *in vitro*. The combination of PLGA-DS/Cu was able to reduce the invasion and migration in MM at a very low concentration *in vitro*. It further suggests that if a potential target is identified, it may elucidate the underlying anticancer mechanism of DS to reverse chemoresistance. PLGA-DS/Cu has shown to enhance the cytotoxicity of first-line drugs in MM hypoxic cultured cell lines. Although combination therapy, consisting of Cisplatin (CIS) and Pemetrexed (PMT), has demonstrated promising prognostic outcomes and a response rate of 41.3%, making it the standard treatment for mesothelioma, overall survival has been a low 16.6 months (Tolani et al.,2018). Therefore, urgent treatments are required for MM. We hypothesise that PLGA-DS/Cu, in combination with anti-MM drugs, can reduce the cytotoxic effects of conventional therapies. These results show that PLGA-DS/Cu enhance anti-MM drugs in cell lines on the graphs (Figure 5.8) but due to high standard deviation and less repeats the CI values do not show complete synergism.

CHAPTER 6

Investigation of the effect of NF-κB activity on stemness, drug sensitivity and invasiveness in MM cell lines.

6.1 Introduction

Hypoxia changes cancer cell metabolism and contributes to therapy resistance by inducing cell quiescence. Hypoxia stimulates a complex cell signalling network in cancer cells, including the HIF, PI3K, MAPK, and NF-κB pathways, which interact with each other causing positive and negative feedback loops and enhancing or diminishing hypoxic effects. Hypoxia causes slow-proliferating stem-cell-like phenotype of cells, decreases senescence, creates chaotic and malfunctioning blood vessels, and augments metastasis, which all together induces therapy resistance. Currently, the assessment of tumour oxygenation and HIF expression pattern helps determine tumour chemo and radio-sensitivity (Barbara Muz et al.,2015). The measure of ROS has shown to be increased in cancer cells exposed to hypoxia. ROS can also activate the differentiation of cancer stem cells, thus encouraging EMT and influence metabolic reprogramming contributing to the resistance of cancer cells (Jing et al.,2019). PI3K/AKT/mTOR, MAPK, and NFκB signalling pathways are also stimulated in a hypoxia-independent manner by several factors such as cytokines, chemokine, and growth factors (Barbara Muz et al.,2015). The pathways controlling survival and cell proliferation include MAPK, PI3K-Akt, and NF-κB (Lin et al.,2010). NF-κB protects DNA-damaged cells from apoptosis and stimulates cell proliferation, which at least partly contributes to its role in promoting cell transformation (Lin et al.,2010). Also, in many types of cancer, chemotherapy and radiotherapy induce constitutive activation of NF-κB, thereby making the tumour non-responsive to the treatment (Chaturvedi et al.,2011).

NF-κB activities are often regulated by its upstream kinase known as Inhibitory kB Kinase (IKK), and activated IKK phosphorylates IkB alpha and beta, the endogenous inhibitors of NF-κB. The phosphorylated IkB alpha and beta gets ubiquitinated and degraded by the proteasome, allowing NF-κB nuclear translocation and transcriptional activation functions (Cheriyan et al., 2014) The half-life of NF-κB is less than 30 min, and maintenance of its activity requires ongoing protein synthesis and continuous stimuli. Thus, the high NF-κB activity in drug-resistant cells is a constitutive and intrinsic feature of the resistant cell lines, IkB degradation is thought to be the main reason for induction and maintenance of high nuclear NF-κB activity (Wang et al.,2013). Although NF-κB is an attractive molecular target for therapeutic intervention, inhibition of NF-κB alone only induces limited cell death (Liu et al., 2012).

Although much of the precise mechanism of the pathogenesis of mesothelioma remains unknown, the involvement of chronic inflammation in the pathogenesis has been proposed. Although the uptake of asbestos often induces cytotoxicity and results in the apoptosis of affected cells, TNF-α produced by macrophages may rescue mesothelial cells from cell death through nuclear factor-κB (NF-κB) dependent pathway. Crucial roles of NF-κB signalling in both malignant transformations have been identified. However, direct evidence regarding NF-κB in triggering mesothelioma formation has been insufficient in clinical cases (Nishkawa et al.,2014). Research has shown increased expression of genes with NF-κB binding sequences in the regulatory regions of lungs and cells *in vitro* after exposure to crocidolite asbestos in lung cancer, and mesothelioma. The fibrous nature of asbestos is essential for activation of NF-κB (Yvonne et al.,1997). *The in vitro* studies evaluating the impact

of asbestos on cell cycle regulation and survival have discovered a significant relationship between activation of NF-κB pathways and cellular protection from the asbestos-induced cell. This effect is further confirmed by selective inhibition of NF-κB, which subjects the exposed cells to programmed cell death (Chandra et al.,2011). We hypothesised that NF-κB drives chemoresistance in MM.

6.2 Materials and Methods

The following section elaborates the specific methods used within this particular study and specifies any experimental changes concerning the general detailed methods explained in chapter 2.

6.2.1 NF-κB -P65 overexpression

6.2.1.1 Culture methods

In this study, MSTO-211H cell line transfected with NF-κB-p65. Amongst fifty clones, two overexpressed clones selected. The transfected clones (C12 and C15) along with MSTO-211H mock, were maintained in RPMI medium containing 50 μg/mL hygromycin and incubated at 37°C and 5% CO_2.

6.2.1.2 Stable transfection

MSTO-211H cell lines were stably transfected with NF-κB -P65. The cDNA of NF-κB-p65 and recombinant vector constructed by inserting the cDNA into pcDNA3.1(+)/hygromycin vector for mammalian expression. The MSTO-211H cells were incubated at a density of 0.4×10^5 cell/well in a 6-well plate for overnight culture. To determine the efficiency of transfection negative (no plasmid) and mock (empty

vector) was used as a control. The pcDNA3.1 NF-κB-p65 and the empty pcDNA3.1 construct was incorporated inside the cells by using lipofectamine^{TM} 2000 reagent and incubated for 24 hours at 37°C and 5% CO2. The cells were then transferred into the fresh RPMI media containing 50 μg/mL hygromycin as the selecting agent for successfully transfected cells. The media was changed after every three days to remove dead cells. After seven days, the successfully transformed colonies were selected and picked carefully. The clones were then screened for ectopic expression by qRT-PCR and western blot analysis. In this study, MSTO-211H cell lines were transfected with an empty vector identified as mock, and the selected MSTO-211H clones with high NF-κB-p65 expression were C12 and C15.

6.2.1.3 Detection of hypoxia-induced proteins by RT-PCR

qRT-PCR was used to measure the mRNA expression of NF-κB-p65 transfected clones C12 and C15 as compared to mock. The qRT-PCR procedure was followed as detailed in chapter 2.2.9.

6.2.1.4. Detection of NF-κB-p65 by Western blot analysis

Flow cytometric analysis was used to measure the presence of CSC markers ALDH, CD133 and ABCG2 in the NF-κB -p65 transfected cells, respectively. A comparison made between NF-κB overexpressed clones and mock, respectively. The detailed methods of staining and detection listed in chapters 2.2.10.

6.2.1.5. Detection of CSC markers

Quantitative RT-PCR method was used to determine the mRNA expression of ESC markers, i.e. SOX-2, NANOG, OCT 4 in NF-κB overexpressed clones. The comparison was made between the overexpressed clones and mock, respectively. The RT-PCR procedure was followed as detailed in chapter 2.2.9. respectively.

6.2.1.6. Detection of EMT markers

Quantitative RT-PCR method was used to determine the mRNA expression of EMT markers, i.e. Snail, Zeb, Slug, Twist, E-Cadherin, N-cadherin, Vimentin and invasiveness markers MMP-2, MMP-7, MMP-9 in NF-κB overexpressed clones. The comparison was made between the overexpressed clones and mock, respectively. The RT-PCR procedure was followed as detailed in chapter 2.2.9. respectively.

6.2.1.7. MTT Cytotoxicity assay

The NF-κB P65 transfected cells were subjected to MTT cytotoxicity assay as detailed in section 2.2.13. The over expressed clones were exposed to serially diluted first line drugs PMT and CIS for 72 hours and placed in their respective cell culture incubators. After incubation the cells were treated with MTT reagent and percentage cell viability was calculated followed by a comparison between the mock and over expressed clones.

6.2.2. Knockout of NF-κB -P65 using CRISPR Cas 9 technology

MSTO-211H cell line was stably transfected with CRISPR Cas-9 lentiviral vectors containing different target sequences of NF-κB p65 gene, i.e. T1, T2 and T3 (Detailed in chapter 2.2.13) purchased from Abm (Canada) by using lipofectamine^{TM} 2000 reagent. The clones were then screened for NF-κB -p65 knock out by RT-PCR and western blot analysis. The MSTO-211H cells were also transfected with a scrambled vector which was used as control.

6.3 RESULTS

6.3.1. Hypoxic culture induced expression of NF-κB

The expression of NF-κB-p65, HIF-1α and HIF-2α examined in hypoxia and normoxia cultured MM cell lines. Figure 6.1 identifies the relative mRNA expression of NF-κB-p65, HIF-1α and HIF-2α, and shows that in comparison with the normoxia-cultured counterparts, the hypoxia-cultured MSTO -211H cells expressed high levels of NF-κB-p65 and HIF-2α. Furthermore, the expression of NF-κB-p65 protein was examined. The overexpression of NF-κB -p65 was detected in the hypoxia-cultured MSTO-211H cells by western blotting analysis

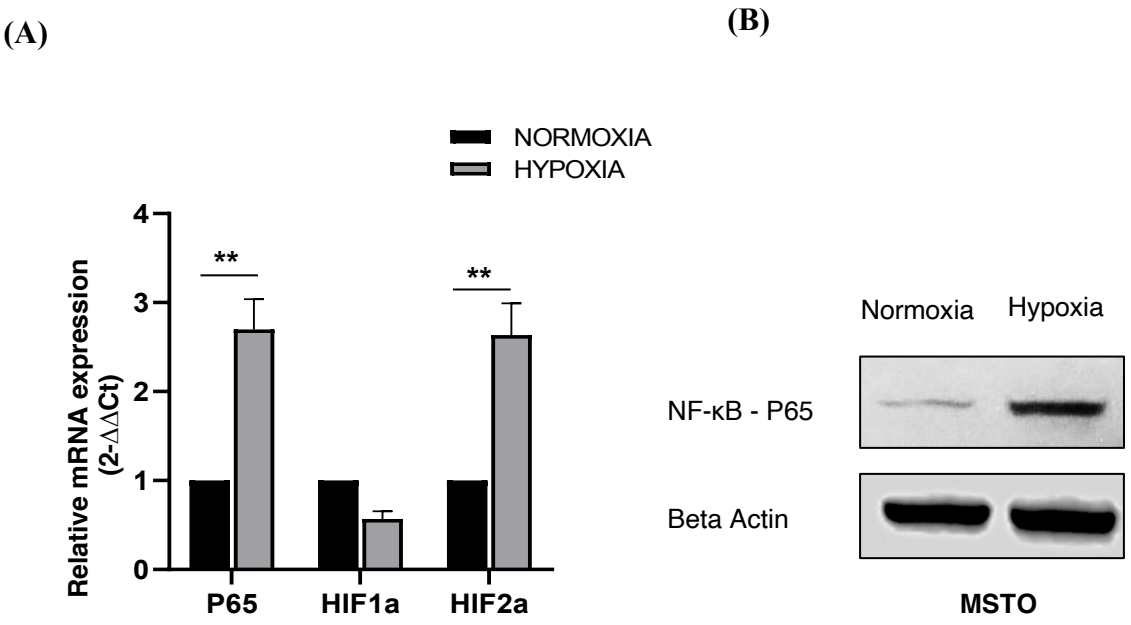

Figure 6.1. Hypoxic cultures demonstrate increased mRNA and protein expression of hypoxia-induced NF-KB-P65. *The relative mRNA and protein expression of hypoxia-induced proteins. (A) mRNA expression in normoxia and hypoxia cultures of MSTO-211H cells. (B) Protein expression in normoxia and hypoxia culture of MSTO-211H cells. n=3, **p<0.01*

6.3.2. Stable transfection of NF-κB-p65 into MSTO-211 cell line

Stable transfection of pcDNA3.1 NF-κB-p65 was performed on MSTO-211H cell line to overexpress NF-κB-p65. Two successfully transfected clones, C12 and C15, with high NF-κB-p65 expression were selected. Figure 6.2. (A) To confirm the success of NF-κB-p65 transfection western blot analysis was performed to identify the whole protein expression of NF-κB-p65. Western blot determined the final screening for the clones (B) To confirm an increase in the relative mRNA expression of NF-κB-p65 in

both C12 and C 15 compared to mock. Figure 6.2 (A) shows an increase in the detection of NF-κB-p65 whole protein signals for both C12 and C15 as compared to the mock. β-Actin used as a loading control for whole protein detection. Figure 6.2 (B) displays a significant increase in the relative mRNA expression of NF-κB-p65 in both C12 and C15 compared to mock, and the results further verify the success of NF-κB-p65 transfected cell lines.

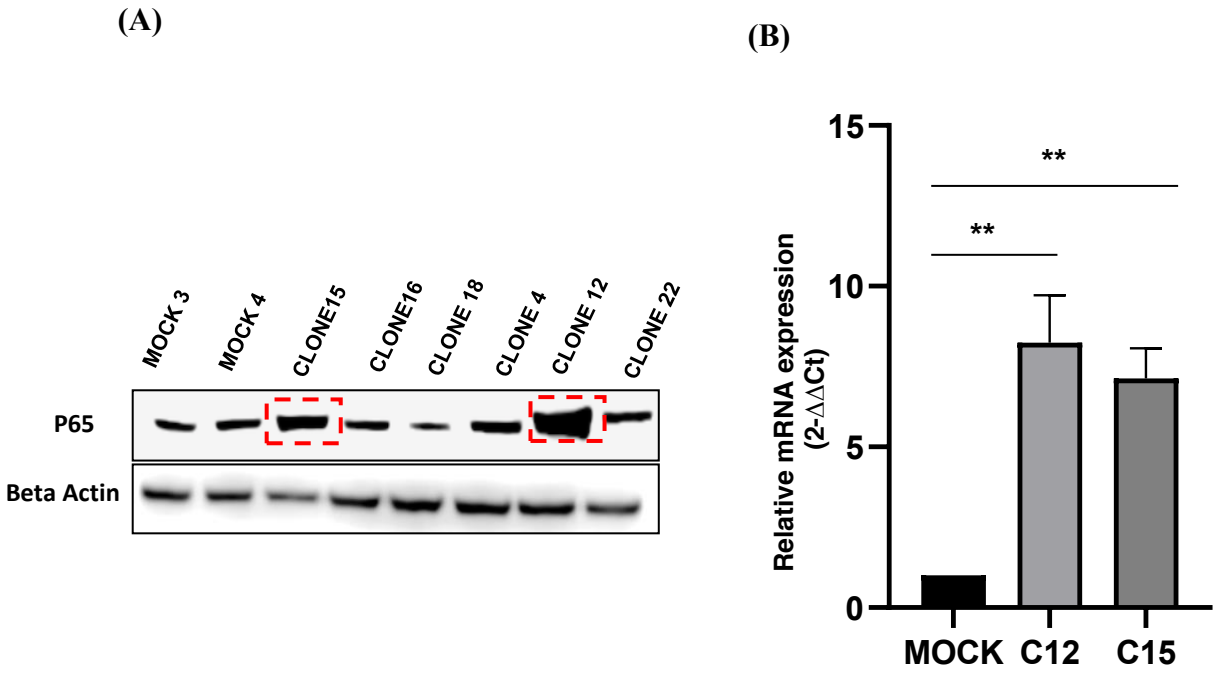

Figure 6.2. Successful stable transfection of NF-κB-p65 in MSTO 211H cell line.

*(A) Western blot analysis used to screen the NF-κB-p65 overexpressed in NF-κB-p65 transfected MSTO-211H cell lines, C12 and C15 demonstrated ectopic expression as compared to mock. β-actin has used as a loading control (B) The relative mRNA expression of NF-κB-p65 was analysed using RT-PCR $2^{-\Delta\Delta Ct}$ method for further confirmation. n=3, **p<0.01*

6.3.3. NF-κB-p65 transfected cell lines does not induce CSC traits

Hypoxic cultures significantly promote the expression of CSC related proteins, but NF-κB-p65 transfected cell lines did not demonstrate an increase in the detection of CSC markers. Figure 6.3. shows the flow cytometric analysis of CSC markers in ALDH, CD133 and ABCG2 in NF-κB-p65 transfected clones C12 and C15 compared to the mock. The transfected cell lines demonstrated statistically no significant increase in the expression of ALDH, ABCG2 and CD133.

(A)

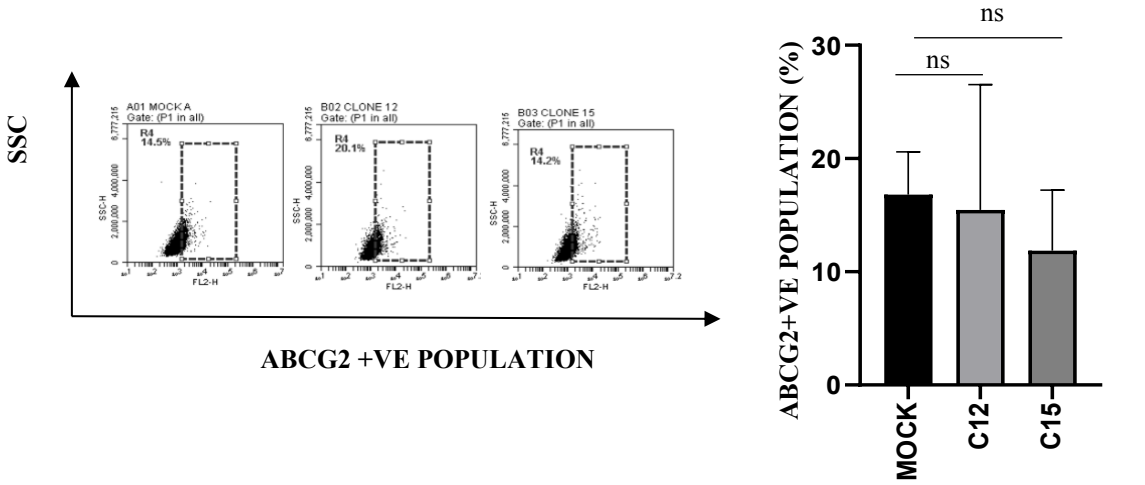

(B)

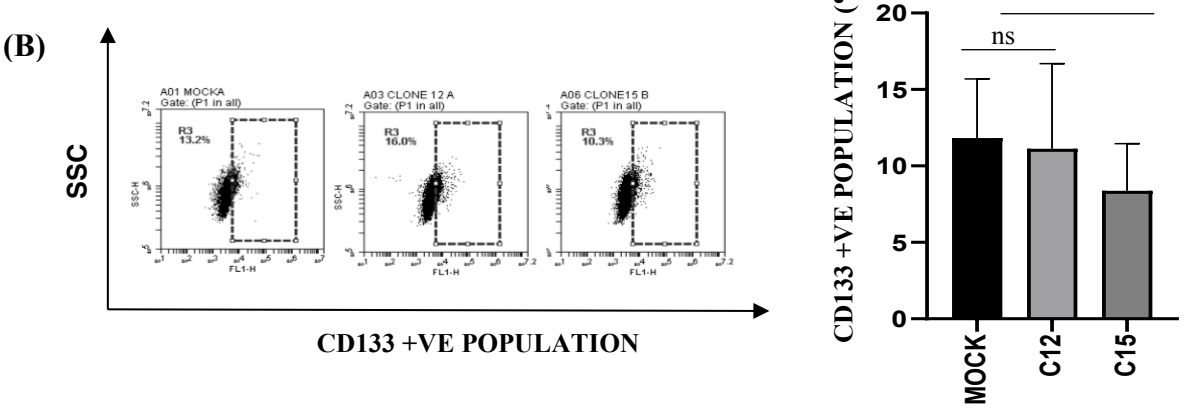

(C)

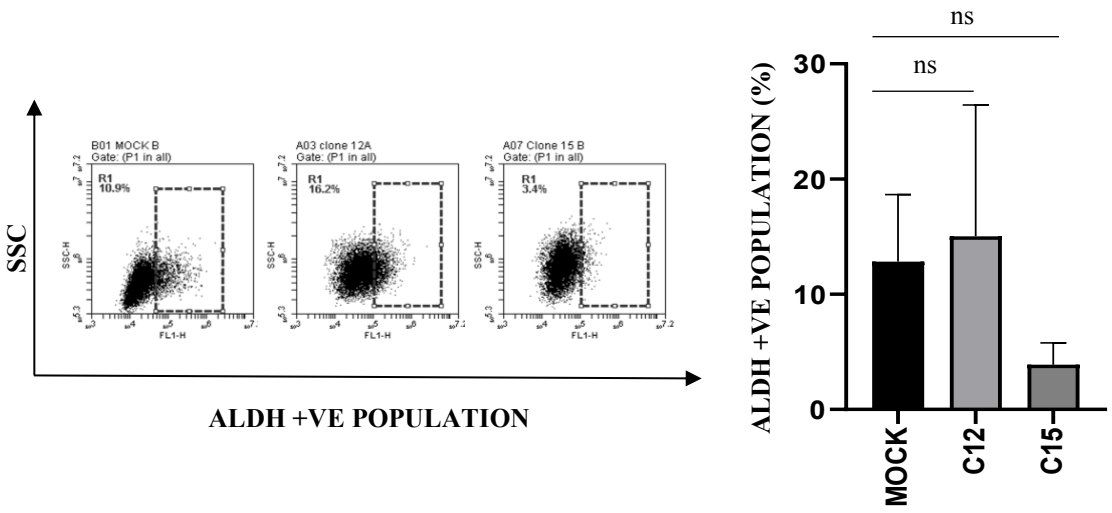

Figure 6.3. NF-κB-p65 overexpression does not induce expression of CSC markers.

The expression of CSC markers was analysed using flow cytometry. (A) ABCG2 using APC conjugated anti-ABCG2, (B) CD133 using FITC conjugated anti-CD133 and (C) ALDH activity using ALDEFUOR. The bar chart displays the population of cells expressing CSC markers.

6.3.4. NF-κB-p65 transfected cell lines does not induce ESC traits

To further identify if NF-κB-p65 expression correlates with CSC characteristics, the relative mRNA expression of ESC transcription factors SOX2, OCT4 and NANOG were analysed by qRT-PCR and shown in Figure 6.4 The bar charts signify non-significant increase in relative mRNA expression for all targets in C12 and C15 compared to mock.

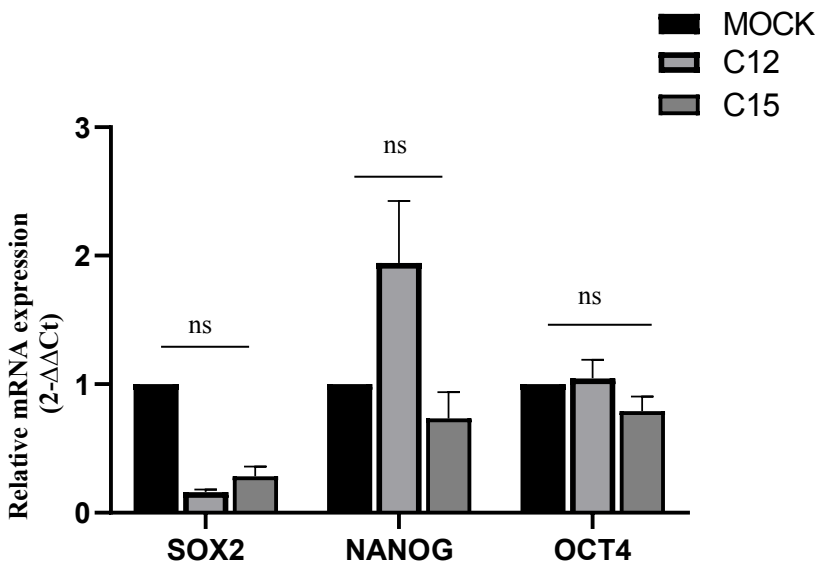

Figure 6.4. NF-κB-p65 transfected MSTO 211H cells demonstrate non-significant increase in the expression of ESC markers.

The relative mRNA expression of ESC markers SOX2, OCT4, NANOG analysed using RT-PCR $2^{-\Delta\Delta Ct}$ method. n =3, ns denotes no- significance ($p \geq 0.05$)

6.3.5. NF-κB-p65 transfected cell lines does not induce EMT and invasiness related markers.

Hypoxic cultures significantly promoted the expression of EMT characteristics, but NF-κB-p65 transfected cell lines did not demonstrate statistically significant increase in the expression of EMT markers. Figure 6.5. shows the relative mRNA expression of (A) EMT markers i.e. Snail 1, Snail 2, ZEB, Twist, E-cadherin, N cadherin, Vimentin and (B) Invasiveness related markers i.e. MMP2, MMP9 and MMP7 in NF-κB-p65 transfected clones C12 and C15 compared to the mock.

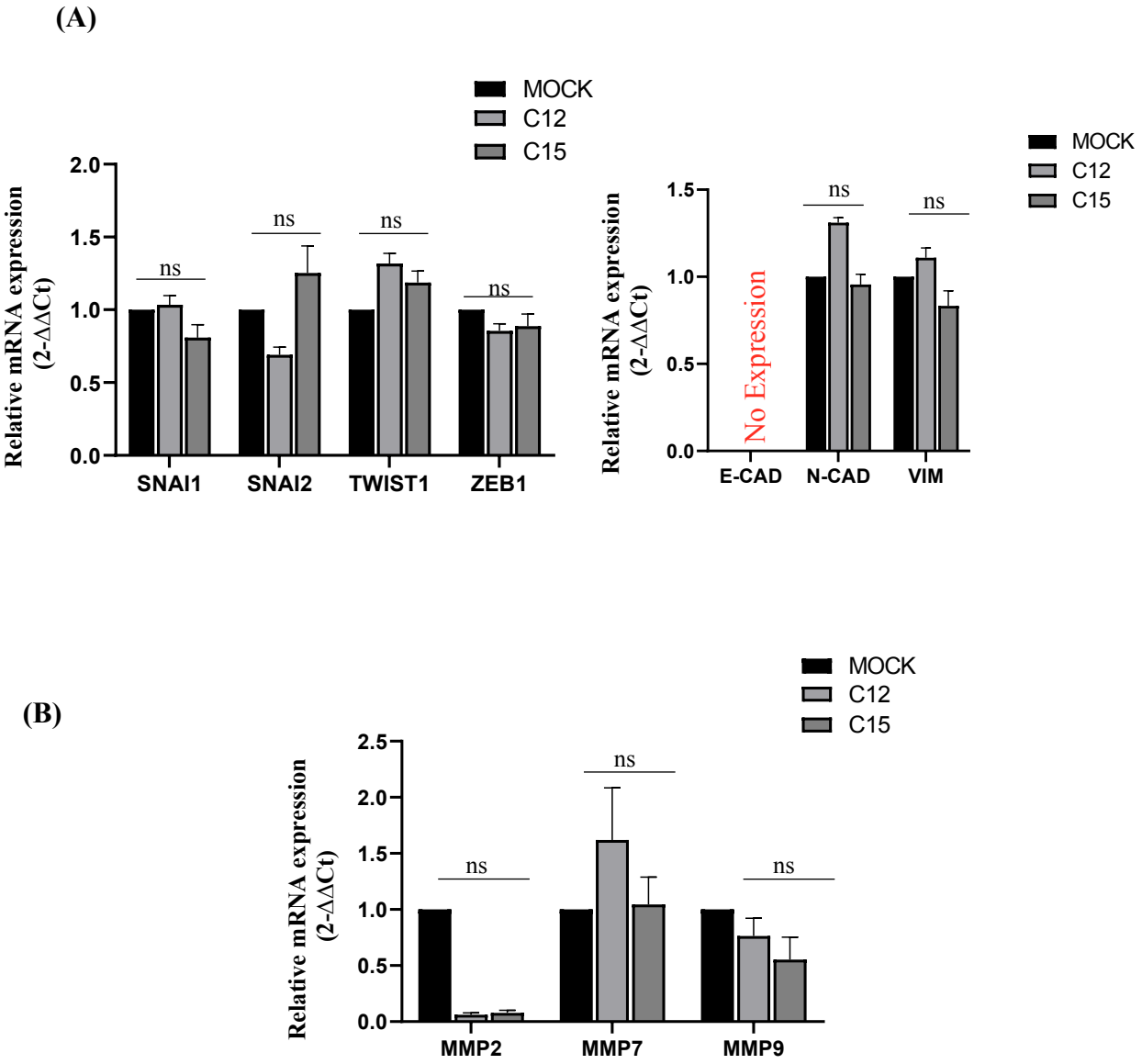

Figure 6.5. NF-κB-p65 transfected MSTO 211H cells demonstrate non-significant increase in the expression of EMT and invasiveness related markers.

The relative mRNA expression of (A) EMT markers i.e., Snail 1, Snail 2, ZEB, Twist, E-cadherin, N cadherin, Vimentin and (B) Invasiveness related markers i.e. MMP2, MMP9 and MMP7 in NF-κB-p65 transfected clones C12 and C15 compared to the mock was analysed using RT-PCR 2-ΔΔCt method. n=3, ns denotes no- significance ($p \geq 0.05$)

6.3.6. NF-κB-p65 transfected cell lines did not show chemoresistantance

Hypoxia stimulated stress drives NF-κB pathway and hypoxic cultures in chapter 3 showed a significant effect of hypoxia on resistance to first line drugs. Figure 6.6. shows the cell viability curves and compares the cytotoxic effect of first line drugs between NF-κB-p65 transfected cell lines. These results demonstrated that the mock showed more resistance to NF-κB -p65 transfected clones, as the curve for the clone declines at lower drug concentration. Table 6.1 shows the calculated values for Mock are greater than the IC50s calculated for the clones C12 and C15 and demonstrate significant resistance to PMT and CIS.

(A)

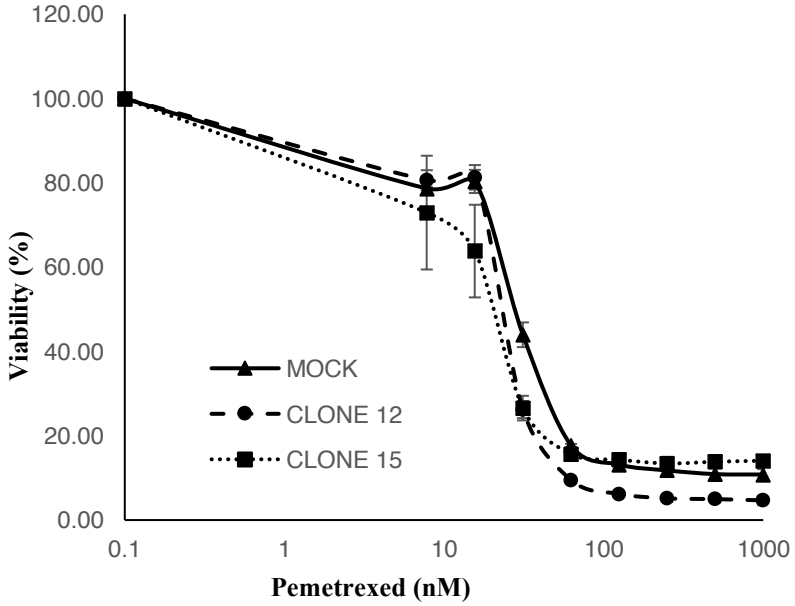

(B)

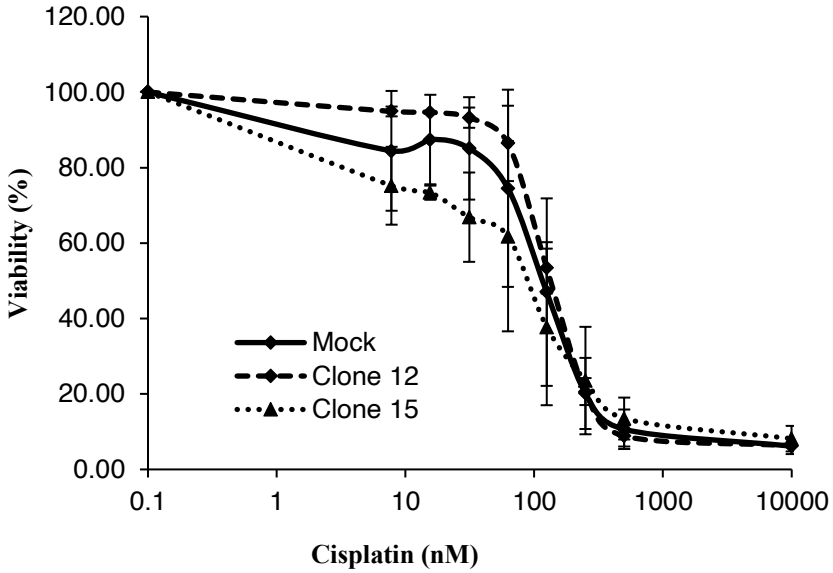

Figure 6.6. NF-κB-p65 transfection does not induces chemoresistance.

The cell viability curves depict the effect of first line drugs on NF-κB-p65 transfected MSTO 211H cell lines, C12 and C15 as compared to mock. The cells were incubated with (A) PMT (B) CIS for 72 hours and then subjected to MTT assay.

Table 4.1. IC50 values for MSTO 211H pcDNA3.1 NF-κB-p65 cell lines (mock, C12 and C15) after 72 hours treatment with anticancer drugs.

	NF-κB -P65 transfected clones		
	Mock	**C12**	**C15**
Pemetrexed	29.41 ± 1.25	25.22 ± 0.73	20.22 ± 4.73
Cisplatin	1179.84 ± 572.36	1036.85 ± 544.34	909.87 ± 626.18

6.3.7. Stable knockout of NF-κB-p65 in MSTO-211 cell line

In order to determine the effect of NF-κB-p65 on MM cells, I also used CRISPR - Cas9 technology to knock out NF-κB-p65 in MSTO-211H cell line. Three successfully transfected clones were selected C2, C13 and C16 during a screening procedure to determine the expression and activity of NF-κB-p65 compared to the scramble vector transfected control cell line. Figure 6.7. (A) To confirm the success of NF-κB-p65 knock out and screening by western blot analysis was performed to identify the whole protein expression of NF-κB-p65 knock out. (B) To confirm an increase in the relative mRNA expression of NF-κB-p65 C2, C13 and C 16 were compared to mock. Figure 6.7. (A) shows no expression of NF-κB-p65 whole protein signals for both C2 and C16 compared to the scrambled. β-Actin was used as a loading control for whole protein detection. Figure 6.7 (B) displays a significant decrease in the relative mRNA expression of NF-κB-p65 in C2, C13 and C16 compared to scrambled, these results further verify the success of NF-κB-p65 knockout in transfected cell lines.

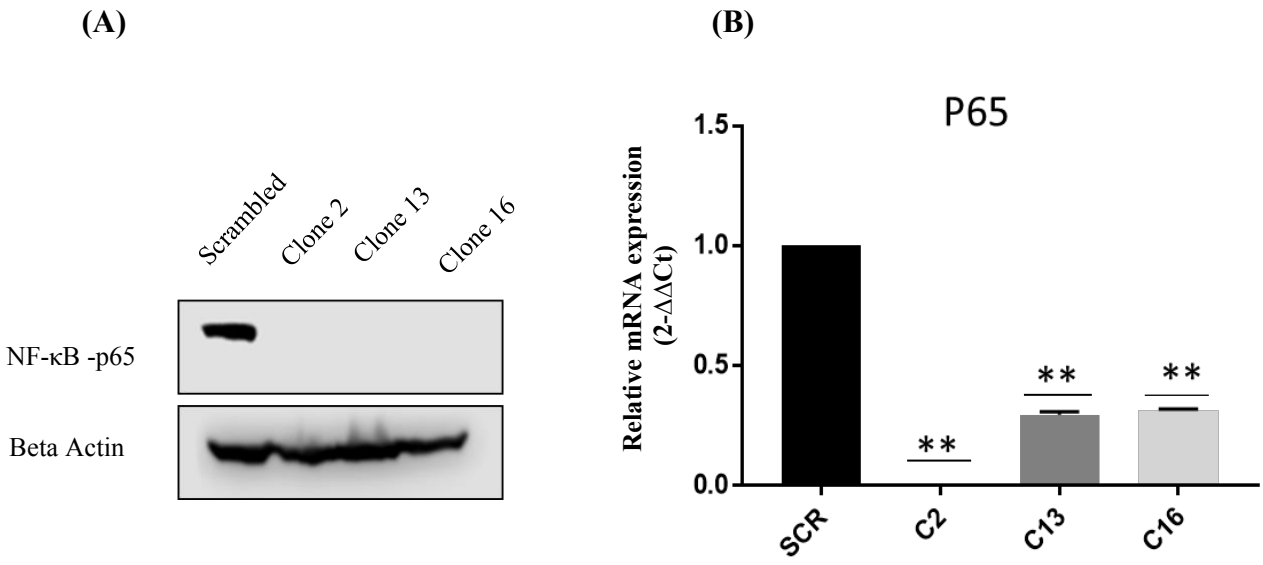

Figure 6.7. Successful stable transfection of NF-κB-p65 knock out in MSTO 211H cell line.

(A) Western blot analysis was used to determine NF-κB-p65 knock out in NF-κB-p65 transfected MSTO-211H cell lines, C2, C13 and C16 demonstrated decreased expression of NF-κB -p65 as compared to mock. β-actin was used as loading control (B) The relative mRNA expression of NF-κB-p65 was analysed using RT-PCR $2^{-\Delta\Delta Ct}$ *method for further confirmation. n=3, **p<0.01.*

Discussion

The previous study identified the hypoxic stimulus as a major contributing factor to the development of CSC traits and chemoresistance in MM. In this chapter, it was shown that MM hypoxic cultures equally demonstrate a significant increase in the expression of transcription factors related to metastasis. Hypoxia generates intra-tumoural oxygen gradients, contributing to the plasticity and heterogeneity of tumors and promoting a more aggressive and metastatic phenotype (Jing et al., 2019). Hypoxia induces NF-κB activation in a wide range of cells and NF-κB plays important role in cell survival, proliferation, invasion, migration and chemoresistance (Liu et al.,2014). NF-κB and its target genes have been implicated as mediators in all of the hallmarks of cancer (Hanahan and Weinberg, 2011). Research have shown increased expression of genes with NF-κB binding sequences in their regulatory regions in lungs and cells *in vitro* after exposure to crocidolite asbestos in lung cancer, and mesothelioma. The fibrous nature of asbestos is essential for activation of NF-KB (Yvonne et al.,1997). *In vitro* models evaluating the impact of asbestos on cell cycle regulation and survival have discovered a significant relationship between activation of NF-κB pathways and cellular protection from asbestos induced cell. This effect has been verified by selective inhibition of NF-κB, which subjects the exposed cells to programmed cell death (Chandra et al.,2011).

Malignant cells are “addicted” to NF-κB signaling, which drives oncogenesis, disease recurrence and therapy resistance in both solid and hematological malignancies, where it induces transcriptional programmers sustaining all hallmarks of cancer (Verzella et al.,2020). As NF-κB is the key transcription factor involved in the inflammatory

pathway, NF-κB is constitutively active in most cancers, and many of the signaling pathways implicated in cancer are likely to be networked to the activation of NF-κB. The cell signaling intermediates that are frequently mutated in human cancers have been directly/indirectly networked with NF-κB pathway (Chaturvedi et al.,2011). NF-κB target genes play an important role in the regulation of many of the pathways involved in the hallmarks of cancer (Godwin et al.,2013). Cheng et al. concluded that HIF-1α-activated NF-κB could promote EMT in pancreatic cancer cells by inhibiting E-cadherin and promoting N-cadherin (Tam et al.,2020) The p65/p50 is the most common NF-κB dimer and plays a major anti-apoptotic role in anticancer drug treated mammalian cells (Wang et al.,2003). The p65 transactivator subunit of NF-κB, RelA, was recognized earlier as the potential oncogene. The p50-p65 heterodimer interacts with many other transcription factors that are regulated by epigenetic modifications at the promoters of responsive genes (Chaturvedi et al.,2011). The canonical pathway for NF-κB activation involves the re-localization of NF-κB p65-p50 dimers to the nucleus (Samuel et al., 2014)

Various oncogenic insults such as in Ras, P53 and EGFR leads to the activation of NF-κB pathway in tumor cells. Due to inflammatory environment and several oncogenic mutations a significant number of neoplasms have constitutive NF-κB activity. As a corollary, the frequent up-regulation of the NF-κB signaling pathway in multiple forms of carcinoma establishes a complimentary microenvironment, which is critical for either tumor initiation or tumor development, or both. (Xia et al.,2014). Our previous work has shown that High NF-κB activity has been identified in drug-resistant cancer cells and ectopic over-expression of NF-κB can block anticancer drug-induced apoptosis (Yip et al.,2011). Exposure of cancer cells to anticancer drugs,

cytokines and radiation can induce the nuclear translocation and DNA binding activity of NF-κB. Human cancer cells with induced NF-κB nuclear activity have demonstrated resistance to apoptosis induced by chemotherapy or radiotherapy (Wang et al.,2003) The mechanism by which NF-κB is induced by drugs or how the genes driven by NF-κB causes drug resistance are not completely understood. The drug driven damage to cancer cell DNA is believed to trigger NF-κB by the protein IKK-gamma. DNA-damage activates ATM kinase, which in turn activates NF-κB essential modifier (NEMO), a component of the IKK complex that induces nuclear translocation of the p65/p50 transcription factor complex (Verzella et al.,2020) Regulation of gene expression is essential for cell maintenance. Transfection is performed to understand the function of gene by enhancing or inhibiting its expression in cells (Kim and Eberwine.,2010) Liu et al transfected Breast cancer (BC) cells with NFκB p65 to determine the importance of NFκB with respect to CSC traits. The transfected clones expressed high levels of BC stem cell markers and were highly resistant to Doxorubicin and Paclitaxel. Therefore, NFκB certainly conferred CSC traits upon BC cells (Liu et al.,2014)

In order to understand the transcriptional activity of NF-κB in MM, stable transfection of NF-κB-p65 over expression and NF-κB p65 knockout was performed on MSTO-211H cell lines. The former study identified specific CSC markers to be overexpressed in hypoxic cultures. Research has revealed that in the bulk of tumors in which NF-κB is constitutively active, it frequently provides cancer cells with a survival advantage by upregulating antiapoptotic genes. Cancer stem-like cells, which utilize the NF-κB pathway, may be responsible for resistance and for re-seeding of the tumor mass after initially effective chemotherapy or radiation (Verzella et al.,2020). We hypothesized

that persistent activation of the NF-κB-p65 pathway drives the maintenance of the stem-like phenotype in MM. This study did not recognize a statistical increase in the expression of CSC, EMT and ESC markers in NF-κB -p65 overexpressed transfected cell lines, indicating NF-κB-p65 may be not be responsible for the generation of CSC in MM. The findings suggest that NF-κB-p65 might not play a pivotal factor in driving CSCs in MM.

It has been shown that in many types of cancer, that chemotherapy and radiotherapy induce constitutive activation of NF-κB, thereby making the tumor non-responsive to the treatment (Chaturvedi et al.,2011). In addition, the previous study demonstrated that the detection of specific CSCs confirms chemoresistant properties in MM hypoxic cultures. NF-κB is also heavily implicated in the development of resistance to platinum-based chemotherapies, such as Cisplatin. Therefore, NF-κB represents an attractive target for anti-cancer therapy particularly as an adjuvant to overcome resistance to platinum-based chemotherapeutics (Godwin et al.,2013). Therefore, we overexpressed and knocked-out NF-kB-P65 to confirm its role in causing chemoresistance in MM. The NF-κB-p65 over expressed transfected cell lines did not demonstrate CSC traits along with no increase in resistance to first line drugs. The MTT assay in this study clearly shows NF-κB-p65 over expressed cell lines did not display a significant increase in resistance to PMT and CIS treatment. One of the reasons speculated here can be that first line drugs elicit their effects in various ways which may not induce apoptosis, therefore, may not be directly affected by NF-κB-p65 overexpression.

Transfection with CRISPR/Cas9 system has been extensively used in easy-to-manipulate cells (Saber et al.,2018). CRISPR/Cas9 is a very powerful gene editing tool for exploring the function of defined genes in cell signalling pathways, proliferation, migration, invasion and potentially chemotherapy resistance (yang et al.,2019). NF-κB -p65 gene was successfully knocked out in MSTO-211H cell line by using CRISPR - Cas9 technology. The result obtained by over expression should be further confirmed by NF-κB -p65 knock out cytotoxicity assay and expression of CSC markers, which would further reconfirm that NF-κB does not drive chemoresistance in MM. Due to time constraints further experiments on NF-κB -p65 knock out could not be performed. This study implicates the possibility if NF-κB-p65 induce CSC traits and chemoresistance in MM.

CHAPTER 7

General Discussion

7.0 Discussion

Malignant Mesothelioma is a highly malignant disease that most often occurs in the pleura of the thoracic cavity, followed by the peritoneum, pericardium, and tunica vaginalis testis (Levy et al.,2019). The standard first-line chemotherapy includes a combination of Cisplatin and Pemetrexed. However, median survival is 12.7 months, and most patients become resistant to chemotherapy and relapse quickly. Currently, there are no second-line treatment options for relapsed patients (Staumont et al. ,2020). Recent research has further shown that MM contains hypoxic regions, which explains the link between tumour hypoxia and poor therapeutic efficacy. However, the underlying mechanism of hypoxia in MM remains largely unknown.

The present study showed that hypoxia promotes aggressive phenotypes in MM cells. By inhibiting apoptosis and inducing drug resistance, hypoxia enhances *in vitro* clonogenicity, migration, invasion in MM cells (Kim at al.,2018). It promotes EMT associated CSC properties, including self-renewal in which CSC enrichment occurs upon exposure to hypoxia-inducible factor HIF-1α *in vivo*; and promote resistance to chemotherapy (Najafi et al.,2019). HIF-1α is commonly expressed in MM and play a significant role in keeping with its aggressive behaviour and chemoresistant phenotype (Klabatsa et al.,2006). Mesotheliomas are particularly hypoxic solid tumour masses. Imaging evidence from [F-18] fluoromisonidazole (FMISO) PET-CT scanning confirms hypoxia being integral to mesotheliomas (Nabavi et al.,2016). Therefore, we observed the effect of hypoxia on chemosensitivity and invasiveness in MM. The results of this study have confirmed that the hypoxic status in MM promotes CSC traits and induces chemoresistance.

Studies have suggested that hypoxia and some hypoxia-regulated transcription factors are the determinants for the stemness of CSCs (Conley et al., 2012). CSCs are a small subpopulation of tumour bulk, but they are mainly responsible for tumour mass renewal, recurrence and chemoresistance (Milosevic et al.,2020). Hypoxia functions to increase CSC number and helps in maintaining their stem-like state allowing the subsequent growth and metastasis and hence considered as a critical physiological component of CSC niche (Yadav and Desai.,2019). Recent research has shown that the generation of CSCs occurs in part as a result of EMT. This hypoxia-induced EMT leads to an increase in CSCs during tumour progression, which subsequently enhances invasion and metastasis (Yeo et al.,2017). EMT is also involved in progresson of cancer and metastasis, and HIF-1 has been identified as a regulator of EMT in human cancers (Zhang et al.,2019). CSCs possess the critical survival mechanisms and properties crucial for the maintenance and propagation of the tumour (Marwa M.,2018).). Both EMT and stemness are associated with resistance to chemotherapy in tumours (Yeo et al.,2017).

We hypothesized that the hypoxic microenvironment/stress of the tumour is responsible for maintaining stemness in CSCs. To further study the effects of hypoxia on MM cell lines, attached monolayer cultures were incubated under hypoxic conditions. The results demonstrated a strong correlation to the hypoxic environmental stress and the expression of CSC specific markers. Chronic, diffusion-limited hypoxia due to an increase in diffusion gap with tumour growth results from excess in oxygen supply and demand (Tameemi et al., 2019). Activation of stem genes along with dedifferentiation, under hypoxic conditions, advances stemness in the cells (Yadav

and Desai.,2019). Also, the hypoxic microenvironment maintains the undifferentiated state of cancer cells and enhances their cloning rate. CSCs can also adapt to a new method of cell energy metabolism and avoid apoptosis caused by hypoxia (Yang et al.,2019). There is growing evidence that CSC are innately resistant to radiation, redistributing the cells in the cell cycle, by stimulating the repair of DNA damaged, increasing activation of the DNA damage checkpoint, and repopulating and reoxygenating areas of hypoxia in the tumour. The reversible conversion capacity of CSCs also attributes to protect themselves from chemo-radiotherapeutic insults (Das et al.,2020). This study confirms the elevated expression of CSC markers, metastasis and invasion related markers in correlation with hypoxia.

The results from this study also demonstrate that CSCs cause chemoresistance in MM cell lines and thus can be potential targets to overcome chemoresistance. Strong preclinical evidence supports the role of hypoxia and MM cancer stem cells (CSCs) in determining tumour resistance to therapies. Indeed, studies have observed that MM includes hypoxic regions and that several signaling pathways are involved in tumour initiation, growth and maintenance, as well as chemo-radio-resistance, are known to trigger the hypoxic microenvironment. Hypoxia also modulates gene and microRNA expression, which are also associated with stemness and to resistance to therapies (Abbott et al.,2020). The CSC and ESC markers were studied in monolayered cultures, and the specific markers studied were CD133, CD24, ABCG2, SOX2, NANOG and OCT 4. CD24 is considered the primary marker of MM in many cases (Yamazaki et al.,2012). It has been shown that Mesothelioma stem cells (MSC) increase and become more resistant after chemoradiation (Wu et al.,2018). Also, elevated levels of OCT4 and other stemness markers in MM cells derived from mesosphere are paralleled by

an increased tumour-initiating capacity (Blum et al.,2017). Overall MM cultures demonstrated a significant increase in the detection of the above markers, and the expression of these markers is associated with poor survival in MM. Also, studying a variety of CSC markers further confirm the significant changes in the phenotype and is beneficial in understanding the molecular interactions and response to anti - MM drugs. The anti-MM drugs used in this study include first-line cytotoxic agents Pemetrexed and Cisplatin. Surgical therapy is only for patients who can handle surgical risks and who have a low tumour stage. Radiation therapy (RT) has a role in MM treatment as well, as it can be in conjunction with chemotherapy and can provide local tumour control if the patient has a good performance status. Toxicity, however, is significant, and thus RT alone has little benefit unless it aims to relieve specific symptoms such as chest pain. Modern targeted therapies have shown benefit in other human tumours - e.g., lung cancers-have so far failed in MM. Although combination therapy, consisting of Cisplatin and Pemetrexed, has shown promising prognostic outcomes and a response rate of 41.3%, making it the standard treatment for MM, overall survival has been a low 16.6 months (Tolani et al.,2018). In the present study, the hypoxic cultured MM cells showed similar traits and demonstrated resistance to anti-MM drugs. When hypoxic MM cells were exposed to high drug concentrations by MTT cytotoxicity assay, the cells showed resistance and demonstrated stemness properties and formed resistant colonies after treatment.

The focus of this study is the betterment of the patient's life and improve current treatment regimes. Therefore, this study focuses on the improvement of first-line anti-MM drugs by synergistically enhancing their efficacy with PLGA-DS + Cu, which can potentially provide the best therapeutic outcomes for MM patients. Drug

repurposing has the potential to surpass many challenges associated with de-novo drug discovery. Repurposing of an existing drug guarantees quick clinical trials due to already established pharmacokinetics, tolerability and toxicity profiles (Kaushik et al.,2020). This study also focused on drug repurposing to target mechanisms responsible for causing chemoresistance in MM. DS/Cu has shown to cause regression of mesothelioma growth *in vivo* in part by stimulating apoptosis (Cheriyan et al.,2014). DS generates oxidative stress through the inhibition of NF-κB activation (Tesson et al., 2017) (Triscott, Rose Pambid and Dunn, 2015) (Li et al., 2017). This study focused on repurposing DS in combination with copper chloride, which demonstrated significant cytotoxicity in MM cell lines. Copper has a crucial role in redox reactions and triggers the generation of ROS in human cells. DS/Cu is a potent ROS inducer and proteasome-NF-κB pathway inhibitor (Chen et al., 2006). Combination of DS with Cu may target cancer cells by simultaneously tackling both ROS and NF-κB (Yip et al., 2011). DS also showed synergy with first-line drugs Pemetrexed and Cisplatin by targeting CSCs and EMT pathway. Conventional anticancer drugs target the proliferating and differentiated tumour bulk but fail to eradicate the CSCs, which become the source of tumour recurrence (Yip et al., 2011). The use of DS in the clinics is limited due to its very short half-life in the blood. It inhibits the ability of intact DS to reach distant tissues and organs due to metabolism in the liver which hampers its chelation with Cu (II) rendering it unfavourable for treating cancer. Therefore, our group coated DS with PLGA nanoparticles and extended its half-Life in the blood, allowing it to chelate Cu (II) at the target site (Wang et al.,2016). The nano-encapsulation protects the thiol groups in DS and extends its half-life in the serum from less than 2 min to over seven hrs. and successfully delivers the intact DS to cancer tissues (Butcher et al., 2018). Our results show that PLGA-DS/Cu enhance anti-MM

drugs in cell lines and can potentially improve treatment options for MM patients with negligible side effects.

MM is a heterogeneous neoplasm. Recent classifications take into account the heterogeneity between patient tumours but not the heterogeneity inside the tumour of each patient (Blum et al.,2019). Tumour heterogeneity can significantly affect drug penetration and distribution (Abbott et al.,2020). Therefore, cancer stemness is highly heterogeneous. Different pathways may express at different times in different tumour types, resulting in distinct stemness characteristics. Activation of stemness pathways can identify in cells expressing distinct CSC markers (Lathia, Liu and Matei.,2020). CSCs has implicated in contributing to tumour heterogeneity and metastasis. For these reasons, CSCs may represent the "root of cancer", and their elimination represents a promising yet investigational therapeutic strategy (Castagnoli et al.,2020). Traditionally, CSCs has been described as preferring hypoxic conditions, and the CSC niche is described as hypoxic and acidic (Steinbichler et al.,2020). Research has shown that CSCs that can form spheres to retain their stem cell properties for many passages, while most differentiated cells die from anoikis (Liu et al.,2020). CSCs can create spheroids in blood circulation. The ability to form spheroids is considered a unique feature of CSCs. These CSC containing spheroids in the blood of cancer patients might generate a "micro-niche" that support CSC survival and adaptation in the bloodstream (Steinbichler et al.,2020). The most commonly used method of function-based CSC enrichment is the sphere reformation assay, in which spheres form CSCs which can grow as non-attached in serum-free medium and form non-adherent 3-dimensional (3D) tumour sphere structures which is characteristic reminiscent of the ability of CSCs to initiate tumours and maintain tumour progression (Liu et al.,2020). This study

used suspension culture and kept it additionally with growth factors and other essential nutrients, which helped to promote the cell aggregation and encouraged the spheroid formation of different shapes and sizes. These spheroids were then treated with different drugs, i.e. Pemetrexed, Cisplatin, Copper, PLGA-DS and PLGA-DS+ Cu. The results showed that the spheroids aggregated again when treated with first-line drugs and Copper and PLGA-DS separately. Still, the combination of PLGA-DS + Cu was able to eliminate sphere reformation in MM cell lines. Therefore, the sphere reformation assay shows that MM spheroid cells are resistant to first-line MM drugs. The results also indicate that certain culture conditions are required to promote CSC expression and induce chemoresistance since the MM cells which survived after treatment again generated spheroid cultures.

Our previous work has shown that hypoxia drives CSCs by activating NF-κB pathway, which also regulates many genes associated with CSC maintenance. The NF-κB pathway has also implicated in EMT and metastasis by transcriptionally up-regulating master-switch transcription factors required for EMT, such as Slug. There is accumulating evidence for an essential link between EMT and the invasion, metastasis and self-renewal traits of cancer cells. Among all the known factors involved in the EMT, the transforming growth factor-beta 1 (TGF-b) signalling pathways have taken centre stage. Coordinated activation of NF-κB and TGF-b signalling cascades effectively induces EMT and the expression of genes related to stemness and cell invasion (Li et al., 2017; Benedetti et al.,2015). High NF-κB activity is identified in drug-resistant cancer cells, and ectopic overexpression of NF-κB can block anticancer drug-induced apoptosis (Wang et al., 1998, 1999, 2004). The p65/p50 subunit is the most common NF-κB dimer and plays a significant anti-apoptotic role in anticancer

drug-treated mammalian cells (Wang et al.,2003). NF-κB induction frequently contributes to a dysregulated apoptotic response in response to chemotherapy, which could mediate chemoresistance (Godwin et al., 2013). Hypoxia induces several complex intracellular signalling pathways such as the major HIF pathway. Other hypoxia-associated pathways include PI3K/AKT/mTOR, MAPK and NF-κB pathway. These pathways have involved in cell proliferation, survival, apoptosis, metabolism, migration, and inflammation (Barbara Muz et al.,2015).

Research has shown increased expression of genes with NF-κB binding sequences in their regulatory regions in lungs and cells *in vitro* after exposure to crocidolite asbestos in lung cancer, and MM. The fibrous nature of asbestos is essential for the activation of NF-κB (Yvonne et al.,1997). Upon contact with asbestos fibres, macrophages produce Tumor Necrosis Factor-alpha (TNF-α), which is a key cytokine involved in inflammatory processes such as acute-phase reaction, systemic inflammation, and chronic inflammation. TNF-α binds to TNF-α Receptor 1 located on mesothelial cells, thereby activating NF-κB. Activation of the NF-κB pathway allows mesothelial cells with DNA damage as a result of exposure to asbestos fibres to survive and proliferate (Hiriart et al.,2019). *In vitro* models evaluating the impact of asbestos on cell cycle regulation and survival have discovered a significant relationship between activation of NF-κB pathways and cellular protection from the asbestos-induced cell. This effect is verified by selective inhibition of NF-κB, which subjects the exposed cells to programmed cell death (Chandra et al.,2011). In line with the previous studies, the hypoxia cultured cells express a high level of NF-κB-p65. Therefore, we hypothesized that hypoxic tumour microenvironment promotes the existence of CSCs by activation of the NF-κB pathway in MM. Extensive bidirectional crosstalk between HIF and NF-κB has also been described, highlighting the influence that hypoxia may have on the

sub adjacent pathways. NF-κB subunits are located in the cytoplasm in an inactive form, allowing a rapid response following an activating stimulus (Tirpe et al.,2019). Since hypoxia activates NF-κB, this study compared the mRNA and protein expression of NF-κB-p65, in attached/normoxic and hypoxic cultures. The results showed an increased expression of NF-κB-p65 in hypoxic cultures as compared to normoxia in both protein level and mRNA levels. Therefore, these findings suggest that hypoxia-induced stress can increase the expression of NF-κB in MM cell lines. NF-κB showed significant support for cancer development and maintenance. Additionally, NF-κB is important for metastasis through epithelial to mesenchymal transition EMT. Hence, the NF-κB pathway is a promising target for cancer therapy (Pires et L.,2018).

A large body of evidence exists to support the rationale of pursuing novel therapies which modulate the NF-κB pathway (Godwin et al., 2013). NF-κB protects DNA-damaged cells from apoptosis and stimulates cell proliferation, which at least partly contributes to its role in promoting cell transformation (Lin et al.,2010). Also, in many types of cancer, chemotherapy and radiotherapy induce constitutive activation of NF-κB, thereby making the tumour non-responsive to the treatment (Chaturvedi et al.,2011). We hypothesized that NF-κB drives chemoresistance in MM. Cisplatin is the first-line drug used as combination chemotherapy for the treatment of MM. Platinum-based drugs cause apoptosis by forming DNA adducts. Cisplatin causes the chronic activation of apoptotic MAPK and c-Jun N-terminal kinase (JNK) pathways. NF-κB can also be activated by this mechanism, resulting in selective apoptotic signalling. By this mechanism, the NF-κB activation can be driven by MAPK pathway in response to Cisplatin treatment. It means that inactivating mutations in the JNK pathway could lead to signalling only via NF-κB pathway in response to Cisplatin

treatment, thereby providing a potential mechanism of resistance (Godwin et al.,2013). Therefore, NF-κB represents an attractive target for anticancer therapy, particularly as an adjuvant to overcome resistance to platinum-based chemotherapeutics (Godwin et al.,2013).

Since NF-κB is shown to be activated in tumour progression, therefore, to understand its role in depth, MSTO-211H cell lines were transfected with pcDNA 3.1 and NF-κB-p65 was successfully overexpressed. Two positive clones were selected based on the relative increase in the mRNA expression determined by qRT-PCR and the increase in protein concentration by western blot analysis. NF-κB proteins are involved in the dimerization of transcription factors, regulate gene expression and affect various CSC biological processes, including inflammation, stress responses, growth, and development of CSCs (Yang et al.,2019). This study did not identify any association between increased expression of NF-κB and CSC traits.

The overexpressed clones did not demonstrate resistance to anti-MM drugs as compared to the mock, and the expression level of CSC markers did not increase as compared to the mock. Therefore, NF-κB did not depict a clear association with chemoresistance caused by CSC traits. Also, the complex mechanism of chemoresistance makes it challenging for finding a promising therapeutic target. Although many previous publications, including our group, has demonstrated that NFκB is responsible for cancer stemness and chemoresistance, I did not have the same findings in MM cell line. Therefore, the role of NFκB may be dependent on cancer type. To further confirm the obtained results from ectopic expression in MM, CRISPR-Cas 9 technology was used to knock out NF-κB-65. Similar to the overexpression, two knocks out clones were selected and compared to scrambled for

cytotoxicity. However, I was not able to carry out further studies because of the time constraints. My findings from the results suggest that NF-κB does not play a prominent role in causing chemoresistance in MM. The current proven therapy for MM is combination chemotherapy and is widely practised along with surgery and radiotherapy where possible, considering the age and status of the disease. Also, this study and recent other studies have shown the importance of CSCs in causing chemoresistance. Therefore, the development of drugs targeting CSC along with conventional anticancer drugs suggests improving the response rate in MM patients.

Drug repurposing promises a quicker and cost-effective alternative for new drugs, especially for orphan cancers like MM. This study focused on repurposing PLGA-DS in combination with Copper to treat MM cell lines. The results of the treatment showed reversed chemoresistance by targeting CSCs. DS could be a way to hit the “Bullseye" given the fact that it not only kills CSCs but also seems to do so by targeting multiple pathways (Triscott, Rose Pambid and Dunn, 2015). Since DS is a bivalent metal ion chelator, DS forms a complex with Cu (DS/Cu) which is more readily taken up by cells (Wu et al., 2018) DS/Cu is a potent ROS inducer (Yip et al., 2011). MTT assay and sphere reformation assay clearly showed that the anticancer activity of DS is directly dependent on Copper in MM cell lines. PLGA-DS/Cu reversed chemoresistance in the hypoxic cultures and inhibited resistant sphere reformation after treatment. The results from my study demonstrated that PLGA-DS/Cu inhibited known MM stemness markers, i.e. CD 24, ABCG2 and CD 133 in MM hypoxia-induced CSC cells. Additionally, PLGA-DS/Cu was able to inhibit ESC markers and eradicated spheroid cultures which further confirmed its ability to target CSCs in MM cell lines. These results confirm that PLGA-DS/Cu demonstrate significant inhibition

of CSC traits, including self-renewal, proliferation and chemoresistance. The successful *in vitro* data from this study and our previous research showing the evidence of PLGA-DS/Cu to target CSCs in NSCLC, glioblastoma and breast cancer makes PLGA-DS/Cu as a potential chemotherapeutic treatment for MM. Further, data from our group has also shown that initial reaction of PLGA-DS chelation with Cu (II) generates extracellular ROS as a byproduct which is lethal to cancerous cells, this is followed by transport of DDC-Cu (a byproduct of PLGA-DS/Cu) which causes intracellular ROS. Thus, making PLGA-DS/Cu work in biphasic reaction and directing the cell towards apoptotic cell death (Tawari et al., 2015).

Remarkably PLGA-DS/Cu also enhanced the cytotoxicity of anti-MM drugs synergistically which improve the efficacy and reduce the toxicity. Further, the study on the key structure of DS, which is responsible for the anti-cancerous activity will aid in the translation of PLGA-DS to the clinic. Our previous study has also shown that PLGA-DS formulation administration by intravenous injection in combination with oral CuGlu significantly improved the efficacy of DS in liver cancer xenografts without causing any side effects (Wang et al., 2017). In line with our previous work, the *in vivo* data based on our study in MM demonstrated significant anti-cancerous activity of PLGA-DS in MM xenograft models. Therefore, the *in vivo* and *in vitro* data confirms the successful combination of DS with Cu as a potential anti-MM drug with little or no known toxicity. It also makes PLGA-DS/Cu as an excellent candidate for combination chemotherapy with conventional anti-MM drugs. It can contribute to the overall improved survival and quality of MM patients.

CHAPTER 8

Conclusions and future work

8.1 Conclusion

To conclude, hypoxic tumour microenvironment plays a significant role in inducing CSC traits and chemoresistance in MM cell lines *in vitro*. CSCs are resistant to all modes of therapies including radio and chemotherapy and possess the ability of self-renewal, proliferation and metastases. Hypoxia generates intra tumoural oxygen gradients which increases the plasticity and heterogeneity in the tumours forming an aggressive phenotype resistant to treatments. Hypoxia induces NF-kB pathway, and many of the target genes transcribed by NF-kB play an essential role in the regulation of various pathways involved in the hallmarks of cancer. DS is a known drug to target cancer stem cells in a copper-dependent manner, with negligible side effects. DS/Cu synergistically enhanced the cytotoxicity of first-line drugs in chemoresistant hypoxic cultures *in vitro*. The intact sulfhydryl group is imperative for DS mechanism of Cu (II) chelation to generate ROS and target cancer cells. Therefore, the success of DS *in vivo* largely depends on copper supplementation along with intact sulfhydryl group to the diseased tissue without getting metabolised. The half-life of DS in the bloodstream is less than 4 minutes. Therefore, our group encapsulated DS with biodegradable polymer PLGA and extended its half-life to ~7 hrs in serum. The encapsulation ensured an adequate ratio of DS to react with the Cu at a distant targeted site. DS is an FDA approved drug for more than 60 years with no known side effects. PLGA-DS/Cu, in combination with anti-MM drugs, can reduce the cytotoxic effects of conventional therapies. This data is consistent with our previous work in treating various other cancers with PLGA-DS/Cu and support translation of PLGA-DS for treating cancer. The successful translation of PLGA-DS to clinics will significantly improve overall survival and quality of life for MM patients.

8.2 Future work

In support of my in vitro studies, CRISPR-Cas9 technology would further elucidate the role of NF-kB in causing chemoresistance in MM cell lines. Due to time constraints, I was not able to further perform experiments on NF-kB-p65 knock out clones to determine the definitive role of NF-kB in MM. I would have also investigated the expression level of EMT and CSC markers on protein level by western blot which would further confirm my results obtained on mRNA level by qRT-PCR. I would also suggest investigating the effect of PLGA-DS on healthy epithelial cells which would indicate that this therapy is selective for malignant cells and not healthy cells. The effect of PLGA-DS Cu and its enhancing effect on conventional anticancer drugs, e.g., cisplatin and pemetrexed on NF-kB transfected cells should also be determined. My results also suggest the active role of HIF 2α in causing chemoresistance in MM. I successfully overexpressed HIF 2α in MSTO 211H cell lines and further experiments would confirm the resistance mechanisms with respect to HIF signalling in MM.

The results obtained in this study showed promising *in vitro* results and was further considered for animal studies which showed valuable insights. But, the translation of PLGA-DS to clinics require various guidelines and mandatory clinical studies. Since mesothelioma is a rare and orphan localised neoplasm, we propose PLGS-DS administration by i.v injection. The ICH guidelines provide the recommendations to support nonclinical evaluations of an anticancer drug before proceeding to clinical trials (ICH Topic S9, 2008). Hence, for clinical trial approvals, we must recognise the detailed pharmacological and toxicological profile of PLGA-DS. This will establish a safe dose for human administration, especially after changing route and formulation.

Scientific poster presentation at conferences

Tyagi, G., Kannappan, V., Zhang, Z., Liu, P., Wang, Y., Szlosarek, P., Wang, Z. and Wang, W., *PLGA-Disulfiram nanoparticles inhibit NF-Kb and PDL-1 pathway and reverse chemoresistance induced by Mesothelioma*.Glasgow, UK, National Cancer Research Institute, November 2019

Tyagi, G., Kannappan, V., Zhang, Z., Liu, P., Wang, Y., Szlosarek, P., Wang, Z. and Wang, W., *PLGA-Disulfiram nanoparticles inhibit NF-Kb and PDL-1 pathway and reverse chemoresistance induced by Mesothelioma*.Wolverhampton, U.K:University of Wolverhampton, June 2019

Tyagi, G., Kannappan, V., Zhang, Z., Liu, P., Wang, Y., Szlosarek, P., Wang, Z. and Wang, W., *PLGA-Disulfiram nanoparticles inhibit NF-Kb and PDL-1 pathway and reverse chemoresistance induced by Mesothelioma*. London, U.K: Mesothelioma Research Network, June 2019

References

Abbott, D., Bortolotto, C., Benvenuti, S., Lancia, A., Filippi, A. and Stella, G., 2020. Malignant Pleural Mesothelioma: Genetic and Microenviromental Heterogeneity as an Unexpected Reading Frame and Therapeutic Challenge. *Cancers*, 12(5), p.1186.

Abu-Serie, M. (2018). Evaluation of the selective toxic effect of the charge switchable diethyldithiocarbamate-loaded nanoparticles between hepatic normal and cancerous cells. *Scientific Reports,* 8(1).

Ahmed I, Ahmed Tipu S, Ishtiaq S. Malignant mesothelioma. *Pak J Med Sci.* 2013;29(6):1433-1438.

Ahmed, M., Chaudhari, K., Babaei-Jadidi, R., Dekker, L. and Shams Nateri, A. (2017). Concise Review: Emerging Drugs Targeting Epithelial Cancer Stem-Like Cells. *STEM CELLS*, 35(4), pp.839-850.

Al Tameemi, W., Dale, T., Al-Jumaily, R. and Forsyth, N., 2019. Hypoxia-Modified Cancer Cell Metabolism. *Frontiers in Cell and Developmental Biology*, 7.

Allensworth, J., Evans, M., Bertucci, F., Aldrich, A., Festa, R., Finetti, P., Ueno, N., Safi, R., McDonnell, D., Thiele, D., Van Laere, S. and Devi, G. (2015). Disulfiram (DSF) acts as a copper ionophore to induce copper-dependent oxidative stress and mediate anti-tumor efficacy in inflammatory breast cancer. *Molecular Oncology*, 9(6), pp.1155-1168.

Arnold, C., Mangesius, J., Skvortsova, I. and Ganswindt, U., 2020. The Role of Cancer Stem Cells in Radiation Resistance. *Frontiers in Oncology*, 10.

Attanoos, R., Churg, A., Galateau-Salle, F., Gibbs, A. and Roggli, V., 2018. Malignant Mesothelioma and Its Non-Asbestos Causes. *Archives of Pathology & Laboratory Medicine*, 142(6), pp.753-760.

Bahmad, H., Elajami, M., El Zarif, T., Bou-Gharios, J., Abou-Antoun, T. and Abou-Kheir, W., 2020. Drug repurposing towards targeting cancer stem cells in pediatric brain tumors. *Cancer and Metastasis Reviews*, 39(1), pp.127-148.

Barroso AS, Leite S, Friões F, et al. Pericardial mesothelioma presenting as a suspected ST-elevation myocardial infarction. *Rev Port Cardiol.* 2017;36(4):307.e1-307.e5.

Benedetti, S., Nuvoli, B., Catalani, S. and Galati, R., 2015. Reactive oxygen species a double-edged sword for mesothelioma. *Oncotarget*, 6(19), pp.16848-16865.

Bianchi, C. and Bianchi, T. (2014). Global mesothelioma epidemic: Trend and features. *Indian Journal of Occupational and Environmental Medicine*, 18(2), p.82.

Bighetti-Trevisan, R., Sousa, L., Castilho, R. and Almeida, L., 2019. Cancer Stem Cells: Powerful Targets to Improve Current Anticancer Therapeutics. *Stem Cells International*, 2019, pp.1-15.

Blum, W., Pecze, L., Felley-Bosco, E., Wu, L., de Perrot, M. and Schwaller, B., 2017. Stem Cell Factor-Based Identification and Functional Properties of In Vitro-Selected Subpopulations of Malignant Mesothelioma Cells. *Stem Cell Reports*, 8(4), pp.1005-1017.

Blum, Y., Jaurand, M., De Reyniès, A. and Jean, D., 2019. Unraveling the cellular heterogeneity of malignant pleural mesothelioma through a deconvolution approach. *Molecular & Cellular Oncology*, 6(4), p.1610322.

Blyth, K. and Murphy, D. (2018). Progress and challenges in Mesothelioma: From bench to bedside. *Respiratory Medicine*, 134, pp.31-41.

Bonomi, M., De Filippis, C., Lopci, E., Gianoncelli, L., Rizzardi, G., Cerchiaro, E., Bortolotti, L., Zanello, A. and Ceresoli, G., 2017. Clinical staging of malignant pleural mesothelioma: current perspectives. *Lung Cancer: Targets and Therapy*, Volume 8, pp.127-139.

Boyer, A., Pasquier, E., Tomasini, P., Ciccolini, J., Greillier, L., Andre, N., Barlesi, F. and Mascaux, C. (2018). Drug repurposing in malignant pleural mesothelioma: a breath of fresh air? *European Respiratory Review*, 27(147), p.170098.

Boyd, P., Major, I., Wang, W. and McConville, C., 2014. Development of disulfiram-loaded vaginal rings for the localised treatment of cervical cancer. *European Journal of Pharmaceutics and Biopharmaceutics*, 88(3), pp.945-953.

Brcic, L. and Kern, I., 2020. Clinical significance of histologic subtyping of malignant pleural mesothelioma. *Translational Lung Cancer Research*, 9(3), pp.924-933.

Brehmer, B., Biesterfeld, S. & Jakse, G. Expression of matrix metalloproteinases (MMP-2 and -9) and their inhibitors (TIMP-1 and -2) in prostate cancer tissue. *Prostate Cancer Prostatic Dis* 6, 217–222 (2003).

Bronte, G., Incorvaia, L., Rizzo, S., Passiglia, F., Galvano, A., Rizzo, F., Rolfo, C., Fanale, D., Listì, A., Natoli, C., Bazan, V. and Russo, A., 2016. The resistance related to targeted therapy in malignant pleural mesothelioma: Why has not the target been hit yet? *Critical Reviews in Oncology/Hematology*, 107, pp.20-32.

Brown JM. The hypoxic cell: a target for selective cancer therapy--eighteenth Bruce F. Cain Memorial Award lecture. *Cancer Res.* 1999 Dec 1;59(23):5863-70.

Butcher, K., Kannappan, V., Kilari, R., Morris, M., McConville, C., Armesilla, A. and Wang, W. (2018). Investigation of the key chemical structures involved in the anticancer activity of disulfiram in A549 non-small cell lung cancer cell line. *BMC Cancer*, 18(1).

Cantini, L., Hassan, R., Sterman, D. and Aerts, J., 2020. Emerging Treatments for Malignant Pleural Mesothelioma: Where Are We Heading? *Frontiers in Oncology*, 10.

Cao, Z., Wang, Z. and Leng, P., 2019. Aberrant N-cadherin expression in cancer. Biomedicine & Pharmacotherapy, 118, p.109320.

Carbone, M., Adusumilli, P., Alexander, H., Baas, P., Bardelli, F., Bononi, A., Bueno, R., Felley-Bosco, E., Galateau-Salle, F., Jablons, D., Mansfield, A., Minaai, M., Perrot, M., Pesavento, P., Rusch, V., Severson, D., Taioli, E., Tsao, A., Woodard, G., Yang, H., Zauderer, M. and Pass, H., 2019. Mesothelioma: Scientific clues for prevention, diagnosis, and therapy. *CA: A Cancer Journal for Clinicians*, 69(5), pp.402-429.

Carbone, M., Ly, B., Dodson, R., Pagano, I., Morris, P., Dogan, U., Gazdar, A., Pass, H. and Yang, H. (2011). Malignant mesothelioma: Facts, Myths, and Hypotheses. *Journal of Cellular Physiology,* 227(1), pp.44-58.

Castagnoli, L., De Santis, F., Volpari, T., Vernieri, C., Tagliabue, E., Di Nicola, M. and Pupa, S., 2020. Cancer Stem Cells: Devil or Savior—Looking behind the Scenes of Immunotherapy Failure. *Cells*, 9(3), p.555.

Challapalli, A., Carroll, L. & Aboagye, E.O. Molecular mechanisms of hypoxia in cancer. *Clin Transl Imaging* 5, 225–253 (2017).

Chaturvedi, M., Sung, B., Yadav, V., Kannappan, R. and Aggarwal, B., 2010. NF-κB addiction and its role in cancer: 'one size does not fit all'. *Oncogene*, 30(14), pp.1615-1630.

Chen YC, Hsu HS, Chen YW, et al. Oct-4 expression-maintained cancer stem-like properties in lung cancer-derived CD133-positive cells. *PLoS One*. 2008;3(7): e2637.

Chen, J., Li, X. and Wei, S. (2014). Critical appraisal of pemetrexed in the treatment of NSCLC and metastatic pulmonary nodules. *OncoTargets and Therapy*, p.937.

Chen, S. and Chang, J., 2019. New Insights into Mechanisms of Cisplatin Resistance: From Tumor Cell to Microenvironment. *International Journal of Molecular Sciences*, 20(17), p.4136.

Chen, X., Wu, C., Zhong, J., Shen, Y. and Zu, X., 2020. Tumorigenesis and Progression as a Consequence of Hypoxic TME : A Prospective View upon Breast Cancer Therapeutic Targets. *Experimental Cell Research*, 395(2), p.112192.

Cheriyan, V., Wang, Y., Muthu, M., Jamal, S., Chen, D., Yang, H., Polin, L., Tarca, A., Pass, H., Dou, Q., Sharma, S., Wali, A. and Rishi, A., 2014. Disulfiram Suppresses Growth of the Malignant Pleural Mesothelioma Cells in Part by Inducing Apoptosis. *PLoS ONE*, 9(4), p.e93711.

Chiodi, I. and Mondello, C., 2020. Lifestyle factors, tumor cell plasticity and cancer stem cells. *Mutation Research/Reviews in Mutation Research*, 784, p.108308.

Cho, E.S., Kang, H.E., Kim, N.H. et al. Therapeutic implications of cancer epithelial-mesenchymal transition (EMT). *Arch. Pharm. Res.* 42, 14–24 (2019).

Christopher, S., Loveitt, A., Goldenberg-Sandau, A., Liu, J., Roy, D. and W. Cohen, L., 2020. Primary Peritoneal Mesothelioma Resulting in Small Bowel Obstruction: A Case Report and Review of Literature.

Chua, T. (2009). Peritoneal mesothelioma: current understanding and management. *Can J Surg*, 52(1).

Clark, D. and Palle, K., 2016. Aldehyde dehydrogenases in cancer stem cells: potential as therapeutic targets. *Annals of Translational Medicine*, 4(24), pp.518-518.

Cohen, L. and Frontario, N., 2015. Primary Peritoneal Mesothelioma Resulting in Small Bowel Obstruction: A Case Report and Review of Literature. *American Journal of Case Reports*, 16, pp.496-500.

Cole, A., Fayomi, A., Anyaeche, V., Bai, S. and Buckanovich, R., 2020. An evolving paradigm of cancer stem cell hierarchies: therapeutic implications. *Theranostics*, 10(7), pp.3083-3098.

Cong, J., Wang, Y., Zhang, X., Zhang, N., Liu, L., Soukup, K., Michelakos, T., Hong, T., DeLeo, A., Cai, L., Sabbatino, F., Ferrone, S., Lee, H., Levina, V., Fuchs, B., Tanabe, K., Lillemoe, K., Ferrone, C. and Wang, X. (2017). A novel chemoradiation targeting stem and nonstem pancreatic cancer cells by repurposing disulfiram. *Cancer Letters,* 409, pp.9-19.

Cortes-Dericks, L., Froment, L., Boesch, R., Schmid, R. and Karoubi, G., 2014. Cisplatin-resistant cells in malignant pleural mesothelioma cell lines show ALDH high $CD44^{+}$ phenotype and sphere-forming capacity. *BMC Cancer*, 14(1).

Creaney, J. and W. S. Robinson, B. (2017). Malignant Mesothelioma Biomarkers from Discovery to Use in Clinical Practice for Diagnosis, Monitoring, Screening, and Treatment. 152(1), pp.143 - 149.

Cvek, B. and Dvorak, Z. (2008). The value of proteasome inhibition in cancer. *Drug Discovery Today*, 13(15-16), pp.716-722.

D.T. Marie-Egyptienne et al., Cancer stem cells, the epithelial to mesenchymal transition (EMT) and radioresistance: Potential role of hypoxia, *Cancer Lett*. 2012.

Das, P., Pillai, S., Rakib, M., Khanam, J., Gopalan, V., Lam, A. and Islam, F., 2020. Plasticity of Cancer Stem Cell: Origin and Role in Disease Progression and Therapy Resistance. *Stem Cell Reviews and Reports*, 16(2), pp.397-412.

Dasari, S. and Bernard Tchounwou, P. (2014). Cisplatin in cancer therapy: Molecular mechanisms of action. *European Journal of Pharmacology*, 740, pp.364-378.

Deng, M., Jiang, Z., Li, Y., Zhou, Y., Li, J., Wang, X., Yao, Y., Wang, W., Li, P. and Xu, B., 2016. Effective elimination of adult B-lineage acute lymphoblastic leukemia by disulfiram/copper complex in vitro and in vivo in patient-derived xenograft models. *Oncotarget*, 7(50), pp.82200-82212.

Dinić, J., Efferth, T., García-Sosa, A., Grahovac, J., Padrón, J., Pajeva, I., Rizzolio, F., Saponara, S., Spengler, G. and Tsakovska, I., 2020. Repurposing old drugs to fight multidrug resistant cancers. *Drug Resistance Updates*, 52, p.100713.

Enomoto LM, Shen P, Levine EA, Votanopoulos KI. Cytoreductive surgery with hyperthermic intraperitoneal chemotherapy for peritoneal mesothelioma: patient selection and special considerations. Cancer Manag Res. 2019 May 7; 11:4231-4241.

Facchetti, G., Petrella, F., Spaggiari, L. and Rimoldi, I. (2017). Malignant Pleural Mesothelioma: State of the art and advanced cell therapy. *European Journal of Medicinal Chemistry,* 142, pp.266-270.

Falls-Hubert, K., Butler, A., Gui, K., Anderson, M., Li, M., Stolwijk, J., Rodman, S., Solst, S., Tomanek-Chalkley, A., Searby, C., Sheffield, V., Sandfort, V., Schmidt, H., McCormick, M., Wels, B., Allen, B., Buettner, G., Schultz, M. and Spitz, D., 2020. Disulfiram causes selective hypoxic cancer cell toxicity and radio-chemo-sensitization via redox cycling of copper. *Free Radical Biology and Medicine*, 150, pp.1-11.

Fels Elliott DR, Jones KD. Diagnosis of Mesothelioma. Surg Pathol Clin. 2020 ; Mar ;13(1):73-89.

Frank, E. (2012). Mesothelioma: A Review. *The Ochsner Journal,* 12, pp.70-79.

Gao, T., Li, J., Lu, Y., Zhang, C., Li, Q., Mao, J. and Li, L., 2016. The mechanism between epithelial mesenchymal transition in breast cancer and hypoxia microenvironment. *Biomedicine & Pharmacotherapy*, 80, pp.393-405.

Garcia-Mayea, Y., Mir, C., Masson, F., Paciucci, R. and LLeonart, M., 2020. Insights into new mechanisms and models of cancer stem cell multidrug resistance. *Seminars in Cancer Biology*, 60, pp.166-180.

Gialeli, C., Theocharis, A. and Karamanos, N., 2010. Roles of matrix metalloproteinases in cancer progression and their pharmacological targeting. *FEBS Journal*, 278(1), pp.16-27.

Gilkes, D., 2016. Implications of Hypoxia in Breast Cancer Metastasis to Bone. *International Journal of Molecular Sciences,* 17(10), p.1669.

Gill, R., Yeap, B., Bueno, R. and Richards, W., 2017. Quantitative Clinical Staging for Patients with Malignant Pleural Mesothelioma. *JNCI: Journal of the National Cancer Institute*, 110(3), pp.258-264.

Gillezeau, C., van Gerwen, M., Ramos, J., Liu, B., Flores, R. and Taioli, E., 2019. Biomarkers for malignant pleural mesothelioma: a meta-analysis. *Carcinogenesis*, 40(11), pp.1320-1331.

Glumac, P. M., & LeBeau, A. M. (2018*)*. The role of CD133 in cancer: a concise review. Clinical and translational medicine*, 7(1), 18.*

Godwin, P., Baird, A., Heavey, S., Barr, M., O'Byrne, K. and Gately, K., 2013. Targeting Nuclear Factor-Kappa B to Overcome Resistance to Chemotherapy. *Frontiers in Oncology*, 3.

Gonzalez-Fierro A, Dueñas-González A. Drug repurposing for cancer therapy, easier said than done. *Semin Cancer Biol*. 2019 Dec 23: S1044-579X (19)30410-9.

Goparaju, C., Blasberg, J., Volinia, S., Palatini, J., Ivanov, S., Donington, J., Croce, C., Carbone, M., Yang, H. and Pass, H., 2011. Onconase mediated NFKβ downregulation in malignant pleural mesothelioma. *Oncogene*, 30(24), pp.2767-2777.

Goudar, R. (2008). Review of pemetrexed in combination with cisplatin for the treatment of malignant pleural mesothelioma. *Therapeutics and Clinical Risk Management,* Volume 4, pp.205-211.

Grzegrzolka J, Biala M, Wojtyra P, Kobierzycki C, Olbromski M, Gomulkiewicz A, Piotrowska A, Rys J, Podhorska-Okolow M, Dziegiel P. Expression of EMT Markers SLUG and TWIST in Breast Cancer. Anticancer Res. 2015 Jul;35(7):3961-8.

Guazzelli, A., Meysami, P., Bakker, E., Bonanni, E., Demonacos, C., Krstic-Demonacos, M. and Mutti, L., 2019. What can independent research for mesothelioma achieve to treat this orphan disease? *Expert Opinion on Investigational Drugs*, 28(8), pp.719-732.

Han, D. Wu G, Chang C *et al* (2015). Disulfiram inhibits TGF-β-induced epithelial-mesenchymal transition and stem-like features in breast cancer via ERK/NF-κB/ Snail pathway. *Oncotarget*, 6(38), pp.40907-19.

Hiddinga, B., Rolfo, C. and van Meerbeeck, J. (2015). Mesothelioma treatment: Are we on target? A review. *Journal of Advanced Research,* 6(3), pp.319-330.

Hiriart, E., Deepe, R. and Wessels, A., 2019. Mesothelium and Malignant Mesothelioma. *Journal of Developmental Biology*, 7(2), p.7.

Hjerpe, A., Own, S. and Dobra, K., 2020. Integrative approach to cytologic and molecular diagnosis of malignant pleural mesothelioma. *Translational Lung Cancer Research*, 9(3), pp.934-943.

Hubert, K. and Butler, A., 2019. Disulfiram Causes Selective Hypoxic Cancer Cell Toxicity and Radio-Chemo-Sensitization via Redox Cycling of Copper. *Free Radical Biology and Medicine*, 145, p.S66.

Hughes, V., Wiggins, J. and Siemann, D., 2018. Tumor oxygenation and cancer therapy—then and now. *The British Journal of Radiology*, p.20170955.

Ibrahim, A., Sadiq, M., Frame, F., Maitland, N. and Pors, K., 2018. Expression and regulation of aldehyde dehydrogenases in prostate cancer. *Journal of Cancer Metastasis and Treatment*, 4(8), p.44.

Jaggupilli, A. and Elkord, E., 2012. Significance of CD44 and CD24 as Cancer Stem Cell Markers: An Enduring Ambiguity. *Clinical and Developmental Immunology*, 2012, pp.1-11.

Jakubowska, K., Pryczynicz, A., Januszewska, J., Sidorkiewicz, I., Kemona, A., Niewiński, A., Lewczuk, Ł., Kędra, B. and Guzińska-Ustymowicz, K., 2016. Expressions of Matrix Metalloproteinases 2, 7, and 9 in Carcinogenesis of Pancreatic Ductal Adenocarcinoma. *Disease Markers*, 2016, pp.1-7.

Janssen YM, Driscoll KE, Howard B, et al. Asbestos causes translocation of p65 protein and increases NF-kappa B DNA binding activity in rat lung epithelial and pleural mesothelial cells. *Am J Pathol*. 1997;151(2):389-401.

Jászai, J. and Schmidt, M., 2019. Trends and Challenges in Tumor Anti-Angiogenic Therapies. *Cells*, 8(9), p.1102.

Jin-Yuan Shih, Pan-Chyr Yang, The EMT regulator slug and lung carcinogenesis. *Carcinogenesis,* Volume 32, Issue 9, September 2011, Pages 1299–1304.

Jing, S., Wang, J. and Xu, Q., 2017. Expression of hypoxia inducible factor 1 alpha and its clinical significance in esophageal carcinoma: A meta-analysis. *Tumor Biology*, 39(7), p.101042831771798.

Jing, X., Yang, F., Shao, C., Wei, K., Xie, M., Shen, H. and Shu, Y., 2019. Role of hypoxia in cancer therapy by regulating the tumor microenvironment. *Molecular Cancer*, 18(1).

Kabakov, A., Yakimova, A. and Matchuk, O., 2020. Molecular Chaperones in Cancer Stem Cells: Determinants of Stemness and Potential Targets for Antitumor Therapy. *Cells*, 9(4), p.892.

Kai, K., D'Costa, S., Yoon, B., Brody, A., Sills, R. and Kim, Y., 2010. Characterization of side population cells in human malignant mesothelioma cell lines. *Lung Cancer*, 70(2), pp.146-151.

Kale, V., Habib, H., Chitren, R., Patel, M., Pramanik, K., Jonnalagadda, S., Challagundla, K. and Pandey, M., 2020. Old drugs, new uses: Drug repurposing in hematological malignancies. *Seminars in Cancer Biology*.

Kaltschmidt, C., Banz-Jansen, C., Benhidjeb, T., Beshay, M., Förster, C., Greiner, J., Hamelmann, E., Jorch, N., Mertzlufft, F., Pfitzenmaier, J., Simon, M., Schulte am Esch, J., Vordemvenne, T., Wähnert, D., Weissinger, F., Wilkens, L. and Kaltschmidt, B., 2019. A Role for NF-κB in Organ Specific Cancer and Cancer Stem Cells. *Cancers*, 11(5), p.655.

Kalyanaraman, B. (2017). "Teaching the basics of cancer metabolism: Developing antitumor strategies by exploiting the differences between normal and cancer cell metabolism." *Redox Biol* 12: 833-842.

Kaushik, I., Ramachandran, S., Prasad, S. and Srivastava, S., 2020. Drug rechanneling: A novel paradigm for cancer treatment. *Seminars in Cancer Biology*.

Kim JY, Lee JY. Targeting Tumor Adaption to Chronic Hypoxia: Implications for Drug Resistance, and How It Can Be Overcome. *Int J Mol Sci*. 2017 Aug 25;18(9):1854.

Kim, J., 2017. Targeting Tumor Adaption to Chronic Hypoxia: Implications for Drug Resistance, and How It Can Be Overcome. *International Journal of Molecular Sciences*, 18(9), p.1854.

Kim, J., Kim, D., Hong, Y., Kim, K., Yoon, Y., Lee, D., Kim, S., Chun, S., Jang, S. and Kim, T. (2018). Mutational Profiling of Malignant Mesothelioma Revealed Potential Therapeutic Targets in EGFR and NRAS. *Translational Oncology*, 11(2), pp.268-274.

Kim, M., Hwang, S., Kim, N. et al. Hypoxia promotes acquisition of aggressive phenotypes in human malignant mesothelioma. *BMC Cancer 18, 819 (2018).*

Kim, M., Hwang, S., Kim, N., Lee, H., Ji, S., Yang, Y. and Kim, Y., 2018. Hypoxia promotes acquisition of aggressive phenotypes in human malignant mesothelioma. *BMC Cancer*, 18(1).
Kim, T. and Eberwine, J., 2010. Mammalian cell transfection: the present and the future. *Analytical and Bioanalytical Chemistry*, 397(8), pp.3173-3178.

Kirtonia, A., Gala, K., Fernandes, S., Pandya, G., Pandey, A., Sethi, G., Khattar, E. and Garg, M., 2020. Repurposing of drugs: An attractive pharmacological strategy for cancer therapeutics. *Seminars in Cancer Biology*.

Klabatsa, A., Sheaff, M., Steele, J., Evans, M., Rudd, R. and Fennell, D., 2006. Expression and prognostic significance of hypoxia-inducible factor 1α (HIF-1α) in malignant pleural mesothelioma (MPM). *Lung Cancer*, 51(1), pp.53-59.

Kumar, S., Liu, S., Lu, H. et al. Acquired cancer stem cell phenotypes through Oct4-mediated dedifferentiation. *Oncogene 31,* 4898–4911 (2012).

Lacerenza, s., Ciregia, f., Giusti, l., Bonotti, A., Greco, v., Giannaccini, g., D'antongiovanni, v., Fallahi, p., Pieroni, l., Cristaudo, a., Lucacchini, a., Mazzoni, m. and FODDIS, R., 2020. Putative Biomarkers for Malignant Pleural Mesothelioma Suggested by Proteomic Analysis of Cell Secretome. *Cancer Genomics - Proteomics*, 17(3), pp.225-236.

Lathia J, Liu H, Matei D. The Clinical Impact of Cancer Stem Cells. *Oncologist.* 2020;25(2):123-131.

Levý M, Boublíková L, Büchler T, Šimša J. Treatment of Malignant Peritoneal Mesothelioma. Maligní peritoneální mezoteliom a jeho léčba. Klin Onkol. 2019;32(5):333-337.

Li Petri, G., El Hassouni, B., Sciarrillo, R., Funel, N., Mantini, G., Zeeuw van der Laan, E., Cascioferro, S., Avan, A., Zucali, P., Zaffaroni, N., Lagerweij, T., Parrino, B., Smid, K., Deraco, M., Granchi, C., Braczko, A., Smolenski, R., Matherly, L., Jansen, G., Assaraf, Y., Diana, P., Cloos, J., Peters, G., Minutolo, F. and Giovannetti, E., 2020. Impact of hypoxia on chemoresistance of mesothelioma mediated by the proton-coupled folate transporter, and preclinical activity of new anti-LDH-A compounds. *British Journal of Cancer*, 123(4), pp.644-656.

Li, C., Rezov, V., Joensuu, E., Vartiainen, V., Rönty, M., Yin, M., Myllärniemi, M. and Koli, K., 2018. Pirfenidone decreases mesothelioma cell proliferation and migration via inhibition

of ERK and AKT and regulates mesothelioma tumor microenvironment in vivo. *Scientific Reports*, 8(1).

Li, H., Wang, J., Wu, C., Wang, L., Chen, Z. and Cui, W., 2020. The combination of disulfiram and copper for cancer treatment. *Drug Discovery Today*, 25(6), pp.1099-1108.

Li, Y., Fu, S., Wang, L., Wang, F., Wang, N., Cao, Q., Wang, Y., Yang, J. and Wu, C. (2015). Copper improves the anti-angiogenic activity of disulfiram through the EGFR/Src/VEGF pathway in gliomas. Cancer Letters, 369(1), pp.86-96.

Li, Y., Wang, L., Zhang, H., Wang, Y., Liu, S., Zhou, W., Yuan, X., Li, T., Wu, C. and Yang, J., 2017. Disulfiram combined with copper inhibits metastasis and epithelial-mesenchymal transition in hepatocellular carcinoma through the NF-κB and TGF-β pathways. *Journal of Cellular and Molecular Medicine*, 22(1), pp.439-451.

Liang, J., Lu, T., Chen, Z., Zhan, C. and Wang, Q., 2019. Mechanisms of resistance to pemetrexed in non-small cell lung cancer. *Translational Lung Cancer Research*, 8(6), pp.1107-1118.

Lin, Y., Bai, L., Chen, W. and Xu, S. (2009). The NF-κB activation pathways, emerging molecular targets for cancer prevention and therapy. *Expert Opinion on Therapeutic Targets*, 14(1), pp.45-55.

Liu, P., Brown, S., Goktug, T., Channathodiyil, P., Kannappan, V., Hugnot, J., Guichet, P., Bian, X., Armesilla, A., Darling, J. and Wang, W. (2012). Cytotoxic effect of disulfiram/copper on human glioblastoma cell lines and ALDH-positive cancer-stem-like cells. *British Journal of Cancer,* 107(9), pp.1488-1497.

Liu, P., Kumar, I., Brown, S., Kannappan, V., Tawari, P., Tang, J., Jiang, W., Armesilla, A., Darling, J. and Wang, W. (2013). Disulfiram targets cancer stem-like cells and reverses resistance and cross-resistance in acquired paclitaxel-resistant triple-negative breast cancer cells. British Journal of Cancer, 109(7), pp.1876-1885.

Liu, P., Wang, Z., Brown, S., Kannappan, V., Tawari, P., Jiang, W., Irache, J., Tang, J., Britland, S., Armesilla, A., Darling, J., Tang, X. and Wang, W., 2014. Liposome encapsulated Disulfiram inhibits NF-κB pathway and targets breast cancer stem cells in vitro and in vivo. *Oncotarget*, 5(17), pp.7471-7485.

Liu, Y., Yang, M., Luo, J. and Zhou, H., 2020. Radiotherapy targeting cancer stem cells "awakens" them to induce tumour relapse and metastasis in oral cancer. *International Journal of Oral Science*, 12(1).

Louw, A., Badiei, A., Creaney, J., Chai, M. and Lee, Y., 2019. Advances in pathological diagnosis of mesothelioma. *Current Opinion in Pulmonary Medicine*, 25(4), pp.354-361.

M.W Janssen, Y., Driscoll, K., Howard, B., Quinlan, T., Treadwell, M., Barchowsky, A. and Mossman, B., 2020. *Asbestos Causes Translocation of p65 Protein and Increases NF-KB DNA Binding Activity in Rat Lung Epithelial and Pleural Mesothelial Cells*.151 (2): pp.389-401

Madden, E., Gorman, A., Logue, S. and Samali, A., 2020. Tumour Cell Secretome in Chemoresistance and Tumour Recurrence. *Trends in Cancer*, 6(6), pp.489-505.
Marie-Egyptienne, D., Lohse, I. and Hill, R., 2013. Cancer stem cells, the epithelial to mesenchymal transition (EMT) and radioresistance: Potential role of hypoxia. *Cancer Letters*, 341(1), pp.63-72.

Marinaccio,1, A., Corfiati, M., Binazzi,, A., Scarselli, A., Ferrante, P., Bonafede, M., Verardo, M., Mirabelli,, D., Gennaro,, V., Mensi, C., Mazzoleni, G., Girardi,, P., Negro,, C., Romanelli, A., Chellini,, E., Silvestri, S., Pascucci,, C., Calisti,, R., Stracci,1, F., Romeo, E., Ascoli,, V., Trafficante, L., Carrozza,, F., Cavone, D., Cauzillo, G., Tallarigo, F., Tumino, R., Melis, M. and Iavicoli,, S., 2020. The epidemiology of malignant mesothelioma in women: gender differences and modalities of asbestos exposure. Occupational and Environmental Medicine. 75.

Mattiuzzi, C. and Lippi, G., 2019. Current Cancer Epidemiology. *Journal of Epidemiology and Global Health*, 9(4), p.217.

McMahon, A., Chen, W. and Li, F., 2020. Old wine in new bottles: Advanced drug delivery systems for disulfiram-based cancer therapy. *Journal of Controlled Release*, 319, pp.352-359.
Mesothelin performance in the diagnosis of malignant mesothelioma. *Lung Cancer,* 90(3), pp.457-464.

Milosevic, V., Kopecka, J., Salaroglio, I., Libener, R., Napoli, F., Izzo, S., Orecchia, S., Ananthanarayanan, P., Bironzo, P., Grosso, F., Tabbò, F., Comunanza, V., Alexa-Stratulat, T., Bussolino, F., Righi, L., Novello, S., Scagliotti, G. and Riganti, C., 2019. Wnt/IL-1β/IL-8 autocrine circuitries control chemoresistance in mesothelioma initiating cells by inducing ABCB5. *International Journal of Cancer*, 146(1), pp.192-207.

Mimeault, M. and Batra, S., 2013. Hypoxia-inducing factors as master regulators of stemness properties and altered metabolism of cancer- and metastasis-initiating cells. *Journal of Cellular and Molecular Medicine*, 17(1), pp.30-54.

Mo W, Zhang JT. Human ABCG2: structure, function, and its role in multidrugresistance. *Int J Biochem Mol Biol.* 2012;3(1):1-27.
Moore, A. J., et al. (2008). "Malignant mesothelioma." *Orphanet J Rare Dis* 3: 34.

Mungo, E., Bergandi, L., Salaroglio, I. and Doublier, S., 2018. Pyruvate Treatment Restores the Effectiveness of Chemotherapeutic Agents in Human Colon Adenocarcinoma and Pleural Mesothelioma Cells. *International Journal of Molecular Sciences*, 19(11), p.3550.

Murphy, D. and Gill, R., 2017. Overview of treatment related complications in malignant pleural mesothelioma. *Annals of Translational Medicine*, 5(11), pp.235-235.

Murray, G., Duncan, M., Arbuckle, E., Melvin, W. and Fothergill, J., 1998. Matrix metalloproteinases and their inhibitors in gastric cancer. *Gut*, 43(6), pp.791-797.

Muz, B., de la Puente, P., Azab, F. and Azab, A., 2015. The role of hypoxia in cancer progression, angiogenesis, metastasis, and resistance to therapy. *Hypoxia*, p.83.

N., Fombon, I., Liu, P., Brown, S., Kannappan, V., Armesilla, A., Xu, B., Cassidy, J., Darling, J. and Wang, W. (2011). Disulfiram modulated ROS–MAPK and NF-κB pathways and targeted breast cancer cells with cancer stem cell-like properties. *British Journal of Cancer*, 104(10), pp.1564-1574.

Nabavi, N., Bennewith, K., Churg, A., Wang, Y., Collins, C. and Mutti, L., 2017. Switching off malignant mesothelioma: exploiting the hypoxic microenvironment. *Genes & Cancer*, 7(11-12), pp.340-354.

Najafi, M., Farhood, B., Mortezaee, K., Kharazinejad, E., Majidpoor, J. and Ahadi, R., 2019. Hypoxia in solid tumors: a key promoter of cancer stem cell (CSC) resistance. *Journal of Cancer Research and Clinical Oncology*, 146(1), pp.19-31.

Najafi, M., Mortezaee, K. and Majidpoor, J., 2019. Cancer stem cell (CSC) resistance drivers. *Life Sciences*, 234, p.116781.

Najlah, M., Ahmed, Z., Iqbal, M., Wang, Z., Tawari, P., Wang, W. and McConville, C., 2017. Development and characterisation of disulfiram loaded PLGA nanoparticles for the treatment of non-small cell lung cancer. *European Journal of Pharmaceutics and Biopharmaceutics*, 112, pp.224-233.

Najlah, M., Said Suliman, A., Tolaymat, I., Kurusamy, S., Kannappan, V., Elhissi, A. and Wang, W., 2019. Development of Injectable PEGylated Liposome Encapsulating Disulfiram for Colorectal Cancer Treatment. *Pharmaceutics*, 11(11), p.610.

Nishikawa, S., Tanaka, A., Matsuda, A., Oida, K., Jang, H., Jung, K., Amagai, Y., Ahn, G., Okamoto, N., Ishizaka, S. and Matsuda, H., 2014. A molecular targeting against nuclear factor-κB, as a chemotherapeutic approach for human malignant mesothelioma. *Cancer Medicine*, 3(2), pp.416-425.

Nowak, A., Brosseau, S., Cook, A. and Zalcman, G., 2020. Antiangiogeneic Strategies in Mesothelioma. *Frontiers in Oncology*, 10. 10.3389/fonc.2020.00126.

Obata, T., Tanaka, M., Suzuki, Y. and Sasaki, T. (2013). The Role of Thymidylate Synthase in Pemetrexed-Resistant Malignant Pleural Mesothelioma Cells. *Journal of Cancer Therapy,* 04(06), pp.1052-1059.

Ortiz-Montero P, Liu-Bordes WY, Londoño-Vallejo A, Vernot JP. CD24 expression and stem-associated features define tumor cell heterogeneity and tumorigenic capacities in a model of carcinogenesis. *Cancer Manag Res*. 2018; 10:5767–5784.

Owunari, G. (2014). Disulfiram and Copper Gluconate in Cancer Chemotherapy; a Review of the Literature. *Cancer Research Journal*, 2(5), p.88.

Papaioannou, M., Mylonas, I., Kast, R. and Bruning, A. (2013). Disulfiram/copper causes redox-related proteotoxicity and concomitant heat shock response in ovarian cancer cells that is augmented by auranofin-mediated thioredoxin inhibition. *Oncoscience*, 1. 2014; 1(1): 21–29.

Peng, L, Wang Z, Brown S *et al* (2014). Liposome encapsulated Disulfiram inhibits NFκB pathway and targets breast cancer stem cells in vitro and in vivo. *Oncotarget*, 5(17), pp.471-85.

Pérez-Mancera, P., González-Herrero, I., Pérez-Caro, M. et al. SLUG in cancer development. *Oncogene* 24, 3073–3082 (2005).

Petrova, V., Annicchiarico-Petruzzelli, M., Melino, G. and Amelio, I., 2018. The hypoxic tumour microenvironment. *Oncogenesis*, 7(1).

Pires, B., Silva, R., Ferreira, G. and Abdelhay, E., 2018. NF-kappaB: Two Sides of the Same Coin. *Genes*, 9(1), p.24.

Porpodis, K. (2019). Malignant pleural mesothelioma : current and future perspective. J *Thorac Dis*, 5(S4), pp S397-S406.

Pozdeyev, N., Berlinberg, A., Zhou, Q., Wuensch, K., Shibata, H., Wood, W. and Haugen, B., 2015. Targeting the NF-κB Pathway as a Combination Therapy for Advanced Thyroid Cancer. *PLOS ONE*, 10(8), p.e0134901.

Qian J, Rankin EB. Hypoxia-Induced Phenotypes that Mediate Tumour Heterogeneity. Adv Exp Med Biol. 2019; 1136:43-55.

Quinn, L., Finn, S., Cuffe, S. and Gray, S. (2015). Non-coding RNA repertoires in malignant pleural mesothelioma. *Lung Cancer*, 90(3), pp.417-426.

Rae, C., Tesson, M., Babich, J., Boyd, M., Sorensen, A. and Mairs, R., 2013. The Role of Copper in Disulfiram-Induced Toxicity and Radiosensitization of Cancer Cells. *Journal of Nuclear Medicine*, 54(6), pp.953-960.

Rankin EB, Nam JM, Giaccia AJ. Hypoxia: Signaling the Metastatic Cascade. *Trends Cancer.* 2016 ;2(6) :295-304.

Redfern, A., Agarwal, V. and Thompson, E., 2019. Hypoxia as a signal for prison breakout in cancer. *Current Opinion in Clinical Nutrition & Metabolic Care*, 22(4), pp.250-263.

Ren, L., Feng, W., Shao, J., Ma, J., Xu, M., Zhu, B., Zheng, N. and Liu, S., 2020. Diethyldithiocarbamate-copper nanocomplex reinforces disulfiram chemotherapeutic efficacy through light-triggered nuclear targeting. *Theranostics*, 10(14), pp.6384-6398.

Richards, W., 2017. Malignant pleural mesothelioma: predictors and staging. *Annals of Translational Medicine*, 5(11), pp.243-243.

Riedel, T., Cavin, S., van den Bergh, H., Krueger, T., Liaudet, L., Ris, H., Dyson, P. and Perentes, J., 2018. Chemo-manipulation of tumor blood vessels by a metal-based anticancer complex enhances antitumor therapy. *Scientific Reports*, 8(1).

Rocha, C., Silva, M., Quinet, A., Cabral-Neto, J. and Menck, C., 2018. DNA repair pathways and cisplatin resistance: an intimate relationship. *Clinics*, 73(Suppl 1).

Rolle, F., Bincoletto, V., Gazzano, E., Rolando, B., Lollo, G., Stella, B., Riganti, C. and Arpicco, S., 2020. Coencapsulation of disulfiram and doxorubicin in liposomes strongly reverses multidrug resistance in breast cancer cells. *International Journal of Pharmaceutics*, 580, p.119191.

Saber, A., Liu, B., Ebrahimi, P. and Haisma, H., 2019. CRISPR/Cas9 for overcoming drug resistance in solid tumors. *DARU Journal of Pharmaceutical Sciences*, 28(1), pp.295-304.

Samuel, T., Fadlalla, K., Gales, D., Putcha, B. and Manne, U., 2014. Variable NF-κB pathway responses in colon cancer cells treated with chemotherapeutic drugs. *BMC Cancer*, 14(1).

Creaney, J. and W. S. Robinson, B. (2017). Malignant Mesothelioma Biomarkers from Discovery to Use in Clinical Practice for Diagnosis, Monitoring, Screening, and Treatment. 152(1), pp.143 - 149.

Sartore-Bianchi, A., Gasparri, F., Galvani, A., Nici, L., Darnowski, J., Barbone, D., Fennell, D., Gaudino, G., Porta, C. and Mutti, L. (2007). Bortezomib Inhibits Nuclear Factor- B

Dependent Survival and Has Potent In vivo Activity in Mesothelioma. *Clinical Cancer Research,* 13(19), pp.5942-5951.

Satelli, A. and Li, S., 2011. Vimentin in cancer and its potential as a molecular target for cancer therapy. *Cellular and Molecular Life Sciences*, 68(18), pp.3033-3046.

Saxena and Jolly, 2019. Acute vs. Chronic vs. Cyclic Hypoxia: Their Differential Dynamics, Molecular Mechanisms, and Effects on Tumor Progression. *Biomolecules*, 9(8), p.339.

Schito, L. and Rey, S., 2018. Cell-Autonomous Metabolic Reprogramming in Hypoxia. *Trends in Cell Biology*, 28(2), pp.128-142.

Schito, L. and Semenza, G., 2016. Hypoxia-Inducible Factors: Master Regulators of Cancer Progression. *Trends in Cancer*, 2(12), pp.758-770.

Schmidtova, S., Kalavska, K., Gercakova, K., Cierna, Z., Miklikova, S., Smolkova, B., Buocikova, V., Miskovska, V., Durinikova, E., Burikova, M., Chovanec, M., Matuskova, M., Mego, M. and Kucerova, L., 2019. Disulfiram Overcomes Cisplatin Resistance in Human Embryonal Carcinoma Cells. *Cancers*, 11(9), p.1224.

Schulte, J. and Husain, A., 2020. Update on the pathologic diagnosis of malignant mesothelioma. *Translational Lung Cancer Research*, 9(3), pp.917-923.

Schulz, A., Meyer, F., Dubrovska, A. and Borgmann, K., 2019. Cancer Stem Cells and Radioresistance: DNA Repair and Beyond. *Cancers*, 11(6), p.862.

Sertedaki, E. and Kotsinas, A., 2020. Drug Repurposing and DNA Damage in Cancer Treatment: Facts and Misconceptions. *Cells*, 9(5), p.1210.

Shavelle, R., Vavra-Musser, K., Lee, J. and Brooks, J. (2017). Life Expectancy in Pleural and Peritoneal Mesothelioma. *Lung Cancer International*, 2017, pp.1-8.

Singh, M., Jun Tian, X., Donnenberg, V., Watson, A., Zhang, J., Stabile, L., Watkins, S., Xing2, J. and Sant, S., 2020. Targeting the temporal dynamics of hypoxia-induced tumorsecreted factors halts tumor migration. 79(11):2962-2977

Singh, V., Gupta, D. and Arora, R., 2015. NF-κB as a key player in regulation of cellular radiation responses and identification of radiation countermeasures. *Discoveries*, 3(1), p.e35.

Sinha, S., Swift, A., Kamil, M., Matthews, S., Bull, M., Fisher, P., De Fonseka, D., Saha, S., Edwards, J. and Johns, C., 2020. The role of imaging in malignant pleural mesothelioma: an update after the 2018 BTS guidelines. *Clinical Radiology*, 75(6), pp.423-432.

Skok, Hladnik, Grm and Crnjac, 2019. Malignant Pleural Effusion and Its Current Management: A Review. *Medicina*, 55(8), p.490.

Skrott, Z., Majera, D., Gursky, J., Buchtova, T., Hajduch, M., Mistrik, M. and Bartek, J., 2019. Disulfiram's anti-cancer activity reflects targeting NPL4, not inhibition of aldehyde dehydrogenase. *Oncogene*, 38(40), pp.6711-6722.

Sørensen, B. and Horsman, M., 2020. Tumor Hypoxia: Impact on Radiation Therapy and Molecular Pathways. *Frontiers in Oncology*, 10. 10. 562. 10.3389/fonc.2020.00562.

Staumont, B., Jamakhani, M., Costa, C., Vandermeers, F., Sriramareddy, S., Redouté, G., Mascaux, C., Delvenne, P., Hubert, P., Safari, R. and Willems, L., 2020. TGFα Promotes Chemoresistance of Malignant Pleural Mesothelioma. *Cancers*, 12(6), p.1484.

Steinbichler, T., Savic, D., Dudás, J., Kvitsaridze, I., Skvortsov, S., Riechelmann, H. and Skvortsova, I., 2020. Cancer stem cells and their unique role in metastatic spread. *Seminars in Cancer Biology*, 60, pp.148-156.

Stockhammer, P., Ploenes, T., Theegarten, D., Schuler, M., Maier, S., Aigner, C. and Hegedus, B., 2020. Detection of TGF-β in pleural effusions for diagnosis and prognostic stratification of malignant pleural mesothelioma. *Lung Cancer*, 139, pp.124-132.

Sun, H., Wang, S., Yan, S., Zhang, Y., Nelson, P., Jia, H., Qin, L. and Dong, Q., 2019. Therapeutic Strategies Targeting Cancer Stem Cells and Their Microenvironment. *Frontiers in Oncology*, 9.

Tam, S., Wu, V. and Law, H., 2020. Hypoxia-Induced Epithelial-Mesenchymal Transition in Cancers: HIF-1α and Beyond. *Frontiers in Oncology*, 10.

Tambuyzer, E., Vandendriessche, B., Austin, C., Brooks, P., Larsson, K., Needleman, K., Valentine, J., Davies, K., Groft, S., Preti, R., Oprea, T. and Prunotto, M., 2020. Publisher Correction: Therapies for rare diseases: therapeutic modalities, progress, and challenges ahead. *Nature Reviews Drug Discovery*, 19(4), pp.291-291.

Tanabe, Shihori & Quader, Sabina & Cabral, Horacio & Ono, Ryuichi. (2020). Interplay of EMT and CSC in Cancer and the Potential Therapeutic Strategies. Frontiers in Pharmacology. 11. 10.3389/fphar.2020.00904.

Tawari, P., Wang, Z., Najlah, M., Tsang, C., Kannappan, V., Liu, P., McConville, C., He, B., Armesilla, A. and Wang, W. (2015). The cytotoxic mechanisms of disulfiram and copper(ii) in cancer cells. *Toxicology Research,* 4(6), pp.1439-1442.

Terry, S., Faouzi Zaarour, R., Hassan Venkatesh, G., Francis, A., El-Sayed, W., Buart, S., Bravo, P., Thiery, J. and Chouaib, S., 2018. Role of Hypoxic Stress in Regulating Tumor Immunogenicity, Resistance and Plasticity. *International Journal of Molecular Sciences*, 19(10), p.3044.

Tertemiz, K., Ozgen Alpaydin, A., Gurel, D., Savas, R., Gulcu, A. and Akkoclu, A., 2014. Multiple distant metastases in a case of malignant pleural mesothelioma. *Respiratory Medicine Case Reports*, 13, pp.16-18.

Tesson, M., Anselmi, G., Bell, C. and Mairs, R., 2017. Cell cycle specific radiosensitisation by the disulfiram and copper complex. *Oncotarget*, 8(39), pp.65900-65916.

Tirpe, A., Gulei, D., Ciortea, S., Crivii, C. and Berindan-Neagoe, I., 2019. Hypoxia: Overview on Hypoxia-Mediated Mechanisms with a Focus on the Role of HIF Genes. *International Journal of Molecular Sciences*, 20(24), p.6140.

Tolani, B., Acevedo, L., Hoang, N. and He, B., 2018. Heterogeneous Contributing Factors in MPM Disease Development and Progression: Biological Advances and Clinical Implications. *International Journal of Molecular Sciences*, 19(1), p.238.

Torre, L., Siegel, R., Ward, E. and Jemal, A., 2015. Global Cancer Incidence and Mortality Rates and Trends--An Update. *Cancer Epidemiology Biomarkers & Prevention*, 25(1), pp.16-27.

Trenti E, Palermo SM, D'Elia C, et al. Malignant mesothelioma of tunica vaginalis testis: Report of a very rare case with review of the literature. Arch Ital Urol Androl. 2018;90(3):212-214.

Triscott, J., Rose Pambid, M. and Dunn, S., 2015. Concise Review: Bullseye: Targeting Cancer Stem Cells to Improve the Treatment of Gliomas by Repurposing Disulfiram. *STEM CELLS*, 33(4), pp.1042-1046.

Trosko, J. (2009). REVIEW PAPER: Cancer Stem Cells and Cancer Nonstem Cells: From Adult Stem Cells or from Reprogramming of Differentiated Somatic Cells. *Veterinary Pathology*, 46(2), pp.176-193.

Vander Linden, C. and Corbet, C., 2019. Therapeutic Targeting of Cancer Stem Cells: Integrating and Exploiting the Acidic Niche. *Frontiers in Oncology*, 9. 159. 10.3389/fonc.2019.00159.

Vaupel, P., Schmidberger, H. and Mayer, A., 2019. The Warburg effect: essential part of metabolic reprogramming and central contributor to cancer progression. *International Journal of Radiation Biology*, 95(7), pp.912-919.

Vega, S., 2004. Snail blocks the cell cycle and confers resistance to cell death. *Genes & Development*, 18(10), pp.1131-1143.

Verzella, D., Pescatore, A., Capece, D., Vecchiotti, D., Ursini, M., Franzoso, G., Alesse, E. and Zazzeroni, F., 2020. Life, death, and autophagy in cancer: NF-κB turns up everywhere. *Cell Death & Disease*, 11(3).

Viscardi, G., Di Liello, R. and Morgillo, F., 2020. How I treat malignant pleural mesothelioma. *ESMO Open*, 4(Suppl 2), p.e000669.

Wang, C., Yang, J., Han, H., Chen, J., Wang, Y., Li, Q. and Wang, Y., 2017. Disulfiram-loaded porous PLGA microparticle for inhibiting the proliferation and migration of non-small-cell lung cancer. *International Journal of Nanomedicine*, Volume 12, pp.827-837.

Wang, C., Yang, J., Han, H., Chen, J., Wang, Y., Li, Q. and Wang, Y. (2017). Disulfiram-loaded porous PLGA microparticle for inhibiting the proliferation and migration of non- small-cell lung cancer. *International Journal of Nanomedicine,* Volume 12, pp.827-837.

Wang, N., Wang, L., Li, Y., Fu, S., Xue, X., Jia, L., Yuan, X., Wang, Y., Tang, X., Yang, J. and Wu, C., 2018. Targeting ALDH2 with disulfiram/copper reverses the resistance of cancer cells to microtubule inhibitors. *Experimental Cell Research*, 362(1), pp.72-82.

Wang, W., McLeod, H. and Cassidy, J., 2003. Disulfiram-mediated inhibition of NF-kB activity enhances cytotoxicity of 5-fluorouracil in human colorectal cancer cell lines. *International Journal of Cancer*, 104(4), pp.504-511.

Wang, Z., Tan, J., McConville, C., Kannappan, V., Tawari, P., Brown, J., Ding, J., Armesilla, A., Irache, J., Mei, Q., Tan, Y., Liu, Y., Jiang, W., Bian, X. and Wang, W., 2017. Poly lactic-co-glycolic acid-controlled delivery of disulfiram to target liver cancer stem-like cells. *Nanomedicine: Nanotechnology, Biology and Medicine*, 13(2), pp.641-657.

Wang, Z., Tan, J., McConville, C., Kannappan, V., Tawari, P., Brown, J., Ding, J., Armesilla, A., Irache, J., Mei, Q., Tan, Y., Liu, Y., Jiang, W., Bian, X. and Wang, W., 2017. Poly lactic-co-glycolic acid-controlled delivery of disulfiram to target liver cancer stem-like cells. *Nanomedicine: Nanotechnology, Biology and Medicine*, 13(2), pp.641-657.

Weina, K., Utikal, J. SOX2 and cancer: current research and its implications in the clinic. Clin Trans Med 3, 19 (2014).

Welsh, S. and Powis, G. (2003). Hypoxia Inducible Factor as a Cancer Drug Target. *Current Cancer Drug Targets*, 3(6), pp.391-405.

Wiggins, H., Wymant, J., Solfa, F., Hiscox, S., Taylor, K., Westwell, A. and Jones, A. (2015). Disulfiram-induced cytotoxicity and endo-lysosomal sequestration of zinc in breast cancer cells. *Biochemical Pharmacology,* 93(3), pp.332-342.

Wilson, M., Weinberg, R., Lees, J. and Guen, V., 2020. Emerging Mechanisms by which EMT Programs Control Stemness. *Trends in Cancer*, 6(9), pp.775-780.
Wu, C., Wang, M. and Chiou, S., 2013. Targeting cancer stem cells: emerging role of Nanog transcription factor. *OncoTargets and Therapy*, p.1207.

Wu, D., Wu, P., Zhao, L., Huang, L., Zhang, Z., Zhao, S. and Huang, J., 2015. NF-κB Expression and Outcomes in Solid Tumors. *Medicine*, 94(40), p.e1687.

Wu, L., Blum, W., Zhu, C., Yun, Z., Pecze, L., Kohno, M., Chan, M., Zhao, Y., Felley-Bosco, E., Schwaller, B. and de Perrot, M., 2018. Putative cancer stem cells may be the key target to inhibit cancer cell repopulation between the intervals of chemoradiation in murine mesothelioma. *BMC Cancer*, 18(1). 18. 471. 10.1186/s12885-018-4354-1.

Wu, X., Xue, X., Wang, L., Wang, W., Han, J., Sun, X., Zhang, H., Liu, Y., Che, X., Yang, J. and Wu, C. (2018). Suppressing autophagy enhances disulfiram/copper-induced apoptosis in non-small cell lung cancer. *European Journal of Pharmacology*, 827, pp.1-12.

Wu, Z., Li, X., Hu, C., Ford, M., Kleer, C. and Weiss, S., 2012. Canonical Wnt signaling regulates Slug activity and links epithelial-mesenchymal transition with epigenetic Breast Cancer 1, Early Onset (BRCA1) repression. Proceedings of the National Academy of Sciences, 109(41), pp.16654-16659.

Xia, Y., Shen, S. and Verma, I., 2014. NF- B, an Active Player in Human Cancers. *Cancer Immunology Research*, 2(9), pp.823-830.

Xia, Y., Wei, X., Gong, H. et al. Aldehyde dehydrogenase serves as a biomarker for worse survival profiles in ovarian cancer patients: an updated meta-analysis. BMC Women's Health 18, 199 (2018).

Yadav, A. and Desai, N., 2019. Cancer Stem Cells: Acquisition, Characteristics, Therapeutic Implications, Targeting Strategies and Future Prospects. *Stem Cell Reviews and Reports*, 15(3), pp.331-355.

Yamazaki, H., Naito, M., Ghani, F., Dang, N., Iwata, S. and Morimoto, C., 2012. Characterization of cancer stem cell properties of CD24 and CD26-positive human malignant mesothelioma cells. *Biochemical and Biophysical Research Communications*, 419(3), pp.529-536.

Yang C-H, Wang H-L, Lin Y-S, Kumar KPS, Lin H-C, Chang C-J, et al. (2014) Identification of CD24 as a Cancer Stem Cell Marker in Human Nasopharyngeal Carcinoma. *PLoS ONE 9(6): e99412.*

Yang, B. and Shi, J., 2020. Developing New Cancer Nanomedicines by Repurposing Old Drugs. *Angewandte Chemie*. 10.1002/ange.202004317.

Yang, H., Bailey, P. and Pilarsky, C., 2019. CRISPR Cas9 in Pancreatic Cancer Research. *Frontiers in Cell and Developmental Biology*, 7. 239. 10.3389/fcell.2019.00239.

Yang, L., Shi, P., Zhao, G. et al. Targeting cancer stem cell pathways for cancer therapy. *Sig Transduct Target Ther* 5, 8 (2020).

Yang, S., Zhang, Z., Hao, Y., Zhao, Y., Qian, F., Shi, Y., Li, P., Liu, C. and Yu, P., 2017. HIF-1α induces the epithelial-mesenchymal transition in gastric cancer stem cells through the Snail pathway. *Oncotarget*, 8(6), pp.9535-9545.

Yang, Y., Li, M., Sun, X., Zhou, C., Wang, Y., Wang, L., Chen, L., Liang, Z., Zhu, L. and Yang, H. (2017). The selective cytotoxicity of DSF-Cu attributes to the biomechanical properties and cytoskeleton rearrangements in the normal and cancerous nasopharyngeal epithelial cells. *The International Journal of Biochemistry & Cell Biology*, 84, pp.96-108.

Yeo, C., Kang, N., Choi, S., Kim, B., Park, C., Kim, J., Kim, Y. and Kim, S., 2017. The role of hypoxia on the acquisition of epithelial-mesenchymal transition and cancer stemness: a possible link to epigenetic regulation. *The Korean Journal of Internal Medicine*, 32(4), pp.589-599.

Yip, N., Fombon, I., Liu, P., Brown, S., Kannappan, V., Armesilla, A., Xu, B., Cassidy, J., Darling, J. and Wang, W., 2011. Disulfiram modulated ROS–MAPK and NF-κB pathways and targeted breast cancer cells with cancer stem cell-like properties. *British Journal of Cancer*, 104(10), pp.1564-1574.

Zandwijk, N., Clarke, C. and Henderson, D. (2013). Guidelines for the diagnosis and treatment of malignant pleural mesothelioma. *J Thorac Dis*, 5(6), pp. E254-E307

Zembko, I., Ahmed, I., Farooq, A., Dail, J., Tawari, P., Wang, W. and Mcconville, C., 2015. Development of Disulfiram-Loaded Poly (Lactic-co-Glycolic Acid) Wafers for the Localised Treatment of Glioblastoma Multiforme: A Comparison of Manufacturing Techniques. *Journal of Pharmaceutical Sciences*, 104(3), pp.1076-1086.

Zha, J., Chen, F., Dong, H., Shi, P., Yao, Y., Zhang, Y., Li, R., Wang, S., Li, P., Wang, W. and Xu, B., 2014. Disulfiram targeting lymphoid malignant cell lines via ROS-JNK activation as well as Nrf2 and NF-kB pathway inhibition. *Journal of Translational Medicine*, 12(1), p.163.
Zhang W, Wu X, Wu L, Zhang W, Zhao X. Advances in the diagnosis, treatment and prognosis of malignant pleural mesothelioma. Ann Transl Med. 2015;3(13):182.

Zhang, J., Pu, K., Bai, S., Peng, Y., Li, F., Ji, R., Guo, Q., Sun, W. and Wang, Y., 2020. The anti-alcohol dependency drug disulfiram inhibits the viability and progression of gastric cancer cells by regulating the Wnt and NF-κB pathways. *Journal of International Medical Research*, 48(6).

Zhang, Y., Xu, L., Li, A. and Han, X., 2019. The roles of ZEB1 in tumorigenic progression and epigenetic modifications. *Biomedicine & Pharmacotherapy*, 110, pp.400-408.

Zonneveld, M., Keulers, T. and Rouschop, K., 2019. Extracellular Vesicles as Transmitters of Hypoxia Tolerance in Solid Cancers. *Cancers*, 11(2), p.154.

Appendix 2: Hypoxia cultured MM cell lines E -58 and 2591 are resistant to first line anti MM drugs

(A)

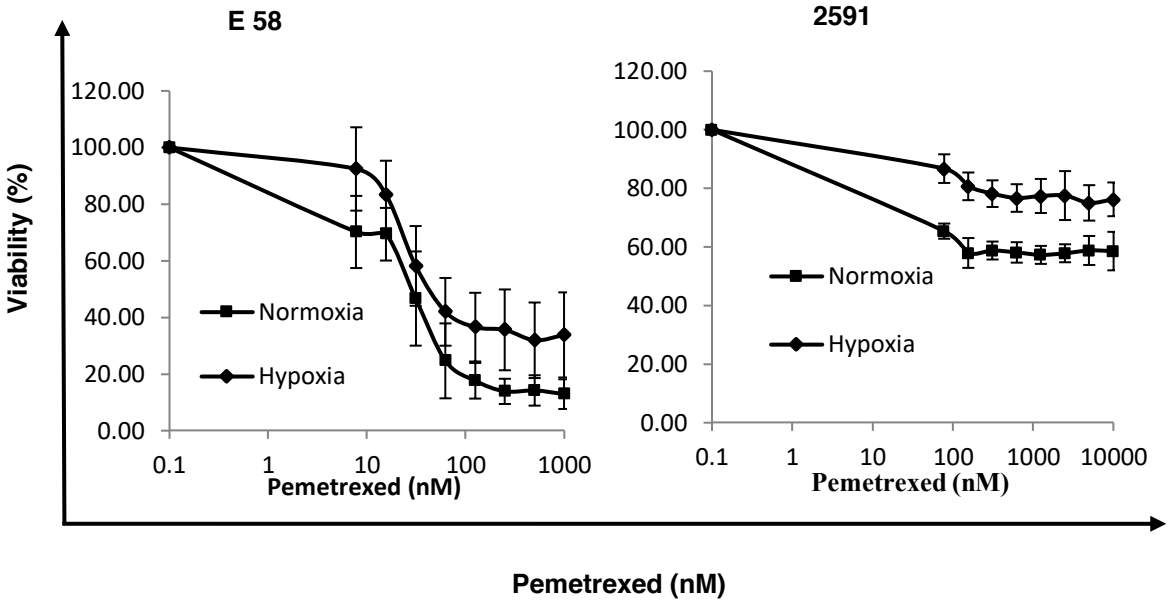

(B)

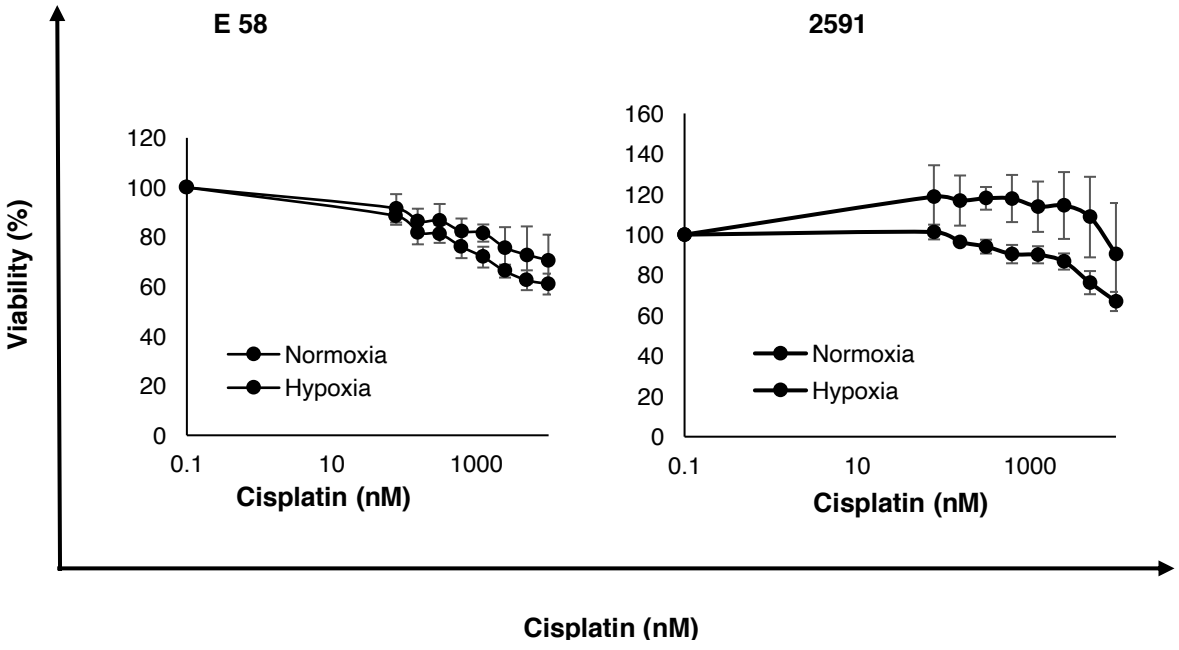

(C) **IC50**

	Normoxia		Hypoxia	
	PMT	CIS	PMT	CIS
E58	913	5025	>1000	>10,000
2591	749	>10,000	>1000	>10,000

The cell viability curve shows the effect of first-line anti-MM drugs on normoxic and hypoxic cultures of E -58 and 2591 cell lines. The cells were treated with (A) Cisplatin (B) Pemetrexed for 72 hours and then subjected to MTT assay (C) IC-50 values for E -58 and 2591 cell lines under normoxia and hypoxia after 72 hours of treatment with anticancer drugs.

Appendix 3: PLGA -DS +Cu synergistically enhances the effect of anti MM drugs

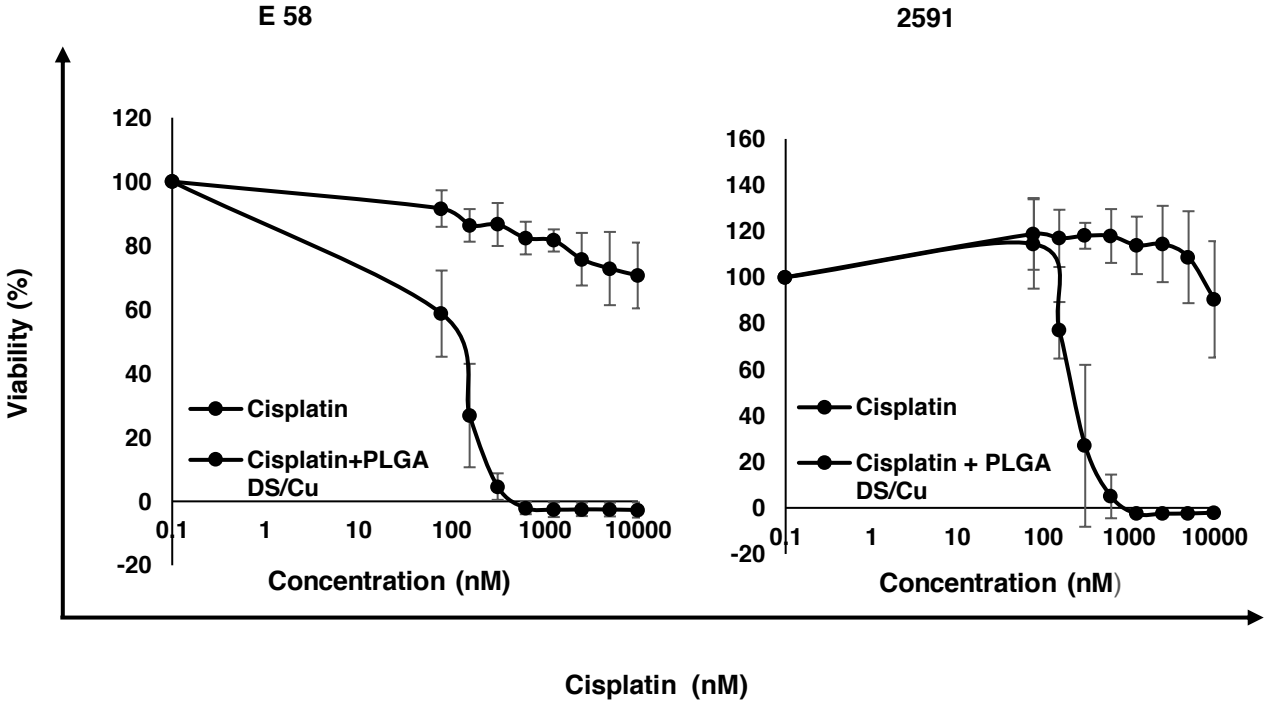

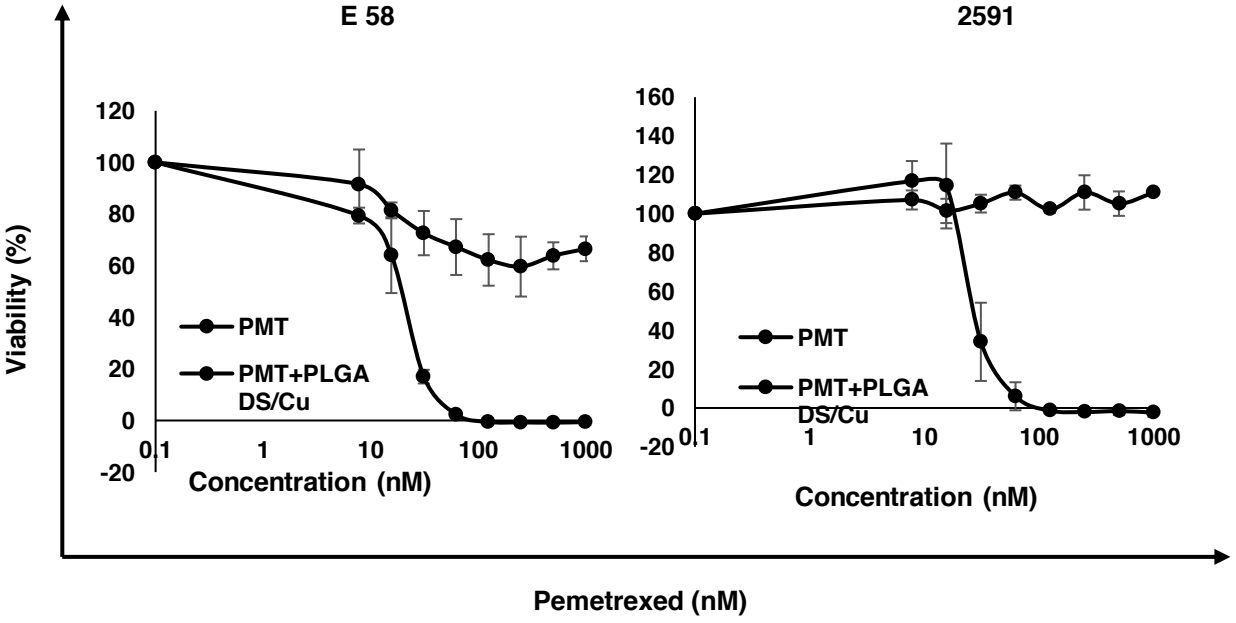

drug in combination with PLGA-DS/Cu(nM)	CI values					
	E58 Hypoxia			2591 Hypoxia		
	ED50	ED75	ED90	ED50	ED75	ED90
Pemetrexed (nM)	0.61	0.51	0.43	0.73	0.94	1.21
Cisplatin (nM)	0.98	0.21	0.50	2.51	0.92	4.81

The above results indicate the effect of PLGA-DS with $CuCl_2$ in hypoxia cultured cell lines. The cells were treated with serial dilution of PLGA-DS μM + $CuCl_2$ μM (1:1) and incubated for 72 hours and then subjected to MTT assay. Combination index (CI) values for hypoxic cultures treated with drug combinations. The effective dose at 50% (ED50) in both cell lines showed a greater synergistic relationship with PMT+PLGA-DS/Cu (1:10) than that of CIS+PLGA-DS/Cu (1:1) (E58 ED50= 0.61, 2591 ED50= 0.73).

Appendix :3 NF-κB-p65 knock out clones did not alter the drug sensitivity in MM cell lines.

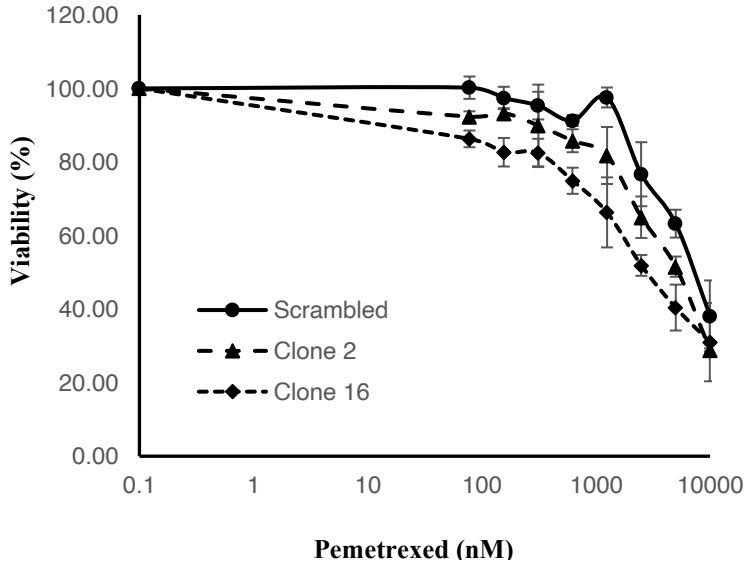

	Scrambled	Clone 2	Clone 16
Pemetrexed (nM)	24.66 ± 1.03	27.28 ± 3.67	28.84 ± 12.63

The above results indicate the effect of Pemetrexed (1μM) in NF-kB-p65 overexpressed clones. The cells were treated with Pemetrexed (1μM) and incubated for 72 hours and then subjected to MTT assay.

Appendix 4: NF-κB-p65 knock out MSTO-211H cells did not demonstrate significant decrease in the expression of (A) ESC markers (B) Invasiveness and (C) EMT related markers.

(A)

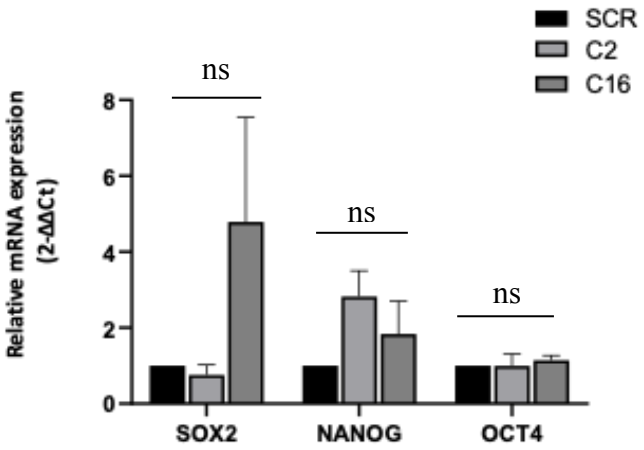

(B)

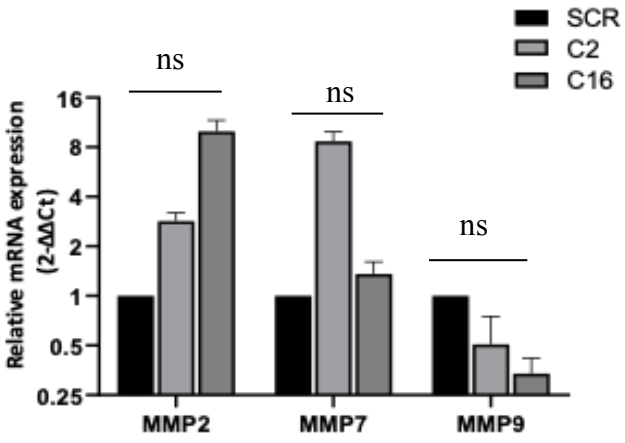

(C)